UDK: 553.411.071:549 DOI: 10.35597/2313-545X-2022-8-1-1

MINERALOGY OF THE VORONTSOVSKOE GOLD DEPOSIT (NORTHERN URALS)

A.V. Kasatkin[1], **S.Yu. Stepanov**[2], **M.V. Tsyganko**[3], **R. Škoda**[4], **F. Nestola**[5], **J. Plášil**[6], **E. Makovicky**[7], **A.A. Agakhanov**[1], **R.S. Palamarchuk**[8]

[1]*Fersman Mineralogical Museum of RAS, Leninsky pr. 18/2, Moscow, 119071 Russia; anatoly.kasatkin@gmail.com*

[2]*Institute of Geology and Geochemistry, UB RAS, ul. Akademika Vonsovskogo 15, Yekaterinburg, 620016 Russia*

[3]*Mineralogical Museum «Shtufnoi Kabinet», ul. Vatutina 17a, Severouralsk, Sverdlovsk oblast, 624480 Russia*

[4]*Masaryk University, Kotlářská 2, Brno, 61137 Czech Republic*

[5]*Università di Padova, Via Gradenigo 6, Padova, 35131 Italy*

[6]*Institute of Physics ASCR, v.v.i., Na Slovance 1999/2, Prague, 18221 Czech Republic*

[7]*University of Copenhagen, Östervoldgade 10, DK-1350, Copenhagen, Denmark*

[8] *Institute of Mineralogy, South Urals Federal Research Center of Mineralogy and Geoecology UB RAS, Miass, Chelyabinsk oblast, 456317 Russia*

Received 18.10.2021, accepted 15.01.2022

Abstract. The Vorontsovskoe gold deposit (Northern Urals) is unique in both Russia and the world because of the diverse and original Tl–Hg–Mn–As–Sb–S mineralization. Based on the available literature and our data, we present a list of 210 minerals found at this deposit. Eight of them are new minerals discovered by the authors: vorontsovite, ferrovorontsovite, tsygankoite, gladkovskyite, luboržákite, pokhodyashinite, gungerite, and auerbakhite. In addition, 41 minerals are found for the first time in the Russian Federation and 89 minerals are new for the deposit. We defined nine major ore mineral assemblages, including seven ones related to carbonate breccias. They contain more than 70 rare sulfides, tellurides and sulfosalts, including 31, 12, and 9 minerals with Tl, Hg and Mn, respectively, as species-defining elements. The paper also describes these mineral assemblages and minerals of the Vorontsovskoe deposit.

Keywords: Vorontsovskoe deposit, Northern Urals, ore mineral assemblage, carbonate breccia, Tl-Hg-Mn sulfosalt, new mineral, first find in Russia.

***For citation*:** Kasatkin A.V., Stepanov S.Yu., Tsyganko M.V., Škoda R., Nestola F., Plášil J., Makovicky E., Agakhanov A.A., Palamarchuk R.S. Mneralogy of the Vorontsovskoe gold deposit (Northern Urals). Mineralogy, **8**(1), 5–93. DOI: 10.35597/2313-545X-2022-8-1-1.

Introduction

The Vorontsovskoe gold deposit is located in the Krasnoturyinsk district of Sverdlovsk Oblast (Northern Urals), 0.5 km west of the settlement of Vorontsovka, 13 km south of Krasnoturyinsk and approximately 310 km north of Yekaterinburg (Figs. 1a, 1b). The deposit was discovered in 1985 and then has been a subject of prospecting and geophysical survey for several years (Gladkovsky, 2002). In 1998, it was acquired by the mining company Polymetal. Exploration of the deposit started in 1999 by northern (now 240 m deep) and southern (now 80 m deep) open pits (Figs. 2a, b). Both primary and oxidized ores are

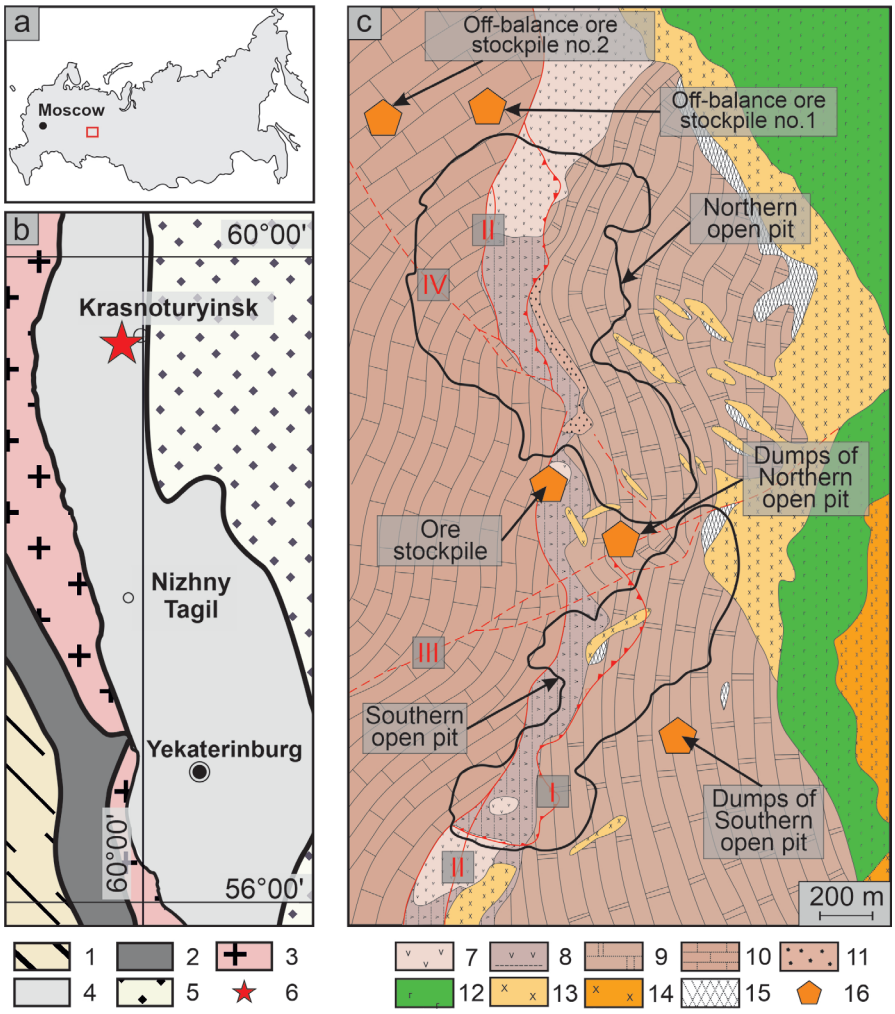

Fig. 1. Geographical location, geological position and structure of the Vorontsovskoe gold deposit:

a – position on map of Russia; b – position in structure of the Urals; c – geological scheme modified after (Vikentyev et al., 2016).

1 – East European Platform; 2 – West Uralian Megazone; 3 – Central Uralian Uplift; 4 – Tagil–Magnitogorsk Megazone; 5 – West Siberian Platform; 6 – Vorontsovskoe deposit; 7 – andesitic porphyrite; 8 – volcanosedimentary rocks; 9 – marble; 10 – limestone; 11 – sedimentary carbonate breccias; 12 – pyroxene–plagioclase porphyrite; 13 – diorite; 14 – quartz diorite; 15 – skarn; 16 – sampling places. Faults: I – Vorontsovsky ore-controlling thrust, II – Vorontsovsky reverse fault, III – Yuzhno-Vorontsovsky fault, IV – Yuzhno-Peschansky fault.

stocked at the ore stockpile near the northern open pit (Fig. 2c), from where the ore is transported to the processing plant located 6 km to the east. The ore is processed by carbon-in-leach (950 Ktpa) and a seasonal heap leach circuit (1000 Ktpa). Waste dumps (Fig. 2d) and off-balance ore stockpiles (Figs. 2e, 2f) are located near the open pits. The location of the main sampling sites of the deposit is shown in Fig. 1c.

Ore processing and gold production at the Vorontsovskoe deposit were maximum in 2010 (5.3 t Au) gradually decreasing to 3.7 t in 2017 and 3.3 t in 2019. Dating at January 1, 2020, the ore reserves of the deposit were estimated at 8.8 Mt with an average Au and Ag grade of 1.5 and 3 g/t, respectively (www.polymetalinternational.com). In 2018 and the middle of 2020, Polymetal company ended the exploration campaign of the southern and northen open pits, respectively. Thus, the plant is currently processing the ore from the previously accumulated off-balance ore stockpiles.

Despite the 35-year history and the status of one of the largest deposits in the Northern Urals, no systematic studies of mineralogy of the Vorontsovskoe deposit have been conducted. Most published data on the deposit concern the features of its geological setting with sketchy mineralogical information. The main aim of this work is to fill this «mineralogical» gap. Using pub-

Fig. 2. Main sites of the mine operating at the Vorontsovskoe deposit:
a – northern open pit; b – southern open pit; c – main ore stockpile; d – dumps of northern open pit; e – off-balance ore stockpile no. 1; f – off-balance ore stockpile no. 2.
Photo: A.V. Kasatkin (a–d), S.Yu. Stepanov (e), M.V. Tsyganko (f).

lished and our data, we composed a list of mineral species of the Vorontsovskoe deposit and provided their mineralogical description, as well as the brief history of the study of the deposit and its geological setting. The description is provided in an alphabetical order on the basis of mineralogical classification. The isostructural minerals (e.g., minerals of the vorontsovite–ferrovorontsovite or dalnegroite–chabournéite series, the members of the apatite supergroup, amphiboles, pyroxenes, etc.) are described together. Most new data result from materials of field trips of 2013–2021 to the open pits, dumps, main ore stockpile and off-balance ore stockpiles and laboratory studies of samples. Most attention is paid to carbonate breccias with extremely rich and diverse Tl–Hg–Mn–As–Sb–S mineralization including numerous rare sulfides and, especially, sulfosalts (both sulfarsenites and sulfantimonites).

Analytical studies of specimens coupled with their detailed observations and systematic documentation *in situ* allowed us to establish nine mineral assemblages with species-defining Tl, Hg, Pb, Cu, and/or Mn. Eight minerals (vorontsovite, ferrovorontsovite, tsygankoite, gladkovskyite, luboržákite, pokhodyashinite, gungerite, and auerbakhite) are new minerals approved in 2016–2020 by the Commission on New Minerals, Nomenclature and Classification of the International Min-

eralogical Association (CNMNC IMA). Along with clerite (Murzin et al., 1996), the total amount of new minerals discovered at the Vorontsovskoe deposit is nine, which is lower than at the Lengenbach deposit in Switzerland (44) and the Allchar deposit in North Macedonia (11), two further deposits famous for their Tl-Hg-As-Sb mineralization. By the amount of minerals with species-defining Tl (31), the Vorontsovskoe deposit is only slightly behind the Lengenbach deposit (33 minerals), but is almost twice ahead of the Allchar deposit (16 minerals). By the total amount of reliable mineral species, the Vorontsovskoe deposit is certainly the richest: 210 mineral species at Vorontsovskoe versus 160 at Lengenbach (Raber, Roth, 2018) and 85 at Allchar deposits (Boev et al., 2012; www.mindat.org). A distinctive feature of the Vorontsovskoe deposit is the Mn enrichment of some mineral assemblages: Mn is a species-defining element of numerous sulfosalts and it also forms rare oxides and hydroxides, which are found in the oxidation zone of the deposit.

The following symbols of minerals are accepted in the paper: Akt, aktashite; Alb, alabandite; And, andorite; Apt, fluorapatite; Apy, arsenopyrite; Ars, native arsenic; As_2O_3, arsenolite/claudetite; Au, native gold; Bar, baryte; Bln, boulangerite; Bnl, benleonardite; Brn, bernardite; Bsc, boscardinite; Cal, calcite; Ccp, chalcopyrite; Chb, chabournéite; Chr, christite; Cln, clinochlore; Clr, clerite; Cnb, cinnabar; Col, coloradoite; Cpb, cupropolybasite; Dfr, dufrénoysite; Dln, dalnegroite; Dol, dolomite; Dps, diopside; Dur, duranusite; Dwt, dewitite; Ecr, écrinsite; Fvr, ferrovorontsovite; Gal, galena; Gcr, geocronite; Gil, gillulyite; Gld, gladkovskyite; Gtr, guettardite; Htr, heteromorphite; Hut, hutchinsonite; Hwl, hawleyite; Imh, imhofite; Jlp, jalpaite; Jos, joséite-A; Lbr, luboržákite; Lft, laffittite; Lor, lorándite; Mgt, magnetite; Mtc, metacinnabar; Orp, orpiment; Oyn, oyonite; Qtz, quartz; Pav, pavonite; Phl, philrothite; Pic, picotpaulite; Pkd, pokhodyashinite; Plb, polybasite; Plg, plagionite; Prn, prehnite; Prp, parapierrotite; Pyr, pyrite; Rbl, rebulite; Rlg, realgar; Rmd, ramdohrite; Rsh, roshchinite; Rtr, routhierite; Sic, sicherite; Sin, sinnerite; Sms, semseyite; Sph, sphalerite; Stb, stibnite; Tdm, tetradymite; Thr, thorite; Til, tilasite; Tnt, tennantite; Tsg, tsygankoite; Tsn, tsnigriite; Twn, twinnite; Ves, vesuvianite; Vik, vikingite; Vor, vorontsovite; Vrb, vrbaite; Wkb, wakabayashilite; Wsb, weissbergite; Znk, zinkenite.

Vorontsovskoe deposit: history of study

The Vorontsovskoe deposit was discovered as a result of prospecting for primary gold in the Peschansko–Vorontsovskoe quartz vein ore field in the mid-1980s by Boris Aleksandrovitch Gladkovsky, a chief geologist of the Vorontsovskoe Geological Survey. In 1985, the karst deposits were trenched 200 m behind the road to the Shikhan recreation center, whereas due to limited funding, previous geochemical and geophysical prospecting for gold was carried out only in a narrow strip of this road along with the western contact of the Auerbakh diorite intrusion. The channel sampling of the trench showed a high Au content and, as a result, several boreholes were drilled near the trench, which exposed primary gold sulfide ores (Vikentyev et al., 2016). The prospecting works of 1985–1987 showed that the exploration of the deposit is profitable by open pit (Gladkovsky, 2002) and were followed by the detailed exploration of the deposit in 1988–1999. The detailed history of the discovery of the deposit and its geological study can be found in a few publications (Kabanov, 2001; Gladkovsky, 2002; Bobrov, 2013; Vikentyev et al., 2016).

First mineralogical studies of the deposit during its exploration were carried out in 1988–1992 by geologists of the Institute of Geology and Geochemistry, Urals Branch, Academy of Sciences of the USSR (Murzin, Sazonov, 1990; Sazonov et al., 1990a, b; Murzin et al., 1990; Grigoriev et al., 1991; Sazonov et al., 1991a, b; Ryabinin et al., 1992). The most detailed data of these studies are published in a monograph (Sazonov et al., 1991a). The monograph describes the geological structure of the ore region and ore complexes and provides a geological and genetic model of the deposit, which was referred for the first time to as Carlin-type gold deposits. The monograph also reports on mineral assemblages of various ore types with a description of minerals identified on the basis of chemical, X-ray diffraction, and optical data. Authors mentioned the presence of numerous rare minerals of the Tl–As–Sb–S and Pb–Tl–As–Sb–S systems, however, only routhierite was studied in detail. Although the authors mainly focused on geological features of the deposit (which was unnamed because of the restrictions on publication of data on gold deposits at that time) and had limited drillcore material for the study, this monograph can be considered the first fundamental mineralogical publication on the Vorontsovskoe deposit. In 1991, V.V. Murzin described benleonardite, a rare Ag sulfosalt found at the deposit (Mineralogy..., 1991).

The publications of the 1990s were mainly devoted to the geological and geochemical features of the deposit (Savel'eva, Kostromin, 1991; Savel'eva et al., 1991; Baryshev et al., 1993; Sazonov et al., 1993; Minina, 1994; Isakovich, 1996; Cheremisin, Zlotnik-Khotkevich, 1997; Rakhov, 1999) and only a few papers addressed particular mineralogical issues, i.e., micas (Sazonov et al., 1995) or morphology of quartz in jasperoids (Begetnev, 1998). The oxidation zone of the deposit was described by N.M. Rindzyunskaya et al. (1995a, b) and A.A. Kabanov (2001), however, withouth detailed study of supergene minerals.

In 1996, the new mineral clerite, $MnSb_2S_4$, was found at the deposit (Murzin et al., 1996). Murzin and Sustavov (1997) suggested the presence of new minerals in the Mn–As–Sb–S, Tl–As–Sb–S, K–As–Sb–S, and As–S systems, but indicated difficulties of their studies due to small sizes and a limited amount of the available material. Sazonov et al. (1998) reported for the first time on S isotopic composition of pyrite, sphalerite, and chalcopyrite of the deposit, as well as O and C of carbonates of host rocks.

The microprobe studies of the late 2000s resulted in the analysis of chemical data on minerals of a gold-sulfide-sulfosalt paragenesis of ore breccias (Murzin, Varlamov, 2010). A paragenesis of native arsenic and arsenopyrite was described by Murzin et al. (2011) and feldspars of the deposit were characterized by Rovnushkin et al. (2010).

In 2016, I.V. Vikentyev and co-authors published a monograph that was focused on the geology and genesis of the deposit based on the results of thermobarometric and isotopic-geochemical studies of ores. These authors described the mineral assemblages of primary and supergene ores providing numerous reflected light and SEM images and the sequence of mineral formation; they also presented new (including LA-ICP-MS and elemental mapping) data on chemical composition of native gold, as well as of a number of main and selected rare ore minerals.

Analytical data on several ore minerals in the matrix of gold-bearing breccias are given by Stepanov et al. (2017). Mineralogy of gangue carbonates of the deposit is studied by Soroka et al. (2017, 2018). Recent publications summarize the results of previous studies of geology, mineralogy, geochemistry and geochronology of the deposit (Murzin et al., 2017; Vikentyev et al., 2019). The latter paper provides a list of 76 ore minerals of the deposit. Thus, previous publications on the Vorontsovskoe deposit were mostly focused on its geology rather than on its mineralogy mainly due to limited analytical resources that prevented from detailed studies of minerals (especially, rare, and μm-sized).

In this paper, we summarize the results of our systematic mineralogical studies of the deposit from 2013 using a multimethodological approach. As a result, 210 mineral species are identified at the deposit including eight new minerals, 41 minerals found for the first time at the territory of the Russian Federation and 89 minerals found for the first time at the deposit. New analytical data are provided for 58 minerals (Table 1). Eight new mineral species include vorontsovite and ferrovorontsovite (Kasatkin et al., 2018a), tsygankoite (Kasatkin et al., 2018b), gladkovskyite (Kasatkin et al., 2019), luboržákite (Kasatkin et al., 2020a), pokhodyashinite (Kasatkin et al., 2022b), gungerite (Kasatkin et al., 2020c, 2022a), and auerbakhite (Kasatkin et al., 2021). Special attention was paid to the study of crystal structure of sulfosalts. The structures of natural parapierrotite (Plášil et al., 2018) and a Pb-free end-member of the chabournéite homeotypic group (Makovicky et al., 2021) were refined on a material from the Vorontsovskoe deposit. The latter was subsequently approved as a new mineral dewitite (Topa et al., 2021b).

Part of our data is published in papers that describe new minerals found at the deposit (Kasatkin et al., 2018a, 2018b, 2019, 2020a), also providing information on relevant mineral assemblages and analytical data on a number of rare sulfosalts. The findings of armenite, chapmanite, claudetite, getchellite, and wakabayashilite are briefly characterized in a review by Kasatkin (2019). Reliable analytical data for picotpaulite, weissbergite, dalnegroite, christite, and philrothite presented here for the first time enable us to consider their first findings at the territory of the Russian Federation.

Geological setting, structure and genetic type of the deposit

The Vorontsovskoe deposit in the Northern Urals is located in the eastern part of the Tagil volcanic zone (Fig. 1b) within a longitudinal volcanoplutonic belt (Sazonov et al., 1998; Murzin et al., 2017). This belt formed as a result of a collision of the Tagil island arc with the East Uralian microcontinent (Yazeva et al., 1991; Sazonov et al., 1998). The Middle Devonian Auerbakh gabbro-diorite-granodiorite pluton (Krasnobaev et al., 2007) occurs in the southern part of the volcanoplutonic belt and its formation was related to the Auerbakh ore region.

Table 1

Minerals of the Vorontsovskoe deposit

Mineral	Formula	Distribution	ID method	Source
Elements				
Native arsenic*	As	+++++	EMPA, XRD, O	Sazonov et al., 1991a; Murzin et al., 2011; Vikentyev et al., 2016; our data
Native copper	Cu	++	O	Vikentyev et al., 2016
Native gold*	Au	+++++	EMPA, O	Sazonov et al., 1991a; Murzin, Varlamov, 2010; Murzin et al., 2011; Vikentyev et al., 2016; our data
Native silver[1]**	Ag	++	EMPA, O	Vikentyev et al., 2016; our data
Sulfides, arsenides, tellurides				
Acanthite**	Ag_2S	++	EMPA, O	our data
Alabandite*	MnS	+++	EMPA, XRD, O	Sazonov et al., 1991a; Murzin, Varlamov, 2010; Murzin et al., 2011; Vikentyev et al., 2016; our data
Arsenopyrite*	FeAsS	+++++	EMPA, XRD, O	Sazonov et al., 1991a; Murzin et al., 2011; Vikentyev et al., 2016; our data
Bismuthinite**	Bi_2S_3	++	EMPA, O	our data
Bornite*	Cu_5FeS_4	+++	EMPA, O	Vikentyev et al., 2016; our data
Chalcopyrite*	$CuFeS_2$	+++++	EMPA, XRD, O	Sazonov et al., 1991a; Vikentyev et al., 2016; our data
Cinnabar*	HgS	++++	EMPA, XRD, O	
Coloradoite*	HgTe	+++	EMPA, XRD, O	Sazonov et al., 1991a; Murzin, Varlamov, 2010; our data
Covellite*	CuS	(++)	EMPA, XRD, O	Vikentyev et al., 2016; our data
Cubanite**	$CuFe_2S_3$	+	EMPA, O	our data
Dimorphite ?	As_4S_3	?	EMPA	Stepanov et al., 2017
Djurleite**	$Cu_{31}S_{16}$	(++)	EMPA, XRD, O	our data
Duranusite ***	As_4S	++	EMPA, O	
Galena*	PbS	+++	EMPA, XRD, O	Sazonov et al., 1991a; Vikentyev et al., 2016; our data
Gersdorfite*	NiAsS	++	EMPA, O	Vikentyev et al., 2016; our data
Getchellite***	$AsSbS_3$	+++	EMPA, XRD, O	Kasatkin, 2019; our data
Greigite*	$Fe^{2+}Fe^{3+}{}_2S_4$	+++	EMPA, XRD, O	Murzin et al., 1996; Murzin, Varlamov, 2010; our data
Hawleyite**	CdS	(++)	EMPA, XRD, O	our data
Hessite[1]**	Ag_2Te	++	EMPA, O	Sazonov et al., 1991a; our data
Ikunolite**	Bi_4S_3	++	EMPA, O	our data
Jalpaite**	Ag_3CuS_2	++	EMPA, O	
Joséite-A**	Bi_4TeS_2	++	EMPA, O	
Löllingite*	$FeAs_2$	+++	EMPA, XRD, O	Vikentyev et al., 2016; our data
Metacinnabar**	HgS	+++	EMPA, XRD, O	
Molybdenite[1]**	MoS_2	++	EMPA, O	
Orpiment*	As_2S_3	+++++	EMPA, XRD, O	Sazonov et al., 1991a; Murzin, Varlamov, 2010; Vikentyev et al., 2016; our data

Pararealgar***	As_4S_4	++	EMPA, XRD, O	our data
Picotpaulite[1]***	$TlFe_2S_3$	++	EMPA, O	Vikentyev et al., 2016; our data
Pyrite*	FeS_2	+++++	EMPA, LA ICP MS, XRD, O	Sazonov et al., 1991a; Murzin, Varlamov, 2010; Vikentyev et al., 2016; our data
Pyrrhotite	$Fe_{1-x}S$	+++	EMPA	Sazonov et al., 1991a; Vikentyev et al., 2016
Realgar*	AsS	+++++	EMPA, XRD, O	Sazonov et al., 1991a; Murzin, Varlamov, 2010; Vikentyev et al., 2016; our data
Sphalerite*	ZnS	+++++	EMPA, XRD, O	Sazonov et al., 1991a; Murzin, Varlamov, 2010; Murzin et al., 2011; Vikentyev et al., 2016; Stepanov et al., 2017; our data
Stibnite*	Sb_2S_3	+++++	EMPA, XRD, O	Sazonov et al., 1991a; Murzin, Varlamov, 2010; Vikentyev et al., 2016; our data
Tetradymite**	Bi_2Te_2S	++	EMPA, O	our data
Wakabayashilite**	$(As,Sb)_6As_4S_{14}$	+++	EMPA, XRD, O	Kasatkin, 2019; our data
Sulfosalts				
Aktashite*	$Cu_6Hg_3As_4S_{12}$	++++	EMPA, XRD, O	Sazonov et al., 1991a; Mineralogy of Urals, 1991; Murzin, Varlamov, 2010; Vikentyev et al., 2016; Stepanov et al., 2017; our data
Andorite*	$AgPbSb_3S_6$	++	EMPA, O	Vikentyev et al., 2016; our data
Argentotetrahedrite-(Fe)	$Ag_6(Cu_4Fe_2)Sb_4S_{13}$	++	EMPA	Sazonov et al., 1991a
Argentotetrahedrite-(Zn)	$Ag_6(Cu_4Zn_2)Sb_4S_{13}$	++	EMPA	
Arsiccioite***	$AgHg_2TlAs_2S_6$	+	EMPA, O	our data
Auerbakhite****	$MnTl_2As_2S_5$	++	EMPA, XRD, O, RS	Kasatkin et al., 2020d
Benavidesite***	$Pb_4MnSb_6S_{14}$	++	EMPA, O	our data
Benleonardite*	$Ag_{15}Cu(Sb,As)_2S_7Te_4$	++	EMPA, O	Mineralogy of Urals, 1991; our data
Bernardite***	$TlAs_5S_8$	++	EMPA, XRD, O	our data
Bernarlottiite ?	$Pb_{12}(As_{10}Sb_6)S_{36}$	?	EMPA	Vikentyev et al., 2016
Boscardinite***	$AgTl_3Pb_4(Sb_{14}As_6)_{\Sigma 20}S_{36}$	+++	EMPA, XRD, O	our data
Boulangerite*	$Pb_5Sb_4S_{11}$	+++	EMPA, XRD, O	Sazonov et al., 1991a; Vikentyev et al., 2016; our data
Bournonite*	$PbCuSbS_3$	++	EMPA, XRD, O	Sazonov et al., 1991a; Vikentyev et al., 2016; our data
Chabournéite*	$AgzTl_{8-x-z}Pb_4 + 2xSb_{40-x-y}AsyS_{68}$	++++	EMPA, XRD, O	Murzin, Varlamov, 2010; Vikentyev et al., 2016; Makovicky et al., 2021; our data
Chalcostibite	$CuSbS_2$	++	EMPA	Sazonov et al., 1991a; Vikentyev et al., 2016
Christite[1]***	$TlHgAsS_3$	+++	EMPA, XRD, O	Vikentyev et al., 2016; our data
Clerite*	$MnSb_2S_4$	++	EMPA, XRD, O, H	Murzin et al., 1996; Murzin, Varlamov, 2010; our data
Cupropolybasite***	$[Cu_6Sb_2S_7][Ag_9CuS_4]$	++	EMPA, O	our data
Dalnegroite[1]***	$Tl_4Pb_2(As,Sb)_{20}S_{34}$	++++	EMPA, XRD, O	Vikentyev et al., 2016; our data
Dewitite***	$Ag_zTl_{10-x-z}Pb_{2x}Sb_{42-x-y}As_yS_{68}$	++	EMPA, XRD, O	described by Makovicky et al., 2021 as a «lead-free end-member of the chabournéite homeotypic family» Topa et al., 2021b

Mineral	Formula	Distribution	ID method	Source
Drechslerite***	$Tl_4(Sb_{4-x}As_x)S_8$; $1 < x < 2$	++	EMPA, O	our data
Dufrénoysite**	$Pb_2As_2S_5$	+	EMPA, O	
Écrinsite***	$AgTl_3Pb_4(As_{11}Sb_9)_{\Sigma 20}S_{36}$	+++	EMPA, XRD, O	
Enargite ?	Cu_3AsS_4	?	EMPA	Vikentyev et al., 2016
Enneasartorite***	$Tl_6Pb_{32}As_{70}S_{140}$	+	EMPA, O	our data
Ferrovorontsovite**	$(Fe_5Cu)_{\Sigma 6}TlAs_4S_{12}$	+++	EMPA, XRD, H, O	Kasatkin et al., 2018a; Kasatkin, Pautov, 2020
Galkhaite**	$(Hg_5Cu)_{\Sigma 6}CsAs_4S_{12}$	+	EMPA	our data
Geocronite*	$Pb_{14}Sb_6S_{23}$	++	EMPA, O	Sazonov et al., 1991a; Vikentyev et al., 2016; our data
Gladkovskyite**	$MnTlAs_3S_6$	+++	EMPA, XRD, H, O, RS	Kasatkin et al., 2019
Guettardite***	$PbAsSbS_4$	+++	EMPA, O	described by Vikentyev et al., 2016 as «twinnite», our data
Guillulyite***	$Tl_2As_{7.5}Sb_{0.3}S_{13}$	++	EMPA, XRD, O, RS	our data
Gungerite**	$TlAs_5Sb_4S_{13}$	+++	EMPA, XRD, H, O, RS	Kasatkin et al., 2020c, 2022a
Heptasartorite***	$Tl_7Pb_{22}As_{55}S_{108}$	+	EMPA, O	our data
Heteromorphite***	$Pb_7Sb_8S_{19}$	++	EMPA, O	
Hutchinsonite***	$TlPbAs_5S_9$	++	EMPA, XRD, O, RS	
Imhofite***	$Tl_{5.8}As_{15.4}S_{26}$	++	EMPA, XRD, O	
Jamesonite*	$Pb_4FeSb_6S_{14}$	+++	EMPA, XRD, O	Sazonov et al., 1991a; Vikentyev et al., 2016; our data
Jordanite**	$Pb_{14}(As,Sb)_6S_{23}$	+	EMPA	our data
Laffittite***	$AgHgAsS_3$	++	EMPA, O	
Lillianite**	$Pb_{3-2x}Ag_xBi_{2+x}S_6$	++	EMPA, O	
Lopatkaite	$Pb_5Sb_3AsS_{11}$	++	EMPA	described by Vikentyev et al., 2016 as «As-boulangerite»
Lorándite***	$TlAsS_2$	++	EMPA, XRD, O, RS	our data
Luboržákite**	Mn_2AsSbS_5	++	EMPA, XRD, H, O	Kasatkin et al., 2020a; our data
Manganoquadratite***	$AgMnAsS_3$	+	EMPA, O	our data
Meneghinite**	$Pb_{13}CuSb_7S_{24}$	++	EMPA, XRD, O	
Nowackiite***	$Cu_6Zn_3As_4S_{12}$	+	EMPA	
Oyonite***	$Ag_3Mn_2Pb_4Sb_7As_4S_{24}$	+	EMPA, O	
Parapierrotite***	$TlSb_5S_8$	++++	EMPA, XRD, O	Plašil et al., 2018; our data
Pavonite**	$AgBi_3S_5$	++	EMPA, O	our data
Philrothite[1]***	$TlAs_3S_5$	++	EMPA, XRD, O	Vikentyev et al., 2016; our data
Pierrotite ?	$Tl_2(Sb,As)_{10}S_{16}$	?	EMPA	Sazonov et al., 1991a; Murzin, Varlamov, 2010
Plagionite*	$Pb_5Sb_8S_{17}$	++	EMPA, O	Sazonov et al., 1991a; our data
Pokhodyashinite**	$Cu_2Tl_3Sb_5As_2S_{13}$	++	EMPA, XRD, H, O	Kasatkin et al., 2022b

Polybasite**	$[Ag_9CuS_4][(Ag,Cu)_6(Sb,As)_2S_7]$	++	EMPA, O	our data
Ramdohrite**	$Pb_6Ag_3Sb_{11}S_{24}$	+	EMPA	
Rebulite***	$Tl_5Sb_5As_8S_{22}$	++	EMPA, XRD, O, RS	
Roshchinite***	$(Ag,Cu)_{19}Pb_{10}Sb_{51}S_{96}$	+	EMPA, O	
Routhierite*	$CuHg_2TlAs_2S_6$	++++	EMPA, XRD, O, H	Sazonov et al., 1991a; Mineralogy of Urals, 1991; Murzin, Varlamov, 2010; Vikentyev et al., 2016; Stepanov et al., 2017; our data
Semseyite**	$Pb_9Sb_8S_{21}$	++	EMPA, O	our data
Sicherite***	$TlAg_2(As,Sb)_3S_6$	+	EMPA, O	
Sinnerite**	$Cu_6As_4S_9$	+	EMPA, O	
Stalderite***	$TlCu(Zn,Fe,Hg)_2As_2S_6$	+	EMPA, O	
Tennantite-(Fe)*	$Cu_6[Cu_4Fe_2]As_4S_{12}S$	+++	EMPA, O	Sazonov et al., 1991a; Murzin et al., 2011; Vikentyev et al., 2016; our data
Tennantite-(Zn)*	$Cu_6[Cu_4Zn_2]As_4S_{12}S$	+++	EMPA, XRD, O	
Tetrahedrite-(Fe)*	$Cu_6[Cu_4Fe_2]Sb_4S_{12}S$	+++	EMPA, O	Sazonov et al., 1991a; our data
Tetrahedrite-(Zn)*	$Cu_6[Cu_4Zn_2]Sb_4S_{12}S$	++++	EMPA, O	Sazonov et al., 1991a; Murzin et al., 2011; Vikentyev et al., 2016; our data
Tsnigriite**	$Ag_9SbTe_3S_3$	++	EMPA, O	our data
Tsygankoite**	$Mn_8Tl_8Hg_2(Sb_{21}Pb_2Tl)_{\Sigma 24}S_{48}$	+++	EMPA, XRD, H, O	Kasatkin et al., 2018b
Twinnite***	$Pb(Sb_{0.63}As_{0.37})_2S_4$	++	EMPA, XRD, O	our data
Veenite***	$Pb_2(Sb,As)_2S_5$	++	EMPA, O	Vikentyev et al., 2016; our data
Vikingite**	$Ag_5Pb_8Bi_{13}S_{30}$	++	EMPA, O	our data
Vorontsovite**	$(Hg_5Cu)_{\Sigma 6}TlAs_4S_{12}$	++++	EMPA, XRD, H, O	Kasatkin et al., 2018a; Kasatkin, Pautov, 2020
Vrbaite***	$Hg_3Tl_4As_8Sb_2S_{20}$	+++	EMPA, XRD, O	our data
Weissbergite[1]***	$TlSbS_2$	++	EMPA, XRD, O	Vikentyev et al., 2016; our data
Zinkenite*	$Pb_9Sb_{22}S_{42}$	+++	EMPA, XRD, O	Sazonov et al., 1991a; Vikentyev et al., 2016; our data
Halides				
Bismoclite**	BiOCl	(+)	EMPA	our data
Oxides and hydroxides				
Akhtenskite**	MnO_2	(++)	EMPA, XRD	our data
Arsenolite[1]**	As_2O_3	(+++)	EMPA, XRD	Murzin et al., 2011; Vikentyev et al., 2016; our data
Asbolane**	$(Ni,Co)_{2-x}Mn^{4+}(O,OH)_4 \cdot nH_2O$	(++)	EMPA, XRD	our data
Birnessite**	$(Na,K,Ca)_{0.6}(Mn^{4+},Mn^{3+})_2O_4 \cdot 1.5H_2O$	(++)	EMPA, XRD	
Bixbyite**	$Mn^{3+}{}_2O_3$	(++)	EMPA, XRD	
Cesàrolite**	$PbMn^{4+}{}_3O_6(OH)_2$	(++)	EMPA, XRD	
Chromite**	$FeCr_2O_4$	++	EMPA	
Claudetite***	As_2O_3	(+++)	EMPA, XRD	Kasatkin, 2019; our data
Coronadite**	$Pb(Mn^{4+}{}_6Mn^{3+}{}_2)_{\Sigma 8}O_{16}$	(+++)	EMPA, XRD	our data
Cryptomelane**	$K(Mn^{4+}{}_7Mn^{3+})O_{16}$	(+++)	EMPA	
Ferberite**	$FeWO_4$	+	EMPA, O	
Fergusonite-(Y)**	$YNbO_4$	+	EMPA	
Geikielite**	$MgTiO_3$	+	EMPA	
Goethite*	FeOOH	[+++++]	EMPA, XRD	Sazonov et al., 1991a; our data
Hematite*	Fe_2O_3	[+++++]	EMPA, XRD	

Mineral	Formula	Distribution	ID method	Source
Hollandite**	$Ba(Mn^{4+}_6Mn^{3+}_2)O_{16}$	(++)	EMPA, XRD	our data
Lithiophorite**	$(Al,Li)(Mn^{4+},Mn^{3+})O_2(OH)_2$	(++)	EMPA, XRD	
Magnesiochromite**	$MgCr_2O_4$	++	EMPA	
Magnetite*	$Fe^{2+}Fe^{3+}_2O_4$	+++++	EMPA, XRD	Vikentyev et al., 2016; our data
Manganite**	$Mn^{3+}O(OH)$	++	EMPA, XRD	our data
Manjiroite**	$Na(Mn^{4+}_7Mn^{3+})O_{16}$	(++)	EMPA, XRD	
Pyrolusite[1]**	MnO_2	+++	EMPA, XRD	Kabanov, 2001; our data
Pyrophanite**	$MnTiO_3$	+	EMPA	our data
Quartz*	SiO_2	+++++	EMPA, XRD, O	Sazonov et al., 1991a; our data
Ramsdellite***	MnO_2	++	EMPA, XRD	our data
Ranciéite**	$(Ca,Mn^{2+})_{0.2}(Mn^{4+},Mn^{3+})O_6\ 0.6H_2O$	(++)	EMPA, XRD	
Romanèchite**	$(Ba,H_2O)_2(Mn^{4+},Mn^{3+})_5O_{10}$	(+++)	EMPA, XRD	
Rutile*	TiO_2	+++	EMPA, O	Murzin, Varlamov, 2010; our data
Todorokite**	$(Na,K,Ca,Ba,Sr)_{1-x}(Mn,Mg,Al)_6O_{12} \cdot 3–4H_2O$	(+++)	EMPA, XRD	our data
Vernadite[1]*	$(Mn,Fe,Ca,Na)(O,OH)_2 \cdot nH_2O$	(++++)	EMPA, XRD	Sazonov et al., 1991a; our data
Carbonates				
Azurite**	$Cu_3(CO_3)_2(OH)_2$	(++)	EMPA, XRD	our data
Calcite*	$CaCO_3$	+++++	EMPA, XRD, LA ICP MS	Sazonov et al., 1991a; Vikentyev et al., 2016; Soroka et al., 2017, 2018; our data
Cerussite**	$PbCO_3$	(++)	EMPA, RS	our data
Dolomite*	$CaMg(CO_3)_2$	+++++	EMPA, XRD, LA ICP MS	Sazonov et al., 1991a; Vikentyev et al., 2016; Soroka et al., 2017, 2018; our data
Kutnohorite**	$CaMn(CO_3)_2$	++	EMPA, XRD	our data
Malachite**	$Cu_2CO_3(OH)_2$	(+++)	EMPA, XRD	
Rhodochrosite**	$MnCO_3$	+++	EMPA, XRD	
Siderite*	$FeCO_3$	+++	CH, EMPA, XRD	Sazonov et al., 1991a; our data
Sulfates				
Anglesite**	$PbSO_4$	(++)	EMPA, XRD	our data
Baryte*	$BaSO_4$	+++++	EMPA	Vikentyev et al., 2016; our data
Beaverite-(Cu)**	$Pb(Fe^{3+}_2Cu)(SO_4)_2(OH)_6$	(++)	EMPA, XRD	our data
Brochantite**	$Cu_4(SO_4)(OH)_6$	(++)	EMPA, XRD	
Chalcanthite**	$CuSO_4 \cdot 5H_2O$	(++)	EMPA, XRD	
Epsomite**	$MgSO_4 \cdot 7H_2O$	(+++)	EMPA, XRD	
Gypsum**	$CaSO_4 \cdot 2H_2O$	(+++)	EMPA, XRD	
Pentahydrite**	$MgSO_4 \cdot 5H_2O$	(++)	EMPA, XRD	
Starkeyite**	$MgSO_4 \cdot 4H_2O$	(++)	EMPA, XRD	

Wolframates				
Scheelite**	$CaWO_4$	+++	EMPA, O	our data
Phosphates, arsenates				
Bayldonite**	$Cu_3PbO(AsO_3OH)_2(OH)_2$	(++)	EMPA, XRD	our data
Chernovite-(Y)**	$YAsO_4$	+	EMPA	
Chlorapatite**	$Ca_5(PO_4)_3Cl$	++	EMPA	
Fluorapatite*	$Ca_5(PO_4)_3F$	++++	EMPA	Murzin, Varlamov, 2010; Murzin et al., 2011; our data
Gasparite-(La)**	$LaAsO_4$	+	EMPA	our data
Hydroxylapatite**	$Ca_5(PO_4)_3(OH)$	++	EMPA	
Svabite**	$Ca_5(AsO_4)_3F$	+	EMPA	
Tilasite**	$CaMg(AsO_4)F$	++	EMPA, XRD, O	
Turneaurite**	$Ca_5(AsO_4)_3Cl$	++	EMPA	
Vivianite	$Fe^{2+}{}_3(PO_4)_2 \cdot 8H_2O$	+++	CH, XRD	Sazonov et al., 1991a
Silicates				
Albite*	$NaAlSi_3O_8$	+++	CM, XRF, EMPA,XRD	Sazonov et al., 1991a; our data
Andradite**	$Ca_3Fe^{3+}{}_2[SiO_4]_3$	++++	EMPA	our data
Armenite***	$BaCa_2Al_6Si_9O_{30} \cdot 2H_2O$	+++	EMPA, XRD, O	Kasatkin, 2019; our data
Augite**	$(Ca,Mg,Fe)_2Si_2O_6$	++	EMPA	our data
Beidellite	$(Na,Ca)_{0.3}Al_2(Si,Al)_4O_{10}(OH)_2 \cdot nH_2O$	[+++]	CH, XRD	Sazonov et al., 1991a
Celadonite**	$KMgFe^{3+}Si_4O_{10}(OH)_2$	+++	EMPA, XRD	our data
Chabazite-Ca**	$Ca_2Al_4Si_8O_{24} \cdot 13H_2O$	+++	EMPA, XRD	
Chamosite*	$(Fe^{2+},Mg,Al,Fe^{3+})_6(Si,Al)_4O_{10}(OH,O)_8$	+++	EMPA, XRD, O	Sazonov et al., 1991a; our data
Chapmanite***	$Fe^{3+}{}_2Sb^{3+}[SiO_4]_2(OH)$	(+++)	EMPA, XRD	Kasatkin, 2019; our data
Chrysotile-2Or_{c1}**	$Mg_3Si_2O_5(OH)_4$	+++	EMPA, XRD	our data
Clinochlore*	$Mg_5Al_2Si_3O_{10}(OH)_8$	+++++	EMPA, XRD, O	Sazonov et al., 1991a; our data
Dickite**	$Al_2Si_2O_5(OH)_4$	[+++]	EMPA, IR	our data
Diopside*	$CaMgSi_2O_6$	++++	EMPA	Sazonov et al., 1991a; our data
Epidote	$Ca_2Al_2Fe^{3+}[Si_2O_7][SiO_4]O(OH)$	++++	CH	Sazonov et al., 1991a
Ferroceladonite**	$KFe^{2+}Fe^{3+}Si_4O_{10}(OH)_2$	+++	EMPA, XRD	our data
Grossular*	$Ca_3Al_2[SiO_4]_3$	+++	EMPA, XRD	Sazonov et al., 1991a; our data
Halloysite-7Å[1]*	$Al_2Si_2O_5(OH)_4$	[+++]	EMPA, XRD	Kabanov, 2001; our data
Harmotome**	$Ba_2Al_4Si_{12}O_{32} \cdot 12H_2O$	++	EMPA	our data
Hemimorphite**	$Zn_4[Si_2O_7](OH)_2 \cdot H_2O$	(++)	EMPA, XRD	
Hingganite-(Y)**	$Y_2\square Be_2[SiO_4]_2(OH)_2$	+	EMPA	
Hingganite-(Nd)***	$Nd_2\square Be_2[SiO_4]_2(OH)_2$	+	EMPA	
Johannsenite**	$CaMnSi_2O_6$	+	EMPA	
Kaolinite*	$Al_2Si_2O_5(OH)_4$	[++++]	EMPA, XRD, IR	Sazonov et al., 1991a; our data
Laumontite*	$CaAl_2Si_4O_{12} \cdot 4H_2O$	+++	EMPA, XRD	
Magnesio-ferri-hornblende	$\square Ca_2(Mg_4Fe^{3+})Si_7AlO_{22}(OH)_2$	++	CH	Sazonov et al., 1991a
Microcline	$KAlSi_3O_8$	+++	CM, XRF, EMPA, XRD	Sazonov et al., 1991a
Montmorillonite	$(Na,Ca)_{0.3}(Al,Mg)_2Si_4O_{10}(OH)_2 \cdot nH_2O$	[+++]	EMPA, XRD	

Mineral	Formula	Distribution	ID method	Source
Muscovite*	$KAl_2(Si_3Al)O_{10}(OH)_2$	++++	EMPA, XRD	Sazonov et al., 1991a; Murzin et al., 2011; our data
Nontronite**	$Na_{0.3}Fe^{3+}{}_2(Si,Al)_4O_{10}(OH)_2 \cdot nH_2O$	(+++)	EMPA, XRD, IR	our data
Orthoclase*	$KAlSi_3O_8$	+++	CM, XRF, XRD, EMPA	Sazonov et al., 1991a; our data
Pargasite**	$NaCa_2(Mg_4Al)Si_6Al_2O_{22}(OH)_2$	+++	EMPA, XRD	our data
Pigeonite**	$(Mg,Fe,Ca)_2Si_2O_6$	+++	EMPA, XRD	
Prehnite[1]**	$Ca_2Al_2Si_3O_{10}(OH)_2$	++++	EMPA	Sazonov et al., 1991a; our data
Pumpellyite-(Mg)**	$Ca_2MgAl_2[Si_2O_7][SiO_4](OH)_2 \cdot H_2O$	++	EMPA	our data
Talc*	$Mg_3Si_4O_{10}(OH)_2$	+++	EMPA, XRD	Murzin, Varlamov, 2010; our data
Thorite**	$Th[SiO_4]$	+	EMPA, O	our data
Titanite*	$CaTi[SiO_4]O$	+++	EMPA, O	Murzin, Varlamov, 2010; our data
Tremolite*	$\square Ca_2Mg_5Si_8O_{22}(OH)_2$	++	EMPA, XRD, O	Sazonov et al., 1991a; our data
Vesuvianite**	$(Ca,Na)_{19}(Al,Mg,Fe)_{13}[SiO_4]_{10}[Si_2O_7]_4(OH,F,O)_{10}$	+++	EMPA	our data
Wollastonite	$CaSiO_3$	++++	EMPA, XRD, O	Sazonov et al., 1991a
Zircon*	$Zr[SiO_4]$	+++	EMPA	Murzin et al., 2010; our data

Note. Occurrence of minerals: +++++ – rock-forming, major gangue and ore, ++++ – abundant, +++ – subordinate, ++ – rare, + – extremely rare (single findings). In third column, supergene minerals are given in round brackets and hypogene and supergene minerals are given in square brackets. The analytical methods of identification of minerals: EMPA – electron microprobe analysis, CM – chemical analysis; XRF – X-ray fluorescence; LA ICP MS – laser ablation inductively coupled plasma mass spectrometry; XRD – X-ray diffraction (single-crystal or powder method); O – optical data; H – micro-indentation hardness; IR – infrared spectroscopy; RS – Raman spectroscopy. CH – mineral is determined by chemistry (method is not specified; only for literature data). Minerals: * – minerals studied by the authors; ** – minerals identified by the authors for the first time at the Vorontsovskoe deposit; *** – minerals identified by the authors for the first time in Russian Federation; **** – new mineral species found by the authors. New mineral species discovered at the Vorontsovskoe deposit are typed in bold. [1] – mineral is mentioned in literature without analytical data and reliable analytical data are published for the first time in this paper; ? – mineral is identified on the basis of chemical composition, however, this identification is doubtful. Formula of boscardinite is given according to (Biagioni, Moëlo, 2017), because it clearer reflects its isostructural correlation with écrinsite rather than IMA formula. The following minerals are not included in Table but they are mentioned in literature without analytical data and any identification features: actinolite, ankerite, apophyllite, hedenbergite, datolite, marcasite, pyrargyrite, stilbite (desmine), thaumasite (Sazonov et al., 1991a); altaite, hessite, digenite, calaverite, tellurobismuthite, jarosite (Kabanov, 2001); aikinite, lead, freibergite (Vikentyev et al., 2016); wittichenite (Vikent'eva, Vikentev, 2016), gruzdevite, polhemusite, silvialite (Stepanov et al., 2017); aurostibite, berthierite, bismuth, dyscrasite, jentschite, cobaltite, russellite (Vikentyev et al., 2019).

The Vorontsovsko-Peschanskaya ore-magmatic system is situated in the southwestern contact of the Auerbakh pluton (Minina, 1994). The Vorontsovskoe deposit is located in the southern part of the system, at some distance from the contact with intrusive rocks of the Auerbakh pluton (Fig. 1c). The host volcanosedimentary rocks of the deposit form a monocline that gently dips to the west and plunges to the north. The basement of this structure represents a limestone sequence about 1 km thick, often recrystallized to marbles, with interlayers of tuffites and siltstones. Limestones are overlain by volcanosedimentary and volcanic rocks: tuff siltstones, tuffites, porphyry diorites, and tuffs. Abundant coarse-clastic breccias with tuff matrix occur at the contact of volcanosedimentary and volcanic rocks with limestones (Korzhinsky, 1948).

The boundaries of the Vorontsovskoe deposit are mainly tectonic with a longitudinal Vorontsovsky fault dipping to the west at an angle of 70–80° in the west and a NW-trending South Peschansky fault in the southwest. The ore bodies are exposed at the surface and eroded in the east and pinch out along the dip and strike in the north (Vikentyev et al., 2016).

The northern open pit of the deposit exposes a wedge-shaped body of volcanosedimentary rocks with dominant tuffs of intermediate composition and tuffaceous sandstones (Fig. 3a). The western part of this body is bounded by a large fault (Fig. 3b). The main volume of ore-bearing breccias is localized in the footwall contact of the body of volcanosedimentary rocks and limestones. Both limestones and volcanosedimentary rocks are brecciated. The breccias consist of semi-rounded and angular limestone fragments up to 25 cm in size in a clay-carbonate and volcanosedimentary matrix (Vikentyev et al., 2016).

Various metasomatic rocks formed over a long period are abundant at the deposit. The earliest skarns are associated with intrusive bodies of the Auerbakh pluton. The thickness of the skarn zones is typically 10–20 m and their length reaches 1.5 km and more. Skarns are replaced by propylites at some distance from intrusive bodies. The propylites replace all volcanosedimentary rocks and compose an outer zone of skarns. Beresites and listvenites are developed after gabbro, mafic to intermediate volcanic rocks, dolerite dikes, and tuffites. The thickness of zones of the beresite–listvenite rocks does not exceed few meters and their length reaches 40–60 m. Abundant quartz–sericite metasomatites are younger than beresites and listvenites and also host a large volume of gold mineralization. Jasperoids occur at the contacts of mafic to intermediate dikes with limestones, as well as in limestones. In the upper horizons of the deposit, rocks affected by clay alteration host low-temperature gold mineralization (Sazonov et al., 1998; Vikentyev et al., 2016). Supergene rocks are also widespread at the Vorontsovskoe deposit. A weathering mantle up to 60 m thick is developed after volcanosedimentary and intrusive rocks of the Auerbakh complex, whereas carbonate rocks are subject to the formation of karst, which is composed of products of displaced weathering mantle up to 120 m thick (Vikentyev et al., 2016).

The ore body with economic Au content at the deposit has a torch-like shape (Cheremisin, Zlotnik-Khotkevich, 1997). Gold mineralization is mainly hosted by breccias and also altered volcanosedimentary rocks. Two main brecciation stages are distinguished at the deposit, which resulted in the formation of (i) large-block breccias with fine-crystalline ore matrix and dominant pyrite after marbles and (ii) breccias with branchy contours and realgar–orpiment matrix in the first stage breccias (Stepanov et al., 2017). The second stage breccias are matrix- and clast-supported in the central and marginal parts of the breccia bodies, respectively.

It was previously concluded that the Vorontsovskoe gold deposit belongs to the Carlin-type (Sazonov et al., 1998; Vikentyev et al., 2016; Murzin et al., 2017). This conclusion is based on a combination of structural and compositional features of gold mineralization including the abundant ore-bearing breccias and Tl minerals, some of which are associated with native gold similarly to the Carlin-type gold deposits (Dickson et al., 1979; Radtke, 1985; Volkov, Sidorov, 2016). Another viewpoint on the genesis of the Vorontsovskoe deposit suggests that, according to a number of features (e.g., origin of breccias, geodynamic setting of the deposit, etc.), some ores (first of all, gold-bearing breccias) can be considered epithermal, which formed in the marginal part of the ore-magmatic system associated with igneous rocks of the Auerbakh complex (Stepanov et al., 2019). The specific features of geological structure of the ore body is composed of breccias; the morphology of limestone fragments, volcanosedimentary rocks and metasomatites, the structures, textures, and mineral composition of breccia matrix indicate a fluid-explosive nature of breccias (Stepanov et al., 2017). The formation of ore breccias could occur due to fluid decompression in near-surface conditions, which is typical of epithermal deposits (White, Hedenquist, 1995). A spatial combination of a large amount of rocks with various geochemical features in breccias

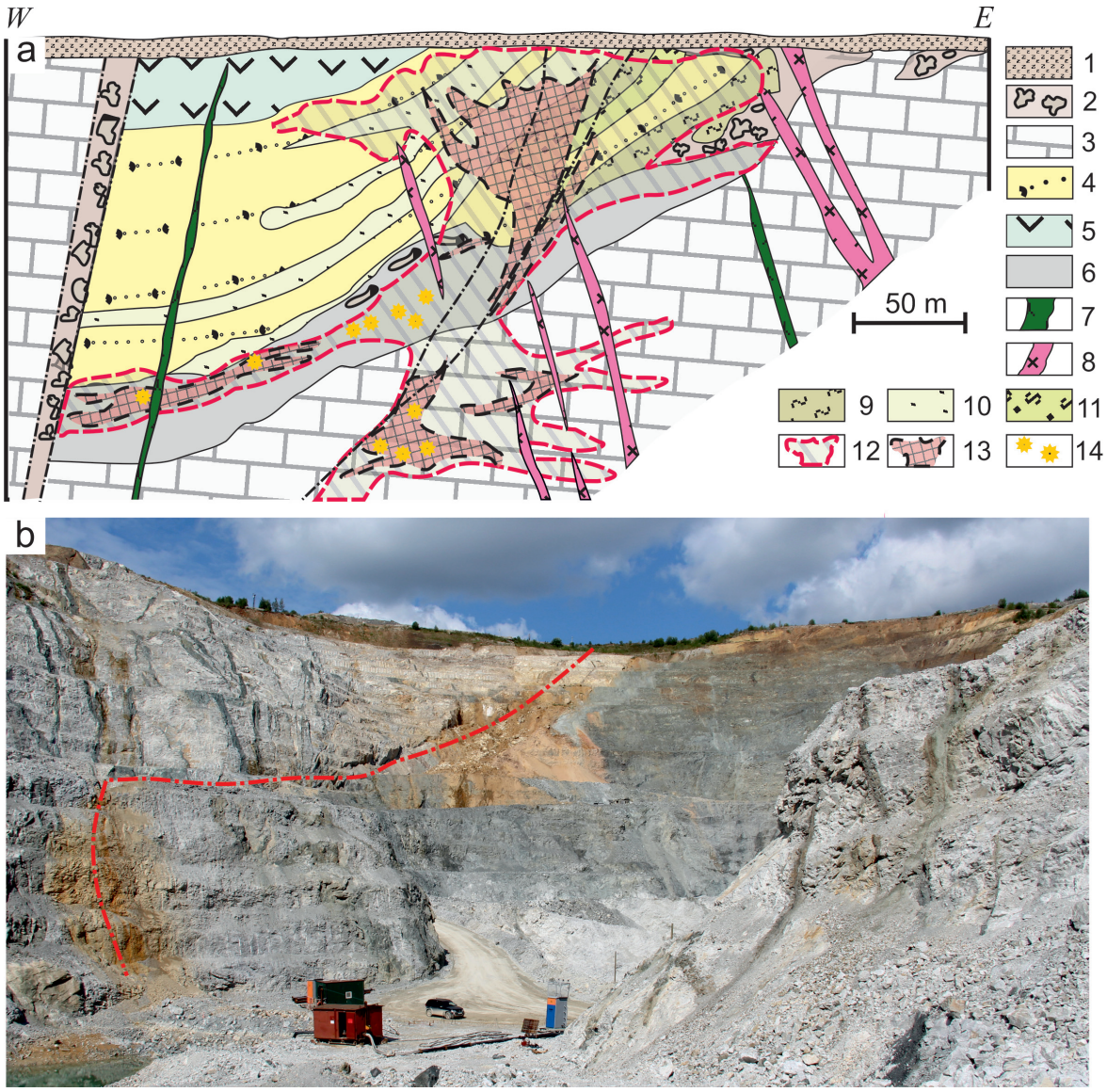

Fig. 3. Cross-sections of the Vorontsovskoe deposit:

a – geological cross-section, modified after (Cheremisin, Zlotnik-Khotkevich, 1977; Sazonov et al., 1998).

1 – Neogene–Quaternary deposits; 2 – Devonian karst; 3 – limestone; 4 – tuff siltstone, tuff sandstone, tuff conglomerate; 5 – andesite, andesitic tuff and lava breccias; 6 – 1st stage breccias; 7 – lamprophyre dikes; 8 – diorite–porphyrite dikes; 9–11 – metasomatites: 9 – quartz–sericite, 10 – quartz–sericite–albite, 11 – berezite–listvenite and chlorite–sericite; 12 – ore shoots with ordinary Au grades; 13 – gold-rich ore shoots; 14 – breccias with realgar–orpiment matrix.

b – photo of the Northern open pit with Vorontsovsky reverse fault (red dotted line).

combined with hydrothermal-metasomatic processes, which accompanied the formation of breccia matrix, resulted in the formation of several unique (including new) minerals, which exhibit contrasting geochemical associations. Gladkovskyite $MnTlAs_3S_6$ (Kasatkin et al., 2019) is a typical example; Mn was probably sourced from Mn-rich carbonate sedimentary rocks, whereas Tl, As, and S could derive from hydrothermal fluids generated by a magmatic source. Thus, the genetic type of the Vorontsovskoe deposit remains a matter of debate.

Ore types and mineral assemblages of the Vorontsovskoe deposit

Several types of ores are identified at the Vorontsovskoe deposit. They are associated with various volcanosedimentary and hydrothermal-metasomatic

rocks: e.g., primary ores in limestones and volcanosedimentary rocks and oxidized ores (Vikentyev et al., 2016). The primary ores include: 1) disseminated gold-magnetite-sulfide ores in calcareous skarns; 2) disseminated gold-polymetallic ores in jasperoids; 3) finely disseminated gold–pyrite–arsenopyrite ores in tuff sandstones and tuff siltstones; 4) finely disseminated gold–pyrite–realgar ores in carbonate breccias, and 5) gold–sulfide–clay ores in argillic rocks. The oxidation zone contains gold–oxihydroxide–clay ores.

Our studies on samples collected at the deposit in 2013–2020 show that the ore breccias after carbonate rocks exhibit the greatest variety of minerals, including all new minerals (sulfarsenites and sulfantimonites with species-defining Tl, Hg, Pb, and Mn) and a number of rare sulfides and sulfosalts, many of which are found for the first time at the territory of the Russian Federation. The names of most mineral assemblages (see below) reflect the findings of these new minerals. Some of them (vorontsovite, gungerite, gladkovskyite, luboržákite, tsygankoite) are new minerals discovered at the deposit, whereas other minerals (boscardinite, parapierrotite, écrinsite) are abundant in these mineral assemblages.

Carbonate breccias are typically composed of fragments of coarse- to medium-grained marblized limestones enclosed in ore matrix. Both marblized limestones and breccias underwent metasomatic alterations, which resulted in the formation of ore minerals. The main gangue minerals of the matrix include calcite and dolomite, which are accompanied by quartz, baryte, prehnite, clinochlore, and muscovite. The fine-grained pyrite and realgar are major minerals of ore matrix and some assemblages can also contain major stibnite, arsenopyrite, orpiment or native arsenic.

The deposition of high-temperature gangue minerals was followed by the formation of a medium-temperature sulfide-polymetallic assemblage (sphalerite, galena, chalcopyrite, alabandite, fahlores, native gold). It is most likely that the mineral assemblage with sulfarsenites and sulfantimonites formed at the last lowest-temperature stage of the hydrothermal process. Although As and Sb sources for sulfosalts are obvious, the source for S has not unambiguously been identified, yet.

A complex character of hydrothermal-metasomatic processes with successive telescoping of ore mineral assemblages developed in various volcanosedimentary and carbonate rocks was partly responsible for the presence of a large number of minerals with a unique chemical composition. For example, the formation of ore breccias and accompanying metasomatic processes in marblized limestones, which are composed of Mn-rich calcite, led to the formation of an endemic sulfarsenite assemblage of Mn- and Tl-bearing minerals. At the last stages of the ore-forming process, the early high- and medium-temperature minerals were replaced by polymetallic ore assemblage (galena, sphalerite, chalcopyrite, etc.) with rare sulfarsenites.

We identified nine most stable ore mineral assemblages, of which seven are found in carbonate breccias and two belong to magnetite skarns and oxidation zone, respectively. Each assemblage is confined to a specific ore type and is characterized by indicative features and unique minerals in comparison with other assemblages. For the sake of brevity, each assemblage is numbered from 1 to 9 (Table 2).

The *boscardinite–écrinsite assemblage* (no. 1) is recognized in carbonate breccias sampled at the lower horizons of the northern open pit (59°39’12’’ N, 60°12’53’’ E). It contains the widest spectrum of ore minerals with very rare Tl sulfosalts including most abundant isostructural boscardinite and écrinsite, which form a solid solution series. Only this assemblage contains O-free minerals such as arsiccioite, getchellite, manganoquadratite, molybdenite, oyonite, pokhodyashinite, native silver, sinnerite, sicherite, stalderite, «tennantite-(Mn)» (a potentially new mineral), weissbergite, as well as oxysalts and oxides (chromite, magnesiochromite, pumpellyite-(Mg), scheelite, svabite, thorite, zircon).

The *vorontsovite–gungerite assemblage* (no. 2). The samples with this mineral assemblage were collected at the ore stockpile of the deposit and off-balance ore stockpile no. 2. It is named after widespread new minerals vorontsovite, ferrovorontsovite (Kasatkin et al., 2018a), and gungerite (Kasatkin et al., 2022a). The assemblage is characterized by a broad isomorphism between various sulfosalts. Vorontsovite and ferrovorontsovite form a continuous solid solution series with a substitution of Hg for Fe. The As ↔ Sb substitution is determined in gungerite and minerals of the chabournéite group. Vorontsovite, ferrovorontsovite and galkhaite also exhibit Tl ↔ Cs isomorphism and cinnabar is characterized by S ↔ Se isomorphic substitution. Both types of isomorphism are rather atypical at the deposit. Only this assemblage contains enneasartorite, ferrovorontsovite, galkhaite, greigite, gungerite, heptasartorite and pararealgar.

The *gladkovskyite (sulfarsenite) assemblage* (no. 3). It is typical of the carbonate breccias, which were collected at the lowest horizons of the northern open pit,

Table 2

Mineral assemblages in ores of the Vorontsovskoe deposit

Assemblage	Ore types	Characteristic features	Minerals			
			Rock-forming, major gangue and major ore	Abundant	Subordinate	Rare
1. Boscardinite–écrinsite	Pyrite–realgar	Largest amount of rare Tl sulfosalts	**Pyrite** **Realgar** Baryte Calcite Clinochlore Dolomite Muscovite Prehnite Quartz	**Aktashite** **Arsenopyrite** **Boscardinite** **Chabournéite** **Écrinsite** **Native gold** **Orpiment** **Parapierrotite** **Routhierite** **Sphalerite** **Stibnite** Armenite	**Chalcopyrite** **Christite** **Cinnabar** **Coloradoite** **Dalnegroite** **Getchellite** **Metacinnabar** **Wakabayashilite** **Weissbergite** **Zinkenite** Diopside Fluorapatite Magnetite Scheelite	**Acanthite** **Alabandite** **Andorite** **Arsiccioite** **Bernardite** **Dewitite** **Drechslerite** **Galena** **Guettardite** **Hutchinsonite** **Imhofite** **Manganoquadratite** **Native arsenic** **Native silver** **Nowackiite** **Oyonite** **Philrothite** **Pokhodyashinite** **Rebulite** **Sicherite** **Sinnerite** **Stalderite** **«Tennantite-(Mn)»** **Tennantite-(Zn)** **Twinnite** **Vorontsovite** **Vrbaite** **UK phase I** **UK phase II** Albite Andradite Augite Chromite Harmotome Magnesiochromite Ba-bearing orthoclase Pumpellyite-(Mg) Rutile Svabite Thorite Titanite Zircon
		Abundant boscardinite and écrinsite forming solid solution series				
		Late propylitization with rock-forming prehnite and abundant armenite				

2. Vorontsovite–gungerite	Pyrite–realgar–stibnite	Numerous minerals of extended solid solutions series (vorontsovite–ferrovorontsovite, dalnegroite–chabournéite) Assemblage with Cs-bearing (galkhaite, vorontsovite, ferrovorontsovite) and Se-bearing (cinnabar) minerals	**Pyrite** **Realgar** **Stibnite** Calcite Clinochlore Dolomite	**Cinnabar** (including Se-bearing) **Dalnegroite** **Ferrovorontsovite** **Gungerite** **Parapierrotite** **Routhierite** **Sphalerite** **Vorontsovite** Quartz	**Chabournéite** **Coloradoite** **Orpiment** Baryte	**Bernardite** **Boscardinite** **Écrinsite** **Enneasartorite** **Galkhaite** **Greigite** **Guettardite** **Heptasartorite** **Hutchinsonite** **Metacinnabar** **Native arsenic** **Native gold** ***Pararealgar*** **Wakabayashilite** **UK phase I** **UK phase II** Goethite Rutile
3. Gladkovskyite (sulfarsenite)	Orpiment–pyrite–realgar	As-bearing stibnite-free ores Strongly dominant As over Sb in chemical composition of sulfosalts Presence of sulfarsenites with species-defining Mn (gladkovskyite, auerbakhite)	**Orpiment** **Pyrite** **Realgar** Baryte Calcite	**Alabandite** **Gladkovskyite** **Native gold** **Routhierite** **Vrbaite** Clinochlore Dolomite Fluorapatite	**Auerbakhite** **Sphalerite**	**Bernardite** **Christite** **Cinnabar** **Coloradoite** **Dalnegroite** **Gillulyite** **Hutchinsonite** **Imhofite** **Lorándite** **Philrothite** **Picotpaulite** **Rebulite** Quartz Talc
4. Cinnabar–coloradoite–parapierrotite	Pyrite–realgar–stibnite	Assemblage with macroscopic cinnabar aggregates Abundant parapierrotite with crystals up to 1 mm in size	**Pyrite** **Realgar** **Stibnite** Calcite Dolomite	**Cinnabar** **Coloradoite** **Orpiment** **Parapierrotite** **Sphalerite** Baryte Clinochlore Quartz Prehnite	**Aktashite** **Metacinnabar** **Native arsenic** **Routhierite** **Zinkenite**	**Acanthite** **Andorite** **Arsenopyrite** **Bernardite** **Chabournéite** **Christite** **Galena** **Gersdorfite** **Guettardite** **Laffittite** **Native gold** **Nowackiite**

Assemblage	Ore types	Characteristic features	Minerals			
			Rock-forming, major gangue and major ore	Abundant	Subordinate	Rare
		Abundant coloradoite with very large grains up to 0.12 × 0.06 mm in size				**Picotpaulite** **Roshchinite** **Tennantite-(Zn)** *Bismoclite* Diopside Ferberite Fluorapatite Microcline Muscovite Rutile
5. Luboržákite–clerite	Pyrite–realgar	Enrichment of ore system in Mn (Mn-bearing calcite, dolomite, sphalerite and sulfosalts)	**Pyrite** **Realgar** Baryte Calcite Dolomite	**Alabandite** **Sphalerite** Clinochlore Diopside	**Aktashite** **Boscardinite** **Clerite** **Luboržákite** **Routhierite**	**Arsenopyrite** **Chabournéite** **Coloradoite** **Écrinsite** **Guettardite** **Native gold** **Orpiment** **Parapierrotite** **Stibnite** **Tennantite-(Zn)** **Twinnite** **UK phase II** Chernovite-(Y) Fluorapatite Muscovite Prehnite
		Presence of Tl-free sulfarsenites and sulfantimonites with species-defining Mn (luboržákite, clerite)				
		Iisomorphic As–Sb substitution in luboržákite, clerite, boscardinite, parapierrotite, chabournéite, and écrinsite				
		Absence of quartz				
6. Assemblage with native arsenic	Native arsenic–arsenopyrite–realgar	Presence of abundant native arsenic	**Arsenopyrite** **Native arsenic** **Realgar** *Arsenolite* *Claudetite* Calcite Dolomite Quartz	**Native gold** **Orpiment** **Pyrite** Baryte Clinochlore Muscovite	**Tetrahedrite-(Zn)** Diopside Fluorapatite Vesuvianite	**Aktashite** **Benavidesite** **Chalcopyrite** **Cubanite** **Galena** **Hessite** **Jamesonite** **Parapierrotite** **Ramdohrite**
		Inclusions of euhedral arsenopyrite crystals up to 1 mm in native arsenic				
		Most abundant and largest inclusions of native gold				

		Absence of Tl- and Hg-bearing minerals except for rare aktashite and parapierrotite Presence of vesuvianite				**Sphalerite** **Stibnite** **Tennantite-(Fe)** **Tennantite-(Zn)** **Tetrahedrite-(Fe)** Rutile Titanite
7. Assemblage with tsygankoite	Arsenopyrite–pyrite–realgar	Presence of major arsenopyrite Enrichment of ore system in Mn (the presence of alabandite and Mn-bearing calcite, dolomite, sphalerite) Presence of sulfantimonites with species-defining Mn (tsygankoite, benavidesite) Presence of zoned fluorapatite crystals with isomorphic P and As, F, Cl and OH up to the formation of chlorapatite and turneaureite	**Arsenopyrite** **Pyrite** **Realgar** Calcite Clinochlore Dolomite	**Alabandite** **Orpiment** **Sphalerite** **Tsygankoite** Fluorapatite Tilasite	**Aktashite** **Duranusite** **Native arsenic** **Native gold** **Routhierite** Titanite	**Benavidesite** **Coloradoite** **Dalnegroite** **Guettardite** **Jordanite** **Veenite** Baryte Chlorapatite Gasparite-(La) Geikielite Hydroxylapatite Pyrophanite Turneaureite
8. Assemblage with Bi minerals	Magnetite–sulfide	Presence of Bi minerals Association with skarns Large arsenopyrite inclusions in massive magnetite Numerous inclusions of sulfides and Bi tellurides in magnetite	**Magnetite** Andradite Calcite	**Arsenopyrite** **Chalcopyrite** **Pyrite** Epidote	**Native gold** **Pyrrhotite** **Sphalerite** Quartz	**Bismuthinite** **Galena** **Native gold** **Ikunolite** **Joséite-A** **Lillianite** **Pavonite** **Tetradymite**
9. Supergene assemblage	Native gold–oxihydroxide–clay	Abundant Fe and Mn oxides and hydroxides and clay minerals including smectites Presence of various sulfates	*Kaolinite* *Goethite* *Montmorillonite* Quartz	**Pyrite** Calcite Dolomite *Gypsum* *Halloysite* *Hematite*	**Arsenopyrite** **Chalcopyrite** **Galena** **Native gold** **Sphalerite** Baryte *Cerussite* *Coronadite* *Cryptomelane* *Dickite* Fluorapatite *Malachite*	**Bornite** ***Covellite*** ***Djurleite*** **Hawleyite** **Tennantite-(Zn)** *Akhtenskite* *Anglesite* *Asbolan* *Azurite* *Bayldonite* *Beaverite-(Cu)* *Birnessite*

Assemblage	Ore types	Characteristic features	Minerals			
			Rock-forming, major gangue and major ore	Abundant	Subordinate	Rare
					Nontronite Pyrolusite Rhodochrosite *Romanèchite* *Todorokite* *Vernadite*	*Bixbyite* *Brochantite* *Cesàrolite* *Chalcanthite* *Epsomite* Hemimorphite *Hollandite* Kutnohorite *Lithiophorite* Manganite *Manjiroite* *Pentahydrite* Ramsdellite *Ranciéite* Rutile *Starkeyite*

Note. Oxygen-free and supergene ore minerals are typed in bold and italic, respectively.

approximately 50 m from its eastern wall (Fig. 4). The assemblage is named after gladkovskyite, a new Mn-Tl-sulfosalt (Kasatkin et al., 2019). This assemblage can alternatively be named sulfarsenite assemblage due to its unique As predominance over Sb, the complete absence of stibnite (as well as sulfantimonites), and general depletion in Sb. Auerbakhite, gillulyite, gladkovskyite, and lorándite occur only in this assemblage.

The *cinnabar–coloradoite–parapierrotite assemblage* (no. 4). Cinnabar, coloradoite, and parapierrotite are rare minerals of the Vorontsovskoe deposit, but they are abundant in assemblage no. 4 and occur either together or in pairs in each studied sample. The carbonate breccias with this assemblage were sampled in the northern open pit. Similarly to the vorontsovite–gungerite assemblage, this one is confined to pyrite–realgar–stibnite ores, but their indicative features and a list of minerals significantly differ. Cinnabar was previously identified as a very rare ore mineral (Sazonov et al., 1991a; Vikentyev et al., 2016), however, in our samples, it forms large macroscopic aggregates. Coloradoite and parapierrotite, which occur almost in all ore assemblages confined to the carbonate breccias as rare grains up to 50 μm, are found in this assemblage as large crystals: up to 0.12 and 1 mm long, respectively. The quality of the parapierrotite crystals from this assemblage allowed us to solve for the first time the structure of this sulfosalt (Plášil et al., 2018). Only this assemblage contains gersdorffite, laffittite, roshchinite, bismoclite, and ferberite.

The *luboržákite–clerite assemblage* (no. 5). It is typical of explosive breccias that contain the fragments of metasomatically altered sedimentary (limestones and marblized limestones) and volcanosedimentary (tuff siltstones and sandstones) rocks and are stored at off-balance ores dump no. 1. Samples of this dump originate from the middle part of a tubular ore breccia body at the contact of a volcanosedimentary wedge and host carbonate rocks. Similar to the boscardinite–écrinsite assemblage, such assemblage is confined to pyrite–realgar ore type with rare arsenopyrite, orpiment, and stibnite. An interesting feature of this assemblage is the enrichment of the ore-forming system in Mn, which is most likely sourced from sedimentary and volcanosedimentary rocks. In addition to higher Mn content in Mn-rich calcite and dolomite and abundance of alabandite and Mn-bearing sphalerite, Mn is often detected in minor amount in accessory sulfosalts (aktashite, boscardinite, chabournéite, écrinsite) in

Fig. 4. Gladkovskyite assemblage *in situ* of the Vorontsovskoe deposit:
a – sampling at the bottom of northern open pit; b – carbonate breccias with gladkovskyite assemblage.
Photo: R.S. Palamarchuk.

contrast to other assemblages. Manganese in this assemblage is also included in the composition of sulfosalts without species-defining Tl (luboržákite and clerite). This assemblage also contains chernovite-(Y).

The *assemblage with native arsenic* (no. 6). The breccias with this assemblage were collected at the dumps of the northern open pit. The main features of this assemblage are the presence of large (up to 3–4 cm) anhedral aggregates, isometric grains and nodules of native arsenic, which intergrows with gangue minerals of breccia matrix (calcite, dolomite, quartz, baryte, clinochlore, muscovite). It is most likely that native arsenic formed during the last low-temperature stage of the hydrothermal process due to the decomposition of the earlier realgar and orpiment. Native arsenic is partly oxidized and replaced by supergene films and crusts, which are composed of two As^{3+} oxides: arsenolite and claudetite. They often form the most part of the studied samples because of fast oxidation of native arsenic (Fig. 5). Native arsenic, arsenolite, and claudetite replace arsenopyrite and realgar and contain numerous largest (up to 0.1 mm) inclusions of native gold. Only this assemblage hosts cubanite, hessite, jamesonite, ramdohrite, tetrahedrite-(Fe), tetrahedrite-(Zn), tennantite-(Fe), and vesuvianite.

The *assemblage with tsygankoite* (no. 7). This was sampled at the main ore stockpile of the deposit. The assemblage is named after tsygankoite, a new mineral with a unique combination of species-defining elements (Kasatkin et al., 2018b). In addition to gladkovskyite and luboržákite-clerite assemblages, this one also contains sulfosalts with species-defining Mn. All three assemblages contain rock-forming Mn-rich calcite and dolomite, alabandite and Mn-bearing sphalerite. A significant difference between the assemblages is related to the types of Mn-sulfosalts: sulfarsenites (gladkovskyite, auerbakhite) in assemblage no. 3, sulfantimonites and sulfarsenites without species-defining Tl (luboržákite, clerite) in assemblage no. 5 and only sulfantimonites (tsygankoite, benavidesite) in assemblage no. 7. Only this assemblage includes duranusite, jordanite, tsygankoite, veenite, chlorapatite, gasparite-(La), geikielite, hydroxylapatite, pyrophanite, and turneaurite.

The *assemblage with Bi minerals* (no. 8). Only two Bi-bearing minerals (vikingite and bismoclite) are found in carbonate breccias. However, several rare Bi sulfides, sulfotellurides and Bi-bearing sulfosalts (bismuthinite, ikunolite, joséite-A, lillianite, pavonite, tetradymite) are identified in magnetite–calcite–andradite–epidote skarns collected at the southern flank of the deposit, in the dumps of the southern open pit.

The *supergene assemblage* (no. 9). The oxidation zone was exposed by the southern open pit at the contact of volcanosedimentary rocks with underlying limestones and is described in a number of publications (Sazonov et al., 1991a; Rindzunskaya et al., 1995a, b; Kabanov, 2001; Vikentyev et al., 2016). The oxidized ores have also been mined at the southern flank of the northern open pit. In the oxidation zone, more than 90 vol. % is comprised of clays (kaolinite, halloysite), smectites (beidellite, montmorillonite, nontronite), hy-

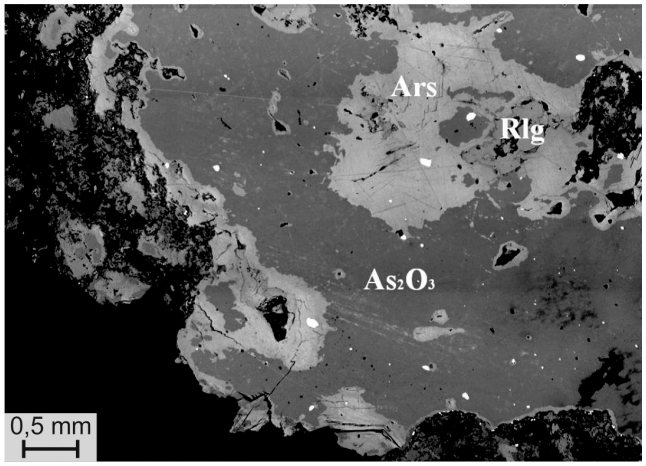

Fig. 5. Assemblage with native arsenic. A fragment of a large nodule of native arsenic with realgar and native gold (small white grains) inclusions, supergene arsenolite/claudetite, and gangue minerals (black).

BSE image.

dromica, quartz, carbonates (calcite, dolomite), fluorapatite, feldspars, etc. The ore minerals (<10 vol. %) mainly include Fe and Mn oxides and hydroxides, native gold, and a small amount of sulfides with dominant pyrite (Kabanov, 2001). The supergene Fe minerals include only goethite and hematite, whereas rare Mn oxides and hydroxides are more diverse, e.g., akhtenskite, birnessite, bixbyite, cesàrolite, manjiroite, etc. (Figs. 6a, 6b; Table 2). This mineral assemblage also comprises supergene sulfides (covellite, djurleite, hawleyite), carbonates (azurite, cerussite, kutnohorite, malachite, rhodochrosite), and sulfates (anglesite, beaverite-(Cu), brochantite, chalcanthite, gypsum, pentahydrite, starkeyite) (Fig. 6c).

Analytical methods

Mineral descriptions are based on the observations under a Zeiss Discovery V8 stereomicroscope. The optical properties of ore minerals in reflected light were studied under a MIN-8 polarizing microscope with an OI-12 opaque illuminator and a Leitz Wetzlar Type 307-107.002 in both the air and immersion using cedar oil (refractive index $n_d = 1.516$). The reflectance spectra were registered using an UMSP-50 universal microspectrophotometer (Opton-Zeiss, Germany) in the air relative to a WTiC standard with a monochromator gap spectral width of 10 nm.

The micromorphology and chemical composition of minerals were studied by scanning electron microscopy (SEM) and electron microprobe analysis (EMPA) using both energy and wavelength dispersive spectrometers (EDS and WDS, respectively). A preliminary study of polished sections and semi-quantitative chemical analysis of minerals were carried out in a laboratory of the Fersman Mineralogical Museum, Russian Academy of Sciences (FMM RAS, Moscow) on a CamScan 4D scanning electron microscope equipped with a Si(Li) energy-dispersive detector and an INCA Oxford microanalyzer at an accelerating voltage of 20 kV, a beam current of 5 nA on metallic cobalt, and a beam diameter of 5 μm.

Quantitative chemical composition was partly analyzed in the laboratory of the FMM RAS on a JCXA-733 Superprobe JEOL microprobe equipped with a Si(Li) energy-dispersive detector with an ATW-2 thin window and an INCA X-MAX (Oxford Instruments) analytical system at an accelerating voltage of

Fig. 6. Supergene assemblage *in situ* of the Vorontsovskoe deposit:

a – dumps of southern open pit with supergene mineralization; b – brown Fe oxy-hydroxides and black Mn oxy-hydroxides; c – white powdery sulfates.

Photo: A.V. Kasatkin.

20 kV, a beam current of 2 nA and a beam diameter of 2 μm. The chemical composition of minerals was also determined by a Cameca SX 100 wavelength electron probe microanalyzer at the Joint Laboratory of Electron Microscopy and Microanalysis of the Department of Geological Sciences at the Masaryk University and Czech Geological Survey, Brno, Czech Republic. The analytical conditions were as follows: an accelerating voltage of 25 kV, a beam current of 2–20 nA, and a beam diameter of 1–2 μm for elements, sulfides, arsenides, tellurides and sulfosalts and an accelerating voltage of 15 kV, a beam current of 10 nA, and a beam diameter of 8 μm, for halides, oxides, and oxysalts. For all minerals, peak counting times (CT) were 10–20 s for major elements and 20–120 s for trace elements with a background CT 5–10 and 10–20 s, respectively.

The standards, analytical X-ray lines and analyzing crystals (in parentheses) were as follows:

– for oxygen-free compounds (except for halides): chalcopyrite, S*K*α line (PET); Mn, Mn*K*α (LIF); FeS_2, Fe*K*α (LLIF); Co, Co*K*α (LLIF); pararammelsbergite, Ni*K*α (LLIF) and As*L*β (TAP); Cu, Cu*K*α (LLIF); ZnS, Zn*K*α (LLIF); PbSe, Se*L*β (TAP) and Pb*M*α (PET); Mo, Mo*L*α (LPET); Ag, Ag*L*α (PET); Cd, Cd*L*β (PET); Sb, Sb*L*β (PET); pollucite, Cs*L*α (LPET); HgTe, Te*L*β (LPET) and Hg*M*α (LPET); Tl(Br,I), Tl*M*α (PET); Bi, Bi*M*β (PET);

– for halides and oxysalts: topaz, F*K*α (PC1); albite, Na*K*α (TAP); pyrope, Mg*K*α (TAP); andalusite, Al*K*α (TAP); wollastonite, Si*K*α (TAP) and Ca*K*α (LPET); fluorapatite, P*K*α (PET); $SrSO_4$, S*K*α (LPET) and Sr*L*α (TAP); vanadinite, Cl*K*α (PET), V*K*α (LLIF) and Pb*M*α (LPET); orthoclase, K*K*α (PET); $ScVO_4$, Sc*K*α (PET); TiO_2, Ti*K*α (LPET); chromite, Cr*K*α (LPET); Mn_2SiO_4, Mn*K*α (LLIF); andradite, Fe*K*α (LLIF); Co, Co*K*α (LLIF); Ni_2SiO_4, Ni*K*α (LLIF); lammerite, Cu*K*α (LLIF) and As*L*α (TAP); gahnite, Zn*K*α (LLIF); YAG, Y*L*α (TAP); zircon, Zr*L*α (TAP); columbite, Nb*L*α (LPET); baryte, Ba*L*α (PET); $LaPO_4$, La*L*α (PET); $CePO_4$, Ce*L*α (PET); $PrPO_4$, Pr*L*β (LLIF); $NdPO_4$, Nd*L*α (LLIF); $SmPO_4$, Sm*L*α (LLIF); $EuPO_4$, Eu*L*β (LLIF); $GdPO_4$, Gd*L*β (LLIF); $TbPO_4$, Tb*L*α (LLIF); $DyPO_4$, Dy*L*α (LLIF); $HoPO_4$, Ho*L*β (LLIF); $ErPO_4$, Er*L*α (LLIF); $TmPO_4$, Tm*L*α (LLIF); $YbPO_4$, Yb*L*α (LLIF); $LuPO_4$, Lu*M*β (TAP); $CrTa_2O_6$, Ta*L*α (TAP); W, W*L*α (LLIF); ThO_2, Th*M*α (LPET); UO_2, U*M*β (LPET).

The raw intensities were converted to concentrations using *X-PHI* matrix-correction software (Merlet, 1994). Inter-*REE* interferences were solved by empirically determined correction factors.

Raman spectra were collected in the Laboratory of Raman spectroscopy of the Masaryk University on a Horiba LabRAM HR Evolution spectrometer equipped with an Olympus BX 41 optical microscope, a diffraction grating with 600 grooves per millimeter, a Peltier-cooled, Si-based charge-coupled device (CCD) detector and three (473, 532, and 633 nm) lasers with a beam power at the sample surface of 5–10 mW. The Raman signal was collected in a range of 100–4000 cm^{-1}; a beam diameter varied from 1 to 2.6 μm and a lateral resolution was 1 to 2 μm. The wavenumber was calibrated using the Rayleigh line and low-pressure Ne-discharge lamp emissions. The wavenumber accuracy was ~0.5 cm^{-1} and the spectral resolution was ~2 cm^{-1}. Band fitting was done after an appropriate background correction, assuming Voigt function, i.e., the convolution of the Lorentzian and Gaussian functions for the individual bands' shapes (*PeakFit*; Jandel Scientific Software).

Raman spectra of good quality were obtained for most transparent and translucent orange and red sulfosalts (auerbakhite, gillulyite, gladkovskyite, gungerite, lorándite, rebulite, hutchinsonite). As for opaque (especially, black sulfides and sulfosalts), these minerals are characterized by high absorption coefficients of laser radiation and a small depth of its penetration into the analyzed sample. This leads to vigorous heating of a laser beam-exposed surface layer of the sample and its local destruction, although the scattered radiation compared to absorbed one is insignificant.

For XRD analysis, the mineral grains preliminary studied by EMPA and, in some cases, Raman spectroscopy, were extracted from polished sections and analyzed in the laboratories of the Department of Geosciences of the University of Padova (Padova, Italy) and the Institute of Physics of the Academy of Sciences of Czech Republic (Prague, Czech Republic).

At the University of Padova, single-crystal (SXRD) and micro-powder X-ray (PXRD) data were collected using a Rigaku Oxford Diffraction SuperNova diffractometer equipped with a Pilatus 200K Dectris detector and an X-ray micro-source (Mo*K*α radiation) at an accelerating voltage of 50 kV, a beam current of 0.12 mA, and a beam size on sample of about 0.12 mm. The detector-to-sample standard distance was 68 mm. The total exposure time for single-crystal data varied from 15 min (determining unit-cell parameters for relatively large crystals) up to 90 h (registration of structural data on 10–15-μm-sized crystals). The powder patterns (up to d_{min} = 0.8 Å) were recorded on the same device in a microdiffraction mode with

0–360° phi rotation scan and an exposure time varied from 30 min to 12 h. The standard powder diffraction patterns were also obtained on a PANalytical θ-θ diffractometer using Co*K*α radiation at an accelerating voltage of 40 kV and a beam current of 40 mA in a stepwise mode (step 0.033° at 2θ) at the Department of Geosciences of the University of Padova.

In the laboratory of the Institute of Physics of the Academy of Sciences of Czech Republic, the studies were carried out on a Rigaku Oxford Diffraction SuperNova single crystal diffractometer equipped with an Atlas S2 CCD detector, at a Mo*K*α radiation, an accelerating voltage of 50 kV, a beam current of 30 mA, and an X-ray beam focus size of 0.3 mm. The sample-to-detector distance was 55 mm for the standard single-crystal data and 120 mm for structural data during the long-time collection. The exposure time varied from 15 min (determination of unit-cells parameters for relatively large crystals) up to 14 days (registration of structural data for the most complex sulfosalts such as gungerite, tsygankoite, etc.). This device also has a Gandolfi mode, which allows collection of the PXRD data. The sample-to-detector distance in this mode was 53.5 mm and the standard exposure time was 25 min.

Description of minerals

Elements

Native arsenic was first described by Sazonov et al. (1991a) as isometric crystals and anhedral grains up to 1 mm in size embedded in the matrix of ore breccias or as tiny inclusions up to 10–15 μm in stibnite. The mineral was identified by its optical properties, chemical composition, and XRD data. Native arsenic contains up to 0.1 wt. % Sb and S. In 2007, large native arsenic aggregates weighing more than 1 t were exposed in the northern open pit (Vikentyev et al., 2016). They are confined to metasomatically altered tuffaceous rocks in the upper part of the deposit. Metasomatite is mainly composed of quartz, which is crossed by brecciation zones up to 5 cm thick with numerous veinlets, lenses, and pockets of native arsenic aggregates up to 3 cm. Native arsenic and prismatic arsenopyrite also occur in rocks beyond the brecciated zones, where they form dense, uniformly dispersed inclusions up 0.5 mm across. Native arsenic contains numerous grains of native gold. According to EMPA, no trace elements were detected in native arsenic. The surface of native arsenic is rapidly oxidized in air and covered by arsenolite films. The mineral assemblage with native arsenic also contains alabandite, sphalerite, fahlores, and Cl-bearing fluorapatite (Murzin et al., 2011).

Our samples with native arsenic-bearing assemblage no. 6 collected in the dumps of the northern open pit most likely derive from the material extracted in 2007. This suggestion is supported by extensive replacement of native arsenic by supergene minerals, which occurred in the dumps. Native arsenic occurs in breccias as veinlets up to 3 cm thick composed of brown to black lamellar aggregates, which are partly oxidized from the surface up to the formation of arsenolite and claudetite, in assemblage with brightly red realgar and yellow orpiment (Figs. 7a–7d, 9l). Native arsenic is a major ore mineral of the assemblage no. 6, where it is found as aggregates up to 3–4 cm in size, isometric grains and nodules intergrown with gangue minerals of the breccia matrix (calcite, dolomite, quartz, baryte, clinochlore, muscovite, etc.) and contains inclusions of realgar, arsenopyrite, pyrite, fahlores, and abundant native gold grains up to 0.1 mm in size. Native arsenic is a host to numerous inclusions of native gold, arsenopyrite, bournonite, and tennantite-(Fe). Native arsenic also rarely occurs in assemblage no. 4, where it forms inclusions up to 50 μm in stibnite and at the contact of the latter with calcite and dolomite (Fig. 8h). The mineral is observed together with various Pb–Cu–Ag-bearing sulfosalts (andorite, tennantite-(Zn), zinkenite), orpiment, realgar, coloradoite, and sphalerite. The parameters of the hexagonal unit cell of native arsenic calculated from powder diffraction pattern are provided in Table 3.

Native copper was observed in the oxidation products of sphalerite and chalcopyrite in garnet skarn (Vikentyev et al., 2016).

Native gold of the deposit is the main target of mining, therefore, it has been studied in details (Sazonov et al., 1991a; Murzin, Varlamov, 2010; Murzin et al., 2011; Vikentyev et al., 2016). In various assemblages, native gold forms small (e.g., < 0.1 mm) rounded and angular particles or interstitial, lamellar, and globular grains. Some grains show crystal faces. Isometric crystals and rounded and elongated grains of native gold are abundant in quartz–mica–carbonate matrix and as inclusions in pyrite, arsenopyrite, native arsenic, Pb sulfosalts, and fahlores. The intergrowths of native gold with realgar are less common. According to Vikentyev et al. (2016), the Ag content of native gold varies from zero in orpiment-realgar ores of carbonate breccias and argillisites, where the fineness of gold reaches 989 and 993 ‰, respectively, up to 37.8 wt. % in pyrite-pyrrhotite ores of skarn (the fine-

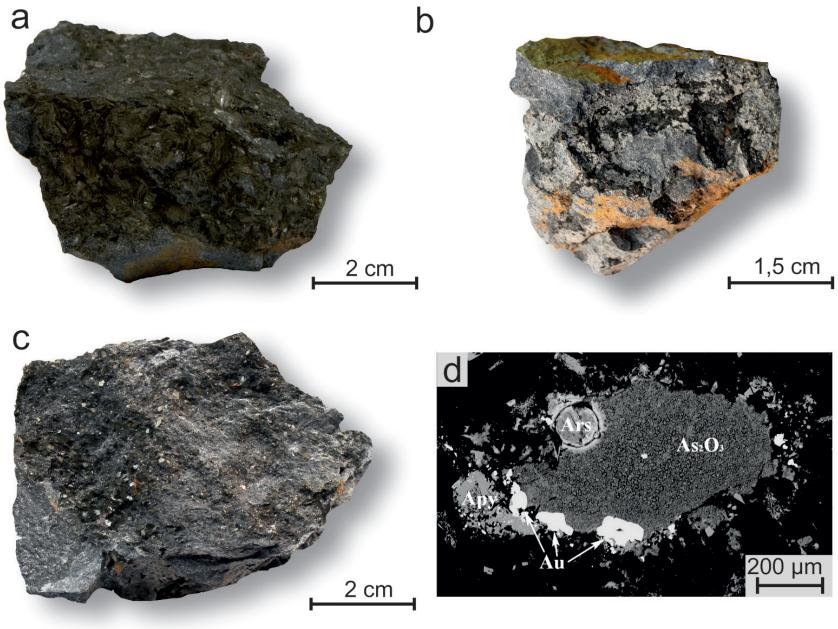

Fig. 7. Morphology of native arsenic of the Vorontsovskoe deposit:

a – monomineral brown segregation; b – black aggregates in assemblage with powdery coatings of white arsenolite/claudetite, films of yellow orpiment and orange realgar; c – coarse-grained aggregate with a perfect cleavage; d – a nodule of native arsenic partly replaced by supergene arsenolite/claudetite in assemblage with native gold and relict arsenopyrite in a matrix composed of quartz, calcite and muscovite.

Collections of A.V. Kasatkin (a, d), Museum «Shtufnoi Kabinet», Severouralsk (b, c). Photo: A.D. Kasatkina (a), M.V. Tsyganko (b, c), BSE image (d).

ness of gold is only 614 ‰). Locally, native gold also contains Hg (up to 5.5 wt. %) and Cu (up to 0.7 wt. %).

In a sample from the main ore stockpile, we found a unique native gold cluster in calcite measuring 1.5 mm long (Fig. 9a). Native gold was also observed in all above mineral assemblages. It is most often found in assemblage no. 6 as grains up to 0.1 mm in size, which are disseminated in gangue minerals of breccias (carbonates, quartz, baryte, muscovite, etc.), native arsenic, arsenolite, and claudetite and at their contact with realgar and arsenopyrite (Figs. 5, 8d). In this assemblage, native gold contains Ag and Hg (average for ten grains, wt. %): 87.12 Au, 8.42 Hg, 5.01 Ag, total 100.55. The empirical formula based on the metal sum of one is $Au_{0.83}Ag_{0.09}Hg_{0.08}$.

Native silver rarely occurs as fine dissemination in ores (Vikentyev et al., 2016). In our samples, the Au-bearing silver («küstelite») forms very rare rounded grains up to 20 μm in diameter in orpiment from assemblage no. 1. The chemical composition of native silver is (wt. %): 71.68 Ag, 28.15 Au, total 99.83; it corresponds to the empirical formula based on the metal sum of one $Ag_{0.82}Au_{0.18}$.

Sulfides, arsenides, tellurides

Acanthite Ag_2S is very rare. It occurs in assemblages nos. 1 and 4 as single rounded grains up to 10 μm in size embedded in calcite. The chemical composition of the mineral is close to the stoichiometric Ag_2S (Table 4).

Alabandite MnS was first recorded by Sazonov et al. (1991a) in one sample as crystals or anhedral grains up to 0.05–0.1 mm across disseminated in carbonate and, locally, intergrown with pyrite. The mineral was identified optically and by chemical composition (up to 3.5 wt. % Fe, up to 0.1 wt. % Cd and Hg). Murzin and Varlamov (2010) described stoichiometric alabandite, which forms aggregates up to 0.15 mm in gangue minerals of breccias in assemblage with greigite, as well as individual crystals and intergrowths with Mn-bearing sulfosalts in realgar. Murzin et al. (2011) also reported on numerous rounded alabandite grains up to 50–70 μm across in native arsenic and arsenopyrite. This alabandite contains Fe (0.6 wt. %) and Zn (0.1 wt. %).

In our samples, alabandite was found in mineral assemblages nos. 1, 3, 5, and 7. In assemblage no. 1, it is rare in comparison with assemblages nos. 3, 5, and 7.

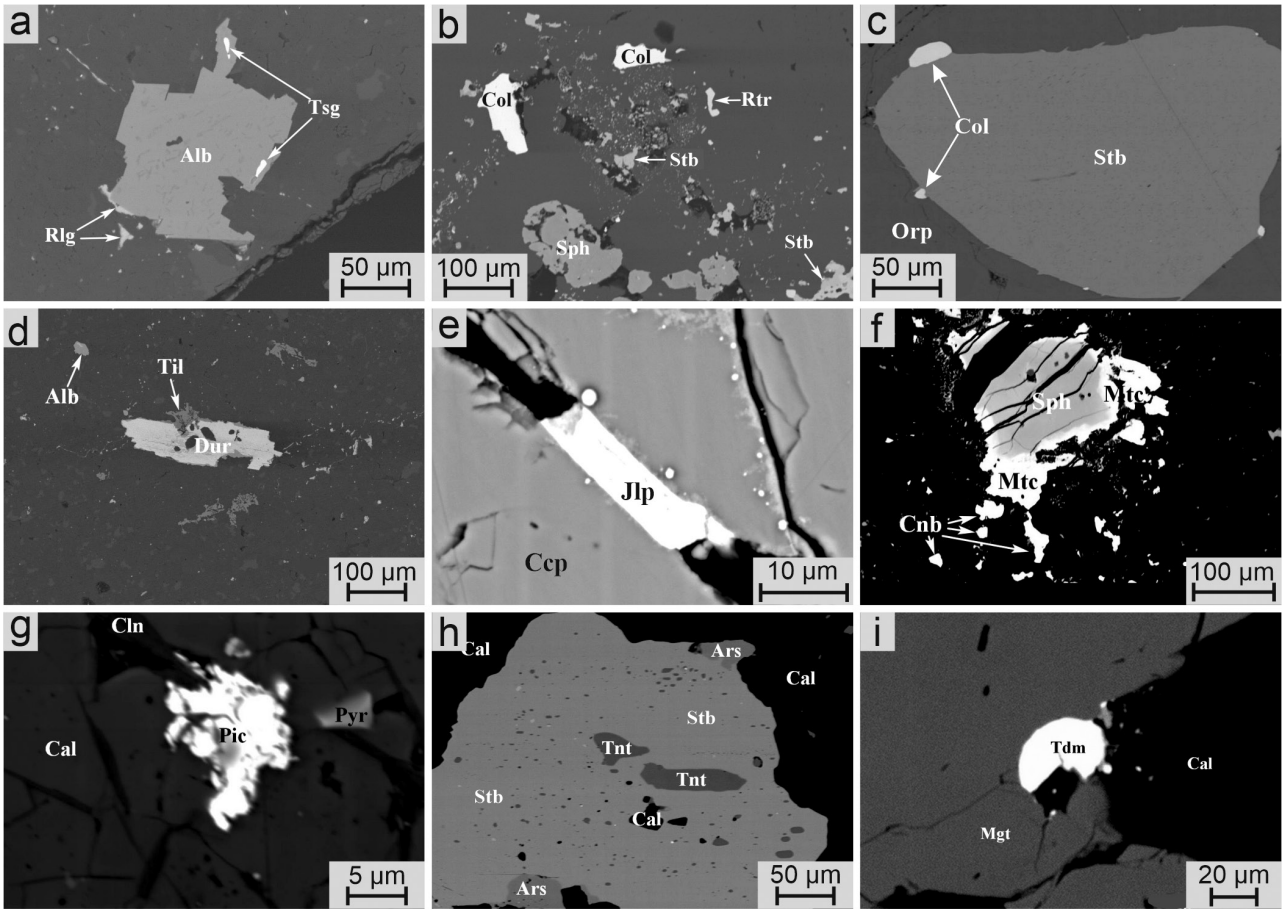

Fig. 8. Sulfides, tellurides and sulfosalts in carbonate breccias of the Vorontsovskoe deposit:

a – crystalline alabandite with inclusions of small tsygankoite crystals and realgar rim in dolomite and calcite; b – coloradoite in assemblage with sphalerite, stibnite, and routhierite in calcite; c – coloradoite grains at the contact with stibnite and orpiment; d – prismatic duranusite crystal rimmed by tilasite in dolomite and calcite with alabandite; e – prismatic jalpaite crystal in chalcopyrite; f – Zn–Mn-bearing metacinnabar around the Hg–Mn-bearing sphalerite grain in a matrix composed of dolomite, calcite, and quartz with cinnabar; g – picotpaulite grain in calcite and clinochlore with a small pyrite crystal; h – stibnite with inclusions of tennantite-(Zn) and native arsenic in calcite; i – rounded tetradymite grain at the contact with magnetite and calcite.

BSE images.

Alabandite typically forms cubic crystals or subhedral grains up to 0.2 mm in size dispersed in gangue minerals of breccias (Figs. 8a, d). Alabandite was a source of Mn for late-stage low-temperature sulfosalts. The relics of alabandite are found in Mn-bearing sulfarsenites and sulfantimonites (gladkovskyite, luboržákite, tsygankoite), which replace it partly or completely (Figs. 17i, 26g). Small inclusions of Mn-bearing sulfosalts in alabandite crystals are observed as well (Fig. 8a). The mineral has black color and submetallic luster. In reflected light, it is grayish white but looks light gray at the contact with tsygankoite, which has higher reflectance. The chemical composition of alabandite is stoichiometric (Table 4). The parameter of the cubic unit cell is provided in Table 3.

Arsenopyrite FeAsS together with pyrite is one of the major ore minerals of altered volcanosedimentary rocks: the contents of both sulfides reach 20–30 vol. %. Arsenopyrite forms metacrystals 0.05 to 2–3 mm in size and also replaces shell walls of mollusks or rock-forming minerals. In breccias, arsenopyrite occurs as acicular crystals up to 0.2 mm long and often intergrows with pyrrhotite. It rarely contains Ni (up to 0.2 wt. %) and Co (up to 0.1 wt. %). Arsenopyrite is also reported from wollastonite metasomatites (Sazonov et al., 1991a).

Arsenopyrite occurs in most mineral assemblages of our samples. In assemblages nos. 6 and 7, it is one of the major ore minerals. In assemblage no. 6, arsenopyrite occurs as euhedral crystals up to 1 mm included

Table 3

Unit-cell parameters of minerals from the Vorontsovskoe deposit (our data)

No.	Mineral name	As. no.	Crystal system	Unit cell parameters							Method
				a, Å	*b*, Å	*c*, Å	α, °	β, °	γ, °	*V*, Å³	
Elements											
1	Arsenic	6	Trig.	3.7395(2)		10.5246(8)				127.46(2)	P
Sulfides, arsenides, tellurides											
2	Alabandite	1	Cub.	5.200(1)						140.61(7)	SC
3	Arsenopyrite	8	Mon.	5.739(5)	5.690(5)	5.775(4)		112.05(8)		174.8(2)	SC
4	Chalcopyrite	1	Tetr.	5.300(3)		10.439(9)				293.2(3)	SC
5	Cinnabar	1	Trig.	4.1590(5)		9.212(2)				138.00(4)	P
6	Cinnabar	4	Trig.	4.1473(3)		9.467(1)				141.01(2)	P
7	Coloradoite	4	Cub.	6.435(11)						266.5(8)	SC
8	Covellite	9	Hex.	3.7863(2)		16.352(2)				203.01(2)	P
9	Djurleite	9	Mon.	26.908(6)	15.722(2)	13.513(2)		90.42(2)		5716(1)	P
10	Galena	9	Cub.	5.9522(10)						211.12(8)	SC
11	Getchellite	1	Mon.	11.910(4)	9.0389 (13)	10.168 (9)		116.23(7)		981.9(9)	SC
12	Greigite	2	Cub.	9.8894(8)						967.20(22)	P
13	Hawleyite	9	Cub.	5.8060(6)						195.71(6)	SC
14	Löllingite	–	Orth.	5.2846(9)	5.9669(8)	2.8736(7)				90.61(2)	P
15	Metacinnabar	4	Cub.	5.7295(3)						188.08(3)	P
16	Orpiment	3	Mon.	11.475(1)	9.528(1)	4.248(1)		90.52(1)		464.52(7)	P
17	Pararealgar	2	Mon.	9.968(3)	9.690(5)	8.574(8)		97.11(5)		821.9(9)	SC
18	Pyrite	1	Cub.	5.4145(4)						158.74(4)	SC
19	Pyrite	9	Cub.	5.408(13)						158.2(6)	SC
20	Realgar	1	Mon.	9.325(1)	13.562(2)	6.586(1)		106.43(2)		798.9(2)	P
21	Sphalerite	1	Cub.	5.4047(4)						157.88(3)	P
22	Stibnite	4	Orth.	11.280(2)	11.276(2)	3.833(1)				487.5(1)	SC
23	Wakabayashilite	1	Orth.	25.21(3)	14.62(3)	6.65(4)				2450(16)	SC
24	Wakabayashilite	2	Orth.	25.40(3)	14.558(10)	6.432(5)				2378(4)	SC
Sulfosalts											
25	Aktashite	5	Trig.	13.639(4)		9.303(7)				1499(1)	SC
26	Auerbakhite	3	Orth.	15.3280(15)	7.662(7)	16.6330(14)				1953.40(18)	SC
27	Bernardite	3	Mon.	15.72(2)	8.18(2)	10.76(4)		91.54(6)		1383.1(2)	SC
28	Boscardinite	1	Tricl.	8.080(1)	8.730(2)	22.474(4)	90.78(1)	97.08(1)	90.93(1)	1572.8(3)	P
29	Boulangerite	–	Mon.	21.592(6)	23.489(15)	8.0758(13)		100.640(19)		4025(3)	SC
30	Bournonite	–	Orth.	8.173(4)	8.704(4)	7.795(10)				554.5(8)	SC
31	Chabournéite	1	Tricl.	16.327(7)	42.677(17)	8.559(9)	95.75(5)	89.11(6)	96.79(3)	5892(7)	SC
32	Christite	3	Mon.	6.11(5)	16.2(2)	6.11(4)		96.7(6)		600(10)	SC
33	Clerite	5	Orth.	11.4021(12)	14.3790(15)	3.7908(4)				621.50(11)	SC
34	Dalnegroite	1	Tricl.	16.33(2)	42.49(3)	8.564(5)	95.32(4)	90.53(4)	96.43(6)	5878(3)	P
35	Dalnegroite? («Protodalnegroite»)	3	Tricl.	8.53(5)	9.16(3)	21.10(2)	93.09(17)	95.70(2)	117.90(5)	1440(10)	SC
36	Dewitite	1	Tricl.	8.63253(19)	16.3055(7)	21.8196(8)	75.094(3)	83.631(2)	89.303(2)	2949.18(18)	SC
37	Écrinsite	1	Tricl.	8.034(8)	8.533(4)	22.320(9)	90.58(5)	96.96(8)	90.63(7)	1519(2)	SC
38	Ferrovorontsovite	2	Cub.	10.2390(7)						1073.43(22)	SC
39	Gillulyite	3	Mon.	9.594(2)	5.677(2)	21.401(7)		100.34(3)		1146.5(4)	SC
40	Gladkovskyite	3	Trig.	9.6392(2)		6.4560(15)				519.49(12)	SC
41	Gungerite	2	Orth.	20.1958(3)	11.5258(2)	20.1430(2)				4688.74(12)	SC
42	Hutchinsonite	3	Orth.	10.82(4)	35.39(2)	8.22(2)				3147.6(2)	SC
43	Imhofite	3	Mon.	8.776(5)	24.430(3)	5.755(2)		108.40(2)		1170.8(2)	SC
44	Lorándite	3	Mon.	12.282(2)	11.240(3)	6.106(2)		104.04(2)		817.8(3)	P
45	Luboržákite	5	Mon.	12.5077(6)	3.8034(2)	16.0517(8)		94.190(4)		761.57(6)	SC

No.	Mineral name	As. no.	Crystal system	Unit cell parameters							Method
				a, Å	*b*, Å	*c*, Å	α, °	β, °	γ, °	*V*, Å³	
46	Meneghinite	–	Orth.	11.320(1)	24.026(3)	4.1435(7)				1127.0(2)	P
47	Parapierrotite (2.0 wt.% As)	4	Mon.	8.0832(5)	19.4057(11)	9.0465(5)		91.908(6)		1418.25(1)	SC
48	Parapierrotite (3.7 wt.% As)	4	Mon.	8.066(6)	19.21(4)	9.123(16)		91.81(7)		1412(4)	SC
49	Parapierrotite (8.6 wt.% As)	2	Mon.	8.104(17)	19.20(3)	9.05(4)		91.7(2)		1408(7)	SC
50	Parapierrotite (15.7 wt.% As)	2	Mon.	8.05(5)	19.39(12)	8.84(6)		92.5(5)		1380(16)	SC
51	Philrothite	3	Mon.	8.102(2)	24.845(5)	11.785(4)		132.65(2)		1744.8(2)	SC
52	Pokhodyashinite	1	Mon.	23.431(5)	3.996(2)	14.070(3)		110.23(3)		1236.1(8)	SC
53	Rebulite	3	Mon.	17.35(3)	7.36(2)	31.94(4)		105.12(2)		3937.4(2)	SC
54	Routhierite	1	Tetr.	9.9724(8)		11.295(2)				1123.2(2)	SC
55	Routhierite	5	Tetr.	9.967(5)		11.382(10)				1131(1)	SC
56	Tennantite-(Zn)	9	Cub.	10.2302(15)						1070.7(3)	SC
57	Tsygankoite	**7**	Mon.	21.362(4)	3.8579(10)	27.135(4)		106.944(14)		2139.19(17)	SC
58	Twinnite	1	Mon.	7.9941(14)	19.507(15)	8.6316(15)		91.066(17)		1346(1)	SC
59	Twinnite	5	Mon.	7.9846(13)	19.472(2)	8.6127(17)		90.817(17)		1338.9(4)	SC
60	Vorontsovite	2	Cub.	10.2956(6)						1091.3(1)	SC
61	Vrbaite	3	Orth.	13.391(5)	23.426(15)	11.294(7)				3543(3)	SC
62	Weissbergite	1	Tricl.	6.11(3)	6.30(6)	12.00(4)	102.3(4)	100.8(5)	104.4(6)	423(5)	SC
63	Zinkenite	–	Hex.	22.13(5)		4.328(9)				1840(7)	SC
Oxides and hydroxides											
64	Akhtenskite	9	Hex.	2.8328(7)		4.330(3)				30.09(2)	P
65	Arsenolite	6	Cub.	11.0412(7)						1346.01(3)	P
66	Asbolane	9	Hex.	2.9602(3)		10.048(5)				76.25(4)	P
67	Birnessite	9	Mon.	5.2094(7)	2.8411(3)	7.2924(9)		104.30(2)		104.59(2)	P
68	Bixbyite	9	Cub.	9.3665(8)						821.7(2)	P
69	Cesàrolite	9	Trig.	2.8378(3)		20.536(3)				143.22(3)	P
70	Claudetite	6	Mon.	5.2467(6)	13.000(2)	4.5398(5)		94.11(1)		308.85(5)	P
71	Coronadite	9	Tetr.	9.923(1)		2.8655(6)				282.16(7)	P
72	Cryptomelane	9	Tetr.	9.828(1)		2.8523(3)				275.52(5)	P
73	Goethite	9	Orth.	9.9711(8)	3.0225(4)	4.6144(4)				139.086(2)	P
74	Hematite	9	Trig.	5.0208(4)		13.735(2)				299.85(5)	P
75	Hollandite	9	Tetr.	9.9124(9)		2.9074(5)				285.67(5)	P
76	Lithiophorite	9	Trig.	2.8873(4)		28.039(3)				202.44(4)	P
77	Magnetite	8	Cub.	8.3990(8)						592.50(17)	P
78	Manganite	9	Mon.	5.302(3)	5.190(1)	5.335(1)		114.69(4)		133.37(5)	P
79	Manjiroite	9	Tetr.	9.7829(5)		2.8560(2)				273.33(2)	P
80	Pyrolusite	9	Tetr.	4.3915(2)		2.8610(1)				55.175(5)	SC
81	Ramsdellite	9	Orth.	4.4939(6)	9.2058(9)	2.8493(4)				117.88(2)	SC
82	Ranciéite	9	Trig.	2.7871(3)		7.699(4)				51.79(2)	P
83	Romanèchite	9	Mon.	13.865(2)	2.8428(5)	9.734(1)		92.472(8)		383.31(6)	P
84	Todorokite	9	Mon.	9.8559(9)	2.8478(4)	9.500(1)		95.271(9)		265.53(4)	P
Carbonates											
85	Azurite	9	Mon.	5.0165(16)	5.856(2)	10.359(5)		92.53(3)		304.0(2)	SC
86	Cerussite	9	Orth.	5.1691(6)	8.503(1)	6.102(1)				268.21(5)	SC
87	Kutnohorite	9	Trig.	4.8272(5)		16.460(4)				332.16(8)	P
88	Malachite	9	Mon.	9.458(1)	11.945(1)	3.2416(4)		98.46(1)		362.24(5)	SC
89	Rhodochrosite	9	Trig.	4.7874(6)		15.655(4)				310.74(9)	P
Sulfates											
90	Anglesite	9	Orth.	8.460(1)	5.3908(6)	6.966(1)				317.71(6)	SC
91	Beaverite-(Cu)	9	Trig.	7.1888(7)		17.096(6)				765.1(2)	P
92	Brochantite	9	Mon.	13.091(1)	9.820(1)	6.0211(8)		103.73(1)		751.90(5)	P

93	Chalcanthite	9	Tricl.	6.101(1)	10.717(2)	5.943(1)	82.49(2)	107.23(2)	102.66(1)	361.18(9)	P
94	Epsomite	9	Orth.	11.840(2)	11.941(8)	6.846(1)				968.0(5)	P
95	Gypsum	9	Mon.	5.6697(9)	15.289(3)	6.551(1)		118.50(2)		499.0(1)	P
96	Pentahydrite	9	Tricl.	6.247(1)	10.561(2)	6.017(1)	82.77(2)	109.13(2)	104.70(1)	362.35(8)	P
97	Starkeyite	9	Mon.	5.9233(8)	13.614(1)	7.956(1)		90.97(1)		641.5(1)	P
					Arsenates							
98	Bayldonite	9	Mon.	10.097(4)	5.8954(7)	13.943(2)		104.14(2)		804.9(3)	P
99	Tilasite	7	Mon.	6.701(1)	8.911(1)	7.5411(6)		121.070(9)		385.73(5)	P
					Silicates							
100	Armenite	1	Orth.	13.727(2)	18.696(2)	10.742(2)				2756.8(5)	SC
101	Celadonite	–	Mon.	5.216(1)	9.049(1)	10.161(1)		100.77(2)		471.17(9)	P
102	Chabazite-Ca	–	Tricl.	9.379(3)	9.346(2)	9.352(1)	94.62(2)	94.29(2)	94.07(2)	812.41(21)	SC
103	Chamosite	–	Tricl.	5.372(1)	9.301(2)	14.279(3)	90.18(3)	97.28(4)	89.75(3)	707.7(2)	P
104	Chapmanite	–	Mon.	5.215(4)	8.998(7)	7.778(8)		101.67(5)		357.4(4)	P
105	Chrysotile-2Or_{c1}	–	Orth.	5.2670(5)	9.203(2)	14.344(2)				695.3(2)	P
106	Clinochlore	–	Tricl.	5.330(1)	9.235(1)	14.457(3)	90.70(1)	98.26(2)	90.43(2)	704.1(2)	P
107	Halloysite-7Å	9	Mon.	5.118(1)	8.907(2)	7.5516(8)		101.07(2)		337.82(7)	P
108	Hemimorphite	9	Orth.	8.359(12)	10.725(15)	5.111(10)				458(1)	SC
109	Kaolinite	9	Tricl.	5.160(1)	8.943(1)	7.3643(8)	91.693(9)	105.31(1)	90.01(1)	327.52(7)	P
110	Laumontite	–	Mon.	7.497(1)	13.279(2)	14.589(1)		111.337(8)		1352.6(2)	SC
111	Muscovite-2M_1	–	Mon.	5.1909(4)	8.949(1)	20.083(2)		95.196(7)		929.12(12)	P
112	Pargasite	–	Mon.	9.8947(7)	18.0247(12)	5.3010(4)		105.563(7)		910.76(9)	P
113	Pigeonite	–	Mon.	9.729(1)	8.957(1)	5.2255(7)		108.56(1)		431.68(6)	P
114	Talc	–	Tricl.	5.2966(9)	9.449(1)	5.329(2)	100.08(2)	120.47(2)	84.96(1)	226.31(9)	P
115	Tremolite	–	Mon.	9.849(1)	18.136(6)	5.261(1)		104.75(1)		908.7(2)	P

Note. P – unit-cell parameters calculated from powder X-ray diffraction data; SC – unit-cell parameters from single-crystal X-ray diffraction data. As. no. – number of mineral.

in native arsenic and arsenolite/claudetite and at their contacts with gangue minerals and native gold (Fig. 7d). The chemical composition of arsenopyrite from assemblage no. 6 is studied in detail (Murzin et al., 2011). In our samples from the dumps of the southern open pit, arsenopyrite forms prismatic crystals up to 1 cm (Fig. 9b) and steel gray aggregates up to 6 × 5 cm in size. The mineral is identified by chemical composition and XRD data (Table 3).

Bismuthinite Bi_2S_3 was found as rare anhedral grains up to 80 μm across in magnetite of assemblage no. 8. The chemical composition of the mineral (Table 4) is close to ideal Bi_2S_3.

Bornite Cu_5FeS_4 together with dominant chalcopyrite occurs in variable amounts in ores developed in the skarn zones in diorites. Both sulfides compose veinlets and pockets 1–10 mm in size and are confined to areas of epidote–calcite, epidote–actinolite–calcite and quartz–sericite–calcite composition. The mineral was identified by chemical composition (Vikentyev et al., 2016). In our samples, bornite was found only in assemblage no. 9 as very rare small (<20 μm) inclusions in calcite and quartz. Its chemical composition is stoichiometric (Table 4).

Chalcopyrite $CuFeS_2$ is a common mineral of the deposit. It is identified in polymetallic mineralization of wollastonite skarns. It occurs as large (up to 5 mm) aggregates and small (up to 0.1 mm) crystals in quartz veinsin beresites and listvenites. In breccia matrix, chalcopyrite forms anhedral grains from 10 μm to 2–3 mm in size in carbonates; it often contains inclusions of sulfosalts, galena, and sphalerite (Sazonov et al., 1991a). In our samples of carbonate breccias, chalcopyrite was found only in assemblages nos. 1 and 6. It occurs more often in assemblage no. 8, where it forms aggregates of distorted tetrahedral crystals up to 0.5 cm across and golden yellow aggregates and is observed together with andradite, calcite, magnetite, arsenopyrite, fahlores, pyrite, and sphalerite (Fig. 9c). In the supergene zone, chalcopyrite occurs as fine oxidized grains in quartz–calcite aggregates. Chalcopyrite is a main source of Cu for supergene carbonates (azurite, malachite) and sulfates (beaverite-(Cu), brochantite, chalcanthite). The chemical composition of chalcopyrite is close to ideal (Table 4). The parameters of its tetragonal unit cell are given in Table 3.

Cinnabar HgS was described as a very rare ore mineral (Sazonov et al., 1991a). Its grains reach

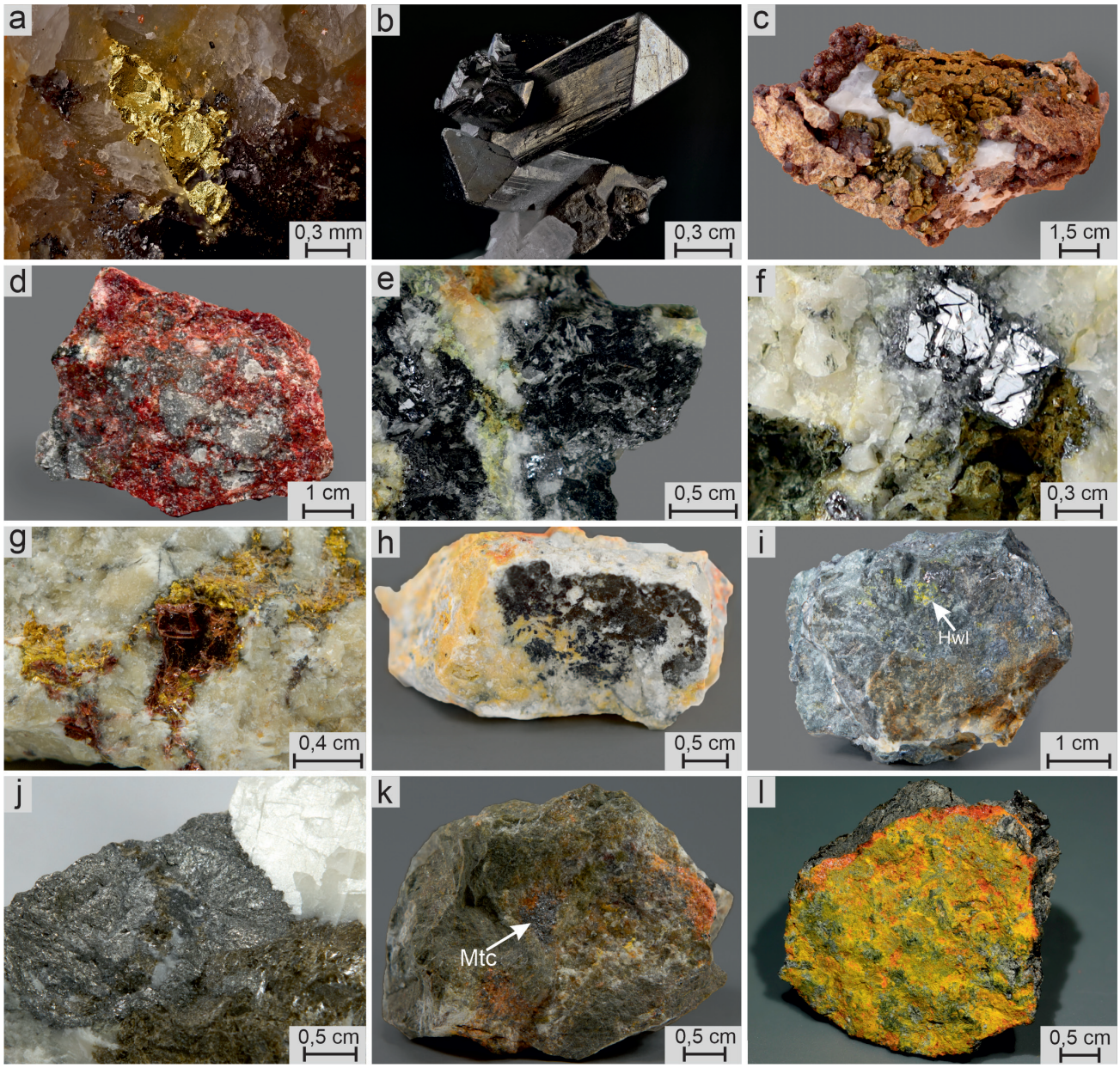

Fig. 9. Elements and sulfides of the Vorontsovskoe deposit , part I:

a – crystalline aggregate of native gold in calcite; b – aggregate of prismatic arsenopyrite crystals; c – aggregates of golden yellow chalcopyrite crystals on calcite and andradite; d – red fine-grained cinnabar in carbonate matrix with stibnite; e – black powdery djurleite and covellite aggregates on galena; f – lead gray isometric galena crystals in quartz matrix; g – dark red platy getchellite crystals in calcite–dolomite matrix with yellow wakabayashilite; h – dark brown greigite crusts on calcite–dolomite marble; i – yellow powdery hawleyite on sphalerite; j – steel gray löllingite with massive brown sphalerite in white calcite; k – iron black metacinnabar grain (in center) in matrix of calcite, dolomite, and realgar; l – veinlet of bright yellow orpiment with bright red realgar in native arsenic.

Collections of Museum «Shtufnoi Kabinet», Severouralsk (a–d), A.V. Kasatkin (e–k), V.V. Levitskiy (l). Photo: T.V. Pashko (a, b), M.V. Tsyganko (c, d), A.D. Kasatkina (e–k), V.V. Levitskiy (l).

0.1–0.3 mm in size and occur together with realgar in thin (1–2 mm) carbonate veinlets in limestone breccias or are included in breccia carbonates in assemblage with realgar and Hg-bearing sphalerite. The chemical composition of cinnabar is close to stoichiometric (Sazonov et al., 1991a). According to our observations, cinnabar is rare in assemblage no. 1 and is abundant in assemblages nos. 2 and 3, where it forms grains up to 0.2 mm across. In assemblage no. 4, cinnabar is one of major ore minerals and occurs as fine-grained dark red

Chemical composition (wt. %) of sulfides, arsenides and tellurides *Table 4*

An. no.	As. no.	Mineral name	Mn	Fe	Cu	Zn	Ag	Hg	Pb	Bi	As	Sb	Te	S	Total	Formula
1	1	Acanthite	–	–	–	–	86.92	–	–	–	–	–	–	12.68	99.60	$Ag_{2.01}S_{0.99}$
2	7	Alabandite	63.18	–	–	–	–	–	–	–	–	–	–	37.04	100.22	$Mn_{1.00}S_{1.00}$
3	8	Bismuthinite	–	–	–	–	–	–	–	81.44	–	–	–	18.76	100.20	$Bi_{2.00}S_{3.00}$
4	9	Bornite	–	11.23	63.45	–	–	–	–	–	–	–	–	25.65	100.33	$Cu_{4.99}Fe_{1.01}S_{4.00}$
5	8	Chalcopyrite	–	30.56	35.15	–	–	–	–	–	–	–	–	35.12	100.83	$Cu_{1.01}Fe_{1.00}S_{2.00}$
6	2	Cinnabar	–	–	–	–	–	78.66	–	–	–	–	–	7.44	99.97	$Hg_{0.98}(S_{0.58}Se_{0.44})_{1.02}$
7		Coloradoite	–	–	–	–	–	61.45	–	–	–	–	39.44	–	100.89	$Hg_{1.00}Te_{1.00}$
8	9	Covellite	–	–	65.23	–	–	–	–	–	–	–	–	35.12	100.35	$Cu_{0.97}S_{1.03}$
9	6	Cubanite	–	41.29	23.69	–	–	–	–	–	–	–	–	35.10	100.08	$Cu_{1.01}Fe_{2.01}S_{2.98}$
10	9	Djurleite	–	–	79.03	–	–	–	–	–	–	–	–	20.46	99.49	$Cu_{31.06}S_{15.94}$
11	7	Duranusite	–	–	–	–	–	–	–	–	91.00	–	–	9.61	100.61	$As_{4.01}S_{0.99}$
12	9	Galena	–	–	–	–	–	–	86.62	–	–	–	–	13.45	100.07	$Pb_{1.00}S_{1.00}$
13	4	Gersdorfite	–	1.06	–	–	–	–	–	–	44.03	–	–	19.82	100.92	$(Ni_{0.64}Co_{0.36}Fe_{0.03})_{1.03}As_{0.96}S_{1.01}$
14	1	Getchellite	–	–	–	–	–	–	–	–	26.06	41.80	–	33.18	101.04	$As_{1.01}Sb_{0.99}S_{3.00}$
15	1	Greigite	–	56.78	–	–	–	–	–	–	–	–	–	42.33	99.11	$Fe_{3.05}S_{3.95}$
16	6	Hessite	–	–	–	–	64.95	–	–	–	–	–	34.92	–	99.87	$Ag_{2.06}Te_{0.94}$
17	8	Ikunolite	–	–	0.04	–	–	–	1.89	82.47	–	–	5.86	8.51	99.56	$Bi_{3.81}Pb_{0.09}Cu_{0.01}(S_{2.56}Te_{0.44}Se_{0.10})_{3.10}$
18		Jalpaite	–	–	14.01	–	70.21	–	–	–	–	–	–	13.89	98.11	$Ag_{2.99}Cu_{1.01}S_{1.99}$
19	8	Joséite-A	–	–	–	–	0.15	–	0.50	79.72	–	–	11.73	5.81	99.04	$Bi_{3.97}Pb_{0.03}Ag_{0.01}Te_{0.96}(S_{1.89}Se_{0.15})_{2.04}$
20		Löllingite	–	28.57	–	–	–	–	–	–	69.44	–	–	1.28	99.29	$Fe_{1.04}As_{1.88}S_{0.08}$
21	4	Metacinnabar	–	–	–	10.85	–	71.60	–	–	–	–	–	17.25	99.70	$(Hg_{0.67}Zn_{0.31})_{0.98}S_{1.01}$
22	4	Metacinnabar	1.70	–	–	15.01	–	64.12	–	–	–	–	–	18.50	99.33	$(Hg_{0.55}Zn_{0.40}Mn_{0.05})_{1.00}S_{1.00}$
23	2	Orpiment	–	–	–	–	–	–	–	–	59.16	1.45	–	38.81	99.42	$(As_{1.96}Sb_{0.03})_{1.99}S_{3.01}$
24	2	Pararealgar	–	–	–	–	–	–	–	–	69.48	–	–	29.85	99.33	$As_{3.99}S_{4.01}$
25	4	Picotpaulite	–	27.21	–	–	–	–	–	–	–	–	–	23.86	100.36	$Tl_{0.98}Fe_{1.99}S_{3.03}$
26		Realgar	–	–	–	–	–	–	–	–	68.89	–	–	29.87	98.76	$As_{0.99}S_{1.01}$
27	4	Sphalerite	3.43	–	–	45.04	–	23.10	–	–	–	–	–	27.73	99.30	$(Zn_{0.80}Hg_{0.13}Mn_{0.07})_{1.00}S_{1.00}$
28		Sphalerite	–	–	–	66.94	–	–	–	–	–	–	–	32.80	99.74	$Zn_{1.00}S_{1.00}$
29	4	Stibnite	–	–	–	–	–	–	0.23	–	0.76	70.69	–	27.90	99.58	$(Sb_{1.99}As_{0.03})_{2.02}S_{2.98}$
30	8	Tetradymite	–	–	–	–	–	–	–	59.14	–	–	36.70	4.15	100.32	$Bi_{2.01}Te_{2.04}(S_{0.92}Se_{0.03})_{0.95}$
31	1	Wakabayashilite	–	–	–	–	–	–	–	–	56.17	6.51	–	36.42	99.1	$As_{9.28}Sb_{0.66}S_{14.06}$

Note. Here and in Tables 5, 7, 9, 10, An. no. – number of analysis; As. no. – number of mineral assemblage (see Table 2). The analytical total includes (wt. %) an. 6 – 13.87 Se; an. 13 – 13.15 Co, 22.86 Ni; an. 17 – 0.79 Se; an. 19 – 1.13 Se; an. 25 – 49.29 Tl; an. 30 – 0.33 Se. Analyses 7 and 26 are the average values of 15 and 20 analyses of coloradoite and realgar from various assemblages. Dash – the content of element is below detection limit.

Samples: Vor-8bis-2 – an. 1; Vor-10-1 – an. 2, 11; Kas172 #11 – an. 3, 17, 19, 30; Vor-08/20-11 – an. 4; 1066A – an. 5; Vor-03/16-6-6 – an. 6; Vor-06/20-11 – an. 8, 10; Vor-01/16-1b – an. 9; Vor-06/20-5 – an. 12; Vor-3 – an. 13, 25; 862G – an. 14; 1099G – an. 15; Vor-01/16-1a – an. 16; Vor-08/20-8 – an. 18; 534L – an. 20; 973M – an. 21; Vor-08/16-11-1 – an. 22, 27; Vor-b/n-9 – an. 23; Vor-08/20-7 – an. 24; 1221S – an. 28; SK-18-19 – an. 29; 610V – an. 31.

The mineral formulas are recalculated to atom sum of two (alabandite, cinnabar, galena, coloradoite, covellite, metacinnabar, realgar, sphalerite), three (acanthite, hessite, löllingite), four (chalcopyrite), five (bismuthinite, duranusite, getchellite, orpiment, stibnite, tetradymite), six (cubanite, gersdorffite, jalpaite, picotpaulite), seven (greigite, ikunolite, joséite-A), eight (pararealgar), ten (bornite), 24 (wakabayashilite) and 47 (djurleite).

aggregates in carbonates, quartz, and baryte in assemblage with Hg-bearing sphalerite, stibnite, metacinnabar, and realgar (Fig. 9d). In assemblage no. 2, cinnabar contains significant amount of Se (13.9 wt. %) (Table 4). The parameters of the hexagonal unit cell of cinnabar from assemblages nos. 1 and 4 are given in Table 3.

Coloradoite HgTe was identified as single grains up to 0.1 mm across intergrown with native arsenic and an unidentified Ag telluride (hessite?) in limestone (Sazonov et al., 1991a) and as aggregates 40–50 μm in size in «pierrotite» in assemblage with native gold (Murzin, Varlamov, 2010). In our samples, coloradoite is present in all mineral assemblages of carbonate breccias except for assemblage no. 6. This telluride typically forms rare rounded grains 5–40 μm in size embedded in calcite and dolomite. It is more abundant in assemblage no. 2 and ubiquitous in assemblage no. 4. In the latter assemblage coloradoite composes large anhedral aggregates up to 0.12 × 0.06 mm in calcite (Fig. 8b), dolomite, and realgar, elongated grains up to 0.04 mm at the contact of orpiment and stibnite (Fig. 8c) and inclusions up to 0.05 mm in stibnite and intergrowths with Hg-bearing sphalerite and zinkenite. Coloradoite is also associated with aktashite, andorite, native arsenic, cinnabar, native gold, guettardite, pyrite, routhierite, and tennantite-(Zn). The mineral contains no trace elements in chemical composition (Table 4). The parameter of the cubic unit cell of coloradoite from assemblage no. 4 is given in Table 3.

Covellite CuS overgrows sphalerite with small chalcopyrite inclusions in garnet skarn samples from the supergene zone (Vikentyev et al., 2016). We found covellite in assemblage no. 9 in oxidized quartz aggregates collected at the dumps of the southern open pit. Covellite is intimately intergrown with djurleite and forms black powdery crusts on galena in assemblage with beaverite-(Cu), malachite, and gypsum (Fig. 9e). Covellite was identified by optical properties, chemical composition (Table 4) and PXRD pattern (Table 3).

Cubanite $CuFe_2S_3$ was found in one sample from assemblage no. 6 as inclusions up to 20 μm in size in dolomite and native arsenic together with chalcopyrite, pyrite, sphalerite, and tetrahedrite-(Zn). The mineral was identified based on chemical composition (Table 4) and optical properties (light brown color in reflected light, strong anisotropy in pinkish brown and grayish blue tones).

Dimorphite As_4S_3 was mentioned by Stepanov et al. (2017) as a low-temperature mineral of the breccia matrix on the basis of three chemical analyzes, which approximately correspond to formula As_4S_3. This finding requires confirmation by XRD, because, according to our analytical experience, the overestimation of As relative to S can be caused by microinclusions of native arsenic in realgar.

Djurleite $Cu_{31}S_{16}$ was found as black powdery crusts overgrowing galena on quartz aggregate in samples with assemblage no. 9 collected from the dumps of the southern open pit (Fig. 9e). Djurleite occurs together with covellite, beaverite-(Cu), malachite, and gypsum. The mineral was identified by EMPA (Table 4) and PXRD data. The strongest reflections of the PXRD pattern are [*d*, Å (*I*)]: 3.27 (30), 3.05 (20), 2.82 (10), 2.63 (10), 2.48 (10), 2.37 (90), 1.96 (100), 1.88 (100). The parameters of the monoclinic unit cell are given in Table 3. In fresh polished thin sections, djurleite looks light gray with a bluish tint, but is quickly covered by an iridescent film.

Duranusite As_4S was found in assemblages nos. 2 and 7. It occurs as coarse prismatic crystals up to 0.2 mm in size enclosed in carbonates of breccias (Fig. 8d). It is locally rimmed by tilasite and contains inclusions of native arsenic. Duranusite formed prior to native arsenic but after realgar and orpiment, being a kind of their intermediate alteration product. Duranusite has a deep red color and a metallic luster. In reflected light, the mineral is light gray, with very weak bireflectance; it is distinctly anisotropic in yellowish tones, with red internal reflections. The chemical composition is stoichiometric (Table 4). This is the first finding of duranusite in the Russian Federation.

Galena PbS was noted as a rare ore mineral in altered wollastonite skarns (Sazonov et al., 1991a; Vikentyev et al., 2016). Together with sphalerite, it forms aggregates up to 3 cm across in greenish rocks, which consist of wollastonite partly replaced by epidote, actinolite, and chlorite. In carbonate breccias, it occurs as rare small anhedral grains up to 0.5 mm in size and occasionally as small inclusions in pyrrhotite. Galena is often intergrown with sphalerite, Pb sulfosalts, and tetrahedrite and replaces arsenopyrite, sphalerite (along cleavage), and pyrite (along microfractures).

In our samples, galena was found as a rare accessory mineral of carbonate breccias and skarns in assemblages nos. 1, 4, 6, and 8. In assemblage no. 9 of the oxidation zone, it is more abundant and forms isometric lead gray crystals up to 1 cm in size (Fig. 9f), as well as elongated aggregates up to 7 cm in size in sphalerite and veinlets with pyrite in quartz. In off-balance ore stockpile no. 2, we collected several samples of white massive carbonate–quartz aggregates with

lead gray galena veins up to 3 mm thick and several centimeters long. These veins contain inclusions of rare Ag- and Te-bearing minerals (hessite, benleonardite, tsnigriite) and geocronite (Fig. 11d). In other samples, galena forms aggregates with rare Pb sulfosalts: boulangerite, heteromorphite, plagionite, and semseyite (Fig. 11i). The chemical composition of galena is close to stoichiometric (Table 4); its XRD data are shown in Table 3.

Gersdorfite NiAsS with a significant Fe content was noted as single 10–20 μm inclusions in pyrite (Vikentyev et al., 2016). We found this mineral in assemblage no. 4 as rare cubic crystals up to 10 μm in calcite. In reflected light, gersdorfite is white, isotropic. It contains Co and Fe in chemical composition (Table 4).

Getchellite $AsSbS_3$ was found in samples from the main ore stockpile (Kasatkin, 2019) as red lamellar aggregates up to 2 cm embedded in calcite–dolomite marble (Fig. 9g). The mineral is transparent and has an adamantine luster and a perfect cleavage parallel to {001}. It belongs to assemblage no. 1 and is associated with orpiment, pyrite, realgar, stibnite and wakabayashilite. The chemical composition (Table 4) is stoichiometric; the parameters of the monoclinic unit cell (Table 3) correspond to getchellite. This is the first reliable find of this mineral in the Russian Federation.

Greigite Fe_3S_4 was first mentioned amid minerals associated with clerite (Murzin et al., 1996). Later, it was noted as anhedral aggregates and, less often, crystals up to 0.15 mm in size enclosed in gangue minerals of the breccia matrix and, locally, rimmed by realgar. Greigite contains Sb and As in chemical composition (Murzin, Varlamov, 2010). We collected samples with macroscopic greigite in the dumps of the southern open pit. This mineral occurs as dark brown crusts and sooty black films on calcite and dolomite and contains inclusions of native arsenic, orpiment, pyrite, realgar, stibnite, and baryte (Fig. 9h). In reflected light, it looks yellowish brown, brighter than As sulfides, but much darker than pyrite and stibnite in its lightest position. Greigite was identified by chemical composition (Table 4) and XRD data (Table 3). It was also found in carbonate breccias from assemblage no. 2 with gungerite, orpiment, and arsenic (Fig. 16c).

Hawleyite CdS was found in samples from the dumps of the southern open pit, where it occurs as yellow powdery veinlets overgrowing sphalerite and galena in assemblage no. 9 (Fig. 9i). Hawleyite is dark gray in reflected light, but looks lighter than sphalerite. At the contact with galena, it acquires a distinct greenish tint. The mineral is isotropic, with yellow internal reflections. Its chemical composition is as follows (wt. %, average of three analyses): 68.72 Cd, 8.25 Zn, 23.45 S, total 100.42. The empirical formula calculated on the based on two atoms is $(Cd_{0.83}Zn_{0.17})_{1.00}S_{1.00}$. The parameter of the cubic unit cell is given in Table 3.

Hessite Ag_2Te was determined in assemblage no. 6 as rare isometric grains up to 15 μm in size in gangue minerals of breccias. It was also identified in calcite–dolomite–quartz aggregates with galena and sphalerite collected at off-balance ore stockpile no. 2. It forms inclusions up to 10 μm in galena and is associated with benleonardite, geocronite, and tsnigriite. The chemical composition of hessite is close to stoichiometric (Table 4).

Ikunolite $Bi_4(S,Se)_3$ represented by a Te-bearing variety was found as single intergrowths with lillianite up to 20 μm enclosed in magnetite from assemblage no. 8. In reflected light, both ikunolite and lillianite are white, but the former has much weaker anisotropy (in faded brownish tones). The chemical composition of ikunolite is given in Table 4.

Jalpaite Ag_3CuS_2 forms tiny prismatic crystals up to 20 × 10 μm in chalcopyrite (Fig. 8e) in assemblage with cupropolybasite, polybasite, pyrite, galena, sphalerite, tetrahedrite-(Fe), calcite, and quartz. The mineral was identified by chemical composition (Table 4). In reflected light, jalpaite looks gray; it is weakly anisotropic.

Joséite-A Bi_4TeS_2 forms rare intergrowths with pavonite in magnetite from assemblage no. 8 (Fig. 21f). The size of the joséite-A grains does not exceed 20 μm. In reflected light, it is creamy white at the contact with pavonite. After several weeks, the joséite-A grains in polished sections are covered by a thin oxide film with a characteristic irridescence. Joséite-A contains a small amount of Se (Table 4).

Löllingite $FeAs_2$ was first found as rosettes and acicular crystals in assemblage with native arsenic and arsenopyrite (Vikentyev et al., 2016). In our samples from the dumps of the northern open pit, the large (up to 3 cm) aggregates of steel gray löllingite are identified in massive brown sphalerite of white calcite–dolomite marble (Fig. 9j). Löllingite has a low S content: up to 1.3 wt. % (Table 4). The parameters of the orthorhombic unit cell are given in Table 3.

Metacinnabar HgS was identified as a rare mineral in assemblages nos. 1–3. It differs from cinnabar by black color, the absence of cleavage, as well as optical properties. In reflected light, metacinnabar is light gray, isotropic and has no internal reflections. In assemblage no. 4, it occurs more often and composes

larger grains (up to 0.5 × 0.5 cm) in carbonates (calcite, dolomite) associating with cinnabar, coloradoite, pyrite, realgar, sphalerite, stibnite, aktashite, routhierite, and baryte (Fig. 9k). It has high Zn contents (Table 4). The isomorphic incorporation of Zn in metacinnabar is also reflected in a PXRD pattern. Each strong reflection ([*d*, Å (*I*)]: 3.318(100), 2.865(80), 2.028(20), 1.735(80), 1.438(20), 1.325(30), 1.175(20), 1.106(20)) is lower by 0.2–0.7 Å than the corresponding reflection of a synthetic cubic HgS phase. Thus, the unit cell volume of metacinnabar from the Vorontsovskoe deposit (Table 3) is significantly smaller than the volume of the synthetic phase: 188 Å^3 versus 200 Å^3. In some cases, the Zn–Mn-bearing metacinnabar forms cubic crystals up to 30 μm or the outer zones 0.08–0.1 mm thick around the Hg–Mn-bearing sphalerite (Fig. 8f).

The chemical compositions of both sulfides are given in Table 4. Vasiliev (2011), who studied solid solutions in the Zn–Hg–S system, concluded on the absence of a continuous isomorphic series in cubic ZnS–HgS sulfides and a miscibility gap in an intermediate range from $(Zn_{0.752}Hg_{0.248})S$ to $(Hg_{0.539}Zn_{0.461})S$. Our data confirm these conclusions; moreover, metacinnabar from the Vorontsovskoe deposit contains 15 wt. % Zn (or 15.4 wt. % when recalculated without Mn and normalized to 100 wt. %), which is close to the maximum possible Zn concentration in metacinnabar (17.7 wt. %).

Molybdenite MoS_2 was recognized in bornite-chalcopyrite ores from diorite skarn zones (Vikentyev et al., 2016). We found it as small oval inclusions up to 20 μm in calcite with pyrite, realgar, sphalerite, dalnegroite, christite, coloradoite, metacinnabar, routhierite, and philrothite in assemblage no. 1. Optically, molybdenite is reliably identified by very strong (especially, in immersion) bireflectance typical for this mineral and very intense anisotropy in light and dark gray and deep black tones. The chemical composition of the mineral is stoichiometric (wt. %): 60.14 Mo, 39.17 S, total 99.31. Its empirical formula based on three atoms is $Mo_{1.02}S_{1.98}$.

Orpiment As_2S_3 is abundant in brecciated limestones and is always associated with more common realgar. The macroscopically visible orpiment aggregates are locally responsible for a lemon yellow color of the ore. The individual anhedral orpiment grains are rare. Its tiny acicular crystals up to 0.3 mm long enclosed in limestone fragments are more abundant. The mineral was identified by chemical composition and XRD data. It contains Sb up to 4.4 wt. % (Sazonov et al., 1991a). Later, orpiment was found in the carbonate breccia matrix as individual grains up to 1 mm, locally, with realgar inclusions (Murzin, Varlamov, 2010; Vikentyev et al., 2016).

In our samples, orpiment in all seven mineral assemblages is confined to carbonate breccias, where it makes a matrix for gangue minerals together with pyrite, realgar and, locally, arsenopyrite, and stibnite. In assemblage no. 3, orpiment is one of the major ore minerals. In assemblage no. 6, it occurs together with realgar forming spectacular yellow red veins in native arsenic nodules (Fig. 9l). In our samples, orpiment contains only <1.5 wt. % Sb (Table 4). The calculated parameters of the monoclinic unit cell are given in Table 3.

Pararealgar As_4S_4 was found in samples from off-balance ore stockpile no. 2 as bright orange powdery aggregates, which partly replace bright red realgar on fragments of carbonate breccias (Fig. 10a). Pararealgar belongs to assemblage no. 2. The associated ore minerals include vorontsovite, ferrovorontsovite, galkhaite, boscardinite, écrinsite, routhierite, stibnite, cinnabar, coloradoite, metacinnabar, pyrite, and sphalerite. The gangue minerals are calcite, Mn-bearing dolomite, and baryte. The identification of pararealgar is confirmed by both EMPA (Table 4) and SXRD (Table 3). Optically, pararealgar is similar to realgar. In reflected light, it looks dull gray; the bireflectance is distinct. Anisotropy is strong and is better observed in slightly crossed-polarized light. In completely crossed-polarized light, it is masked by abundant yellow and orange internal reflections. Pararealgar is known as a product of light-induced transformation of realgar (Bonazzi et al., 1995, Bindi et al., 2003) in oxidized contiditions. Therefore, it is likely that pararealgar formed directly in the ore stockpile. This is the first reliable find of pararealgar in the Russian Federation.

Picotpaulite $TlFe_2S_3$ is the only sulfide with species-defining Tl found at the deposit. It was identified in two polished sections in assemblages nos. 3 and 4 as rare small (no more than 15 × 12 μm) inclusions in gangue minerals of breccias (calcite, dolomite, baryte, clinochlore) and intergrowths with realgar. In assemblage no. 3, picotpaulite is also associated with gladkovskyite, native gold, and routierite and, in assemblage no. 4, it occurs together with chabournéite, christite, cinnabar, coloradoite, metacinnabar, orpiment, parapierrotite, and pyrite (Fig. 8g). In reflected light, the mineral is creamy pinkish and, in aggregates with realgar, it looks much brighter than the latter. Bireflectance is distinct. Picotpaulite is strongly anisotropic in gray-violet tones. Its chemical composition is

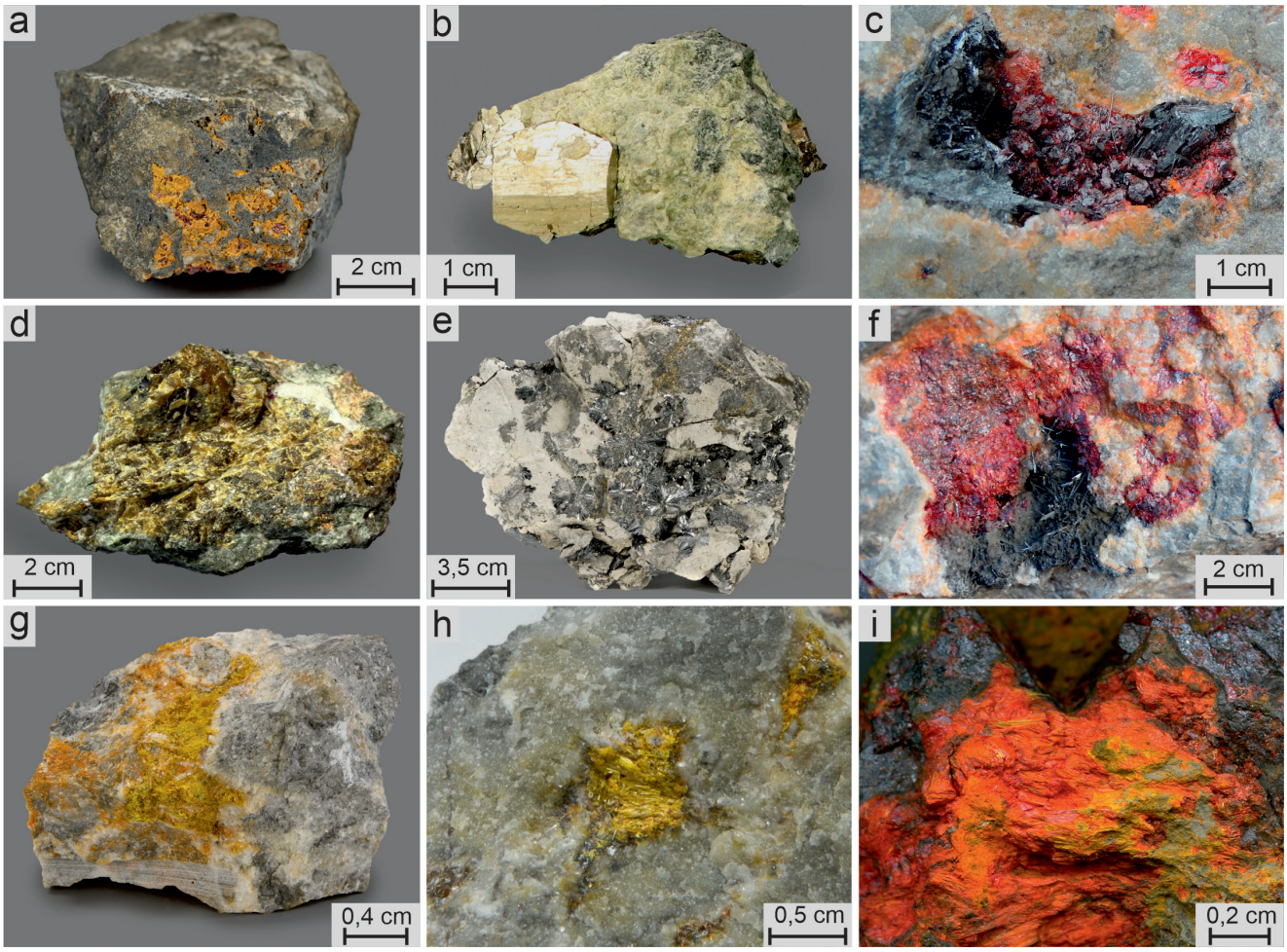

Fig. 10. Sulfides of the Vorontsovskoe deposit, part II:

a – bright orange pararealgar crusts on deep red realgar in carbonate breccia; b – pyrite crystal in carbonate matrix with pigeonite; c – dark red realgar crystals with gray stibnite in a cavity of silicified limestone; d – massive yellow–brown sphalerite; e – radial aggregates of lead gray stibnite crystals on dolomite and calcite in assemblage with golden yellow pyrite; f – acicular stibnite crystals up to 1 cm in cavities of carbonate matrix with bright red realgar; g – bright yellow fibrous wakabayashilite crystals in calcite and dolomite with dark pyrite and stibnite; h – bright yellow wakabayashilite in breccia; i – yellow fibrous wakabayashilite colored by bright red powdery realgar.

Collections of A.V. Kasatkin (a, e, g, h), Museum «Shtufnoi Kabinet», Severouralsk (b, d, f, i), V.V. Levitskiy (c). Photo: A.D. Kasatkina (a, e, g, h), M.V. Tsyganko (b, d, f, i), V.V. Levitskiy (c).

close to the ideal formula $TlFe_2S_3$ (Table 4). This is the first finding of picotpaulite in the Russian Federation.

Pyrite FeS_2 is the major ore mineral of various rocks of the deposit. In metasomatites, its content is 1–10 %, but often is <1 %. Several morphological varieties of pyrite of various sizes are known. Abundant pyrite grains of 0.01–0.1 mm in size occur as fine inclusions in other minerals; metacrystals up to several millimeters in size are less common. The calcite–grossular skarns host pyrite crystals up to 1 cm in size. In quartz veins in beresites and listvenites, pyrite is characterized by two generations: cubic pyrite-1 crystals 0.5–1 mm (rarely up to 5 mm) in size and small (about 0.1–0.2 mm) pyrite-2 crystals of complex morphology. Pyrite typically contains numerous microinclusions of other ore minerals, mainly, chalcopyrite and pyrrhotite. Together with magnetite, pyrite is the only ore mineral of unaltered skarns, where it occurs as irregular interstitial aggregates up to several millimeters in size. In altered skarns, pyrite forms large (1–10 mm) aggregates and often crystals of complex morphology in quartz–calcite matrix. It forms dissemination of crystals 0.1–0.3 mm (locally, up to 2 cm) in size in propylitized rocks or in matrix of ore breccias. Pyrite is the major ore mineral of altered volcanosedimentary rocks, where its content, together with arsenopyrite,

reaches 20–30 wt. %. Pyrite forms metacrystals of 0.05–3 mm in size and replaces shell walls of mollusks or rock-forming minerals. Pyrite is extremely abundant in carbonate breccia matrix in form of metacrystals and crystal aggregates up to 1.5 cm in size (Sazonov et al., 1991a). In a sample from the dumps of the southern open pit, we found a well-formed pyrite crystal of an atypical light silvery color 25 × 25 mm in size in an aggregate of calcite, dolomite, and pigeonite (Fig. 10b). Pyrite of the deposit contains up to 1.1 wt. % Co, Ni, and As (Sazonov et al., 1991a; Murzin, Varlamov, 2010; Vikentyev et al., 2016).The results of XRD analyses of pyrite from mineral assemblages nos. 1 and 9 are given in Table 3.

Pyrrhotite $Fe_{1-x}S$ is a rare mineral of the deposit (Sazonov et al., 1991a; Vikentyev et al., 2016). It was found as inclusions up to 0.5 mm in sphalerite and at the contact of sphalerite and galena in wollastonite skarns.Pyrrhotite together with chalcopyrite forms aggregates up to several centimeters in altered skarns. In the breccia matrix, it occurs as rare crystals up to 0.1 mm in carbonates, rounded or drop-like inclusions up to 0.05 mm in size in earlier pyrite, arsenopyrite or sphalerite.

Realgar AsS is the major ore mineral in breccias, where it is disseminated in limestone fragments and is responsible of a reddish color of breccia. Its small-sized (up to 0.2 mm) and larger (up to 5 mm) individuals are characterized by angular anhedral morphology and occur between carbonate. Realgar locally fills microfractures in pyrite metacrystals. The largest realgar aggregates often contain inclusions of pyrite, sphalerite, and Tl and Hg sulfosalts (Sazonov et al., 1991a). The free-standing realgar crystals up to 0.5 cm in size were found at the main ore stockpile (Fig. 10c). According to Murzin and Varlamov (2010), realgar contains Sb (up to 1.6 wt. %). We found that realgar melts during the EMPA under standard conditions for sulfides and sulfosalts (WDS, 25 kV, 20 nA, 1 μm). Satisfactory analytical conditions for chemical analyses of realgar were achieved at a lower accelerating voltage of 15 kV and a beam rastering at a 10 × 10 μm area. In most assemblages, realgar contains only As and S (Table 4). The parameters of the monoclinic unit cell are given in Table. 3.

Sphalerite ZnS is one of the major ore minerals of the deposit. Together with galena, it forms aggregates 2–3 cm in size in wollastonite skarns. In altered skarns, sphalerite occurs as veins or inclusions in pyrite and typically contains small chalcopyrite and pyrrhotite grains. In breccia matrix, it forms euhedral and anhedral aggregates 0.05–0.4 mm in size enclosed in carbonates or quartz and intergrown with baryte, pyrite, and fahlores. Sphalerite often contains (up to) Hg (23.1 wt. %), Mn (4.9 wt. %), Fe (8.5 wt. %), Cd (1.3 wt. %), Cu (0.7 wt. %), and Ag (0.4 wt. %) (Sazonov et al., 1991a; Murzin, Varlamov, 2010). The Mn-bearing sphalerite (up to 7.6 wt. % Mn) was described as rounded and oval inclusions up to 50–70 μm in size in native arsenic and arsenopyrite (Murzin et al., 2011).

Samples from the dumps of the southern open pit and off-balance ore stockpile no. 2 contain dark green sphalerite aggregates up to 20 cm in size with galena inclusions. This sphalerite contains only Zn and S. The yellow–brown sphalerite from samples of the main ore stockpile (Fig. 10d) is also nearly trace element-free (Table 4, an. 28). The parameter of its cubic unit cell is given in Table 3. In assemblage no. 4, the Hg–Mn-bearing sphalerite grains up to 0.2 mm in size are enclosed in carbonates (dolomite, calcite) and are often surrounded by rims of Zn–Mn-bearing metacinnabar up to 40 μm thick (Fig. 8f). The chemical composition of this sphalerite is given in Table 4, an.27. In reflected light, Hg–Mn-bearing sphalerite shows dark red internal reflections.

Stibnite Sb_2S_3 is widely abundant at the deposit. In ore breccias, it occurs as acicular crystals up to 0.2 mm long or anhedral aggregates up to 3 mm, locally forms intergrowths with zinkenite and chalcostibite and contains inclusions of native gold and native arsenic. Stibnite was determined by its optical properties and chemical composition. It often contains As (up to 3.5 wt. %) (Sazonov et al., 1991a). Murzin and Varlamov (2010) described this mineral as rare grains and anhedral aggregates in carbonates ~0.1 mm in size, which it is often intergrown with Hg and Tl sulfosalts. It contains up to 7.5 wt. % As.

In a large specimen from ore zone of the northern open pit, stibnite forms spectacular radial aggregates up to 2 cm in diameter of lead gray prismatic and acicular crystals, which are located in an open cavity of the dolomite–calcite rock in assemblage with pyrite and arsenopyrite (Fig. 10e). In assemblage no. 4, stibnite is the major ore mineral in addition to pyrite and realgar. It forms acicular crystals up to 1 cm in size and irregular grains intergrowing with orpiment and realgar in the dolomite–calcite rock (Fig. 10f). Stibnite contains numerous small inclusions of various Pb–Cu–Ag-bearing sulfosalts (andorite, tennantite-(Zn), zinkenite), coloradoite, and native arsenic as well (Fig. 8h). The chemical composition of stibnite in given in Table 4 and its XRD data are provided in Table 3.

Tetradymite Bi_2Te_2S was found in skarns in assemblage no. 8 as rounded grains up to 40 μm in size at the contact with magnetite and calcite (Fig. 8i). The chemical composition of tetradymite is close to stoichiometric (Table 4).

Wakabayashilite $(As,Sb)_6As_4S_{14}$ was first identified in samples collected in the main ore stockpile (Kasatkin, 2019). It belongs to assemblage no. 1 and is associated with cinnabar, getchellite, orpiment, pyrite, realgar, stibnite, and rare Tl- and Hg-bearing sulfosalts, which occur as tiny inclusions in wakabayashilite: boscardinite, chabournéite, coloradoite, dalnegroite, écrinsite, parappierrotite, routhierite, etc. Wakabayashilite is one of the most spectacular minerals of the deposit. It occurs as columnar and fibrous aggregates and irregular crystals up to 2 cm in size in calcite–dolomite marble (Figs. 10g–i). Wakabayashilite is bright yellow to yellow-orange with a strong silky luster. Perfect cleavage is observed along {010}, {100}, and {101}. In reflected light, the mineral is grayish white; it is weakly anisotropic with abundant internal lemon yellow reflections. Wakabayashilite was also detected in assemblage no. 2, where it forms rare small (no more than 50 μm in size) inclusions in carbonates together with vorontsovite and ferrovorontsovite. The chemical composition (Table 4) and the orthorhombic unit cell parameters of wakabayashilite from both assemblages (Table 3) correspond to this mineral.

Sulfosalts

This mineral group is unambiguously of great interest, because it is the largest in terms of a number of mineral species identified at the Vorontsovskoe deposit. Sulfosalts include all Vorontsovskoe type locality minerals and most first findings of previously unknown minerals at the territory of the Russian Federation. The most sulfosalts are found in carbonate breccias characterized by the ultimate variety of mineral species.

Aktashite $Cu_6Hg_3As_4S_{12}$ was first described by Sazonov et al. (1991a) as anhedral, rarely euhedral light gray aggregates up to 0.05 mm across in limestones. The mineral was identified by its optical properties and chemical composition. It contains Zn (up to 2.0 wt. %), Cd (up to 0.9 wt. %), and Fe (up to 0.5 wt. %). Murzin and Varlamov (2010) reported on the aktashite grains up to 0.15 mm in size intergrown with sphalerite, baryte, chabournéite, and other Tl sulfosalts, which were found in the carbonate matrix and siliceous fragments of breccias. The mineral contains up to 3.9 wt. % Zn and up to 2.8 wt. % Sb.

We identified aktashite in five mineral assemblages. Its largest aggregates (up to 0.2 mm in size) are typical of assemblage no. 1 at the contact of orpiment and gangue minerals (prehnite, calcite) and as intergrowths with sphalerite (Fig. 11a). In assemblage no. 4, aktashite occurs as anhedral grains up to 50 μm across enclosed in carbonates (calcite, dolomite) and is observed together with cinnabar, coloradoite, parapierrotite, routhierite, sphalerite and stibnite. In other assemblages, aktashite composes individuals 20–30 μm in size in gangue minerals of breccias. In reflected light, the mineral looks light gray, brighter than orpiment and sphalerite, but darker than all other neighboring ore minerals. In general, the effects of anisotropy in the air are weak, but, in some grains of aktashite from assemblage no. 1, they are distinct, in brownish tones, much stronger in immersion. According to chemical composition (Table 5), aktashite contains Zn, Fe, and Mn (all isomorphic to Hg) and up to 2.6 wt. % Sb (= 0.35 apfu) (a gruzdevite component). The parameters of the hexagonal unit cell (Table 4) correspond to aktashite.

Nowackiite $Cu_6Zn_3As_4S_{12}$, a Zn analog of aktashite, was determined in two specimens from assemblages nos. 1 and 4. In sample Vor-SS-6, nowackiite occurs as tiny (less than 10 μm in size) grains in diopside and pyrite and is associated with écrinsite, native gold, orpiment, parapierrotite, realgar, baryte and fluorapatite. In sample VD-7.1b, a small nowackiite zone (Table 5) was detected in a 40-μm inclusion of Zn-rich aktashite in prehnite with parapierrotite, pyrite, and realgar. Optically, nowackiite is indistinguishable from aktashite. This mineral was found for the first time in the Russian Federation.

Andorite $AgPbSb_3S_6$ was found in polymineral sulfosalt veinlets up to 5 mm thick in limestones and as small inclusions in bournonite (Vikentyev et al., 2016). One chemical analysis given in this work shows a deficiency of Ag (9.3 wt. % = 0.73 apfu) and the presence of Fe (2.8 wt.% = 0.43 apfu) and Cu (1.0 wt. % = 0.13 apfu).

We identified andorite in assemblages nos. 1 and 4, where it forms small (<15 μm in size) inclusions in stibnite with orpiment (Fig. 11b), coloradoite, realgar, tennantite-(Zn), zinkenite, and native arsenic. In reflected light, andorite is white, almost indistinguishable from the host stibnite in its lightest position; however, when the table is rotated by 90°, weakly bireflectant andorite becomes clearly visible in comparison with gray stibnite in its darkest position. In crossed polars, the difference between weakly anisotropic andorite and

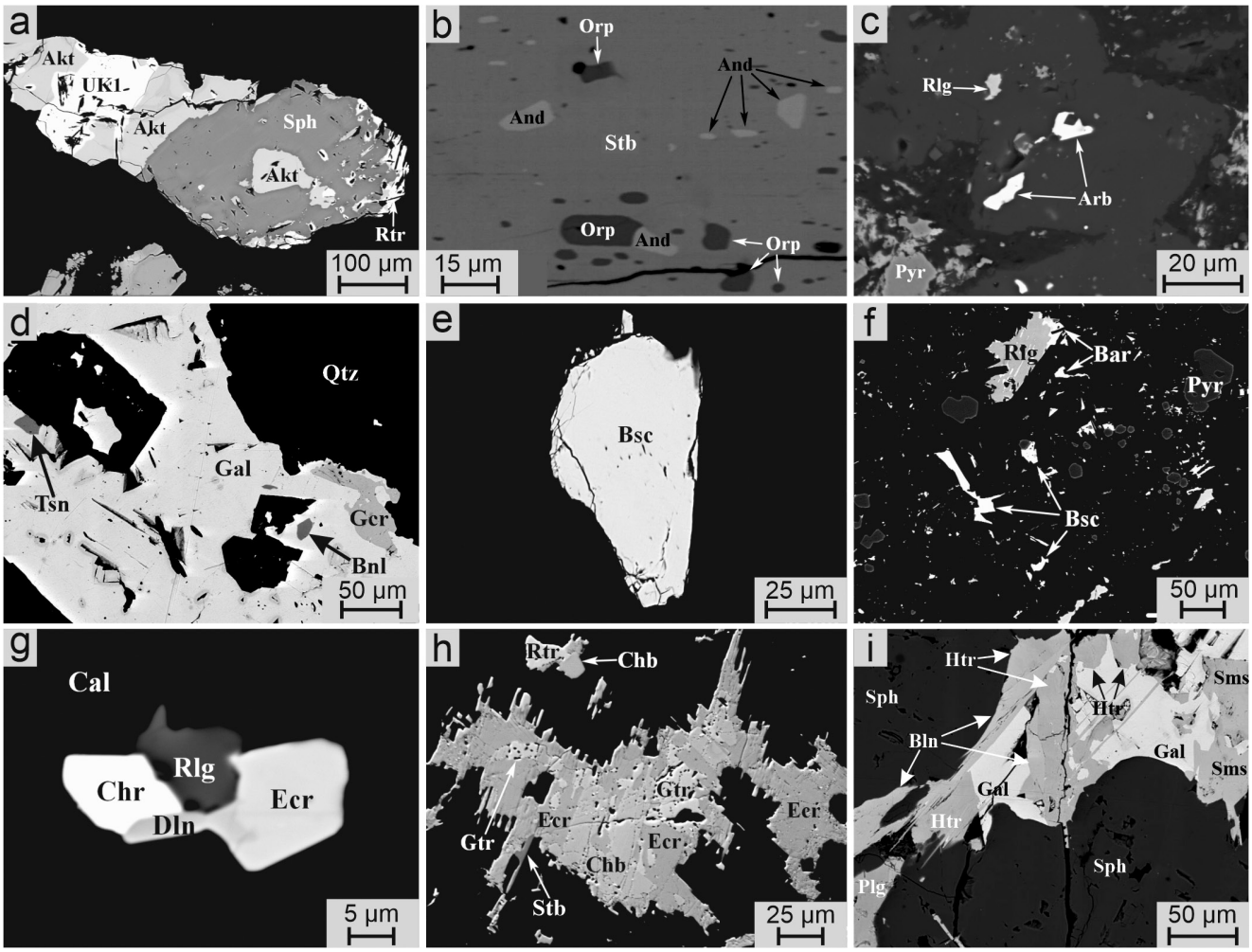

Fig. 11. Sulfosalts of the Vorontsovskoe deposit, part I:

a – aktashite intergrown with Mn–Hg-bearing sphalerite, an unnamed phase I (UK1), and routhierite in calcite; b – andorite and orpiment inclusions in stibnite; c – auerbakhite inclusions in calcite with realgar and pyrite; d – benleonardite, geocronite, and tsnigriite inclusions in galena with quartz; e – large monomineral boscardinite aggregate in calcite; f – boscardinite crystals and grains in calcite (black) in assemblage with realgar, baryte, and pyrite; g – aggregate of écrinsite with christite, dalnegroite, and realgar in calcite; h – aggregate of écrinsite with chabournéite and guettardite in calcite/dolomite in assemblage with routhierite and stibnite; i – aggregate of boulangerite, heteromorphite, plagionite, semseyite, and galena at the contact of sphalerite with pyrite.

BSE images.

very strongly anisotropic stibnite with bright color effects becomes more pronounced. The composition of the mineral better corresponds to andorite-VI; it contains Cu, Mn, and As in chemical composition (Table 5).

Auerbakhite $MnTl_2As_2S_5$ is one of eight new mineral species found at the deposit (Kasatkin et al., 2021). Its name honors Alexander Andreevich Auerbakh (1844–1916), a Russian mining engineer, manufacturer and mineralogist. At the end of the 19th century, his activities were closely related to the Northern Urals. In 1884, he founded the Turyinsk Mining School at the famous Turyinsk Copper Mines. In 1881–1896, he managed the Bogoslovskiy mining district, developed and improved the copper smelting production of the region. The Auerbakh intrusion and Auerbakh ore district with the Vorontsovskoe gold deposit are also named after him. A.A. Auerbakh is the author of several mineralogical papers published in «Gornyi Zhurnal» («Mining Magazine») and was the first one in Russia, who used microscopic techniques to study minerals.

Samples with auerbakhite were collected directly in the bottom of the northern open pit of the deposit. Auerbakhite occurs in assemblage no. 3 and was found

Table 5

Chemical composition (wt. %) of sulfosalts

An. no.	As. no.	Mineral name	Mn	Fe	Cu	Zn	Ag	Hg	Tl	Pb	As	Sb	S	Total	Formula
1	1	Aktashite	–	1.58	25.48	2.76	–	24.29	–	–	19.80	0.49	25.45	99.85	$Cu_{6.06}(Hg_{1.83}Zn_{0.64}Fe_{0.43})_{2.90}(As_{3.99}Sb_{0.06})_{4.05}S_{11.99}$
2	4		–	–	23.07	–	–	35.13	–	–	16.23	2.60	23.50	100.53	$Cu_{6.01}Hg_{2.90}(As_{3.59}Sb_{0.35})_{3.94}S_{12.14}$
3	5		1.02	–	26.19	3.01	–	25.75	–	–	18.30	0.94	25.38	100.59	$Cu_{6.25}(Hg_{1.95}Zn_{0.70}Mn_{0.28})_{2.93}(As_{3.70}Sb_{0.12})_{3.82}S_{12.00}$
4	4	Andorite	0.14	–	1.00	–	11.89	–	0.08	20.88	3.35	38.74	22.85	99.05	$Ag_{0.93}Pb_{0.85}Cu_{0.13}Mn_{0.02}(Sb_{2.68}As_{0.38})_{3.06}(S_{6.00}Se_{0.01})_{6.01}$
5	1	Arsiccioite	0.11	0.26	3.09	3.81	5.75	27.78	21.83	–	14.34	2.68	20.19	99.84	$(Ag_{0.51}Cu_{0.46})_{0.97}(Hg_{1.32}Zn_{0.56}Fe_{0.04}Mn_{0.02})_{1.94}Tl_{1.02}(As_{1.83}Sb_{0.21})_{2.04}S_{6.02}$
6	3	Auerbakhite	7.34	–	–	–	–	–	51.89	0.50	18.79	–	20.70	99.22	$Mn_{1.04}Tl_{1.97}Pb_{0.02}As_{1.95}S_{5.02}$
7	6	Benavidesite	1.57	1.11	–	–	–	–	–	40.03	–	35.83	21.97	100.51	$Pb_{3.95}Mn_{0.59}Fe_{0.41}Sb_{6.02}S_{14.03}$
8	7		2.64	–	–	–	–	–	–	40.24	1.21	33.60	22.08	99.77	$Pb_{3.97}Mn_{0.98}(Sb_{5.64}As_{0.33})_{5.97}S_{14.08}$
9	–	Benleonardite	–	–	0.68	–	63.07	–	–	–	1.12	7.12	8.47	99.50	$Ag_{15.67}Cu_{0.29}(Sb_{1.57}As_{0.40})_{1.97}Te_{4.00}S_{7.08}$
10	1	Bernardite	–	–	–	–	–	–	22.80	–	21.34	29.58	27.08	100.80	$Tl_{1.05}(As_{2.69}Sb_{2.29})_{4.98}S_{7.97}$
11	2		–	–	–	–	–	–	21.40	0.13	25.32	25.39	27.98	100.22	$Tl_{0.96}Pb_{0.01}(As_{3.10}Sb_{1.92})_{5.02}S_{8.01}$
12	3		–	–	–	–	–	–	25.55	0.22	42.25	1.31	30.07	99.40	$Tl_{1.07}Pb_{0.01}(As_{4.82}Sb_{0.09})_{4.91}S_{8.01}$
13	1	Boscardinite	–	–	–	–	2.01	–	12.60	17.82	12.19	30.86	24.22	99.70	$Ag_{0.89}Tl_{2.95}Pb_{4.11}(Sb_{12.12}As_{7.78})_{19.90}S_{36.14}$
14	1		0.14	0.20	0.02	–	1.51	–	12.60	21.32	12.19	29.16	24.52	101.71	$Ag_{0.66}Fe_{0.17}Mn_{0.12}Cu_{0.01}Tl_{2.92}Pb_{4.87}(Sb_{11.33}As_{7.70})_{19.03}S_{36.19}$
15	1		0.08	0.25	–	–	1.53	–	12.81	20.87	12.22	29.12	24.46	101.33	$Ag_{0.67}Fe_{0.21}Mn_{0.07}Tl_{2.97}Pb_{4.78}(Sb_{11.35}As_{7.74})_{19.09}S_{36.20}$
16	1		–	–	–	–	1.66	–	13.53	18.50	13.16	29.41	24.28	100.54	$Ag_{0.73}Tl_{3.15}Pb_{4.25}(Sb_{11.49}As_{8.36})_{19.85}S_{36.03}$
17	1		–	0.15	–	–	1.51	–	12.71	19.15	13.51	27.06	24.06	98.13	$Ag_{0.68}Fe_{0.13}Tl_{3.01}Pb_{4.47}(Sb_{10.74}As_{8.71})_{19.45}S_{36.27}$
18	1		0.13	0.07	–	–	1.54	–	12.23	21.89	14.38	25.93	25.14	101.34	$Ag_{0.67}Mn_{0.11}Fe_{0.06}Tl_{2.79}Pb_{4.93}(Sb_{9.93}As_{8.95})_{18.88}(S_{36.56}Se_{0.02})_{36.58}$
19	1		0.15	0.05	0.02	–	1.74	–	12.64	21.77	15.27	25.12	25.1	101.87	$Ag_{0.75}Mn_{0.13}Fe_{0.04}Cu_{0.02}Tl_{2.87}Pb_{4.87}(Sb_{9.57}As_{9.45})_{19.02}(S_{36.30}Se_{0.01})_{36.31}$
20	2		0.14	0.03	0.02	–	1.49	–	13.23	21.53	15.44	25.13	24.75	101.77	$Ag_{0.64}Mn_{0.12}Fe_{0.03}Cu_{0.02}Tl_{3.02}Pb_{4.85}(Sb_{9.64}As_{9.62})_{19.26}S_{36.05}$
21	5		0.14	–	0.02	–	1.51	–	12.60	21.32	12.19	29.16	24.52	101.46	$Ag_{0.66}Mn_{0.12}Cu_{0.01}Tl_{2.93}Pb_{4.88}(Sb_{11.37}As_{7.72})_{19.09}S_{36.30}$
22	–	Boulangerite	–	–	–	–	–	–	–	55.53	–	25.92	19.07	100.52	$Pb_{4.98}Sb_{3.96}S_{11.06}$
23	–		–	–	–	–	–	–	–	54.84	–	26.02	18.85	99.85	$Pb_{4.96}Sb_{4.00}S_{11.01}Se_{0.03}$
24	–	Bournonite	–	–	13.63	–	–	–	–	44.30	6.60	14.78	20.49	99.80	$Pb_{1.00}Cu_{1.01}Sb_{0.57}As_{0.41}S_{3.00}$
25	1	Chabournéite	–	–	–	–	–	–	18.47	11.15	13.89	32.97	25.22	101.70	$Tl_{7.81}Pb_{4.65}Sb_{23.41}As_{16.03}S_{68.00}$
26	2		–	–	–	–	–	–	17.47	10.96	13.86	32.89	24.85	100.03	$Tl_{7.50}Pb_{4.64}Sb_{23.70}As_{16.23}S_{68.00}$
27	5		0.03	–	0.01	–	0.07	–	18.85	10.31	16.61	29.83	25.46	101.17	$Ag_{0.06}Mn_{0.05}Cu_{0.01}Tl_{7.90}Pb_{4.26}Sb_{20.98}As_{18.98}S_{68.00}$
28	1	Christite	–	–	–	–	–	34.5	35.73	–	12.62	–	16.40	99.25	$Tl_{1.02}Hg_{1.01}As_{0.98}S_{2.99}$
29	1		–	–	–	–	–	33.36	35.65	0.28	13.25	0.08	17.03	99.65	$Tl_{1.00}Hg_{0.95}Pb_{0.01}As_{1.01}S_{3.03}$
30	4		–	–	–	–	–	34.64	36.01	–	12.55	–	16.49	99.69	$Tl_{1.03}Hg_{1.01}As_{0.98}S_{2.99}$
31	5	Clerite	13.77	–	–	–	–	–	–	–	4.64	51.91	30.87	101.19	$Mn_{1.03}(Sb_{1.75}As_{0.25})_{2.00}S_{3.96}$
32	–	Cupropolybasite	–	–	18.05	–	54.04	–	–	–	–	11.59	17.01	100.69	$Ag_{9.00}Cu_{1.00}(Cu_{4.84}Ag_{1.30})_{6.14}Sb_{1.96}S_{10.91}$
33	1	Dalnegroite	–	–	–	–	0.12	2.22	20.14	10.95	26.58	14.80	26.12	100.93	$Ag_{0.05}Hg_{0.46}Tl_{4.06}Pb_{2.18}As_{14.63}Sb_{5.01}S_{33.61}$
34	1		–	–	–	–	0.10	–	19.53	10.39	23.13	21.08	26.36	100.59	$Ag_{0.04}Tl_{3.95}Pb_{2.74}As_{12.77}Sb_{7.16}S_{34.01}$
35	1		0.02	0.04	0.20	0.20	0.19	0.03	18.25	11.79	17.63	28.25	25.27	101.89	$Cu_{0.14}Zn_{0.13}Ag_{0.08}Fe_{0.03}Mn_{0.02}Tl_{3.80}Pb_{2.42}As_{10.00}Sb_{9.87}S_{33.52}$
36	2		0.03	–	–	–	0.07	–	18.85	10.31	17.61	27.83	25.96	100.66	$Ag_{0.03}Mn_{0.03}Tl_{3.91}Pb_{2.11}As_{9.95}Sb_{9.68}S_{34.29}$

An. no.	As. no.	Mineral name	Mn	Fe	Cu	Zn	Ag	Hg	Tl	Pb	As	Sb	S	Total	Formula
37	2	Dalnegroite	–	–	–	–	–	–	19.20	9.99	21.04	23.43	25.82	99.48	$Tl_{3.97}Pb_{2.04}As_{11.86}Sb_{8.13}S_{34.01}$
38	3	Dalnegroite?	0.30	–	–	–	–	–	24.38	0.27	22.34	25.24	26.98	99.51	$Mn_{0.21}Tl_{4.87}Pb_{0.07}As_{12.14}Sb_{8.43}S_{34.28}$
39	3	(«protodalnegroite»)	0.07	–	0.02	–	–	–	20.78	7.71	19.53	26.47	26.19	100.77	$Mn_{0.05}Cu_{0.01}Tl_{4.25}Pb_{1.56}As_{10.90}Sb_{9.09}S_{34.15}$
40	1	Dewitite	–	–	–	–	–	–	23.10	0.25	16.08	35.12	26.30	100.85	$Tl_{9.37}Pb_{0.10}Sb_{23.91}As_{17.79}S_{68.00}$
41	1	Drechslerite	–	–	–	–	–	–	53.46	–	5.17	24.73	16.80	100.19	$Tl_{3.96}(Sb_{3.07}As_{1.04})S_{7.93}$
42	1		–	–	–	–	–	–	54.67	–	7.24	20.62	17.09	99.62	$Tl_{4.01}(Sb_{2.54}As_{1.45})S_{8.00}$
43	–	Dufrénoysite	–	–	–	–	–	–	–	55.98	15.43	6.87	21.37	99.65	$Pb_{2.03}(As_{1.55}Sb_{0.42})_{1.97}S_{5.00}$
44	1	Écrinsite	–	0.23	–	–	1.64	–	14.17	16.50	16.50	26.06	24.67	99.77	$Ag_{0.71}Fe_{0.19}Tl_{3.23}Pb_{3.71}(As_{10.27}Sb_{9.99})_{20.26}S_{35.89}$
45	1		–	0.25	–	–	1.55	–	8.72	26.04	17.84	20.78	24.28	99.62	$Ag_{0.68}Fe_{0.21}Tl_{2.01}Pb_{5.93}(As_{11.24}Sb_{8.06})_{19.30}(S_{35.76}Se_{0.10})_{35.86}$
46	2		0.30	–	–	–	1.21	–	8.41	30.71	15.74	19.92	24.77	101.06	$Ag_{0.53}Mn_{0.26}Tl_{1.95}Pb_{7.01}(As_{9.94}Sb_{7.74})_{17.68}S_{36.56}$
47	5		–	–	–	–	0.18	0.27	13.77	20.03	19.83	20.70	25.79	100.57	$Ag_{0.08}Hg_{0.06}Tl_{3.07}Pb_{4.40}(As_{12.05}Sb_{7.74})_{19.79}S_{36.61}$
48	2	Enneasartorite	–	–	–	–	–	–	6.69	35.05	18.94	14.83	24.08	99.59	$Tl_{6.11}Pb_{31.60}(As_{47.22}Sb_{22.75})_{69.97}S_{140.31}$
49	2	Ferrovorontsovite	–	9.89	3.95	1.16	0.45	25.13	12.93	0.04	17.83	2.15	24.91	99.28	$[(Fe_{2.74}Hg_{1.94}Zn_{0.27})_{4.95}(Cu_{0.96}Ag_{0.06})_{1.02}](Tl_{0.98}Cs_{0.05})_{1.03}$ $(As_{3.68}Sb_{0.27}Te_{0.05})_{4.00}S_{12.00}$
50	2	Galkhaite	–	2.47	3.25	0.91	–	45.20	5.05	–	15.96	1.24	21.58	100.43	$[(Hg_{4.01}Fe_{0.79}Zn_{0.25})_{\Sigma5.05}Cu_{0.91}]_{5.96}(Cs_{0.64}Tl_{0.44})_{1.08}(As_{3.79}$ $Sb_{0.18})_{3.97}S_{11.99}$
51	–	Geocronite	–	–	–	–	–	–	–	67.58	4.37	9.80	17.23	98.98	$Pb_{13.99}(Sb_{3.45}As_{2.50})_{5.95}S_{23.05}$
52	3	Gillulyite	–	–	–	–	–	–	29.49	0.19	40.02	1.73	29.52	100.95	$Tl_{2.04}Pb_{0.01}(As_{7.54}Sb_{0.21})_{7.75}S_{13.00}$
53	3	Sb-gillulyite?	0.12	–	–	–	–	–	24.54	1.27	21.47	26.95	26.73	101.08	$Tl_{1.86}Pb_{0.10}Mn_{0.03}(As_{4.44}Sb_{3.43})_{7.87}S_{12.93}$
54	3	Gladkovskyite	8.28	–	–	–	–	–	30.04	0.23	31.80	2.27	28.58	101.20	$Mn_{1.01}Tl_{0.99}Pb_{0.01}As_{2.86}Sb_{0.13}S_{6.00}$
55	1	Guettardite	–	–	–	–	–	–	5.14	33.25	13.66	22.30	24.17	98.52	$Pb_{0.86}Tl_{0.13}As_{0.98}Sb_{0.98}S_{4.04}$
56	2		–	–	–	–	–	–	2.45	37.42	15.82	20.06	24.60	100.35	$Pb_{0.95}Tl_{0.06}As_{1.11}Sb_{0.86}S_{4.02}$
57	4		–	0.01	–	–	0.05	–	0.15	39.82	15.73	21.42	24.49	101.67	$Pb_{1.00}As_{1.09}Sb_{0.92}S_{3.98}$
58	2	Gungerite	–	–	–	–	–	–	13.68	–	26.77	30.97	28.02	99.44	$Tl_{0.99}As_{5.29}Sb_{3.77}S_{12.95}$
59	2	Heptasartorite	–	–	–	–	–	–	9.51	31.38	19.21	15.35	23.93	99.38	$Tl_{6.73}Pb_{21.91}(As_{37.10}Sb_{18.24})_{55.34}S_{108.01}$
60	–	Heteromorphite	–	–	–	–	–	–	–	48.69	0.42	30.85	19.65	99.76	$Pb_{7.21}Sb_{7.77}As_{0.17}S_{18.79}Se_{0.06}$
61	–		–	–	–	–	–	–	–	49.37	0.25	30.59	19.95	100.28	$Pb_{7.25}Sb_{7.65}As_{0.10}S_{18.95}Se_{0.05}$
62	1	Hutchinsonite	–	0.10	0.01	0.03	–	–	18.09	18.15	29.79	6.40	25.74	98.31	$Fe_{0.02}Zn_{0.01}Tl_{0.99}Pb_{0.98}(As_{4.44}Sb_{0.59})_{5.03}S_{8.97}$
63	2		–	–	–	–	–	–	18.84	18.51	30.05	5.52	25.93	98.85	$Tl_{1.03}Pb_{0.99}(As_{4.47}Sb_{0.50})_{4.97}S_{9.01}$
64	3		–	–	–	–	–	–	19.14	18.68	31.25	4.73	26.54	100.34	$Tl_{1.02}Pb_{0.98}(As_{4.55}Sb_{0.42})_{4.97}S_{9.03}$
65	3	Imhofite	–	–	–	–	–	–	36.30	–	30.02	8.43	25.37	100.12	$Tl_{5.83}(As_{13.14}Sb_{2.27})_{15.41}S_{25.96}$
66	6	Jamesonite	0.53	1.97	–	–	–	–	–	40.47	–	34.74	21.56	99.27	$Pb_{4.08}Fe_{0.74}Mn_{0.20}Sb_{5.95}S_{14.03}$
67	–		–	2.59	–	–	–	–	–	40.18	–	35.18	21.80	99.75	$Pb_{4.01}Fe_{0.96}Sb_{5.97}S_{14.06}$
68	7	Jordanite	–	–	–	–	–	–	–	69.05	6.90	5.89	17.55	99.39	$Pb_{14.03}(As_{3.88}Sb_{2.04})_{5.92}S_{23.05}$
69	4	Laffittite	–	–	–	–	23.10	40.90	–	–	15.95	–	20.16	100.11	$Ag_{1.02}Hg_{0.97}As_{1.01}S_{2.99}$
70	8	Lillianite	–	–	0.22	–	6.54	–	–	27.72	–	–	16.80	101.39	$Pb_{1.52}Ag_{0.69}Cu_{0.04}Bi_{2.67}(S_{5.95}Se_{0.13})_{6.08}$
71	3	Lorándite	–	–	–	–	–	–	58.49	0.42	20.57	0.45	19.37	99.30	$Tl_{0.98}Pb_{0.01}(As_{0.94}Sb_{0.01})_{0.95}S_{2.06}$

72	5	Luboržákite	21.23	–	0.29	–	0.56	–	–	1.90	15.25	27.03	33.23	99.49	$Mn_{1.86}Pb_{0.04}Ag_{0.03}Cu_{0.02}As_{0.98}Sb_{1.07}S_{5.00}$
73	5	Pb-luboržákite?	16.14	–	0.07	–	–	0.05	0.09	9.01	9.20	34.15	29.99	98.70	$Mn_{1.58}Pb_{0.23}Cu_{0.01}As_{0.66}Sb_{1.50}S_{5.02}$
74	1	Manganoquadratite	17.84	–	–	–	30.73	–	–	–	21.78	–	30.06	100.41	$Ag_{0.93}Mn_{1.06}As_{0.95}S_{3.06}$
75	–	Meneghinite	–	–	1.45	–	–	–	–	61.31	–	19.4	17.55	99.71	$Pb_{12.98}Cu_{1.00}Sb_{6.99}S_{24.02}$
76	4	Nowackiite	–	2.03	27.34	6.09	–	15.62	–	–	20.66	1.73	27.72	101.19	$Cu_{6.00}(Zn_{1.30}Hg_{1.09}Fe_{0.51})_{2.90}(As_{3.85}Sb_{0.20})_{4.05}S_{12.06}$
77	1	Oyonite	3.09	0.03	0.15	–	10.62	0.25	0.17	24.64	8.77	28.57	24.49	100.78	$Mn_{1.78}Fe_{0.02}Ag_{3.11}Cu_{0.07}Hg_{0.04}Pb_{3.75}Tl_{0.03}Sb_{7.41}As_{3.69}S_{24.11}$
78	4	Parapierrotite	–	–	–	–	–	–	19.49	–	2.02	54.78	24.14	100.43	$Tl_{1.01}(Sb_{4.75}As_{0.28})_{5.03}S_{7.95}$
79	4		–	–	–	–	–	–	19.01	0.31	2.4	54.91	24.34	101.00	$Tl_{0.97}Pb_{0.02}(Sb_{4.72}As_{0.33})_{5.05}S_{7.95}$
80	4		–	–	–	–	–	–	19.20	0.26	2.77	54.10	24.39	100.82	$Tl_{0.98}Pb_{0.01}(Sb_{4.65}As_{0.39})_{5.04}S_{7.96}Se_{0.01}$
81	4		–	–	–	–	–	–	19.75	0.55	3.49	53.77	24.64	102.29	$Tl_{1.00}Pb_{0.03}(Sb_{4.57}As_{0.48})_{5.05}S_{7.90}Se_{0.01}$
82	4		–	–	–	–	–	–	19.02	0.35	3.73	52.63	24.09	99.82	$Tl_{0.98}Pb_{0.02}(Sb_{4.55}As_{0.53})_{5.08}S_{7.92}$
83	4		–	–	–	–	–	–	20.1	–	8.61	46.08	25.17	99.96	$Tl_{1.00}(Sb_{3.85}As_{1.17})_{5.02}S_{7.98}$
84	4		0.06	–	0.04	–	0.08	–	20.56	0.27	11.90	41.43	24.65	98.99	$Tl_{1.03}Pb_{0.01}Mn_{0.01}Cu_{0.01}Ag_{0.01}(Sb_{3.47}As_{1.62})_{5.09}S_{7.84}$
85	4		–	–	–	–	–	–	22.69	–	15.32	35.46	25.75	99.22	$Tl_{1.10}(Sb_{2.89}As_{2.03})_{4.92}S_{7.98}$
86	2		–	–	–	–	–	–	20.32	–	15.70	38.09	26.84	100.95	$Tl_{0.95}(Sb_{3.00}As_{2.01})_{5.01}S_{8.03}$
87	4		–	–	–	–	–	–	23.05	0.91	16.51	32.89	26.03	99.39	$Tl_{1.11}Pb_{0.04}(Sb_{2.66}As_{2.17})_{4.83}S_{8.01}$
88	5		1.36	–	–	–	–	–	22.4	–	17.09	32.68	26.78	100.31	$Tl_{1.05}Mn_{0.24}Sb_{2.56}As_{2.18}S_{7.98}$
89	5		1.59	–	–	–	–	–	22.58	–	17.55	31.70	26.82	100.24	$Tl_{1.05}Mn_{0.28}Sb_{2.48}As_{2.23}S_{7.96}$
90	8	Pavonite	–	–	0.31	–	11.12	–	–	2.68	–	–	18.20	99.10	$(Ag_{0.92}Cu_{0.04})_{0.96}(Bi_{2.82}Pb_{0.11}Te_{0.01})_{2.94}(S_{5.05}Se_{0.05})_{5.10}$
91	3	Philrothite	–	–	–	–	–	–	33.17	0.59	34.40	3.94	27.06	99.16	$Tl_{0.97}Pb_{0.02}(As_{2.75}Sb_{0.19})_{2.94}S_{5.06}$
92	–	Plagionite	–	–	–	–	–	–	–	40.53	–	38.58	21.48	100.88	$Pb_{4.95}Bi_{0.02}Sb_{8.02}S_{16.96}Se_{0.04}$
93	1	Pokhodyashinite	–	–	4.59	–	3.79	–	27.88	0.42	7.63	32.95	21.89	99.15	$Cu_{0.70}Ag_{0.34}Tl_{1.32}Pb_{0.02}Sb_{2.63}As_{0.99}S_{6.625}$
94	–	Polybasite	–	–	9.05	–	64.60	–	–	–	–	10.75	16.10	100.50	$Ag_{9.00}Cu_{1.00}(Ag_{4.04}Cu_{2.10})_{6.14}Sb_{1.92}S_{10.94}$
95	6	Ramdohrite	2.36	0.74	2.27	0.32	5.75	–	0.80	33.61	2.16	29.91	22.15	100.07	$Ag_{1.83}Mn_{1.47}Cu_{1.23}Fe_{0.45}Zn_{0.17}Tl_{0.13}Pb_{5.57}(Sb_{8.43}As_{0.99})_{9.42}S_{22.03}$
96	1	Rebulite	–	–	–	–	–	–	34.80	0.36	22.98	16.82	24.23	99.19	$Tl_{4.96}Pb_{0.05}(As_{8.94}Sb_{4.03})_{12.97}S_{22.02}$
97	1		–	–	–	–	–	–	36.04	–	20.32	18.89	25.13	100.38	$Tl_{5.09}(As_{7.82}Sb_{4.48})_{12.30}S_{22.61}$
98	3		–	–	–	–	–	–	36.10	0.29	30.63	7.08	25.34	99.44	$Tl_{4.92}Pb_{0.04}(As_{11.39}Sb_{1.62})_{13.01}S_{22.03}$
99	4	Roshchinite	0.16	–	0.02	–	15.7	2.72	0.10	14.16	11.43	30.59	25.07	99.95	$Ag_{18.08}Hg_{1.68}Mn_{0.36}Cu_{0.04}Pb_{8.49}Tl_{0.06}(Sb_{31.21}As_{18.95})_{50.16}S_{97.13}$
100	4		0.15	0.02	0.02	–	15.02	2.98	0.13	14.32	10.69	31.05	25.06	99.44	$Ag_{17.42}Hg_{1.86}Mn_{0.34}Fe_{0.04}Cu_{0.04}Pb_{8.65}Tl_{0.08}(Sb_{31.91}As_{17.85})_{49.76}S_{97.80}$
101	1	Routhierite	0.11	0.08	3.93	3.76	4.70	27.42	21.74	0.17	14.17	2.65	20.28	99.01	$(Cu_{0.59}Ag_{0.42})_{1.01}(Hg_{1.31}Zn_{0.55}Mn_{0.02}Fe_{0.01})_{1.89}Tl_{1.02}Pb_{0.01}(As_{1.81}Sb_{0.21})_{2.02}S_{6.05}$
102	2		–	–	5.92	0.51	0.25	38.87	19.21	–	13.97	1.72	19.03	99.48	$(Cu_{0.94}Ag_{0.02})_{0.96}(Hg_{1.96}Zn_{0.08})_{2.04}Tl_{0.95}(As_{1.89}Sb_{0.14})_{2.03}S_{6.01}$
103	5		–	–	5.98	1.02	0.63	36.52	20.95	0.09	14.52	1.30	18.60	99.61	$(Cu_{0.95}Ag_{0.06})_{1.01}(Hg_{1.84}Zn_{0.16})_{2.00}Tl_{1.04}Pb_{0.01}(As_{1.96}Sb_{0.11})_{2.07}S_{5.87}$
104	–	Semseyite	–	–	–	–	–	–	–	52.78	–	27.92	19.08	99.93	$Pb_{8.95}Sb_{8.06}S_{20.92}Se_{0.07}$
105	1	Sicherite	–	0.10	–	–	23.83	–	22.63	0.22	16.71	13.69	21.61	98.79	$Tl_{0.99}Pb_{0.01}(Ag_{1.97}Fe_{0.02})_{\Sigma1.99}(As_{1.99}Sb_{1.00})_{\Sigma2.99}S_{6.02}$
106	1	Sinnerite	–	–	38.58	–	0.10	–	–	–	29.74	0.27	28.71	97.40	$Cu_{6.06}Ag_{0.01}(As_{3.96}Sb_{0.02})_{3.98}S_{8.94}$

An. no.	As. no.	Mineral name	Mn	Fe	Cu	Zn	Ag	Hg	Tl	Pb	As	Sb	S	Total	Formula
107	1	Stalderite	0.10	–	4.07	8.16	4.92	20.49	22.24	–	15.02	2.50	21.29	98.79	$(Cu_{0.58}Ag_{0.41})_{0.99}(Zn_{1.12}Hg_{0.92}Mn_{0.02})_{2.06}Tl_{0.98}(As_{1.81}Sb_{0.18})_{1.99}S_{5.98}$
108	1	«Tennantite–(Mn)»	2.70	1.82	36.08	0.12	5.79	6.87	–	–	16.70	3.09	26.01	99.18	$(Cu_{9.15}Ag_{0.87}Mn_{0.79}Hg_{0.55}Fe_{0.53}Zn_{0.03})_{11.92}(As_{3.59}Sb_{0.41})_{4.00}S_{13.08}$
109	4	Tennantite–(Zn)	0.01	1.47	39.10	6.35	3.23	0.41	0.04	0.10	13.81	8.53	26.49	99.54	$(Cu_{9.65}Ag_{0.47}Zn_{1.52}Fe_{0.41}Hg_{0.03}Pb_{0.01})_{12.09}(As_{2.90}Sb_{1.10})_{4.00}S_{12.97}$
110	–	«Tetrahedrite–(Mn)»	3.20	2.62	38.80	0.17	0.07	–	–	–	3.25	25.68	26.01	99.80	$(Cu_{9.61}Ag_{0.01}Mn_{0.92}Fe_{0.74}Zn_{0.04})_{11.32}(Sb_{3.32}As_{0.68})_{4.00}S_{12.77}$
111	–	Tsnigriite	–	–	–	–	62.02	–	–	–	–	7.32	5.94	100.09	$Ag_{9.07}Sb_{0.95}Te_{3.07}S_{2.92}$
112	7	Tsygankoite	6.29	–	–	–	–	5.42	26.05	5.84	3.39	30.89	21.87	99.75	$Mn_{8.06}Tl_{8.00}Hg_{1.90}(Sb_{17.87}As_{3.19}Pb_{1.99}Tl_{0.97})_{24.02}S_{48.03}$
113	1	Twinnite	–	–	–	–	–	–	2.80	33.43	12.23	26.63	23.58	98.67	$Pb_{0.87}Tl_{0.07}(Sb_{1.18}As_{0.88})_{2.06}S_{3.98}$
114	5		–	–	–	–	–	–	2.95	34.02	10.40	27.77	24.41	99.55	$Pb_{0.88}Tl_{0.08}(Sb_{1.22}As_{0.74})_{1.96}S_{4.08}$
115	7	Veenite	–	–	–	–	–	–	6.77	45.99	8.72	18.39	21.32	101.19	$Pb_{1.68}Tl_{0.25}(Sb_{1.14}As_{0.88})_{2.02}S_{5.04}$
116	–	Vikingite	–	–	0.58	–	6.07	–	–	28.84	–	–	17.01	99.23	$Ag_{3.28}Cu_{0.53}Pb_{8.13}Bi_{13.03}S_{30.97}Se_{0.05}$
117	2	Vorontsovite	–	5.36	3.42	1.26	0.64	35.70	11.53	0.04	15.98	2.35	22.70	99.76	$[(Hg_{3.02}Fe_{1.63}Zn_{0.33})_{4.98}(Cu_{0.91}Ag_{0.10})_{1.01}]Tl_{0.96}Cs_{0.04})_{1.00}(As_{3.62}Sb_{0.33}Te_{0.05})_{4.00}S_{12.01}$
118	1	Vrbaite	–	0.17	–	–	–	19.72	27.67	0.24	20.20	8.54	22.00	98.54	$Hg_{2.88}Fe_{0.09}Tl_{3.96}Pb_{0.03}As_{7.89}Sb_{2.05}S_{20.09}$
119	3		–	–	–	–	–	20.42	28.52	–	20.61	8.57	22.32	100.44	$Hg_{2.94}Tl_{4.02}As_{7.93}Sb_{2.03}S_{20.08}$
120	1	Weissbergite	–	–	–	–	–	–	51.12	0.69	0.47	31.08	16.53	99.89	$Tl_{0.97}Pb_{0.01}(Sb_{0.99}As_{0.02})_{1.01}S_{2.00}$
121	1		–	–	–	–	–	–	53.31	–	3.42	27.81	16.61	101.15	$Tl_{0.99}(Sb_{0.87}As_{0.17})_{1.04}S_{1.97}$
122	–	Zinkenite	–	–	–	–	–	–	–	31.87	–	45.03	22.64	99.54	$Pb_{9.13}Sb_{21.95}S_{41.92}$
123	1		–	–	–	–	–	–	–	32.91	7.55	35.07	23.90	99.43	$Pb_{8.97}(Sb_{16.26}As_{5.69})_{21.95}S_{42.08}$
124	4		–	–	–	–	–	–	–	32.02	4.28	40.37	23.42	100.09	$Pb_{8.86}(Sb_{19.00}As_{3.27})_{22.27}S_{41.87}$
125	1	UK phase I	2.38	–	–	–	2.53	0.47	10.52	24.48	17.98	16.76	24.96	100.08	$Mn_{1.99}Ag_{1.08}Hg_{0.11}Tl_{2.36}Pb_{5.42}As_{11.01}Sb_{6.32}S_{35.72}$
126	1	UK phase II	3.29	0.30	0.50	–	12.26	0.58	0.11	15.46	8.58	32.83	25.47	99.38	$Mn_{0.91}Ag_{1.73}Cu_{0.12}Fe_{0.08}Hg_{0.04}Tl_{0.01}Pb_{1.14}Sb_{4.11}As_{1.75}S_{12.11}$

Note. The analytical total includes (wt.%): an. 4 – 0.12 Se; an. 9 – 19.04 Te, an. 23 – 0.14 Se; an. 45 – 0.16 Se; an. 50 – 4.77 Cs; an. 59 – 0.15 Se; an. 60 – 0.12 Se; an. 70 – 49.20 Bi, 0.91 Se; an. 80 – 0.09 Se; an. 81 – 0.10 Se; an. 90 – 66.21 Bi, 0.10 Te, 0.48 Se; an. 92 – 0.12 Se, 0.17 Bi; an. 104 – 0.15 Se; an. 49 – 0.40 Te, 0.44 Cs; an. 111 – 24.81 Te; an. 116 – 0.07 Se, 46.66 Bi; an. 117 – 0.02 Se, 0.41 Te, 0.35 Cs. The low analytical total of an. 106 is due to subtraction of pyrite from the matrix. Analysis 110 was taken from (Murzin et al., 2011). Dash – the content of element is below detection limit.

Samples: Vor-8-2 – an. 1, 41; Vor-10-8 – an. 2; Vor-19-01emf – an. 3, 27; SK-18-19 – an. 4, 109; Vor-10/2017-2 – an. 5, 35, 107; VK-27-3 – an. 6, 91; Vor-08-18-13 – an. 7, 66; Vor-10-6 – an. 8, 68; Vor-08/20-20 – an. 9, 51, 111; Vor-8-3 – an. 10; Vor-03/16-6-3 – an. 11, 102; VK-27-4 – an. 12, 53, 54; Vor-10/2017-2b – an. 13, 18, 19; Vor-10/2017-2v – an. 14; Vor-10/2017-2d – an. 15, 17, 44, 105; Vor-01/19-16 – an. 16, 106; Vor-08/20-7 – an. 20, 46, 50; Vor-19-05emf – an. 21; 905B – an. 22; Vor-08/20-22 – an. 23, 60, 61, 92, 104; Vor-08/20-14 – an. 24; Vor-10bis-3c – an. 115; Vor-10/2017-1 – an. 93, 101, 120; Vor-08/20-26 – an. 116; Vor-

in limestone breccias composed of calcite, dolomite, baryte, clinochlore, fluorapatite, and quartz, which are enclosed in realgar, orpiment, and pyrite. Auerbakhite is associated with alabandite, bernardite, christite, cinnabar, coloradoite, dalnegroite, gillulyite, native gold, hutchinsonite, imhofite, lorándite, metacinnabar, philrothite, rebulite, routhierite, sphalerite, and vrbaite. Auerbakhite forms rare small short-prismatic crystals and irregular grains measuring maximum 15 × 5 μm in size (or even smaller) (Fig. 11c). Auerbakhite is transparent and has a bright red color and an adamantine luster. It is brittle, with an uneven fracture. No cleavage was observed. The calculated density is 5.245 g/cm^3. In reflected light, auerbakhite is light gray, weakly bireflectant. It is distinctly anisotropic in light gray and brown tones. The mineral exhibits abundant bright red internal reflections. In transmitted light, auerbakhite is moderately pleochroic from orange-red to dark red. The reflectance spectra are shown in Fig. 12. The reflectance values for the wavelengths recommended by the Commission on Ore Mineralogy of the IMA are (R_{min}/R_{max}, %): 25.2/27.1 (470 nm), 24.0/25.2 (546 nm), 23.7/24.7 (589 nm), 23.0/24.0 (650 nm). The chemical composition of the holotype sample is shown in Table 5. Its empirical formula (based on the atom sum of 10) is $Mn_{1.04}Tl_{1.97}Pb_{0.02}As_{1.95}S_{5.02}$. Auerbakhite is orthorhombic, space group *Cmce*, Z = 8. The unit cell parameters are given in Table 3.

In the Raman spectrum of auerbakhite (Fig. 13a), the most high-force-strength bonds are Mn–S. Bands of *M*–S stretching vibrations in the Raman spectra of pyrite-type compounds MS_2 (*M* = Mn, Co, Ni, Cu, Zn) with 3D systems of vertice-sharing MS_6 octahedra are observed in a range of 380–500 cm^{-1} (Anastassakis, Perry, 1976). Slightly lower frequencies should be expected for auerbakhite, which contains 1D system of MnS_6 octahedra. This conclusion is in agreement with the positions of the strong high-frequency bands observed in a range of 350–400 cm^{-1}. By analogy with the Raman spectra of orpiment and realgar (Forneris, 1969; Minceva-Sukarova et al., 2003), the bands in a range of 300–350 cm^{-1} are assigned to As–S stretching vibrations. The assignment of the Raman bands with wavenumbers below 260 cm^{-1} is ambiguous. These bands possibly correspond to mixed soft modes involving bending vibrations, as well as Tl–S stretching vibrations.

The crystal structure of auerbakhite (Fig. 14) is identical to the structure of a synthetic phase $Tl_2MnAs_2S_5$ (Gostojić et al., 1982). It consists of complex (001) layers based on a set of MnS_4 columns, which

03/16-5-4 – an. 36, 48, 59, 117; Vor-CC-10 – an. 96, 108, 118; VK-27 – an. 119; Vor-01/19-23 – an. 55, 77; Vor-03/16-3-1 – an. 26, 56; Vor-08/18-5 – an. 57, 99, 100; VK-27-1-1 – an. 52; Vor-03/16-6-6 – an. 49, 58; Vor-01/19-15 – an. 29, 33, 34; Vor-03/16-3-5 – an. 37; VK-27-4-1 – an. 38; VK-27-3-1 – an. 39, 64; Vor-08/20-13 – an. 67; Vor-8bis-1 – an. 42; Vor-08/20-9 – an. 43; Vor-01/19-16 – an. 106; VK-27-2 – an. 65; Vor-01/19-10b – an. 31; Vor-2013-8-7b – an. 28; VK-37 – an. 30; Vor-08/20-8 – an. 32, 94; Vor-08/18-19 – an. 69; Kas172 #11 – an. 70, 90; VK-27-4-new – an. 71; Vor-01/19-10g – an. 47, 72, 73; Vor-CC-15 – an. 74; 1365M – an. 75; VD-7.1b – an. 76; 1038P – an. 78; Vor-9-1 – an. 79, 80, 81; Vor-9-2 (940P) – an. 82; VD-20 – an. 83; SK-18-4bis – an. 84; Vor-CC-1a – an. 85; 939P – an. 86; Vor-2 – an. 87; Vor-01/19-1b – an. 88, 89; Vor-08/18-13 – an. 95; Vor-01/19-25 – an. 97; VK-27-4-2 – an. 98; Vor-EMF-6 – an. 103; Vor-CC-5 – an. 113; Vor-2019-4nf – an. 114; Vor-01/19-22 – an. 62; Vor-b/n-9 – an. 63; 287Z – an. 122; Vor-CC-12 – an. 123; Vor-b/n-5 – an. 124; Vor-10-3 – an. 112; Vor-11 – an. 25; VK-23 – an. 40; Vor-CC-07 – an. 45; Vor-01/19-3tf – an. 125; Vor-CC-9 – an. 126.

The mineral formulas are recalculated to atom sum of 4 (weissbergite, lorándite), 6 (bournonite, christite, laffittite, manganoquadratite), 7 (guettrdite, clerite, twinnite), 9 (veenite, dufrénoysite, luboržákite, pavonite, philrothite), 10 (auerbakhite), 11 (andorite, gladkovskyite, lillianite), 12 (arsiccioite, sicherite, routhierite), 14 (bernardite, parapierrotite), 16 (drechslerite, hutchinsonite, tsnigriite, stalderite), 19 (sinnerite), 20 (boulangerite), 22 (phase II), 22.8 (gillulyite), 23 (vorontsovite, galkhaite, gungerite, ferrovorontsovite), 25 (aktashite, benavidesite, jamesonite, nowackiite), 29 (benleonardite, cupropolybasite, polybasite, tennantite-(Zn), «tennantite-(Mn)», «tetrahedrite-(Mn)»), 30 (plagionite), 34 (heteromorphite), 37 (vrbaite), 38 (semseyite), 40 (rebulite), 43 (geocronite, jordanite), 44 (oyonite, ramdohrite), 45 (menegh inite), 47.2 (imhofite), 56 (vikingite), 60 (dalnegroite), 64 (boscardinite, écrinsite, phase I), 73 (zinkenite), 90 (tsygankoite), 176 (roshchinite), 192 (heptasartorite), 248 (enneasartorite). The formulas of chabournéite (an. 25–27) and dewitite (an. 40) are recalculated to 68 S atoms, that of pokhodyashinite (an. 93) to cation sum of 6.

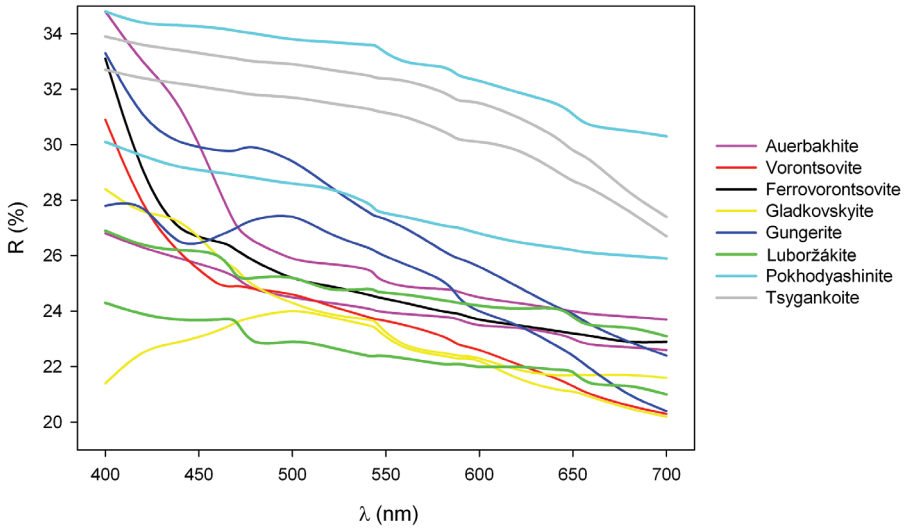

Fig. 12. Reflectance spectra of new sulfosalts from the Vorontsovskoe deposit.

are parallel to [010] and are composed of edge-sharing modestly irregular MnS_6 octahedra. The columns are framed by paired AsS_3 pyramids with lone electron pairs oriented into interlayer space. Highly irregular $Tl2S_6$ coordination polyhedra are situated in the interlayers and share ligands with the layers. Tl1 is part of the complex (001) layer, however, interconnecting the Mn octahedral rods within this particular layer.

Benavidesite $Pb_4MnSb_6S_{14}$ was found for the first time in assemblage no. 7 (Kasatkin et al., 2018b) as intergrowths with sphalerite up to 20 μm in size in calcite with clinochlore. In assemblage no. 6, it forms rounded grains up to 40 μm in size in a vesuvianite–diopside rock. In reflected light, benavidesite is white with a faint greenish tint; bireflectance is distinct in air and strong in immersion. In crossed-polarized light, the mineral is strongly anisotropic in brownish tones. The chemical composition varies depending on the assemblage: in assemblages no. 6 and 7, benavidesite contains significant contents of Fe, which isomorphically substitutes for Mn, and low amount of As, which is isomorphic with Sb, respectively (Table 5). Our finding is probably the first in the Russian Federation.

Jamesonite $Pb_4FeSb_6S_{14}$, a Fe analog of benavidesite, is more common at the deposit. It was first identified by XRD in a sample with boulangerite and bournonite (Sazonov et al., 1991a). Later, jamesonite was found as inclusions <0.5 mm in size in gangue minerals of the breccia matrix, where it intergrows with boulangerite, zinkenite, chalcostibite and stibnite (Vikentyev et al., 2016). In our sample, jamesonite was found in assemblage no. 6, where it occurs as intergrowths with tetrahedrite-(Zn) up to 50 μm in size in carbonates with vesuvianite and diopside. It was also identified in samples from off-balance ore stockpile no. 2 as inclusions up to 0.1 mm in size in pyrite, sphalerite, and carbonates (dolomite, calcite). The optical properties of jamesonite and benavidesite are identical. Jamesonite from assemblage no. 6 contains some amount of Mn in contrast to Mn-free jamesonite from off-balance ore stockpile no. 2 (Table 5).

Benleonardite $Ag_{15}Cu(Sb,As)_2S_7Te_4$ was found by V.V. Murzin (Mineralogy..., 1991) at the western flank of the deposit in a mineralization zone, which is composed of epidote–actinolite–chlorite–carbonate metasomatites with disseminated galena, sphalerite, chalcopyrite, and pyrrhotite. Together with pyrargyrite, benleonardite forms lamellar aggregates up to 0.06 mm in size along the cleavage planes in galena. The mineral was identified by its chemical composition and optical properties. In comparison with the theoretical composition, benleonardite from the Vorontsovskoe deposit is characterized by an almost complete absence of Cu. Recently, Bindi et al. (2015) refined the structure of benleonardite and considered it as a member of the pearceite–polybasite group with Cu as an essential element in its structure. Benleonardite from different localities, including the type material from the Bambolla Mine, Mexico, however, is depleted in Cu or even Cu-free (Stanley et al., 1986; Bindi et al., 2015), similarly to our mineral from Vorontsovskoe deposit.

In our samples, benleonardite was found in calcite–dolomite–quartz aggregates with galena and sphalerite in samples from off-balance ore stockpile no. 2. Benleonardite forms small (up to 20 μm in size) inclusions in galena and is associated with geocronite,

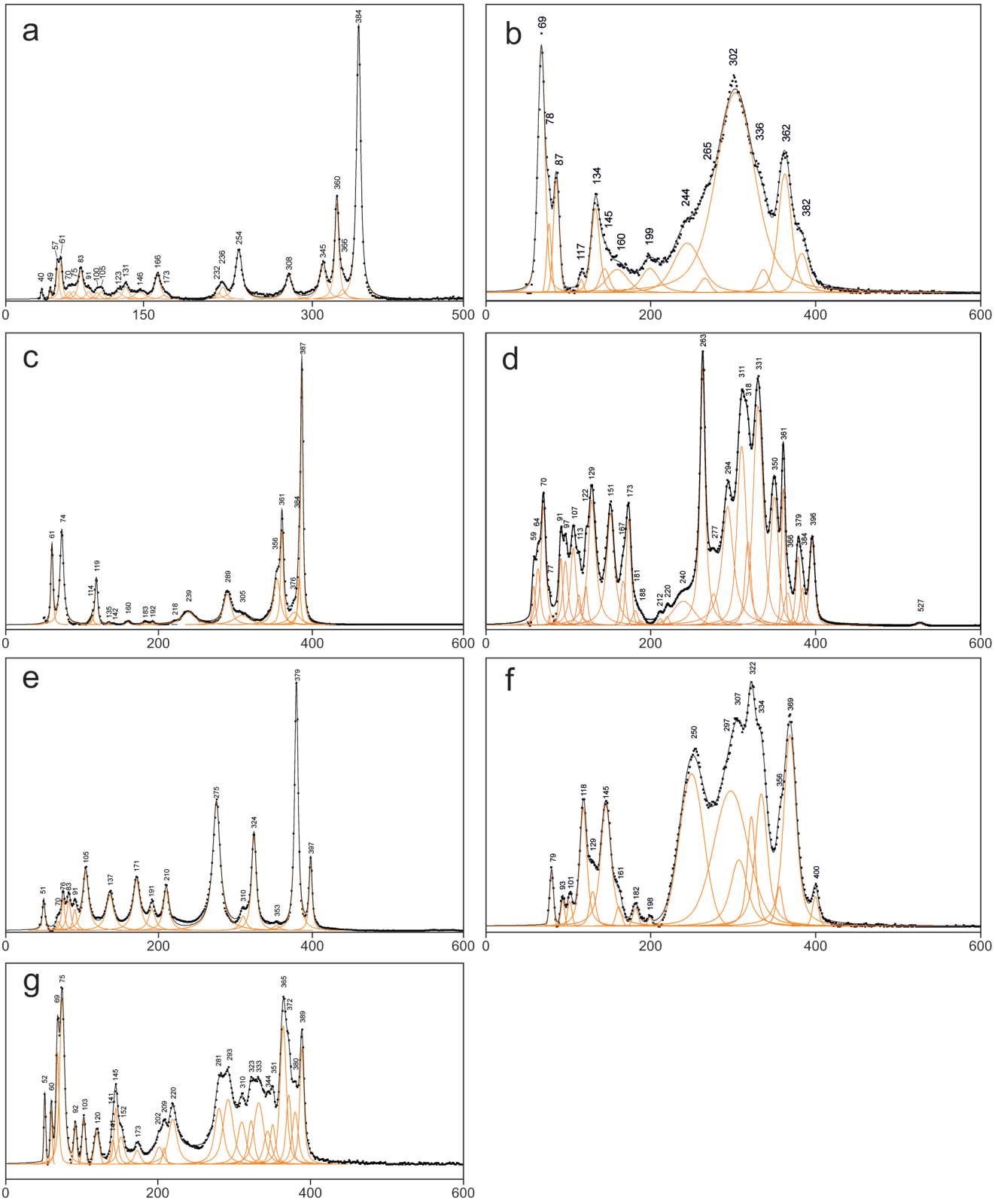

Fig. 13. Raman spectra of sulfosalts from the Vorontsovskoe deposit:

a – auerbakhite; b – gillulyite; c – gladkovskyite; d – gungerite; e – lorándite; f – rebulite; g – hutchinsonite. Intensity and wavenumbers (cm^{-1}) are shown vertically and horizontally, respectively. The measured spectrum is shown by dots. The black curve matching the dots is a result of spectral fit as a sum of individual Voigt peaks (orange).

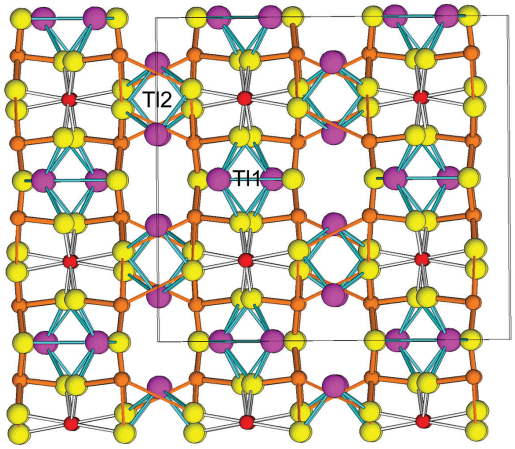

Fig. 14. The crystal structure of auerbakhite projected along [010].

Axis *c* axis is horizontal. Columns of Mn-coordinated octahedra (perpendicular to the projection plane; red spheres) are alternated with Tl1 polyhedra (large mauve spheres) in layers parallel to plane (001). The Tl2 coordination polyhedra (large mauve spheres) are located in interlayers. The As and S atoms of AsS_3 pyramids are shown as orange and lemon yellow spheres, respectively

hessite, and tsnigriite (Fig. 11d). The mineral is also characterized by a deficit of Cu (Table 5). The reflectance of benleonardite is moderate: in reflected light, it looks light gray in comparison with the host white galena, whereas the mineral exhibits distinct anisotropy in brownish and bluish tones.

Bernardite $TlAs_5S_8$ was found for the first time in the Russian Federation in assemblages nos. 1–4 as rare small (up to 50 μm in size) anhedral grains in gangue minerals of breccias (calcite, baryte, clinochlore) and single intergrowths with parapierrotite and vorontsovite. In reflected light, bernardite is light gray; its bireflectance is weak. The effects of anisotropy are very strong in white and brownish tones; the internal reflections are orange-red. The chemical composition of the mineral is heterogeneous: the Sb contents ranges from 1.3 wt. % in assemblage no. 3 to 29.6 wt. % in assemblage no. 1 (Table 5). The monoclinic unit cell parameters of most stoichiometric bernardite from assemblage no. 3 are given in Table 3.

Bernarlottiite $Pb_6(As_5Sb_3)S_{18}$ of a problematic chemical composition was indicated in the gold–pyrite–realgar assemblage as a mineral intergrowing with sphalerite and enclosing enargite (Vikentyev et al., 2016).

Boscardinite and its As-dominant isostructural analogue écrinsite were found for the first time in the Russian Federation in assemblages nos. 1, 2, and 5. Boscardinite was initially described at the Monte Arsiccio Mine (Tuscany, Italy) as a new mineral with formula $TlPb_4(Sb_7As_2)_9S_{18}$ (Orlandi et al., 2012). Further structural studies of new material from the same locality (Biagioni, Moëlo, 2017) revealed a widely variable chemical composition of the mineral up to $AgTl_3Pb_4(Sb_{14}As_6)_{20}S_{36}$ and different occupancy of ten structural sites by Sb and As. In particular, in holotype As was dominant only in one site in contrast to three dominated positions in new material. Despite these chemical and structural differences (including different contents and distribution of Pb and Tl in structural sites), it was the same mineral, boscardinite, with a species-defining feature of $Sb_{tot}>As_{tot}$ (Biagioni, Moëlo, 2017). Écrinsite with the formula $AgTl_3Pb_4As_{11}Sb_9S_{36}$, an As-dominant isostructural analog of boscardinite, was described at the French Jas Roux deposit in the same year (Topa et al., 2017a).

At the Vorontsovskoe deposit, boscardinite and écrinsite show a very broad Sb ↔ As substitution. In assemblage no. 1, they form a solid solution series ranging from $Bsc_{74}Ecr_{26}$ to $Bsc_{17}Ecr_{83}$ with a gap in the écrinsite field from $Bsc_{18}Ecr_{82}$ to $Bsc_{39}Ecr_{61}$ (Fig. 15). Both minerals occur as small anhedral grains (less than 50 μm in size, with some individuals up to 0.2 mm in size) in carbonates and quartz, rims around pyrite grains and aggregates with realgar and various Tl sulfosalts (christite, dalnegroite) (Figs. 11e–11g). In one sample with assemblage no. 1, écrinsite forms a complex 0.3 mm intergrowth with chabournéite, guettardite, and stibnite (Fig. 11h). In assemblages nos. 2 and 5, boscardinite and écrinsite are less common and form aggregates up to 50 μm in size enclosed in Mn-bearing carbonates and realgar and, in assemblage no. 5, they are intergrown with luboržákite and realgar (Fig. 21b). In reflected light, both minerals are white and look light gray at the contact with pyrite that is in agreement with the original data on their reflectance values: at λ = 546 nm R = 32.1–38.0 % for boscardinite (Orlandi et al., 2012) and 35.2–36.7 % for écrinsite (Topa et al., 2017a). Bireflectance is noticeable only in boscardinite (only in most Sb-rich grains). Both minerals are distinctly anisotropic in various tints of gray. No internal reflections are observed. The chemical composition of boscardinite and écrinsite from different assemblages is given in Table 5. Strong reflections of the PXRD pattern of boscardinite are [d, Å (I)]: 3.74(40), 3.55(50), 3.46(40), 2.98(40), 2.81(100), 2.71(90), 2.32(50), 2.18(40). The parameters of the triclinic unit cell of both minerals (SXRD data for écrinsite) are given in Table 3.

Boulangerite $Pb_5Sb_4S_{11}$ was described as acicular crystals up to 1 mm long dispersed in carbonates of breccias or as aggregates up to 1 cm across (Sazonov et al., 1991a; Vikentyev et al., 2016). It is closely associated with bournonite, jamesonite, and fahlores. The mineral was determined by chemical composition and optical properties. One analysis of As-boulangerite exhibits 3.05 wt. % As, thus, the empirical formula of the mineral $Pb_{5.07}Bi_{0.1}Sb_{2.94}As_{0.76}Se_{0.07}S_{11.04}$ formally corresponds to the homeotype of boulangerite, **lopatkaite** $Pb_5Sb_3AsS_{11}$ (Topa et al., 2013). The presence of the latter at the Vorontsovskoe deposit, however, still requires confirmation by XRD studies.

In samples from the dumps of the northern open pit, boulangerite occurs as lead gray hairy and acicular crystals up to 2 cm long in cavities of calcite–dolomite breccias in assemblage with tiny arsenopyrite and chalcopyrite crystals (Fig. 16a). Boulangerite was identified by chemical composition (Table 5) and SXRD data (Table 3). This sulfosalt was also found in an aggregate of sulfantimonites and galena in a sample from the off-balance ore stockpile no. 2. The mineral forms veinlets up to 0.5 mm at the contact with sphalerite and pyrite and aggregates with galena, heteromorphite, and plagionite (Fig. 11i). It has low Se contents (Table 5).

Bournonite $PbCuSbS_3$ was described as anhedral grains or acicular crystals up to 1 mm long in gangue minerals of breccias often intergrown with boulangerite and hosting small andorite inclusions (Sazonov et al., 1991a; Vikentyev et al., 2016). The mineral was identified by chemical composition and optical properties. In our samples, bournonite was found as rare inclusions in native arsenic and lead gray grains up to 5 mm in size in calcite–dolomite marble in assemblage with galena, pyrite, and tetrahedrite-(Zn). Bournonite is enriched in As (up to 6.6 wt. %; 0.41 apfu) (Table 5). The identification of bournonite was confirmed by SXRD data (Table 3).

Chabournéite $Tl_4Pb_2(Sb,As)_{20}S_{34}$**,** recently redefined by CNMNC IMA (Miyawaki et al., 2021), and its As-dominant isostructural analogue **dalnegroite** $Tl_4Pb_2(As,Sb)_{20}S_{34}$ often occur in four assemblages. The size of their grains is typically <0.1 mm. Both minerals form anhedral grains and, rarely, short-prismatic crystals up to 50 μm in size dispersed in ore matrix of breccias (Figs. 17a, 26d, 26k). They are associated with boscardinite–écrinsite, christite, cinnabar, guettardite, parapierrotite, realgar, and routhierite and form inclusions in these minerals (Figs. 11g, 11h) or epitaxial overgrowths on stibnite. Both minerals are opaque, have black color and metallic luster. In reflected light,

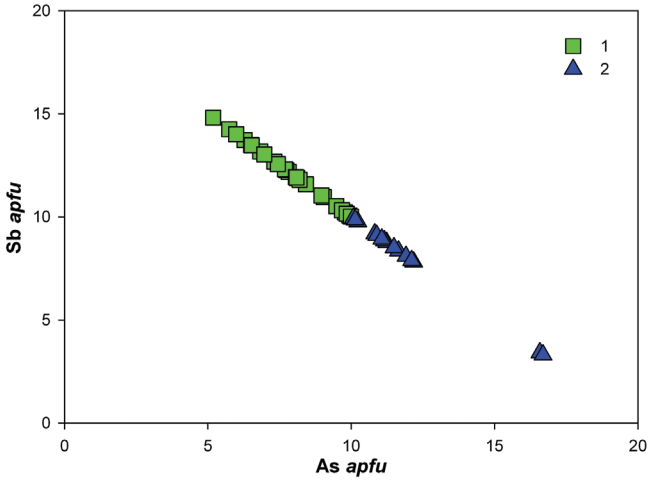

Fig. 15. Sb–As correlation in boscardinite (1) and ecrinsite (2).

they are white, but dalnegroite has slightly higher reflectance values. The bireflectance of both minerals is distinct. In crossed-polarized light, these sulfosalts are strongly anisotropic in brownish and bluish gray tones, with red internal reflections, which are especially distinct in immersion.

The chemical composition of chabournéite and dalnegroite is given in Table 5. The parameters of the triclinic cell of chabournéite according to SXRD data are given in Table 3. The strongest reflections of the PXRD pattern of dalnegroite from assemblage no. 1 are [*d*, Å (*I*)]: 3.918(100), 3.774(50), 3.614(50), 3.128(50), 2.932(40), 2.869(60), 2.572(30), 2.101(60). The calculated parameters of its triclinic unit cell are shown in Table 3 No 34. In assemblage no. 2, dalnegroite and chabournéite form an extended series of solid solutions (data of 61 analysis), they often transit into each other even within the same grain. This series extends from $Dln_{63}Chb_{37}$ to $Dln_{26}Chb_{74}$ with two gaps in $Dln_{27}Chb_{73}$–$Dln_{33}Chb_{67}$ and $Dln_{43}Chb_{57}$–$Dln_{46}Chb_{54}$ ranges (Fig. 18).

Our finding of dalnegroite is the first at the territory of the Russian Federation. As for chabournéite, it was first mentioned by Murzin and Varlamov (2010) among Tl sulfosalts included in carbonate breccias of the deposit. The mineral was conditionally ascribed to chabournéite based on chemical analysis. Later, chabournéite was described as anhedral grains up to 0.5 mm in size together with other Tl sulfosalts in late hydrothermal parageneses of carbonate breccias (Vikentyev et al., 2016). The Tl minerals are associated with aktashite, sphalerite, and baryte.

In one sample of assemblage no.1, large (up to 0.4 × 0.1 mm in size) prismatic crystals and grains of a cha-

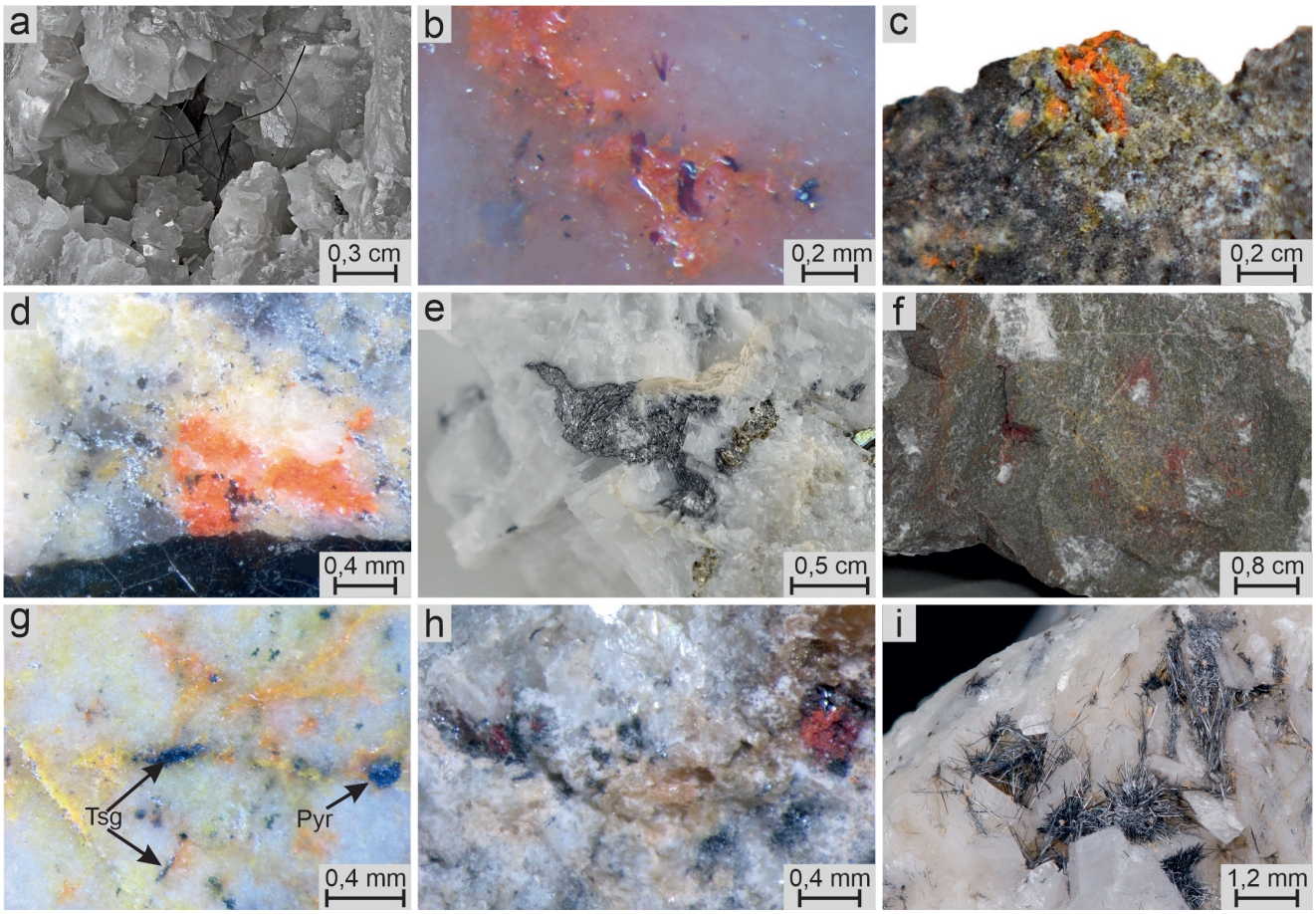

Fig. 16. Sulfosalts of the Vorontsovskoe deposit, part II:

a – lead gray hairy boulangerite crystals in the cavity of calcite–dolomite breccia; b – dark cherry red prismatic gladkovskyite crystals in carbonate aggregates with orange realgar; c – bright orange gungerite aggregates on carbonate breccia covered by a black greigite film ; d – bright orange gungerite in calcite and dolomite; e – lead gray meneghinite in calcite with pyrite; f – dark red routhierite aggregates in dolomite–calcite matrix; g – elongated lath-like tsygankoite crystals in white dolomite/calcite with veinlets of orange orpiment/realgar and pyrite; h – black vorontsovite–ferrovorontsovite grains in calcite and dolomite with red cinnabar; i – lead gray acicular zinkenite crystals in calcite.

Collection of A.V. Kasatkin. Photo: T.V. Pashko (a), A.V. Kasatkin (b, d, g, h), A.D. Kasatkina (c, e, f), M.D. Milshina (i).

bournéite-like mineral were found in calcite associated with quartz, realgar (Fig. 17b), aktashite, coloradoite, native gold, orpiment, parapierrotite, pyrite, routhierite, stibnite, baryte, and prehnite. A specific feature of this mineral is the lack of Pb in chemical composition and higher Tl and Sb contents. Despite that $2Pb^{2+} \leftrightarrow Tl^{+} + Sb^{3+}$ substitution is typical of chabournéite, a Pb-free variety was described only once at the Jas Roux deposit in France without structural studies (Johan et al., 1981) in contrast to Pb-rich chabournéite (Biagioni et al., 2015). The crystal structure of the Pb-free end-member of the homeotypic chabournéite family was first solved by us using crystals from the above sample (Makovicky et al., 2021). Soon after our paper was published, the CNMNC IMA approved the chabournéite group (Miyawaki et al., 2021), where chabournéite *sensu stricto* was redefined as a Pb-rich mineral with the formula $Ag_zTl_{8-x-z}Pb_{4+2x}Sb_{40-x-y}As_yS_{68}$ (with $0.00 \le x \le 0.40$, $16.15 \le y \le 19.11$, $0.04 \le z \le 0.11$), whereas our «Pb-free end-member of the chabournéite homeotypic family» became identical to the new mineral **dewitite** (Topa et al., 2021b) by both chemical composition (Table 5) and SXRD data (Table 3). Our finding of dewitite is also first in the Russian Federation.

Assemblage no. 3 hosts another phase chemically similar to dalnegroite. It forms short-prismatic crystals up to 60 × 5 μm in size, as well as anhedral and euhedral grains up to 0.15 mm in size in calcite, orpiment, and realgar and often intergrowths with pyrite and routhierite. Macroscopically, this phase has

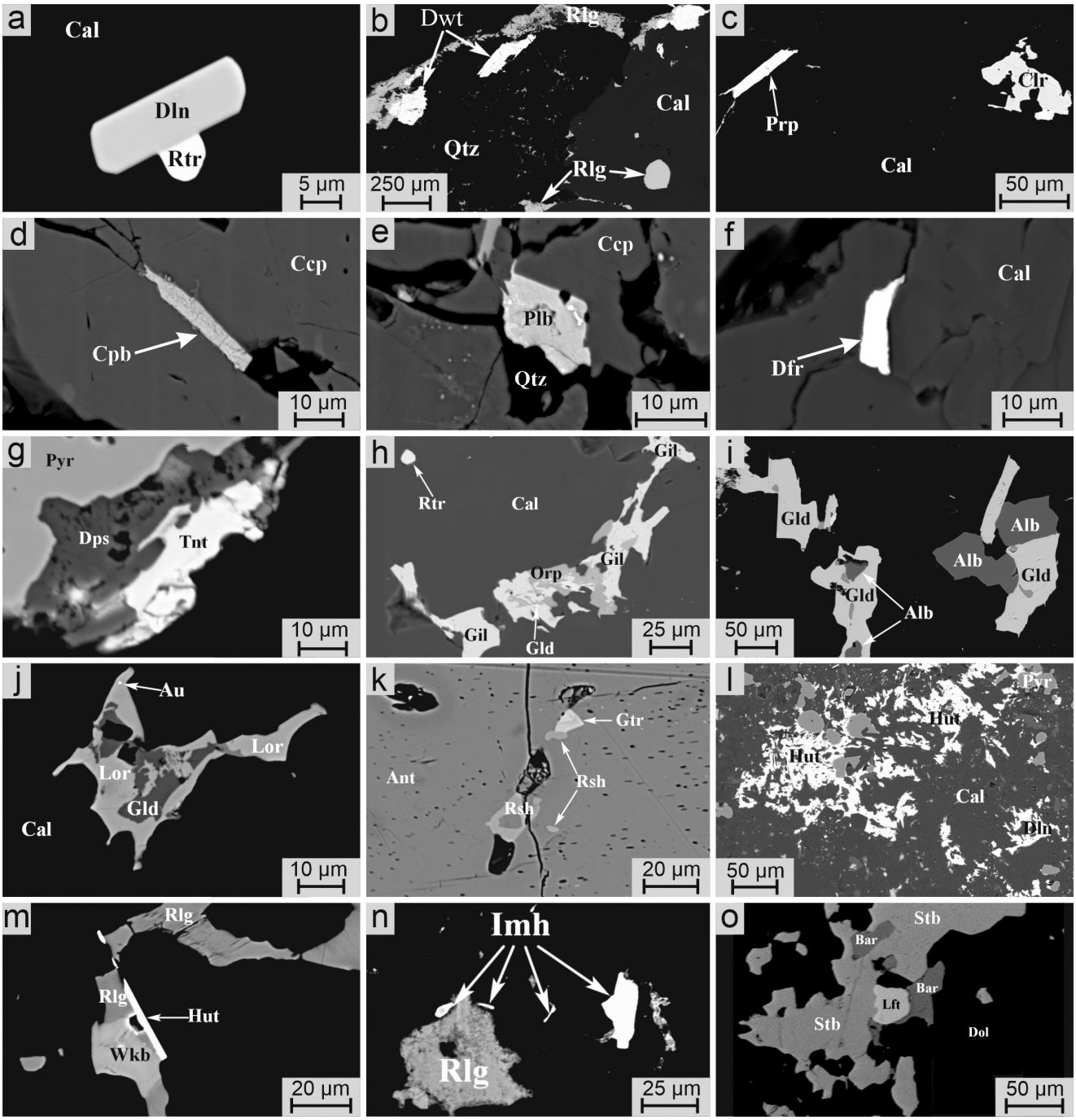

Fig. 17. Sulfosalts of the Vorontsovskoe deposit, part III:

a – short-prismatic dalnegroite crystal intergrown with routhiérite in calcite; b – dewitite crystals and grains in quartz and calcite with realgar; c – clerite and parapierrotite grains in calcite; d – prismatic cupropolybasite crystal in chalcopyrite; e – polybasite grain between chalcopyrite and quartz; f – short-prismatic dufrénoysite crystal in calcite; g – «tennantite-(Mn)» and diopside rim around pyrite crystal; h – intergrowths of gillulyite with orpiment and gladkovskyite in calcite with a small routhierite grain; i – pseudomorphs of gladkovskyite after alabandite in calcite; j – gladkovskyite and lorandite aggregate in calcite; k – small guettardite and roshchinite inclusions in stibnite; l – dendritic hutchinsonite aggregates in calcite with dalnegroite and pyrite; m – acicular hutchinsonite crystal at the contact with wakabayshilite and realgar in calcite; n – imhofite and realgar grains in calcite; o – laffittite grain at the contact of stibnite with baryte in dolomite.

BSE images.

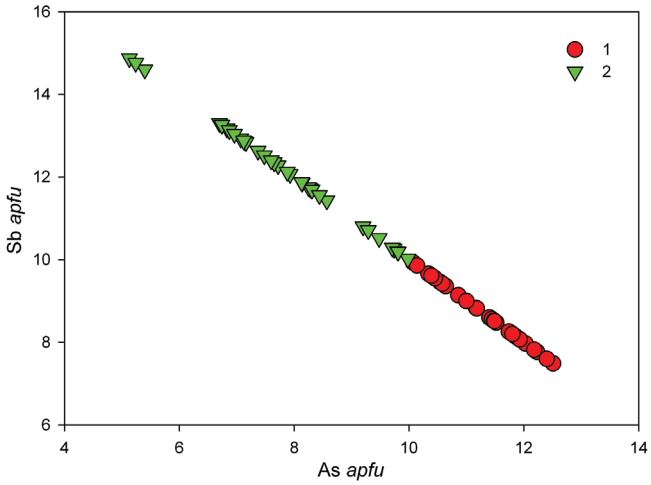

Fig. 18. As–Sb correlation in dalnegroite (1) and chabournéite (2) of the Vorontsovskoe deposit.

a black color and metallic luster; it is opaque, brittle, with an uneven fracture. Cleavage is absent. In reflected light, it is white with a faint pinkish tint, the reflectance values are lower than those of pyrite (R = 54 %), but higher than those of routhierite (R = 28–30 %). Bireflectance is distinct. This phase is strongly anisotropic in bluish gray and brownish tones. Its chemical composition is characterized by widely variable Pb contents from Pb-free to Pb-rich varieties (Table 5 an. 38–39). The parameters of the triclinic unit cell of the Pb-free variety according to SXRD data (Table 3 No. 35) allow us to refer it to the chabournéite group (Miyawaki et al., 2021). A Sb branch of this group currently includes four mineral species: chabournéite (Johan et al., 1981; Biagioni et al., 2015; Makovicky et al., 2021; Miyawaki et al., 2021), protochabournéite (Orlandi et al., 2013; Miyawaki et al., 2021), dewitite (Topa et al., 2021b; Makovicky et al., 2021), and shimenite (Topa et al., 2021a), whereas an As branch contains only dalnegroite (Nestola et al., 2009; Bindi et al., 2010). The unit cell parameters with a volume four time smaller than that of dalnegroite and the chemical composition indicate that the phase from assemblage no. 3 could be the As analog of protochabournéite («protodalnegroite»).

Chalcostibite $CuSbS_2$ was identified as 0.05–0.2 mm grains of stoichiometric composition overgrowing large (up to 5 mm) stibnite aggregates in limestone breccias (Sazonov et al., 1991a).

Christite $TlHgAsS_3$ was found in assemblages nos. 1, 3, and 4. It forms rounded grains up to 20 μm in size in gangue matrix of breccias (carbonates, armenite, baryte, clinochlore, muscovite, prehnite) (Fig. 11g). It is typically associated nearly with all abundant ore minerals of above assemblages, as well as other Tl- and Hg-bearing sulfosalts. Christite is bright orange to dark orange, translucent, with an adamantine luster. Cleavage is perfect on {010}. The mineral is grayish white with a bluish tint and is distinctly anisotropic in brownish tones. The orange-red internal reflections are observed. The mineral is stoichiometric (Table 5). The identification is confirmed by SXRD data (Table 3). This is the first reliable finding of this mineral at the territory of the Russian Federation.

Clerite $MnSb_2S_4$ is the first new mineral described at the Vorontsovskoe deposit (Murzin et al., 1996). This Mn-analog of berthierite $FeSb_2S_4$ was found in silicified limestones from the core drilled in the central part of the deposit. Clerite occurs as isometric grains 0.01–0.2 mm in size, is mostly included in realgar or intergrown with aktashite and alabandite, and is associated with As-bearing pyrite, orpiment, stibnite, cinnabar, greigite, sphalerite, fahlores, zinkenite, chalcostibite, routhierite, and native gold. Murzin and Varlamov (2010) noted the constant presence of As (up to 5 wt. %) in the composition of the mineral.

In our samples, clerite was found in assemblage no. 5 as anhedral grains up to 80 μm in size in Mn-bearing calcite and dolomite (Fig. 17c) and as tiny inclusions in baryte. Clerite is associated with luboržákite, aktashite, alabandite, boscardinite, chabournéite, native gold, orpiment, parapierrotite, pyrite, realgar, routhierite, Hg-Mn-bearing sphalerite, stibnite, and twinnite. In reflected light, clerite is white with a faint yellowish tint. Bireflectance is distinct in the air and strong in immersion. The effects of anisotropy are strong in yellow-brown tones. Clerite contains up to 4.6 wt. % As (Table 5). The parameters of the orthorhombic unit cell according to SXRD data (Table 3) are close to those calculated from PXRD by (Murzin et al., 1996).

Cupropolybasite $[Cu_6Sb_2S_7][Ag_9CuS_4]$ and **polybasite** $[Ag_9CuS_4][(Ag,Cu)_6(Sb,As)_2S_7]$, two isostructural minerals of the polybasite series, were found in a sample consisting of calcite, quartz, chalcopyrite, pyrite, galena, and sphalerite, which was collected at the off-balance ore stockpile no. 2. Cupropolybasite forms long prismatic crystals up to 30 × 5 μm in size enclosed in chalcopyrite (Fig. 17d) and polybasite occurs as tabular crystals and grains up to 15 ×10 μm in size at the contact between chalcopyrite or pyrite and quartz (Fig. 17e). In addition to these minerals, this sample contained jalpaite and tetrahedrite-(Fe). Cupropolybasite and polybasite from the deposit are characterized by a wide isomorphism between Cu and Ag. Table 5 shows the chemical composition of the Cu-richest cupropoly-

basite and Ag-richest polybasite. The optical properties of both minerals are almost identical. Their reflectance values are significantly lower than those of host chalcopyrite and pyrite, thus, at the contact with them, cupropolybasite and polybasite look gray. Bireflectance and anisotropy effects in greenish and lilac tones are clearly visible in immersion. At high magnification, especially in immersion, cupropolybasite exhibits dark red internal reflections. The finding of cupropolybasite is probably the first in the Russian Federation.

Dufrénoysite $Pb_2As_2S_5$ was tentatively identified in sample Vor-08/20-9 collected at off-balance ore stockpile no. 2 as rare inclusions up to 15 μm in size in calcite (Fig. 17f) in assemblage with native gold, pyrite, diopside, and fluorapatite. The mineral contains up to 6.9 wt. % Sb (Table 5). Its optical properties are consistent with dufrénoysite: white in reflected light and anisotropic in grayish violet tones.

Enargite Cu_3AsS_4 was mentioned in a gold–pyrite–realgar assemblage (Vikentyev et al., 2016), however, the chemical analyses most likely correspond to a mineral mixture.

Enneasartorite $Tl_6Pb_{32}As_{70}S_{140}$ and **heptasartorite** $Tl_7Pb_{22}As_{55}S_{108}$ were determined in sample Vor-03/16-5-4 of assemblage no. 2 on the basis of chemical composition (Table 5). They compose rare prismatic crystals and grains up to 20 μm in size in a calcite-dolomite rock and are associated with minerals of the chabournéite–dalnegroite and vorontsovite–ferrovorontsovite series, cinnabar, parapierrotite, pyrite, routhierite, and stibnite. The optical properties (white color and distinct anisotropy) correspond to minerals of the sartorite group. Both minerals were previously unknown at the territory of the Russian Federation.

Fahlores at the deposit form aggregates of rounded grains up to 0.1–0.3 mm in size in carbonates and are often intergrown with stibnite, pyrite, and zinkenite (Sazonov et al., 1991a). The Ag-rich fahlores rim bournonite, boulangerite, chalcopyrite, and sphalerite. Small (up to 0.05 mm) fahlore crystals are locally enclosed in sphalerite. The chemical analyses provided by (Sazonov et al., 1991a) demonstrate a wide isomorphism between both the formally monovalent (Cu and Ag) and divalent (Fe and Zn) components. Their recalculation yields the compositions corresponding to seven members of the tetrahedrite group in accordance with a recently approved nomenclature (Biagioni et al., 2020): **tennantite-(Fe), tennantite-(Zn), tetrahedrite-(Fe), tetrahedrite-(Zn), argentotetrahedrite-(Fe), argentotetrahedrite-(Zn),** and **kenoargentotetrahedrite-(Zn)**.

Murzin et al. (2011) reported on fahlores of variable composition as rounded or oval inclusions up to 50–70 μm in size in native arsenic and arsenopyrite. Despite the presence of As-rich fahlores, both tennantite and tetrahedrite are recorded. The recalculated compositions correspond to tennantite-(Zn), tetrahedrite-(Zn), and a possibly new mineral «tetrahedrite-(Mn)» (Table 5). We also found the Fe-dominant members of the group in the same mineral assemblage: tennantite-(Fe) and tetrahedrite-(Fe). Tennantite-(Zn) was also identified as a rare accessory mineral in assemblages nos. 1, 4, 5, 7, and 9. In samples from assemblage no. 4, it composes anhedral grains and elongated inclusions up to 80 μm in stibnite with native arsenic (Fig. 8h), andorite, coloradoite, orpiment, realgar, and zinkenite. Assemblage no. 9 contains the largest (up to 2 × 2 cm) steel gray tennantite-(Zn) aggregates in quartz cavities with bayldonite, hemimorphite, malachite, and pyrite. This tennantite-(Zn) contains low amounts of Fe and Ag (Table 5) and the parameter of its cubic unit cell (Table 3) corresponds to the structural type of fahlores.

In assemblage no. 1, we found an elongated grain 40 × 15 μm in size at the margin of pyrite crystal overgrown by diopside, which corresponds to «tennantite-(Mn)», another possible new member of the tetrahedrite group (Fig. 17g; Table 5).

Geocronite $Pb_{14}(Sb,As)_6S_{23}$ was first mentioned by Sazonov et al. (1991a). It forms aggregates <0.1 mm in size in gangue minerals of breccias or intergrowths with galena and arsenopyrite. The mineral was ascribed to geocronite on the basis of a ratio between main components and optical properties. Vikentyev et al. (2016) showed that the mineral contains a significant amount of As (up to 3.8 wt. % = 2.21 apfu). We found geocronite in samples with calcite–dolomite–quartz aggregates, galena, and sphalerite collected at off-balance ore stockpile no. 2. Geocronite forms anhedral grains up to 0.1 mm enclosed in galena or at the contact of the latter with quartz and is associated with benleonardite, hessite, and tsnigriite (Fig. 11d). The As content in the mineral reaches 4.4 wt. % (Table 5).

Jordanite $Pb_{14}(As,Sb)_6S_{23}$ was tentatively identified in assemblage no. 7 based on chemical data (Table 5). The mineral forms sporadic small (<7 μm in size) grains in dolomite and calcite and is associated with tsygankoite, alabandite, and tilasite. Although geocronite and jordanite often form continuous solid solution series (Moëlo et al., 2008), they occur at the Vorontsovskoe deposit in different assemblages and show no intermediate compositions.

Gillulyite $Tl_2As_{7.5}Sb_{0.3}S_{13}$ is determined in assemblage no. 3, where it forms anhedral grains up to 80 μm and intergrowths up to 0.2 mm with gladkovskyite and orpiment in calcite (Fig. 17h). The mineral is dark red, translucent in thin sections, with adamantine luster. Perfect cleavage is observed along {001}. In reflected light, gillulyite is light gray; bireflectance is noticeable in air and strong in immersion in pale pink tones. The mineral looks dark red due to abundant bright red internal reflections and is distinctly anisotropic in gray and brownish tones. The chemical composition and parameters of the monoclinic unit cell of gillulyite are given in Tables 5 and 3, respectively. In the Raman spectrum (Fig. 13b), a range of 240–400 cm^{-1} corresponds to the stretching vibrations of As–S bonds. The lower-frequency bands are assigned to the mixed lattice modes involving bending vibrations of the As,Sb,S-bond system and stretching vibrations of Tl–As and Tl–S bonds. Unlike auerbakhite and gladkovskyite, in spectra of which the strongest peaks are observed at 384–387 cm^{-1} due to the contribution of vibrations of Mn–S bond, the strongest peaks in gillulyite (as in hutchinsonite) are observed in the lower frequency region. Our finding of gillulyite is the first in the Russian Federation and second in the world after its type locality, South Mercur Pit in Utah, USA (Wilson et al., 1991). In addition to a chemically «normal» gillulyite, which contains only 0.2–0.3 apfu Sb similarly to the Utah holotype, we detected few rare small (up to 20 × 20 μm) grains of a Sb-rich gillulyite (up to 3.43 apfu Sb; Table 5, an. 53).

Gladkovskyite $MnTlAs_3S_6$ is a new sulfosalt described at the Vorontsovskoe deposit (Kasatkin et al., 2019). It honors the discoverer of the deposit Boris Aleksandrovich Gladkovsky (1937–1990). The mineral occurs in limestone breccias enclosed in abundant realgar, orpiment, baryte, and pyrite, as well as minor clinochlore, fluorapatite, quartz, and talc. Gladkovskyite occurs as long-prismatic crystals and grains up to 0.2 mm in realgar and orpiment (Fig. 16b) and, locally, forms partial pseudomorphs after alabandite (Fig. 17i) and intergrowths with gillulyite and lorándite (Figs. 17h, 17j). In one sample, we found a gladkovskyite veinlet 2 mm long and up to 0.3 mm thick in calcite.

The mineral is transparent and has a dark cherry red color, a red streak and an adamantine luster. It is brittle, with uneven fracture and neither cleavage nor parting. The Vickers microhardness is 94 kg/mm^2 corresponding to a Mohs hardness of 2–2½. The calculated density is 4.356 g/cm^3. In reflected light, the mineral looks

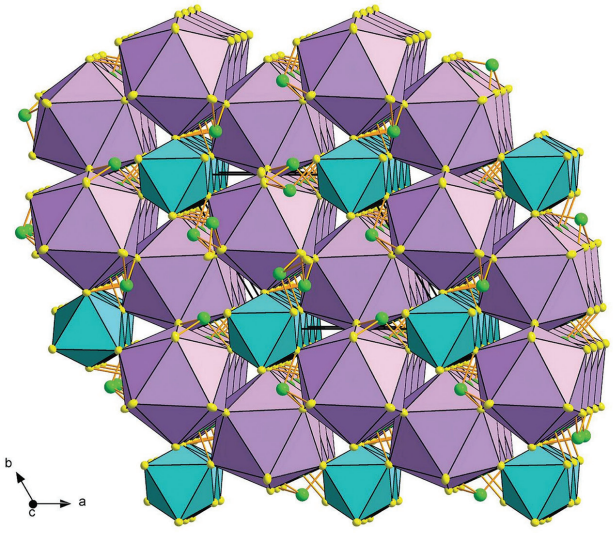

Fig. 19. Crystal structure of gladkovskyite.

Purple – TlS_9 polyhedra, turquoise – Mn-centered octahedra, ball-and-stick model representation (green As and yellow S atoms) – AsS_3 pyramids. All S atoms are shown as thermal ellipsoids.

light gray; bireflectance is barely noticeable. The mineral is strongly anisotropic with clear effects in dark gray, light gray and brownish tones. Some grains look dark red due to abundant bright red internal reflections, especially intense in immersion. In transmitted light, gladkovskyite is strongly pleochroic from orange–red to dark red. The reflectance spectra are shown in Fig. 12. The reflectance values for wavelengths recommended by the Commission on Ore Mineralogy of the IMA are as follows (R_{min}/R_{max}, %): 23.6/25.5 (470 nm), 23.3/23.5 (546 nm), 22.3/22.4 (589 nm), 21.1/21.7 (650 nm). The chemical composition of the holotype sample is given in Table 5. Its empirical formula based on the sum of all atoms of 11 is $Mn_{1.01}(Tl_{0.99}Pb_{0.01})_{1.00}(As_{2.86}Sb_{0.13})_{2.99}S_{6.00}$. Gladkovskyite is trigonal, $R31c$, $Z = 2$. The unit cell parameters are given in Table 3. The strongest reflections of the PXRD pattern are as follows [*d*, Å (*I*, %) (*hkl*)]: 5.11(80)(101), 4.83(70)(110), 3.49(50)(201), 3.23(30)(002), 2.86(100)(–2–11, 211), 2.68(30)(112), 2.55(60) (301, 202).

The Raman spectrum of gladkovskyite is similar to that of auerbakhite (Fig. 13c). The bands of Mn–S stretching vibrations are observed in a range 350–400 cm^{-1}. The bands at 289 and 305 cm^{-1} are assigned to As–S stretching vibrations. The Raman bands with wavenumbers below 250 cm^{-1} are possibly related to mixed soft modes involving bending vibrations and Tl–As and Tl–S stretching vibrations and phonons. The crystal structure of gladkovskyite belongs to rare

cyclic sulfosalts and contains infinite chains of face-sharing MnS_6 octahedra, TlS_9 polyhedra and pyramidal AsS_3 groups (Fig. 19).

Guettardite $PbAsSbS_4$ was identified in five mineral assemblages. It forms rare small (typically <10 μm in size) inclusions in orpiment, stibnite, and gangue minerals of breccias (calcite, dolomite, baryte, quartz, clinochlore, fluorapatite). It is also associated with aktashite, cinnabar, coloradoite, native gold, laffittite, metacinnabar, pyrite, realgar, routhierite, sphalerite, and other minerals. In assemblage no. 1, the guettardite inclusions up to 30 μm were found in chabournéite and écrinsite (Fig. 11h) and, in assemblage no. 4, guettardite is intergrown with roshchinite (Fig. 17k). In reflected light, guettardite is white with a bluish tint; bireflectance is distinct. It is strongly anisotropic in brownish tones. Several larger grains exhibit weak reddish internal reflections. The chemical composition of the mineral is close to stoichiometric $PbAsSbS_4$ (Table 5). This is the first finding of the minerals at the Russian Federation.

Gungerite $TlAs_5Sb_4S_{13}$ is a new mineral found at the Vorontsovskoe deposit (Kasatkin et al., 2020c, 2022a). The mineral was named after Yuri Vladimirovich Gunger (born in 1961), a mining engineer and surveyor, a famous historian and expert of Northern Urals, a former director of the Fedorov Geological Museum in Krasnoturyinsk. Gungerite was found in limestone breccias mainly composed of calcite and dolomite and enclosed in orpiment, pyrite, realgar, and stibnite and minor baryte and quartz. Gungerite is associated with bernardite, minerals of the chabournéite–dalnegroite and vorontsovite–ferrovorontsovite series, cinnabar, coloradoite, native gold, greigite, hutchinsonite, parapierrotite, and routhierite. Amid all new minerals found at the deposit, only gungerite forms macroscopic fine-grained bright orange aggregates up to 0.5 × 0.2 cm size on the breccia surface (Figs. 16c, 16d). The mineral has an orange streak, a greasy luster and a perfect cleavage on {010}; it is translucent in thin fragments. Gungerite is brittle, with an uneven fracture. The Vickers microhardness is 84 kg/mm^2 corresponding to a Mohs hardness of 2–2½. The calculated density is 4.173 g/cm^3. In reflected light, gungerite is yellowish white, but looks light gray with a weak bluish tint at the contact with stibnite. Bireflectance is very weak. The mineral is distinctly anisotropic, but anisotropy effects are masked by bright orange internal reflections. The internal reflections are visible even in plane-polarized light and are extremely abundant and strong in cross-polarized light in air and, especially, in immersion. The reflectance spectra are shown in Fig. 12. The reflectance values for the wavelengths recommended by the Commission on Ore Mineralogy of the IMA are as follows (R_{min}/R_{max}, %): 27.0/29.8 (470 nm), 26.1/27.4 (546 nm), 24.5/25.9 (589 nm), 22.4/23.9 (650 nm).

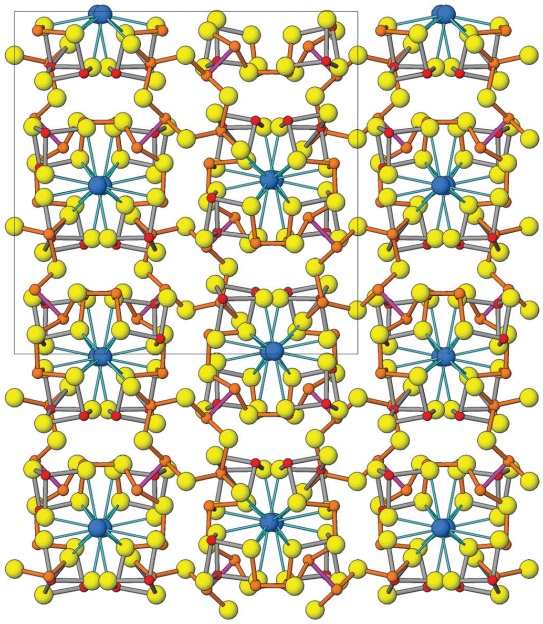

Fig. 20. Crystal structure of gungerite projected along [010].

Axes ***a*** and ***c*** are horizontal and vertical, respectively. The space between the rods is filled with lone-electron Sb and As pairs . Yellow, blue, red, and brown – S, Tl, Sb and As, respectively; lilac – covalent As–As bonds.

The chemical composition of the holotype sample is given in Table 5. Its empirical formula based on the sum of all atoms of 23 is $Tl_{0.99}As_{5.29}Sb_{3.77}S_{12.95}$. Gungerite is orthorhombic, space group *Pbcn*, Z = 8. The unit cell parameters are given in Table 3. The strongest reflections of its PXRD pattern are as follows [*d*, Å (*I*, %) (*hkl*)]: 5.755(100)(020), 3.030(10)(424), 2.901(10)(620), 2.878(14)(040), 2.821(10)(141).

According to the current nomenclature of sulfosalts (Moëlo et al., 2008), gungerite belongs to a rare class of subchalcogenides, which are characterized by a S deficiency relative to those with «normal» valences and relative excess of positive charges with respect to the charge balance (+2 for the ideal formula of gungerite, when the charge loss due to the covalent As–As bonding is ignored). The crystal structure of gungerite (Fig. 20) is the most complex among all new sulfosalts of the deposit. It contains 23 atomic sites, in which one site is occupied by Tl, one site is occupied by Sb, three

sites are occupied by As, three Sb and two As sites are mixed-occupied and remaining 13 sites are occupied by S atoms.

The crystal structure consists of (As,Sb)–S clusters, which have van der Waals contacts to most surroundings, and are connected to them only by sparse metal cation–sulfur bonds (Kasatkin et al., 2022a). These clusters have a peculiar arrangement, being «stacked» on, around, and along the Tl–S rods parallel to [010]. An individual cluster, always doughnut-shaped (or toroid-shaped), has a central Tl polyhedron half-inserted into it. The cluster is formed by a chelating mirror-symmetrical group that has Sb–As «defect coordination cubes» as forceps (with some atoms missing from a perfect cube-model). Its two mirror-related arms are connected by the coordination pyramid of As3. One arm of the chelating group has an eyelet of doubly interconnected Sb1 and Sb3 as its terminal portion. Through the coordination pyramid of As1, the eyelet is connected to the centrally positioned pyramid of As3, from which starts the other arm of the chelating group. In the order of appearance, this arm consists of the coordination pyramid of As2, a terminal eyelet of Sb2 and Sb4. These two Sb atoms are doubly interconnected *via* two sulfurs. A radially oriented «tail group» points out of the cluster and is formed by a covalent As–As bond, which connects As3 with As4. After the As4 polyhedron (which still is in a mirror-symmetric position with the rest of the «molecule») As5 follows, which points sideways, counter to the *m* symmetry of the group. An As5 polyhedron from an adjacent «molecule», however, is a mirror-symmetrical «plug» that closes the doughnut body from the side, which was left open by the original group.

In the Raman spectrum of gungerite (Fig. 13d), the wavenumbers in a range of 280–370 cm^{-1} refer to as As–S stretching vibrations. A strong band at 294 cm^{-1} with a shoulder at 240 cm^{-1} can be assigned to the bending mode of SbS_3 units (Frost et al., 2010). The bands in the ranges of 302–310, 334, 282, and 270 cm^{-1} are assigned to antisymmetric, symmetric, symmetric, and antisymmetric bending modes of SbS_3, respectively (Kharbish et al., 2009). It is noteworthy that no strong Raman bands of Tl sulfosalts, except for gungerite, are observed in a range of 250–265 cm^{-1} in the literature (Kharbish, 2011; Makreski et al., 2014) and our Raman spectra. Unlike other Sb-bearing Tl sulfosalts with pyramidal $(As,Sb)S_3$ units, gungerite is characterized by the presence of a As–As bond in the crystal structure and the presence of a strong band at 263 cm^{-1} in the Raman spectrum. Thus, the band at 263 cm^{-1} was assigned to As–As stretching vibrations that is in good agreement with the Raman spectrum of arsenolamprite with the strongest Raman band observed at 253 cm^{-1} (Thomas, Davidson, 2010). The assignment of the Raman bands with wavenumbers below 250 cm^{-1} is ambiguous and, probably, they correspond to soft mixed lattice modes involving As–S–As bending and Tl–S stretching vibrations.

Heteromorphite $Pb_7Sb_8S_{19}$ was found in a complex aggregate of sulfantimonites and galena in a sample collected at off-balance ore stockpile no. 2. The mineral forms grains up to 0.12 mm in sphalerite, which are intergrown with galena and boulangerite (Fig. 11i), and is associated with plagionite, semseyite, and pyrite. It contains low As and Se amounts (Table 5) and the atomic Pb/(Sb+As) ratio ranges from 0.910 to 0.935, which is within a Pb/Sb range (0.86–0.96) for heteromorphite from various deposits (Mozgova et al., 1971). In reflected light, heteromorphite is white, almost identical in brightness to galena and boulangerite, slightly darker than pyrite, but much brighter than sphalerite. Its bireflectance is strong. Heteromorphite differs from all neighboring minerals by strong anisotropy effects in brownish–yellowish and greenish tones. Several references to heteromorphite findings in Russia (Ivashchenko et al., 2004; Bryzgalov et al., 2011; Kemkina et al., 2018; Gvozdev et al., 2020) provide no sufficient information for its precise identification. Thus, we consider our finding at the Vorontsovskoe deposit the first reliable in Russia.

Hutchinsonite $TlPbAs_5S_9$ is a rare mineral identified in assemblages nos. 1, 2, and 3. In each assemblage, it is characterized by specific morphology. In assemblage no. 1, the mineral composes dendritic aggregates up to 0.2 × 0.1 mm in size in a calcite–prehnite rock and is associated with pyrite, realgar, dalnegroite, native gold, routhierite, sphalerite, baryte, and fluorapatite (Fig. 17l). In assemblage no. 2, hutchinsonite forms long-prismatic to acicular crystals up to 50 × 5 μm in size in calcite and, locally, is intergrown with realgar and wakabayashilite (Fig. 17m). In assemblage no. 3, hutchinsonite occurs as dissemination of tiny grains (<15 μm in size) in calcite.

The mineral has a cherry red color and an adamantine luster and it is translucent in thin sections. A good cleavage on {010} is observed. In reflected light, hutchinsonite is bluish gray; its bireflectance is distinct. It is strongly anisotropic in bluish and brownish tones. The internal reflections are carmine red, especially strong in immersion. Hutchinsonite from all assemblages contains a low Sb amount (Table 5). The

parameters of its orthorhombic unit cell are given in Table 3. In the Raman spectrum (Fig. 13g), a range of 280–400 cm^{-1} corresponds to the stretching vibrations of As–S bonds. The bands with lower wavenumbers cannot unambiguously be assigned and are probably related to mixed lattice modes involving bending vibrations of As–S bonds, as well as the stretching vibrations of the Tl and Pb coordination polyhedra (these vibrations can resonate with each other and cover large regions in the crystal). Our finding of hutchinsonite is the first in Russia.

Imhofite $Tl_{5.8}As_{15.4}S_{26}$ was determined in assemblages nos. 1 and 3, where it composes rare anhedral grains up to 30 μm in size in calcite with realgar (Fig. 17n). The mineral is bright red; it is translucent in thin fragments. In reflected light, imhofite is light gray; bireflectance is weak in the air and distinct in immersion. Strong anisotropy in grayish–brownish tones and red internal reflections are observed. The chemical composition of the mineral and its monoclinic unit-cell parameters are given in Tables 5 and 3, respectively. Imhofite was discovered in the Lengenbach quarry (Burri et al., 1965) and was later described in the Shimen deposit, China (Roth et al., 2017). Our finding is, thus, the first in the Russian Federation and, most likely, third in the world.

Laffittite $AgHgAsS_3$ was found in assemblage no. 4 as individual grains up to 30 μm in size in dolomite and baryte or in aggregates with stibnite (Fig. 17o). It is associated with coloradoite, guettardite, orpiment, parapierrotite, and roshchinite. Laffitite is transparent and has a dark red color and an adamantine luster. In reflected light, the mineral is bluish white. It is moderately anisotropic from bluish gray to dark gray; the effects of anisotropy are strongly enhanced in immersion. The red internal reflections are distinct. The chemical composition of the mineral is close to theoretical (Table 5). This is the first finding of laffittite in the Russian Federation.

Lillianite $Pb_3Bi_2S_6$ forms rare inclusions up to 20 μm in size in magnetite and intergrowths of the same size with Te-bearing ikunolite from assemblage no. 8. In reflected light, the mineral is creamy white. It is distinctly anisotropic with more intense effects than of the neighboring ikunolite. Lillianite also demonstrates a typical so-called «gustavite» isomorphic substitution according to $2Pb^{2+} \leftrightarrow Ag^{+}+Bi^{3+}$ scheme (Makovicky, 2019) (Table 5); the substitution percentage *L*% is 72.3.

Lorándite $TlAsS_2$ was identified in assemblage no. 3 as individual grains up to 20 μm in size included in calcite, as well as the intergrowths with gladkovskyite up to 50 μm in size (Fig. 17j) and with philrothite and orpiment up to 0.1 mm in size. The mineral is bright red, transparent, with an adamantine luster, very brittle. Cleavage is perfect on {100} and good on {001} and {201}. In reflected light, lorándite is grayish white, slightly lighter than gladkovskyite and philrothite. No bireflectance is observed in the air in contrast to immersion. Lorándite exhibits strong anisotropy in yellowish–brownish tones, but anisotropy in some grains is masked by abundant red internal reflections. The chemical composition of the mineral is stoichiometric (Table 5).

The strong reflections of the PXRD pattern are as follows [*d*, Å (*I*)]: 5.25(20), 3.80(20), 3.57(100), 2.99(20), 2.88(90), 2.63(30), 2.37(10), 1.85(10). The parameters of the monoclinic unit cell (Table 3) are almost identical to those of lorándite from the type locality Allchar deposit in North Macedonia (Fleet, 1973). The Raman spectrum (Fig. 13e) corresponds to that of lorándite (Kharbish, 2011; Makreski et al., 2014). All bands in a range of 250–400 cm^{-1} are due to vibrations of As–S bonds: a strong band at 397 cm^{-1} and a most intense band at 379 cm^{-1} (as well as a weak band at 353 cm^{-1}) are assigned to ν_1 (symmetric stretching vibrations) and ν_3 (antisymmetric stretching vibrations), respectively. A strong band at 324 cm^{-1} with a shoulder at 310 cm^{-1} and a strong band at 275 cm^{-1} are assigned to ν_2 (symmetric bending vibrations) and ν_4 (antisymmetric bending vibrations), respectively. The wavenumbers below 210 cm^{-1} correspond to mixed lattice modes. In Russia, lorándite was mentioned in assemblage with lermontovite without optical or analytical data at the Beshtau U deposit in Northern Caucasus (Melkov et al., 1983). Thus, we consider our data the first reliable for lorándite in the Russian Federation.

Luboržákite Mn_2AsSbS_5 is a second new mineral without species-defining Tl discovered at the deposit (Kasatkin et al., 2020a) after clerite. It honors Lubor Žák (1925–2008), a prominent Czech crystallographer and mineralogist, an expert in sulfosalts, and Professor at the Faculty of Science of the Charles University in Prague. Luboržákite forms long-prismatic crystals up to 70 × 20 μm in size and similar-sized anhedral grains in Mn-bearing dolomite and calcite (Fig. 21a). Luboržákite is associated with pyrite, orpiment, realgar, stibnite, aktashite, alabandite, boscardinite, chabournéite, coloradoite, clerite, écrinsite, native gold, routhierite, sphalerite, twinnite, baryte, chernovite-(Y), diopside, fluorapatite, hyalophane, muscovite, and prehnite.

Luboržákite is black, opaque with a metallic luster and a black streak. It is brittle and has an uneven frac-

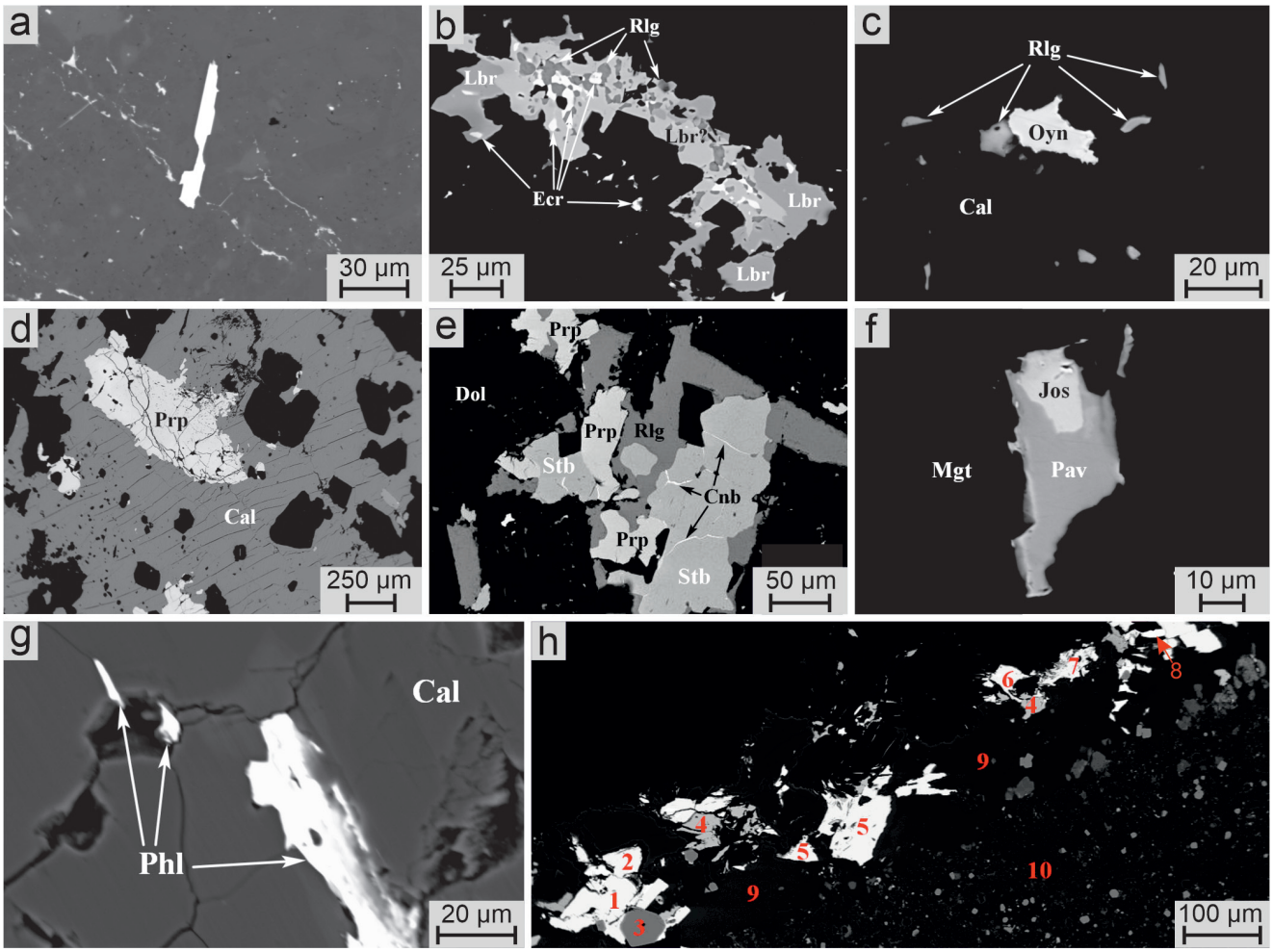

Fig. 21. Sulfosalts of the Vorontsovskoe deposit, part IV:

a – long-prismatic luboržákite crystal in carbonate aggregate; b –intergrowth of luboržákite, its Pb-rich variety (Lbr?), écrinsite, and realgar in Mn-bearing calcite and dolomite; c – oyonite grain in calcite with realgar; d – parapierrotite crystals in calcite; e – aggregate of parapierrotite, stibnite, realgar and cinnabar in dolomite; f – aggregate of pavonite and joseite-A in magnetite; g – prismatic philrothite crystals in calcite; h – pokhodyashinite (1) with parapierrotite (2), pyrite (3), sphalerite (4), dalnegroite (5), routhierite (6), realgar (7), weissbergite (8) in calcite (9) with clinochlore (10).

BSE images.

ture. No cleavage and parting were observed. The Vickers microhardness (VHN, 30 g load) is 242 kg/mm^2 corresponding to a Mohs hardness of 4–4½. The calculated density is 4.181 g/cm^{-3}. In reflected light, luboržákite is tin white; bireflectance is moderate. It is distinctly anisotropic with rotation tints varying from light gray to brownish. Kasatkin et al. (2020a) described no internal reflections, however, red internal reflections, especially noticeable in immersion, were observed in recently found larger grains (up to 80 × 50 μm in size). The reflectance spectra are shown in Fig. 12. The reflectance values for the wavelengths recommended by the Commission on Ore Mineralogy of the IMA are as follows (R_{min}/R_{max}, %): 23.6/25.3 (470 nm), 22.4/24.7 (546 nm), 22.1/24.3 (589 nm), 21.8/23.8 (650 nm).

The chemical composition of the holotype sample is shown in Table 5. Its empirical formula based on the sum of all atoms of 9 is $Mn_{1.86}Pb_{0.04}Ag_{0.03}Cu_{0.02}As_{0.98}Sb_{1.07}S_{5.00}$. Luboržákite is monoclinic, space group $C2/m$, $Z = 4$. The unit cell parameters are given in Table 3. The crystal structure of luboržákite (Fig. 22) contains ten atomic sites with one Sb site, one Mn site, five S sites and three mixed-occupied sites (two As/Mn and one Mn/Sb sites). The structural formula of the mineral is $[Mn_{0.5}SbS_2]^{thin\_layer} \cdot [(Mn,Sb)_{0.5}(AsMn)_{\Sigma 2}S_3]^{thick\_layer}$ individualizes two layers in its structure.

Luboržákite is a new member of the pavonite homologue series with $N = 5$. These structures resemble the unit-cell-twinned lillianite, in which slabs of PbS-like arrangement are cut along $(311)_{PbS}$ and twinned using

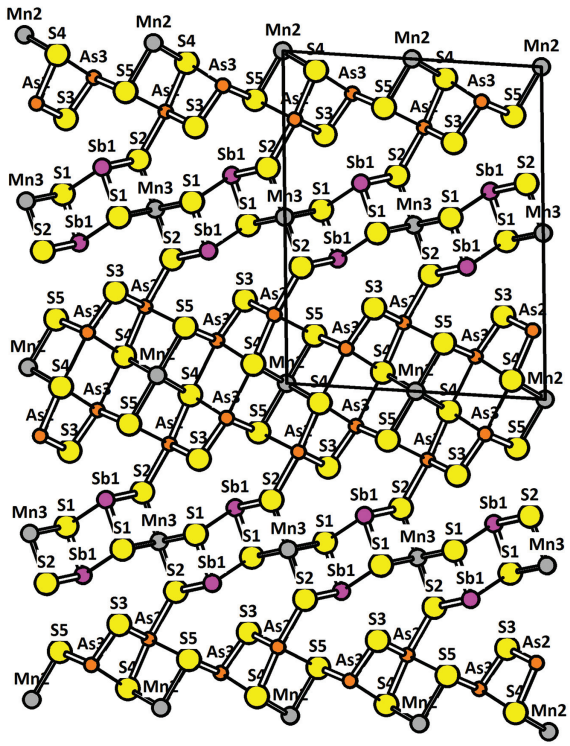

Fig. 22. Projection of the crystal structure of luboržákite down b.

Only strong short bonds are indicated.

these planes *via* bi-capped trigonal coordination prisms (mostly, of Pb). In the pavonite series, one orientation of these slabs is always only one octahedron-wide, whereas the other intervening slab orientation can be several cation-coordination octahedra wide (up to eight octahedra). The bi-capped trigonal coordination prisms on twin planes become distorted and are usually occupied by the lone electron pair of Bi (or Sb) situated in one of the prism's caps. In luboržákite, the thinner layer's octahedron is occupied by Mn3, whereas the caps of 'empty' only moderately distorted trigonal coordination prisms have the cap oriented into this layer filled by a coordination prism of Sb1.

In one aggregate about 0.2 mm long consisting of luboržákite, écrinsite, and realgar, we identified a phase optically similar to luboržákite differing in a significant Pb content, a deficiency of Mn and a distinct Sb/As ratio (Table 5, an. 73). An intimate intergrowth of this phase with other minerals (Fig. 21b) prevent from its XRD studies. Another clerite-like phase with formula $Mn(Sb,As)S_4$ was previously noted in assemblage with clerite (Murzin, Varlamov, 2010). In comparison with luboržákite, it has lower Mn and higher Sb contents.

Manganoquadratite $AgMnAsS_3$ was identified by chemical composition (Table 5) as rare inclusions about 10 μm in size in sphalerite in assemblage no. 1. In reflected light, the mineral looks light gray, noticeably lighter than the host sphalerite. No additional optical characteristics are determined due to a small grain size of manganoquadratite. Our finding of this mineral is the first in Russia and third in the world after its type locality Uchucchacua Mine in Peru (Bonazzi et al., 2012) and Săcărâmb deposit in Romania (Dincă, Popescu, 2019).

Meneghinite $Pb_{13}CuSb_7S_{24}$ was found in samples from the dumps of the southern open pit. It forms lead gray pockets up to 1 × 0.5 cm in calcite in assemblage with cubic pyrite crystals and white talc coatings (Fig. 16e). In reflected light, meneghinite is white. It is strongly anisotropic in greenish tones. The chemical composition of the mineral is stoichiometric (Table 5). The strong reflections of the PXRD pattern are as follows [*d*, Å (*I*)]: 5.81(30), 3.87(40), 3.70(50), 3.48(70), 3.27(90), 2.93(100), 2.73(70), 2.54(10), 2.08(60). The parameters of the orthorhombic unit cell correspond to meneghinite (Table 3).

Oyonite $Ag_3Mn_2Pb_4Sb_7As_4S_{24}$ was identified by chemical composition in assemblage no. 1 (Table 5). It occurs as a single grain 30 × 15 μm in size, which is enclosed in calcite with realgar, boscardinite, coloradoite, pyrite, sphalerite, stibnite, and twinnite (Fig. 21c). In reflected light, oyonite is grayish white, significantly brighter than the hosting realgar. It exhibits a distinct anisotropy in grayish and brownish tones. This is the first finding of the mineral in Russia and second in the world after its type locality the Uchucchacua Ag mine in Peru (Bindi et al., 2018).

Parapierrotite $TlSb_5S_8$ is one of the five most abundant Tl minerals at the deposit along with chabournéite, dalnegroite, routhierite, and vorontsovite. Murzin and Varlamov (2010) first reported on the chemical composition of a Tl sulfosalt that was conditionally ascribed to pierrotite or parapierrotite. We found parapierrotite in five assemblages. In assemblages nos. 2 and 4, abundant parapierrotite forms short-prismatic black crystals with a metallic luster and anhedral grains in gangue minerals of breccias (calcite, dolomite, baryte, quartz, clinochlore, prehnite, diopside, etc.) and is associated with cinnabar, orpiment, pyrite, realgar, routhierite, cinnabar, minerals of the vorontsovite–ferrovorontsovite and chabournéite–dalnegroite series, etc. The largest individuals of parapierrotite reaching 1 mm in size were found in assemblage no. 4 (Fig. 21d). The mineral structure

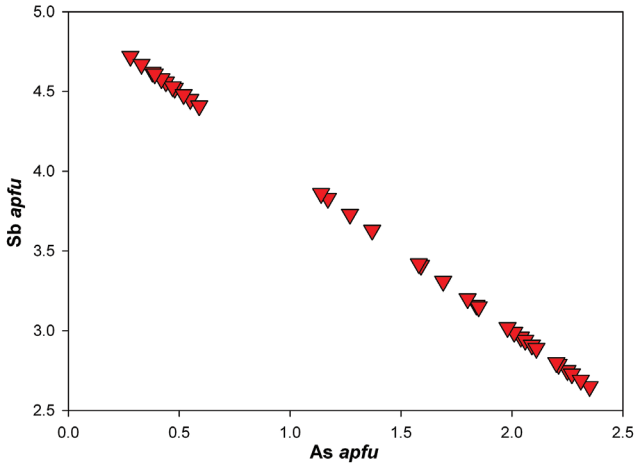

Fig. 23. Sb–As correlation in parapierrotite.

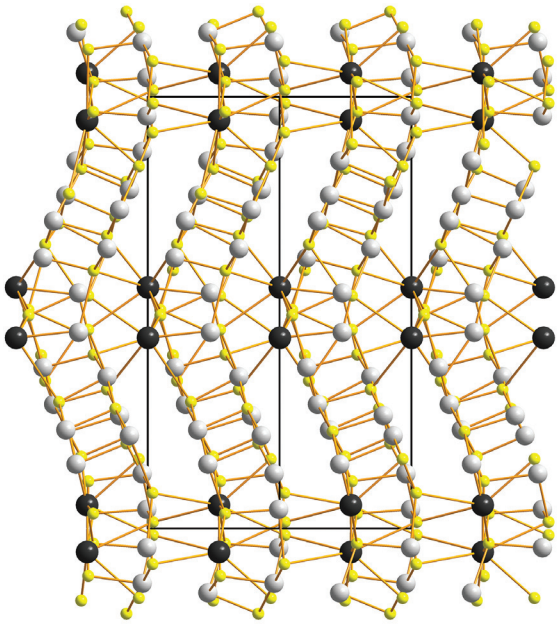

Fig. 24. Crystal structure of parapierrotite along [–101]. Black – Tl atoms, light gray – Sb and As sites, yellow – S atoms. Black lines – unit-cell edges.

was solved using one of these large crystals (Plášil et al., 2018). Smaller parapierrotite grains often occur as inclusions in pyrite and intergrowths with realgar, stibnite, and cinnabar (Fig. 21e). In reflected light, the mineral is white with a weak grayish tint; bireflectance is moderate. It is distinctly anisotropic in gray brownish and gray bluish tones. Red internal reflections are rare. The As content of the mineral widely varies from 2.0 (0.28 apfu) to 17.6 (2.23 apfu) wt. % (Table 5). The Sb–As isomorphic substitution extends from $Sb_{94}As_6$ to $Sb_{53}As_{47}$ with an obvious miscibility gap between $Sb_{88}As_{12}$ and $Sb_{77}As_{23}$ (Fig. 23).

The crystal structure of the natural parapierrotite (Fig. 24) is identical to a structure of a synthetic phase $TlSb_5S_8$ (Engel, 1980), in which Tl occupies two sites, whereas 10 and 16 sites are occupied by Sb and S, respectively. The refinement of the structure of parapierrotite from the Vorontsovskoe deposit shows that As isomorphically substitutes for Sb only in half of ten sites (Plášil et al., 2018). The reasons of partial ordering of As and Sb atoms are related to a stereochemical behavior of Sb^{3+} and the formation of more clear-cut AsS_3 pyramids in comparison with Sb^{3+}. Substitution of some Sb^{3+} atoms by smaller As^{3+} ones obviously leads to a decrease in the volume of the unit cell of the mineral. The more significant the decrease, the higher the As^{3+} content in the composition of the mineral (Table 3). In addition, our SXRD experiments with parapierrotite grains of various chemical compositions show that the XRD quality also directly depends on the Sb/As ratio of the mineral: the larger the As content, the worse the X-ray pattern. As a result, a crystal with a minimum As content (2.0 wt. %) yielded the best structural data.

Parapierrotite is rare in assemblage no. 5. It composes prismatic crystals up to 50 μm in size in aggregates of Mn-bearing carbonates and is associated with clerite (Fig. 17c), luboržákite, alabandite, pyrite, and realgar. An interesting feature of parapierrotite is the presence of Mn up to 1.6 wt. % (0.28 apfu) and a deficiency in Sb and As sites: 4.71–4.74 apfu Sb + As (Table 5, an. 88–89). By analogy with luboržákite, it is suggested that the deficiency is compensated by isomorphic entry of Mn in some of the Sb/As sites. The finding of parapierrotite at the Vorontsovskoe deposit is the first in the Russian Federation.

Pavonite $AgBi_3S_5$ forms anhedral grains up to 30 μm in size and intergrowths with joséite-A up to 50 μm in size in magnetite from assemblage no. 8 (Fig. 21f). In reflected light, pavonite is white at the contact with magnetite and has a faint pinkish cream tint at the contact with joséite-A. The effects of anisotropy in pavonite are more intense than in joséite-A, in bluish gray tones. Bireflectance is weak in the air and significant in immersion. The mineral contains a low Pb contents (Table 5).

Philrothite $TlAs_3S_5$ was identified in assemblages nos. 1 and 3 of carbonate breccias, where it forms scarce short-prismatic crystals up to 70 × 15 μm in size in calcite and dolomite (Fig. 21g). In rare cases, philrothite is intergrown with lorándite, realgar and

rounded grains of native gold. The mineral is black and opaque. In reflected light, it looks light gray, slightly darker than neighboring lorándite but brighter than realgar. Bireflectance in the air is noticeable. The mineral is strongly anisotropic in light gray and brown tones. The chemical composition and parameters of the monoclinic unit cell of philrothite are given in Tables 5 and 3, respectively. This is the first finding of this mineral in the Russian Federation and second world finding after its type locality at the Lengenbach quarry (Bindi et al., 2014).

Pierrotite $Tl_2(Sb,As)_{10}S_{16}$ was described as rounded or anhedral inclusions up to 60 × 30 μm in size in large (up to 3 mm) realgar aggregates (Sazonov et al., 1991a). In reflected light, it is white with a greenish or bluish tint. The anisotropy is distinct. The internal reflections are dark red. The chemical formula provided by these authors $(Tl_{1.86}Ag_{0.01}Cu_{0.11}Fe_{0.02})_{2.00}(As_{7.20}Sb_{3.72})_{10.92}S_{16.08}$, however, does not correspond to pierrotite, because the latter is a Sb-dominant mineral. We believe that the indicated optical and chemical data better match bernardite, although this suggestion requires the XRD study. Murzin and Varlamov (2010) reported on the chemical composition of a Tl sulfosalt, which is consistent with both pierrotite and parapierrotite. We cannot exclude the presence of pierrotite in ores of the Vorontsovskoe deposit due to its chemical composition and optical data similar to parapierrotite, however, all 15 grains of the mineral studied by XRD were parapierrotite.

Plagionite $Pb_5Sb_8S_{17}$ forms prismatic crystals or anhedral grains less than 0.1 mm in size in quartz or carbonates of breccias (Sazonov et al., 1991a). It is occasionally recorded from the central parts of zonal intergrowths with other sulfides. Plagionite was determined by its chemical composition and optical properties. It was identified in an aggregate of sulfantimonites and galena in a sample collected at off-balance ore stockpile no. 2. Plagionite occurs as grains up to 50 μm in sphalerite or at the contact with galena and pyrite (Fig. 11i) and is associated with boulangerite, heteromorphite, and semseyite. The mineral contains minor Bi and Se amounts (Table 5). Plagionite is creamy white in reflected light, slightly darker than galena in the air and much darker in immersion. Bireflectance is distinct. The effects of anisotropy are strong (especially, in immersion) in gray, pinkish and brownish tones.The red–brown internal reflections are also observed in immersion.

Pokhodyashinite $CuTlSb_2(Sb_{1-x}Tl_x)AsS_{7-x}$ is the rarest new mineral of the Vorontsovskoe deposit (Kasatkin et al., 2022b). It was found in two polished sections of carbonate breccia collected at the main ore stockpile. The new mineral is named in honor of Maksim Mikhailovich Pokhodyashin (1708–1780), a Russian merchant, manufacturer, and owner of mines and smelter plants in Northern Urals. He was a pioneer of mining engineering and smelting works in the region, who founded the Bogoslovskiy mining district, opened and operated famous Turyinsk copper mines, established three copper smelters, and built important roads connecting the mines and the smelters. Pokhodyashinite forms anhedral grains up to 0.1 × 0.05 mm in size in calcite and is associated with major orpiment, pyrite and, realgar and minor baryte, clinochlore, As-bearing fluorapatite, harmotome, prehnite, arsiccioite, boscardinite, chabournéite, coloradoite, dalnegroite, écrinsite, native gold, parapierrotite, routhierite, sicherite, sphalerite, stalderite, tennantite-(Zn), and weissbergite in assemblage no. 1 (Fig. 21h).

Pokhodyashinite is black, opaque, with a metallic luster and a black streak. It is brittle, with an uneven fracture and a poor cleavage on {010}. The Vickers hardness (VHN, 20 g load) is 55 kg/mm^2 corresponding to a Mohs hardness of 2. The calculated density is 5.169 g/cm^3. In reflected light, pokhodyashinite is grayish white, bireflectance is distinct. It is strongly anisotropic; rotation tints vary from dark brownish gray to light bluish gray. No internal reflections are observed. The reflectance spectra are shown in Fig. 12. The reflectance values for the wavelengths recommended by the Commission on Ore Mineralogy of the IMA are as follows (R_{min}/R_{max}, %): 28.9/34.6 (470 nm), 27.6/33.4 (546 nm), 26.7/32.4 (589 nm), 26.1/31.1 (650 nm).

The chemical composition of the holotype sample is shown in Table 5. Its empirical formula based on the sum of all cations of 6 is $Cu_{0.70}Ag_{0.34}Tl_{1.32}Pb_{0.02}Sb_{2.63}As_{0.99}S_{6.625}$. Pokhodyashinite is monoclinic, space group $C2/m$, $Z = 4$. The unit cell parameters are given in Table 3. The structure of pokhodyashinite contains 13 atomic sites: one Tl, two Sb, one As, seven S, and two mixed-(one Sb/Tl and one Cu/Ag) sites (Fig. 25). Its structure can be described as wavy slabs of a complex structure based on double-rods of (primarily) Sb-coordination pyramids and lone-electron-pair interspaces/micelles, separated by wavy interlayers consisting of paired columns of Tl and rods of paired Cu-coordination polyhedra.

Ramdohrite $(Cd,Mn,Fe)Ag_{5.5}Pb_{12}Sb_{21.5}S_{48}$ was probably found in assemblage no. 6 as tiny inclusions up to 8 μm in size in an arsenopyrite grain, which is enclosed in vesuvianite (Fig. 26a). The mineral con-

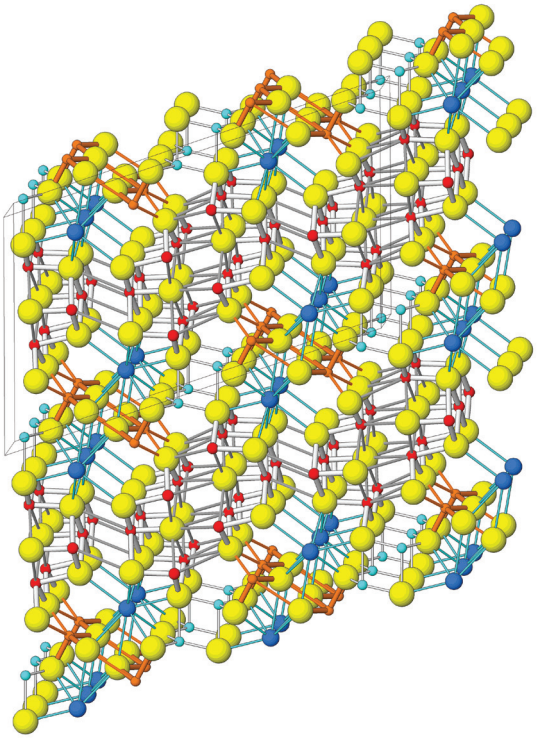

Fig. 25. Projection of the crystal structure of pokhodyashinite along [010] (slightly inclined).

Blue, azure, orange, red, and yellow – Tl, Cu/Ag, Sb, As, and S atoms, respectively. The unit-cell edges are indicated.

tains Mn, Cu, Fe, and Zn, which possibly substitute to Ag (Table 5).

Rebulite $Tl_5Sb_5As_8S_{22}$ was determined in assemblages nos. 1 and 3. The mineral occurs as rare prismatic individuals up to 20 μm long and angular grains up to 40 × 30 μm in size in calcite–quartz aggregates. It is observed together with boscardinite, chabournéite, orpiment, parapierrotite, pyrite, realgar, routhierite, Mn–Hg-bearing sphalerite, baryte, diopside, prehnite, and fluorapatite (Fig. 26b). Sample Vor-SS-10 from assemblage no. 1 contained one large rebulite grain (0.2 × 0.1 mm in size) with a small inclusion of vrbaite (Fig. 26c). Rebulite has a dark red color and a luster varying from metallic to adamantine. In reflected light, it is grayish white. It is distinctly anisotropic in grayish and brownish tones with red internal reflections.

The chemical composition of the mineral and the parameters of its monoclinic unit cell are given in Tables 5 and 3, respectively. Its Raman spectrum (Fig. 13f) is identical to that of rebulite described by (Makreski et al., 2014). The bands with maxima in a range of 330–400 cm^{-1} are assigned to As–S and Sb–S stretching ($\nu_1 + \nu_3$) vibrations and the bands with maxima at 322 and 250 cm^{-1} are due to bending ($\nu_2 + \nu_4$) vibrations of short (2.2–2.6 Å) and long (2.9–3.9 Å) Sb–S bonds, respectively. The bands below 205 cm^{-1} belong to the mixed lattice modes. Rebulite was first described at the Allchar deposit (Balić-Žunić et al., 1982) and remained its endemic for a long time. In the late 2010s, it was also discovered at the Shimen As deposit in the Hunan province, China (Roth et al., 2017). Our finding is the first in Russia and third in the world.

Roshchinite $Ag_{19}Pb_{10}Sb_{51}S_{96}$ was probably found in one sample from assemblage no. 4, which was composed of dolomite, baryte, and large (up to 3 mm) stibnite aggregates. Roshchinite is included in stibnite and is intergrown with guettardite (Fig. 17k). The sizes of the individual inclusions and intergrowths do not exceed 20 and 15 μm, respectively. It is also associated with coloradoite, laffittite, orpiment, and parapierrotite. Roschinite contains Mn (up to 0.2 wt. %), Hg (up to 3.0 wt. %), and As (up to 11.4 wt. %) (Table 5). The lower contents of the same trace elements (up to 0.04, 0.9, and 5.6 wt. %, respectively) were also determined in roshchinite from its type locality at the Kvartsitovye Gorki Au deposit in Northern Kazakhstan (Spiridonov et al., 1990).

The optical properties of the studied mineral are consistent with those of roshchinite: it is grayish white with a slightly bluish tint in reflected light and is moderately anisotropic without color effects. In terms of the reflectance values, roshchinite is close to guettardite and host stibnite but is characterized by weaker (almost invisible) bireflectance and weaker anisotropy. Small grain size of roshchinite prevented from XRD studies. Our finding of this sulfosalt is probably the first in the Russian Federation.

Routhierite $Tl(Cu,Ag)(Hg,Zn)_2(As,Sb)_2S_6$ together with chabournéite, dalnegroite, parapierrotite, and vorontsovite is one of the most abundant Tl sulfosalts of the deposit. It was first described as interstitial anhedral aggregates up to 0.5 mm in size between carbonate grains and smaller isometric crystals in realgar or Pb–Tl-bearing sulfosalts (Sazonov et al., 1991a). Routhierite was confirmed by optical properties, including reflectance spectra, microhardness, chemical composition, PXRD pattern and refined parameters of the unit cell. It contains Zn (up to 1 wt. %), Ag (up to 0.3 wt. %) and Sb (4.3 wt. %). Murzin and Varlamov (2010) provided additional chemical analyses including one analysis with a higher Sb content (up to 7.15 wt. %).

In our samples, routhierite occurs in six assemblages, typically, as dissemination up to 0.5 × 0.5 cm in size in carbonates of breccias (Fig. 16f). The color

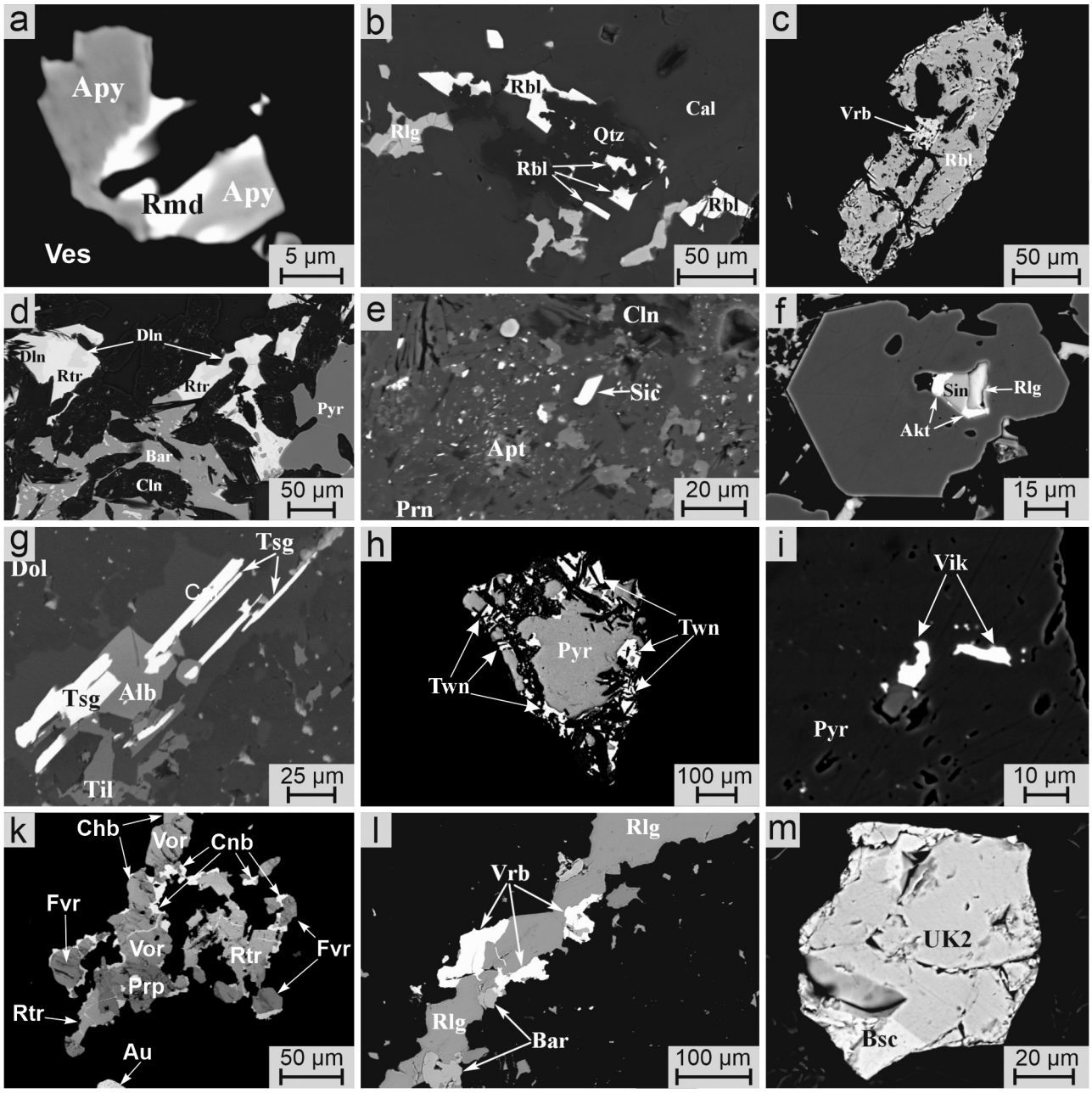

Fig. 26. Sulfosalts of the Vorontsovskoe deposit, part V:

a – ramdohrite inclusions in arsenopyrite enclosed in vesuvianite; b – rebulite crystals and grains in calcite and quartz in assemblage with realgar; c – rebulite grain with a vrbaite inclusion; d – Ag-rich routhierite intergrown with dalnegroite in clinochlore with baryte and pyrite; e – sicherite inclusion in prehnite with As-bearing fluorapatite, Mn-bearing clinochlore, and pyrite (light gray rounded grains); f – intergrowth of sinnerite with aktashite and realgar included in pyrite crystal (dark gray) and calcite (black); g – pseudomorphs of tsygankoite crystals after alabandite in assemblage with tilasite in dolomite and calcite; h – twinnite grains around pyrite; i – vikingite inclusions in pyrite; k – intergrowth of vorontsovite, ferrovorontsovite, chabournéite, parapierrotite, and cinnabar in calcite with native gold; l – aggregate of vrbaite with realgar and baryte in calcite; m – an unknown phase II (UK2) intergrown with boscardinite.

BSE images.

of the mineral varies from bright red to dark red and its luster is either metallic or adamantine. Routhierite is translucent in thin fragments. In reflected light, routherite is light gray. It is distinctly anisotropic in gray and brownish tones; however, routhierite from assemblage no. 7 is characterized by very weak ani-

sotropy. Abundant internal reflections are bright red and especially strong in immersion. The parameters of the tetragonal unit cell of routhierite from assemblages nos. 1 and 5 are given in Table 3. Most grains contain only minor amount of Ag (up to 0.06 apfu) and Zn (up to 0.16 apfu) (Table 5). The grains of Ag- and Zn-rich routhierite up to 80 μm in size intergrown with dalnegroite were found in assemblage no. 1 (Fig. 26d). The EMPA of these grains showed a wide substitution according to Ag → Cu and Zn → Hg schemes up to the compositions corresponding to other members of the routhierite group: **arsiccioite** (Ag > Cu and Hg > Zn) and **stalderite** (Cu > Ag and Zn > Hg) (Table 5, an. 5 and 107, respectively). Both arsiccioite and stalderite have previously been described at the Monte Arsiccio mine in Tuscany, Italy (Biagioni et al., 2014) and Lengenbach quarry (Graeser et al., 1995), respectively. Our findings are the first in the Russian Federation and second in the world for each of these species.

Semseyite $Pb_9Sb_8S_{21}$ was determined in an aggregate of sulfantimonites and galena in a sample collected at off-balance ore stockpile no. 2. The mineral forms grains up to 70 μm in size, which are intergrown with galena (Fig. 11i) at the contact with sphalerite and pyrite and is associated with boulangerite, heteromorphite, and plagionite. Semseyite contains a minor amount of Se (Table 5). It is grayish white in reflected light, slightly darker than pyrite, but much lighter than sphalerite. Semseyite and galena have close reflectance values and look bright in the air, but, at the contact with galena, semseyite looks slightly greenish. In immersion, the difference between these minerals becomes more obvious: semseyite is much darker. Bireflectance is distinct. The effects of anisotropy are strong in both the air and immersion.

Sicherite $TlAg_2(As,Sb)_3S_6$ was identified by chemical composition in sample from assemblage no. 1 (Table 5). This extremely rare sulfosalt was found as a single grain 10 × 5 μm in size in prehnite in assemblage with boscardinite–écrinsite, chabournéite, parapierrotite, pyrite, routhierite, sphalerite, weissbergite, baryte, Mn-rich clinochlore, and As-bearing fluorapatite (Fig. 26e). In reflected light, the mineral looks white. Sicherite was known only from the Lengenbach quarry (Graeser et al., 2001). Our finding is, therefore, the first in Russia and second in the world.

Sinnerite $Cu_6As_4S_9$ was tentatively identified in a sample from assemblage no. 1 as a single grain 13 × 9 μm in size, which was intergrowth with aktashite and realgar in a pyrite crystal enclosed in calcite (Fig. 26f). Other minerals of this assemblage include the minerals of the chabournéite–dalnegroite series, coloradoite, native gold, orpiment, routhierite, baryte, hyalophane, fluorapatite, and cerussite. In reflected light, sinnerite looks light gray, is indistinguishable from aktashite and significantly darker than host pyrite and lighter than realgar. This is relatively consistent with the reference reflectance values for all four minerals in white light: R = 29, 30, 54 and 19–21 % for sinnerite, aktashite, pyrite, and realgar, respectively (Chvileva et al., 1988). In spite of the tiny grain size, its chemical composition is perfectly recalculated to the formula of a typical sinnerite (Table 5). The analytical total is slightly lower due to the subtraction of a small admixture of pyrite from the matrix. In the Russian Federation, sinnerite has previously been identified in the Elbrus polymetallic deposit in Northern Caucasus at the contact with chalcopyrite and fahlores (Bezsmertnaya et al., 1973). Our finding is the first in the Urals.

Tsnigriite $Ag_9SbTe_3S_3$ was identified in samples collected at off-balance ore stockpile no. 2 in calcite–dolomite–quartz aggregates with galena and sphalerite. Tsnigriite forms inclusions up to 30 μm in size in galena and is associated with benleonardite, geocronite, and hessite (Fig. 11d). Its chemical composition is close to ideal (Table 5). In reflected light, tsnigriite looks light gray with a faint greenish blue tint in comparison with white galena. It is anisotropic in brownish and grayish tones. In Russia, it was previously described as single microinclusions in galena from gold-polymetallic ores of the Berezitovoe deposit in Amur oblast (Vakh et al., 2016, 2019).

Tsygankoite $Mn_8Tl_8Hg_2(Sb_{21}Pb_2Tl)S_{48}$ is a new mineral with a unique set of species-defining elements (Kasatkin et al., 2018b). It was named after Mikhail Vladimirovich Tsyganko (born 1979), an amateur mineralogist and collector from Severouralsk, a founder of the Mineralogical Museum «Shtufnoi Kabinet» («Mineral Cabinet») and one of the authors of this work. A number of rare minerals were found in samples collected by him. Tsygankoite occurs as lath-like elongated crystals up to 0.2 mm in size in gangue minerals of carbonate breccias (dolomite, calcite, clinochlore) enclosed in arsenopyrite, pyrite, orpiment, and realgar (Fig. 16g). It often forms partial pseudomorphs after alabandite (Fig. 26g) and intergrowths with routhierite and sphalerite.

Tsygankoite is opaque, has a black color and streak and a metallic luster; it is brittle, with an uneven fracture. No cleavage is observed. The Vickers microhardness (VHN, 10 g load) is 144 kg/mm^2 corresponding to a Mohs hardness of ~3. The calculated density is

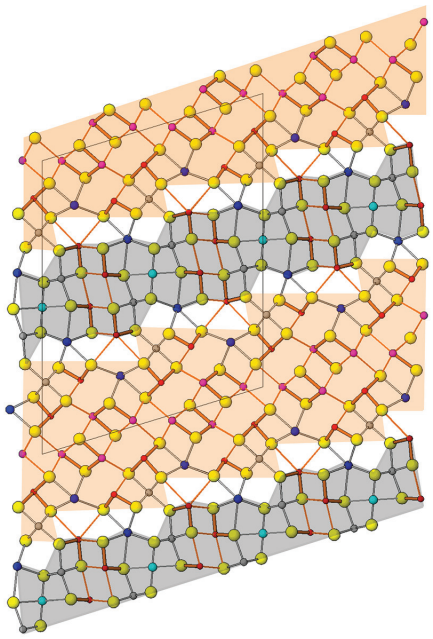

Fig. 27. Crystal structure of tsygankoite in projection on plane (010).

Yellow, blue, turquoise, red, lilac, and gray – atoms of S, Tl, Hg, Sb and (Sb,As), (Sb,Pb,Tl), and Mn, respectively. Thick orange lines – short strong Sb–S bonds, thin lines – longer distances. Other cation–anion bonds correspond to distances defining the complete coordination polyhedron. Axis c is vertical and slightly inclined.

5.450 g/cm^{-3}. In reflected light, tsygankoite looks white at the contact with alabandite, routhierite, and sphalerite and light gray at the contact with pyrite and arsenopyrite. Bireflectance is weak in the air and distinct in immersion from white to pale yellow. Tsygankoite is strongly anisotropic in grayish white and pinkish gray tones; rare internal reflections are light gray. The reflectance spectra are shown in Fig. 12. The reflectance values for the wavelengths recommended by the Commission on Ore Mineralogy of the IMA are as follows (R_{min}/R_{max}, %): 31.9/33.1 (470 nm), 31.2/32.4 (546 nm), 30.2/31.6 (589 nm), 28.7/29.8 (650 nm). The chemical composition of the holotype is given in the Table 5. Its empirical formula based on the sum of all atoms of 90 is $Mn_{8.06}Tl_{8.00}Hg_{1.90}(Sb_{17.87}As_{3.19}Pb_{1.99}Tl_{0.97})_{24.02}S_{48.03}$.

Tsygankoite is monoclinic, space group *C*2/*m*, *Z* = 1. The unit cell parameters are given in Table 3. The strongest reflections of its PXRD pattern are as follows [*d*, Å (*I*, %) (*hkl*)]: 3.587(100)(112), 3.353(70)(−114), 3.204(88)(405), 2.841(72)(−513), 2.786(99)(−514). The crystal structure of tsygankoite contains 11 independent cation sites (four of which are mixed sites that were refined with one set of coordinates each) and 12 different sulfur sites (Fig. 27). It consists of an alternation of two thick layer-like arrays based on PbS- and SnS-archetypes, respectively. Both are typical of sulfosalt structures. The array based on the PbS-archetype (i.e., with a PbS-like topology) contains a Hg site with a typical bond scheme, a Tl site, an octahedrally coordinated Mn1 site, and two Sb sites labeled Sb1 and Sb2. The alternating array based on the SnS-archetype (an array with a more pronounced steric role of lone electron pairs) with a general bond scheme represented by that observed in SnS [10] contains four distinct Sb sites, all of which are statistically mixed either with heavier cations (refined as Pb or Tl component) or As. A Tl site (refined as «Tl3») is embedded in this array and a Mn^{2+} site is apical to the second array. Close spatial relationship of large Tl^{+} and small Mn^{2+} polyhedra in the former array and along of its contact with the latter array is of interest.

Twinnite $Pb_{0.8}Tl_{0.1}Sb_{1.3}As_{0.8}S_4$ was noted in the realgar-bearing ores as dissemination of anhedral grains and intergrowths with aktashite (Vikentyev et al., 2016). Three chemical analyses given in this work, however, have higher totals (up to 105 wt. %) and correspond by stoichiometry to guettardite. The reliable twinnite was identified by us in assemblages nos. 1 and 5 as anhedral grains up to 0.3 mm in size. In some cases, twinnite forms intergrowths with boscardinite around pyrite grains (Fig. 26h). It is also associated with aktashite, minerals of the boscardinite–écrinsite series, chabournéite, native gold, orpiment, realgar, and routhierite. Twinnite is black, opaque with a metallic luster. Perfect cleavage is observed along {100}. In reflected light, twinnite is white, locally, with greenish or bluish tints. Bireflectance is distinct in the air and strong in immersion. Twinnite is moderately anisotropic without color effects. The chemical composition and parameters of the monoclinic unit cell of twinnite from both assemblages are given in Tables 5 and 3, respectively. Our finding of twinnite is the first in the Russian Federation.

Veenite $Pb_{16}Sb_{9-x}As_{7+x}S_{40}$ (where x~0.0–0.5) was identified only in one sample from assemblage no. 7. The mineral forms rare 30-μm inclusions in gangue minerals of breccia (calcite, dolomite, clinochlore) and is associated with pyrite, arsenopyrite, sphalerite, native arsenic and tsygankoite. In reflected light, veenite looks white. It is distinctly anisotropic in dark gray tones. The mineral contains high Tl amount (Table 5), which is typical of all members of the sartorite group (Topa et al., 2017b; Topa, Kolitsch, 2018). Vikentyev

et al. (2016) reported on two chemical compositions of «veenite with Cu and Hg» and only trace amount of As (0.38 and 0.18 wt. %). The refinement of the veenite crystal structure, however, shows that As is a species-defining element of this sulfosalt (Topa, Makovicky, 2017). The recalculations of analyses given by Vikentyev et al. (2016) better correspond to rouxelite $Cu_2HgPb_{22}Sb_{28}S_{64}(O,S)_2$, however, this identification requires additional optical and XRD studies. In Russia, «veenite» was previously noted as gray tabular crystals in «carbonatites» of the Krestovozdvizhensky mine in the Southern Urals (Popov, Kolisnichenko, 2008). The high As and low Sb contents of the Southern Urals mineral, however, contradict its identification as veenite. Our finding is the first in the Russian Federation.

Vikingite $Ag_5Pb_8Bi_{13}S_{30}$ was tentatively identified in a sample mainly consisting of quartz, pyrite, galena, sphalerite, and chalcopyrite collected at off-balance ore stockpile no. 2. Vikingite forms rare small (up to 15 μm in size) inclusions in pyrite (Fig. 26i). Compared to the ideal formula of vikingite, our sulfosalt is Ag-deficient (Table 5), which is similar to some previously published compositions (Moëlo et al., 1987). The optical properties of the mineral match those of vikingite: in reflected light, it looks grayish white and is slightly darker than the host pyrite; it is weakly anisotropic in grayish tones.

Vorontsovite $(Hg_5Cu)_{\Sigma6}TlAs_4S_{12}$ and **ferrovorontsovite** $(Fe_5Cu)_{\Sigma6}TlAs_4S_{12}$ are new minerals discovered at the deposit (Kasatkin et al., 2018a). Vorontsovite is named after its type locality, Vorontsovskoe deposit, and also indirectly honors a mining engineer Vladimir Vasil'evich Vorontsov (1842–after 1908), who was a superintendent of the Bogoslovskiy mining district and organized extensive geological survey and prospecting work that resulted in the discovery of an iron deposit. The nearby mining settlement of Vorontsovka and the Vorontsovskoe iron deposit were also named after him. The adjacent Vorontsovskoe gold deposit, which was discovered in 1985, was named after the settlement of Vorontsovka. Ferrovorontsovite is named for its chemical composition, as a Fe analogue of vorontsovite.

Vorontsovite and ferrovorontsovite occur in assemblage no. 2 as numerous anhedral grains up to 0.5 (vorontsovite) and 0.2 (ferrovorontsovite) mm in size in gangue minerals of breccias (calcite, dolomite, clinochlore) and as inclusions in orpiment, realgar, and stibnite (Fig. 16h). Both minerals are often intergrown with each other, as well as with cinnabar, parapierrotite, routhierite, and minerals of the chabournéite group and form polymineral aggregates up to 0.2 mm in size (Fig. 26k). In contrast to ferrovorontsovite, vorontsovite was also found in assemblage no. 1 as rare small (<10 μm) grains in calcite and baryte. Both minerals are opaque, black, with a dark red streak and a metallic luster. They are brittle, with uneven fracture. No cleavage is observed. The Vickers hardness (VHN, 10g load) is 172 kg/mm^2 for vorontsovite and 170 kg/mm^2 for ferrovorontsovite corresponding to a Mohs hardness of ~ 3½. The calculated density is 5.140 and 4.744 g/cm^3, respectively.

In reflected light, both sulfosalts are light gray with a bluish tint; they are isotropic with abundant internal reflections, which are distinct in the air and strong in immersion (Kasatkin, Pautov, 2020). The color of internal reflections varies from dark red to bright red in vorontsovite and from dark red to dark brown in ferrovorontsovite. Their reflectance spectra are shown in Fig. 12. The reflectance values for the wavelengths recommended by the Commission on Ore Mineralogy of the IMA are as follows (*R*, %; vorontsovite /ferrovorontsovite): 24.9/26.2 (470 nm), 23.7/24.5 (546 nm), 22.8/23.9 (589 nm), 21.3/23.2 (650 nm).

The chemical composition of the holotype samples of both minerals is given in Table 5. Their empirical formulas are recalculated on the basis of 23 atoms *pfu*: $[(Hg_{3.02}Fe_{1.63}Zn_{0.33})_{4.98}(Cu_{0.91}Ag_{0.10})_{1.01}](Tl_{0.96}Cs_{0.04})_{1.00}(As_{3.62}Sb_{0.33}Te_{0.05})_{4.00}S_{12.01}$ (vorontsovite) and $[(Fe_{2.74}Hg_{1.94}Zn_{0.27})_{4.95}(Cu_{0.96}Ag_{0.06})_{1.02}](Tl_{0.98}Cs_{0.05})_{1.03}(As_{3.68}Sb_{0.27}Te_{0.05})_{4.00}S_{12.00}$ (ferrovorontsovite). Both minerals are cubic, space group *I*-43*m*, *Z* = 2. The parameters of their unit cells are given in Table 3. The strongest reflections of the PXRD patterns are [*d*, Å (*I*, %) (*hkl*); vorontsovite/ferrovorontsovite]: 4.198(79)/4.175(93)(211), 2.970(100)/2.952(100)(222), 2.749(66)/2.735(57)(321), 1.818(49)/1.810(40)(440), 1.550(31)/1.543(24)(622).

Vorontsovite and ferrovorontsovite are Tl and Tl–Fe analogs of galkhaite $(Hg_5Cu)_{\Sigma6}CsAs_4S_{12}$, respectively. All three minerals form the galkhaite group. Similarly to galkhaite, the crystal structure of vorontsovite and ferrovorontsovite is characterized by three independent crystallographic sites (Fig. 28). The first site is occupied by metal atoms in tetrahedral coordination: Hg (dominant in vorontsovite and galkhaite), Fe (dominant in ferrovorontsovite), Zn, Cu, and Ag. The second site is a 12-fold coordinated site occupied by Tl atoms (Cs atoms in galkhaite) centering Laves polyhedra TlS_{12} (CsS_{12} in galkhaite). The third site is a trigonal pyramid with As coordinating three S. Our EMPA results show an isomorphic substitution in each of three crystallographic sites. The largest degree of

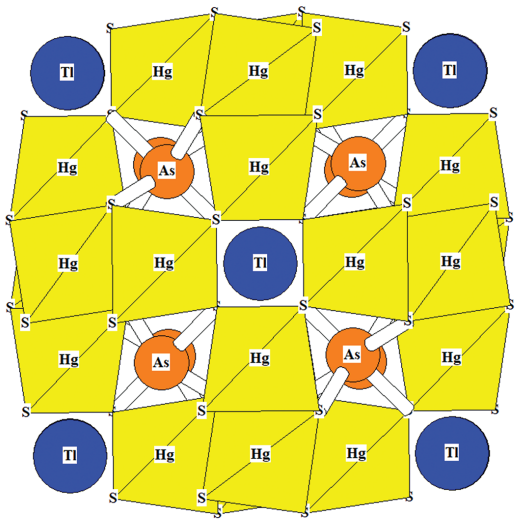

Fig. 28. Crystal structure of vorontsovite/ferrovorontsovite along [001].

For simplicity, the site occupied by (Hg, Fe, Zn, Cu, Ag), (Tl, Cs), and (As, Sb) are indicated as Hg, Tl, and As, respectively.

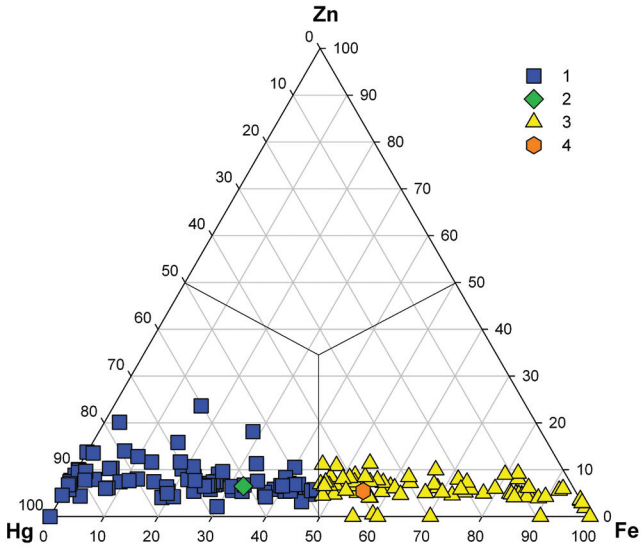

Fig. 29. Hg : Fe : Zn ratios for tetrahedral sites in vorontsovite and ferrovorontsovite.

1 – vorontsovite; 2 – vorontsovite holotype; 3 – ferrovorontsovite; 4 – ferrovorontsovite holotype.

substitution is recorded in tetrahedral sites following a Hg ↔ Fe scheme that leads to a continuous solid solution series extending from Fe-free vorontsovite to Hg-free ferrovorontsovite. The compositions corresponding to vorontsovite and ferrovorontsovite were determined in 89 and 77 analyses, respectively (Fig. 29). The Zn content does not exceed 1.4 wt. % (0.34 apfu) in vorontsovite and 1.4 wt. % (0.33 apfu) in ferrovorontsovite. The substitution of As for Sb in the third site is limited that is similar to the 12-fold coordinated site with Tl–Cs substitution, where the maximum Cs content was only 0.7 wt. % (0.09 apfu) in vorontsovite and 0.8 wt. % (0.08 apfu) in ferrovorontsovite (Kasatkin et al., 2018a).

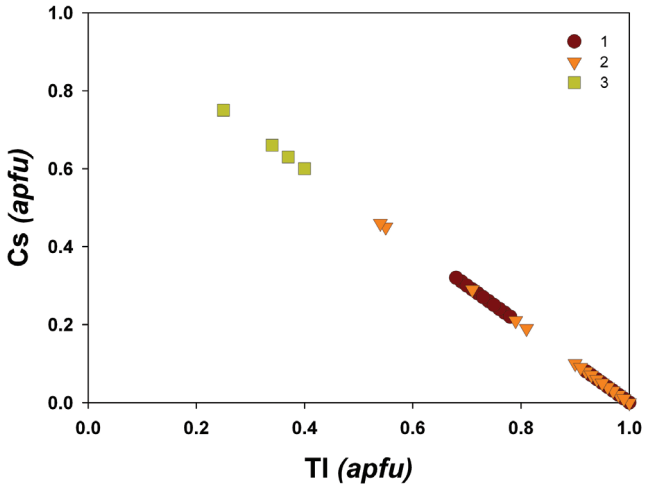

Fig. 30. Tl–Cs correlation in minerals of the galkhaite group.

1 – ferrovorontsovite; 2 – vorontsovite; 3 – galkhaite.

At off-balance ore stockpile no. 2, we later collected carbonate breccias with numerous inclusions of vorontsovite and ferrovorontsovite, which are characterized by significantly higher Cs content (Fig. 30). One of Cs-rich vorontsovite contained zones with Cs > Tl, which formally correspond to galkhaite (Table 5; Fig. 30). This is the first mineral with species-defining Cs found at the Vorontsovskoe deposit and the second finding of galkhaite in the Russian Federation after the Gal-Khaya deposit in Yakutia (Gruzdev et al., 1972). The highest Cs content in ferrovorontsovite reaches 0.38 apfu.

Vrbaite $Hg_3Tl_4As_8Sb_2S_{20}$ was identified in assemblages nos. 1 and 3 as anhedral intergrowths with realgar and baryte up to 0.2 mm in size, which are enclosed in carbonates, and small inclusions in rebulite (Figs. 26c, 26l). The mineral is orange-red, transparent in thin sections and has a metallic luster. In reflected light, vrbaite is grayish white; bireflectance is weak in the air and noticeable in immersion. It is distinctly anisotropic with faded color effects. Abundant orange-red internal reflections are especially strong in immersion. The chemical composition of vrbaite is stoichiometric (Table 5). The parameters of the orthorhombic unit cell are given in Table 3. Similarly to lorándite, vrbaite was mentioned in a list of minerals associated with

lermontovite from the Beshtau U deposit in Northern Caucasus without analytical data (Melkov et al., 1983). We consider our finding the first one in the Russian Federation.

Weissbergite $TlSbS_2$ was found in assemblage no. 1, where it forms elongated grains up to 50 μm in size in carbonates, inclusions in arsenopyrite, thin rims around realgar aggregates and intimate intergrowths with pokhodyashinite (Fig. 21h). It is also associated with aktashite, bernardite, boscardinite, chabournéite, dalnegroite, native gold, parapierrotite, pyrite, and routhierite. In reflected light, weissbergite is grayish white and looks gray at the contact with arsenopyrite. Bireflectance is weak in the air and noticeable in immersion from white to light gray. The mineral is strongly anisotropic in bluish, brownish, and beige tones. Rare orange-red internal reflections are weak in the air and distinct in immersion. Chemically, most grains correspond to the end-member $TlSbS_2$ (Table 5, an. 120); however, some grains contain As (Table 5, an. 121). The compositions, where As exceeds 1 apfu (calculated for S = 8), correspond to the field of isostructural **drechslerite** $Tl_4(Sb_{4-x}As_x)S_8$, which was recently approved and occupies an intermediate position in the weissbergite–lorándite system (Topa et al., 2019). Optically, drechslerite and weissbergite are similar, but the former has more noticeable bireflectance in the air. The identification of weissbergite was supported by SXRD data (Table 3). Our findings of both sulfosalts are the first in the Russian Federation.

Zinkenite $Pb_9Sb_{22}S_{42}$ was described as acicular crystals or anhedral aggregates up to 0.2–0.3 mm across in carbonate breccias (Sazonov et al., 1991a). It intergrows with stibnite, fills microfractures in arsenopyrite and contains realgar inclusions. The mineral was identified by its chemical composition and optical properties. Later, zinkenite was found as anhedral grains and acicular crystals less than 1 mm in size and fibrous aggregates up to 2 cm in size in marblized limestones (Vikentyev et al., 2016). Locally, it contains As up to 7.6 wt. %.

A sample with zinkenite from the Vorontsovskoe deposit in our collection corresponds to the above description and, most likely, originates from the same mineral assemblage (Fig. 16i). The chemical composition of zinkenite from this sample and its hexagonal unit-cell parameters are given in Tables 5 and 3, respectively. The As-bearing zinkenite was also found in assemblage no. 1, where it occurs as rounded grains up to 0.2 mm in size in carbonates, and assemblage no. 4 (Table 5), where it forms acicular crystals up to 1 mm size in quartz–carbonate rock, oval inclusions up to 0.1 mm in size in realgar and native arsenic and small intergrowths with coloradoite and pyrite. In assemblage no. 1, zinkenite is associated with aktashite, boscardinite, chabournéite, écrinsite, hutchinsonite, orpiment, parapierrotite, pyrite, routhierite, stibnite, magnetite, baryte, etc. In assemblage no. 4, zinkenite is observed with aktashite, andorite, cinnabar, routhierite, Hg-bearing sphalerite, and tennantite-(Zn). In reflected light, zinkenite is white and its bireflectance and anisotropy are distinct, especially, in immersion. Red internal reflections are observed.

Some analyses of sulfosalts cannot be recalculated to certain minerals, e.g., phases of compositions Mn–Ag–Pb–Tl–As–Sb–S and $MnPbAg_2Sb_4As_2S_{12}$.

Phase I of the Mn–Ag–Pb–Tl–As–Sb–S composition (Table 5) was found in assemblages nos. 1 and 2. In assemblage no. 1, the mineral occurs as intergrowths with aktashite and grains at the contact of aktashite and Mn–Hg-bearing sphalerite. The maximum size of grains is 0.18 × 0.1 mm (Fig. 11a). In assemblage no. 2, this phase composes small inclusions (up to 10 μm) in realgar and carbonate aggregates. It is possible that phase I is a Mn–Ag-bearing variety of écrinsite.

Phase II of the approximate composition $MnPbAg_2Sb_4As_2S_{12}$ (Table 5) was identified in assemblages nos. 1 and 5 in form of 100-μm intergrowths with boscardinite and isometric grains up to 20 μm in size in pyrite (Fig. 26m). It is opaque, has a black color and a metallic luster. In reflected light, this phase is white; the bireflectance is very weak; it is strongly anisotropic in light gray and pinkish–brownish tones. No internal reflections are observed. The reflectance values for the wavelengths recommended by the Commission on Ore Mineralogy of the IMA are as follows (R_{min}/R_{max}, %): 33.8/34.4 (470 nm), 32.8/33.6 (546 nm), 32.0/32.9 (589 nm), 30.5/31.5 (650 nm). In terms of the chemical composition and stoichiometry, phase II is similar to oyonite, but contains almost half less of Pb.

Oxyhalides

Bismoclite BiOCl was detected in assemblage no. 4 as tiny (<10 μm) rare inclusions in calcite–prehnite–diopside rock in assemblage with chabournéite, native gold, parapierrotite, pyrite, and realgar. Its chemical composition is as follows (wt. %, average of 3 analyses): 88.72 Bi_2O_3, 12.99 Cl, 2.94 –O = Cl_2 (total 98.77). The empirical formula based on two anions is $Bi_{1.01}O_{1.03}Cl_{0.97}$.

Oxides and hydroxides

Akhtenskite MnO_2 was identified in samples from the dumps of the southern open pit in form of black sparkling plates up to 0.5 mm in size, composing a zone of ~1 × 1 cm in massive brown limonite and dull black goethite with quartz (Fig. 31a). According to EMPA, the mineral contains only Mn and O. The strongest reflections of the PXRD pattern are as follows [*d*, Å (*I*)]: 2.41(70), 2.10(30), 1.63(100), 1.43(40), 1.07(10). The calculated parameters of the hexagonal unit cell correspond to akhtenskite (Table 3).

Arsenolite As_2O_3 was mentioned in the oxidation products of massive dark gray nodules and veinlets of native arsenic up to 2–3 cm thick in an aggregate of layered silicate and as fine dissemination in breccias (Vikentyev et al., 2016). Arsenolite and its dimorph **claudetite** were also identified in samples from the dumps of the northern open pit (Kasatkin, 2019). Both minerals are intergrown with each other and form grayish white powdery aggregates replacing native arsenic from assemblage no. 6 with arsenopyrite, native gold, orpiment, calcite, quartz, muscovite-2M_1 and Cl-bearing fluorapatite (Figs. 7b, 7d, 31b). According to EMPA, the minerals contain only As and O. The PXRD data of a sample with both oxides are given in Table 6. The calculated parameters of the unit cells of arsenolite and claudetite are given in Table 3. This is the first finding of claudetite in the Russian Federation.

Asbolane $Mn^{4+}(O,OH)_2 \cdot (Co,Ni,Mg,Ca)_x(OH)_{2x} \cdot nH_2O$ was found in samples of the oxidation zone collected in the dumps of southern open pit. It occurs as black sooty grains up to 1 mm in size in calcite and quartz with nontronite (Fig. 31c). The mineral contains up to 2.5 wt. % Co and 12.6 wt. % Cu, as well as traces of Al, Si, V, Fe, and Zn. The strong reflections of the PXRD pattern are as follows: [*d*, Å (*I*)]: 9.66(100), 4.80(100), 2.42(40), 2.39(20), 1.92(10), 1.53(50), 1.43(50). The calculated parameters of the hexagonal unit cell are given in Table 3.

Birnessite $(Na,Ca,K)_{0.6}(Mn^{4+},Mn^{3+})_2O_4 \cdot 1.5H_2O$ was identified in samples from the dumps of the southern open pit in dark brown soft crusts composed of kaolinite (~80 vol. %), quartz, and supergene Mn oxides (birnessite, vernadite). These crusts overgrow black goethite pseudomorphs after a large pyrite crystal (Fig. 31d). Birnessite was identified according to a strong predominance of Mn and subordinate amounts of Na > K > Ca in chemical analysis and PXRD pattern with the following reflections: [*d*, Å]: 7.13(vs), 3.55(s), 2.53, 2.43, 2.14, 1.82, 1.46. The calculated parameters of the monoclinic unit cell are given in Table 3.

Bixbyite $Mn^{3+}{}_2O_3$ was found in samples from the dumps of the southern open pit. It occurs in dark brown to black powdery aggregates composed of kaolinite and Mn oxides (bixbyite, vernadite) in assemblage with cryptomelane, calcite, and quartz. The Mn/Fe ratio of the mineral is close to 2 : 1; it also exhibits traces of Ti and Ca. The strongest reflections of the PXRD pattern ([2.69 (vs), 1.65 (s), 3.85, 2.34, 1.99, 1.80, 1.45, 1.40, 1.29 Å]) and the calculated parameters of the cubic unit cell correspond to bixbyite (Table 3).

Cesàrolite $PbMn^{4+}{}_3O_6(OH)_2$ forms dark earthy brown aggregates that overgrow hemimorphite crystals in samples collected at the dumps of the southern open pit (Fig. 31e). The chemical composition of the mineral is as follows (wt. %, average of five analyses; H_2O calculated by stoichiometry): 45.55 PbO, 4.25 Fe_2O_3, 46.07 MnO_2, 3.45 H_2O (total 99.32). The empirical formula based on eight O atoms, two of which are assigned to hydroxyl groups, is $Pb_{1.06}(Mn^{4+}{}_{2.76}Fe^{3+}{}_{0.28})_{\Sigma 3.04}O_6(OH)_2$. The strongest reflections of the PXRD pattern ([(*d*, Å (*I*, %)): 3.41(40), 2.21(100), 2.11(50), 1.88(20), 1.77(40), 1.58(50), 1.49(10), 1.42(20)]) and the calculated parameters of the hexagonal unit cell correspond to cesàrolite (Table 3).

Minerals of the **chromite–magnesiochromite** series are rare in metasomatites after carbonate breccias. Chromite and magnesiochromite were found in assemblage no. 1, where they form anhedral grains up to 0.15 mm in size in armenite, augite, and prehnite. Their chemical composition varies and some grains are characterized by both compositions. The associated minerals with chromite and magnesiochromite include realgar, pyrite, aktashite, arsenic, arsenopyrite, coloradoite, native gold, and weissbergite. The chemical composition of chromite/magnesiochromite is as follows (wt. %, average of three analyses for each mineral; Fe^{2+}/Fe^{3+} ratio is calculated from the charge balance): 9.45/10.89 MgO, 18.45/16.65 FeO, 5.35/6.29 Al_2O_3, 61.97/61.72 Cr_2O_3, 5.14/4.94 Fe_2O_3 (total 100.36/100.49). The empirical formulas on the basis of four O atoms and three metal cations are $(Fe^{2+}{}_{0.52}Mg_{0.48})_{\Sigma 1.00}(Cr_{1.66}Al_{0.21}Fe^{3+}{}_{0.13})_{\Sigma 2.00}O_4$ and $(Mg_{0.54}Fe^{2+}{}_{0.46})_{\Sigma 1.00}(Cr_{1.63}Al_{0.25}Fe^{3+}{}_{0.12})_{\Sigma 2.00}O_4$, respectively.

Minerals of the coronadite group of the hollandite supergroup locally occur in the oxidation zone of the Vorontsovskoe deposit. Samples from the dumps of the southern open pit contain four members of this group: coronadite, cryptomelane, hollandite, and manjiroite. **Coronadite** $Pb(Mn^{4+}{}_6Mn^{3+}{}_2)O_{16}$ forms

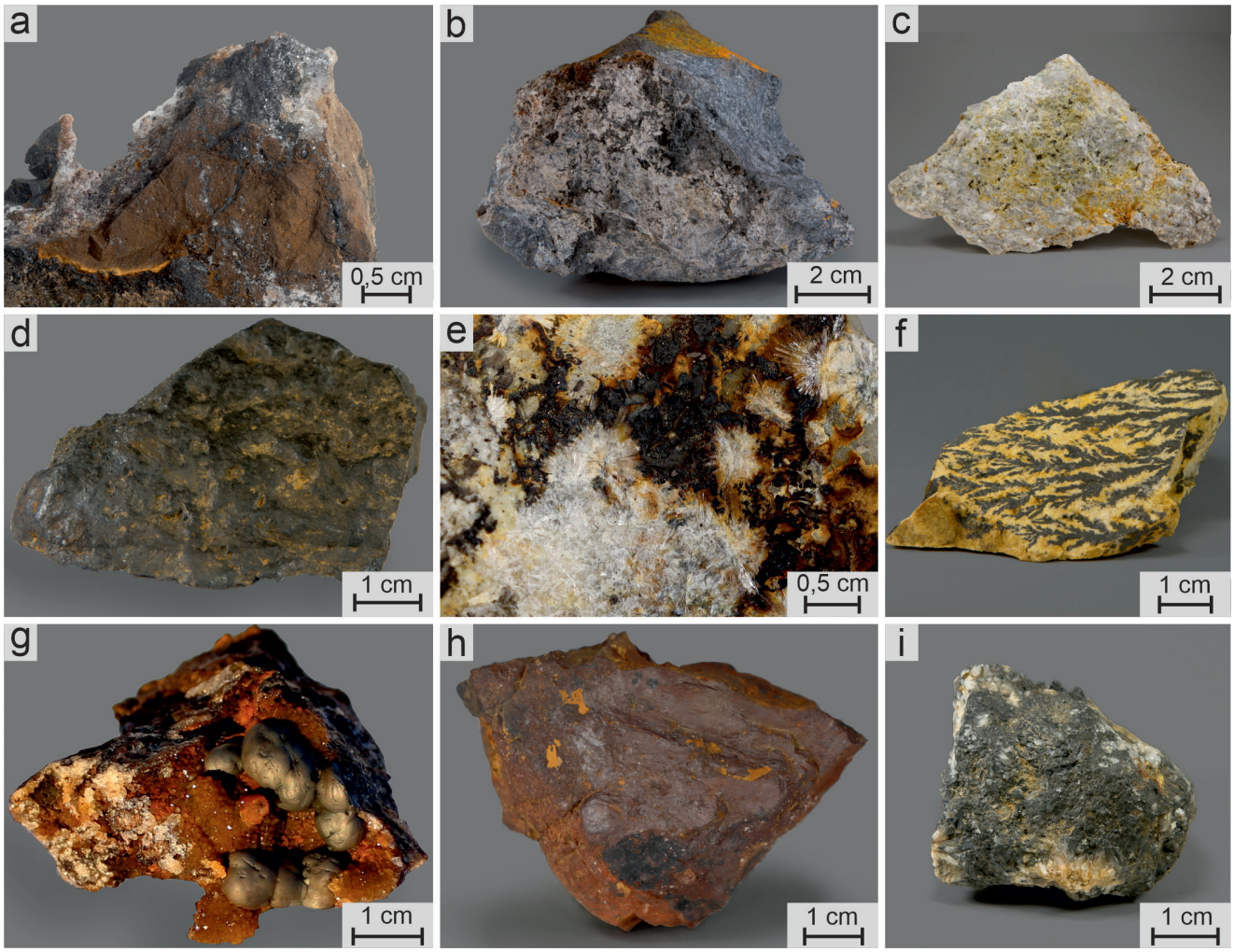

Fig. 31. Oxides and hydroxides of the Vorontsovskoe deposit, part I:

a – black shiny akhtenskite plates on black dull goethite and orange limonite; b – grayish white powdery aggregates composed of arsenolite and claudetite on native arsenic; c – black sooty grains of Co–Cu-bearing asbolane in calcite with yellow nontronite; d – dark brown crust composed of birnessite, vernadite, kaolinite, and quartz on goethite pseudomorph after pyrite; e – dark brown earthy cesàrolite crusts on colorless radial hemimorphite aggregates; f – black dendrites on calcite; g – black cryptomelane spherulites on quartz; h – dark red massive hematite with black crust (in the bottom) of hollandite and lithiophorite; i – black crusts of manjiroite (with microinclusions of rutile) on quartz.

Collections: A.V. Kasatkin (a–f, h, i), Museum «Shtufnoi Kabinet», Severouralsk (g). Photo: A.D. Kasatkina (a–f, h, i), M.V. Tsyganko (g).

black dendrites up to 4 cm long on quartz with calcite and fine-grained pyrite (Fig. 31f). **Cryptomelane** $K(Mn^{4+}_{7}Mn^{3+})O_{16}$ composes spectacular dark brown to black spherulites up to 1 cm in diameter on oxidized quartz (Fig. 31g). **Hollandite** $Ba(Mn^{4+}_{6}Mn^{3+}_{2})O_{16}$ intergrown with lithiophorite occurs as black opaque fine-grained crusts up to 3 × 1 cm on dark red hematite (Fig. 31h). **Manjiroite** $Na(Mn^{4+}_{7}Mn^{3+})O_{16}$ forms dull black crusts on quartz (Fig. 31i) and contains rutile microinclusions. The chemical composition of minerals of the coronadite group is given in Table 7. The strongest reflections in the PXRD patterns are [*d*, Å (*I*)] 6.90(40), 3.47(40), 3.12(100), 2.40(80), 2.20(40), 2.12(20), 1.86(10), 1.56(10) for coronadite; 6.93(90), 4.90(50), 3.11(70), 2.39(100), 2.16(40), 1.83(40), 1.54(40), 1.42(20) for cryptomelane; 3.13(s), 2.38(s), 6.96, 3.47, 2.16, 1.87, 1.81, 1.60, 1.55 for hollandite and 6.96(90), 4.91(70), 3.48(30), 3.12(100), 2.40(100), 2.15(40), 1.83(40), 1.55(40) for manjiroite. The parameters of the tetragonal unit cells of all four minerals are given in Table 3.

Ferberite $Fe^{2+}(WO_4)$ was found as rare short-prismatic crystals up to 20 × 15 μm in size in quartz with calcite and muscovite in assemblage no. 4. It

Table 6

Powder XRD data of sample 1810K with claudetite and arsenolite

d, Å (*I*, %) sample 1810K	Claudetite [JCPDS-ICDD, 15-0778]	Arsenolite [JCPDS-ICDD, 36-1490]	Quartz [JCPDS-ICDD, 46-1045]	Muscovite-2M_1 [JCPDS-ICDD, 06-0263]
10.01(30)				9.95(95)
6.37(50)	6.496(10)	6.3993(44)		
4.98(15)	4.924(25)			4.97(30)
4.45(20)				4.47(20)
4.24(25)	4.277(4)		4.2549(16)	
3.86(10)				3.88(14)
3.70(10)	3.717(2)			3.73(18)
3.47(15)	3.454(50)			3.48(20)
3.33(100)	3.356(20), 3.328(18)	3.3410(2)	3.3434(100)	3.34(25), 3.32(100)
3.24(25)	3.245(100)			
3.18(50)		3.1993(100)		3.19(30)
2.98(15)				2.987(35)
2.85(10)				2.859(25)
2.76(15)	2.771(35)	2.7698(26)		2.789(20)
2.66(8)	2.640(16)			
2.55(40)		2.5422(34)		2.566(55)
2.44(10)			2.4568(9)	2.450(8)
2.40(10)				2.398(10)
2.25(12)	2.264(25), 2.253(6)	2.2619(6)	2.2814(8), 2.2361(4)	2.254(10)
2.12(15)	2.104(6)	2.1327(12)	2.1277(6)	2.132(20)
1.98(15)			1.9798(4)	1.993(45)
1.95(25)		1.9587(22)		1.951(6)
1.87(5)	1.857(12)	1.8728(4)		1.871(4)
1.81(30)			1.8179(13)	
1.66(25)	1.6477(4)	1.6701(14)	1.6717(4), 1.6591(2)	1.662(12)
1.60(8)	1.5988(2)	1.5990(5)		1.603(6)
1.54(20)		1.5515(14)	1.5415(9)	1.541(4)
1.50(12)				1.504(30)
1.44(8)		1.4422(7)	1.4528(2)	1.453(4)

Table 7

Chemical composition (wt. %) of minerals of the coronadite group from assemblage no. 9

An. no.	Mineral	K_2O	CaO	BaO	Mn_2O_3	Fe_2O_3	MnO_2	Total	Formula
1	Coronadite	0.20	0.76	–	12.30	4.79	60.38	99.36	$Pb_{0.82}Ca_{0.12}K_{0.04}(Mn^{4+}_{6.10}Mn^{3+}_{1.37}Fe^{3+}_{0.53})_8O_{16}$
2	Cryptomelane	5.02	0.64	1.49	10.90	–	81.20	100.10	$K_{0.79}Ca_{0.08}Ba_{0.07}(Mn^{4+}_{6.90}Mn^{3+}_{1.02}V^{3+}_{0.08})_8O_{16}$
3	Hollandite	–	0.14	18.88	17.30	2.58	60.45	99.35	$Ba_{1.04}Ca_{0.02}(Mn^{4+}_{5.88}Mn^{3+}_{1.85}Fe^{3+}_{0.27})_8O_{16}$
4	Manjiroite	0.88	–	–	8.89	1.58	86.64	101.59	$Na_{0.82}K_{0.13}(Mn^{4+}_{7.06}Mn^{3+}_{0.80}Fe^{3+}_{0.14})_8O_{16}$

Note. The Mn^{4+}/Mn^{3+} ratio is calculated from charge balance. The analyses contain (wt. %): 20.93 PbO (an. 1), 0.85 V_2O_3 (an. 2), 3.60 Na_2O (an. 4). Samples: 1721K – an. 1; 1808K – an. 2; 1214G – an. 3; 1316M – an. 4.

occurs together with native arsenic, baryte, cinnabar, coloradoite, fluorapatite, orpiment, parapierrotite, pyrite, realgar, sphalerite, and stibnite. In reflected light, ferberite has a grayish white color in comparison with hosting quartz. Bireflectance is weak and anisotropy is distinct. Rare dark brown-red internal reflections are observed in immersion. In chemical composition, ferberite contains a low amount of a hubnerite component (wt. %, average of three analyses): 2.31 MnO, 21.15 FeO, 75.98 WO_3 (total 99.44). The empirical formula on the basis of four O atoms is $(Fe_{0.90}Mn_{0.10})_{\Sigma 1.00}W_{1.00}O_4$.

Fergusonite-(Y) $YNbO_4$ was tentatively identified in a sample collected from the main ore stockpile of the deposit. The mineral occurs as rare small (<7 μm) inclusions in dolomite–calcite rock and is associated with baryte, hingganite-(Y), hingganite-(Nd), Cr-bearing magnetite, pyrite, realgar, routhierite, and wakabayashilite. The chemical composition of the mineral is as follows (wt. %, average of three analyses): 0.40 CaO, 27.13 Y_2O_3, 0.57 Ce_2O_3, 1.61 Nd_2O_3, 1.56 Sm_2O_3, 4.03 Gd_2O_3, 0.57 Tb_2O_3, 4.70 Dy_2O_3, 3.44 Er_2O_3, 0.71 Tm_2O_3, 2.57 Yb_2O_3, 0.39 Lu_2O_3, 0.48 TiO_2, 0.78 ThO_2, 47.63 Nb_2O_5, 0.56 Ta_2O_5, 2.32 WO_3 (total 99.45). The empirical formula on the basis of four O atoms is $(Y_{0.65}\ Dy_{0.07}Gd_{0.06}Er_{0.05}Yb_{0.04}Nd_{0.03}Sm_{0.02}\ Ce_{0.01}Tb_{0.01}Tm_{0.01}Lu_{0.01}\ \ Ca_{0.02}Th_{0.01})_{\Sigma 0.99}(Nb_{0.97}W_{0.03}Ti_{0.02}\ Ta_{0.01})_{\Sigma 1.03}O_4$. In addition to fergusonite-(Y), we found in ore breccias of the deposit four minerals with species-defining REEs: **gasparite-(La)**, **chernovite-(Y)**, **hingganite-(Y),** and **hingganite-(Nd)**. The ore breccias of the deposit are enriched in REEs and HREEs are dominant over LREEs (Murzin et al., 2010; Stepanov et al., 2017). The total REE content varies from 3.7 to 54.8 ppm increasing in more brecciated rocks.

Geikielite $MgTiO_3$ and **pyrophanite** $Mn^{2+}TiO_3$ from the ilmenite group were found in assemblage no. 7. They form rare anhedral grains up to 30 μm in calcite–dolomite–clinochlore rock, which contain zones corresponding to both minerals in chemical composition (Mg-richest geikielite/Mn-richest pyrophanite, wt. %, average of three analyses for each mineral): 16.77/11.38 MgO, 23.08/30.71 MnO, 59.88/57.81 TiO_2 (total 99.73/99.90). The empirical formulas on the basis of three O atoms are $Mg_{0.56}Mn_{0.44}Ti_{1.00}O_3$ and $Mn_{0.60}Mg_{0.39}Ti_{1.01}O_3$, respectively.

Goethite FeO(OH) was identified in several polymineralic samples by strong reflections of the PXRD pattern (Sazonov et al., 1991a). In addition to its hydrated variety, goethite is a main component of the oxidation zone. In our samples from the dumps of the southern open pit, goethite occurs as fine-grained, botryoidal, and stalagmite-like aggregates of black to brown color (Figs. 32a, 32b) and pseudomorphs after pyrite. Black botryoidal goethite was studied by EMPA and XRD. It contains only Fe and O in chemical composition. According to the PXRD pattern, the mineral correspond to goethite. Its unit cell parameters are given in Table 3.

Hematite Fe_2O_3 occurs at the flanks of stringer-disseminated gold mineralization zones (Sazonov et al., 1991a). In altered skarns, it replaces magnetite and, rarely, forms lamellar aggregates in calcite. It was determined by PXRD data. Abundant hematite was identified in assemblage no. 9. Its dark red aggregates are locally covered by black crusts composed of hollandite and lithiophorite (Fig. 31h). It contains only Fe and O in chemical composition. Its PXRD pattern belongs to hematite. The unit-cell parameters are given in Table 3.

Lithiophorite $(Al,Li)(Mn^{4+},Mn^{3+})O_2(OH)_2$ was found in samples from the dumps of the southern open pit. It composes black crusts together with hollandite on dark red massive hematite (Fig. 31h). The mineral was identified by its qualitative chemical composition (dominant Mn and O contents with subordinate Al amount) and PXRD pattern (strong reflections at 9.48 (vs), 4.75 (vs), 2.38 (s), 3.13, 2.47, 1.87, 1.55, 1.42 Å; the calculated parameters of the hexagonal unit-cell are given in Table 3).

Magnetite $Fe^{2+}Fe^{3+}{}_2O_4$ in various quantities occurs in skarns. Magnetite and pyrite are exclusive ore minerals of unaltered skarns, where magnetite forms tiny (0.1–0.2 mm) isometric crystals or inclusions in pyrite. In metasomatites, the amount of magnetite does not exceed hundredth part of a percent (Sazonov et al., 1991a). In magnetite–sulfide ores of the calcite–garnet–epidote skarns at the southern flank of the deposit, magnetite composes euhedral iron black grains up to 0.5 cm in size and massive aggregates. They contain abundant dissemination of major arsenopyrite and pyrite, subordinate sphalerite, chalcopyrite, and galena and rare microinclusions of Bi-Te-bearing sulfides and sulfosalts (assemblage no. 8). Magnetite contains only Fe and O in chemical composition. According to the PXRD pattern, the mineral corresponds to magnetite; the refined parameter of its cubic unit cell is given in Table 3.

Manganite $Mn^{3+}O(OH)$ was identified in a sample collected from the dumps of the southern open pit. It occurs as fine-grained particles in crusts and spherulites of kutnohorite and is responsible for its dark gray color (Fig. 33b). Manganite contains only Mn and O in chemical composition. The strongest reflections of the PXRD pattern [3.40 (s), 2.63, 2.41, 1.80, 1.67 Å] and the refined parameters of the monoclinic unit cell are consistent with manganite (Table 3).

Pyrolusite MnO_2 was found in samples collected at the main ore stockpile and dumps of the northern open pit. It occurs as black columnar crystals up to 5 mm in size with a strong metallic luster, which are grouped into radial aggregates that fill veinlets up to 3–4 cm thick and 10 cm long. (Fig. 32c). Pyrolusite contains only Mn and O in chemical composition. The parameters of the tetragonal unit cell correspond to pyrolusite (Table 3).

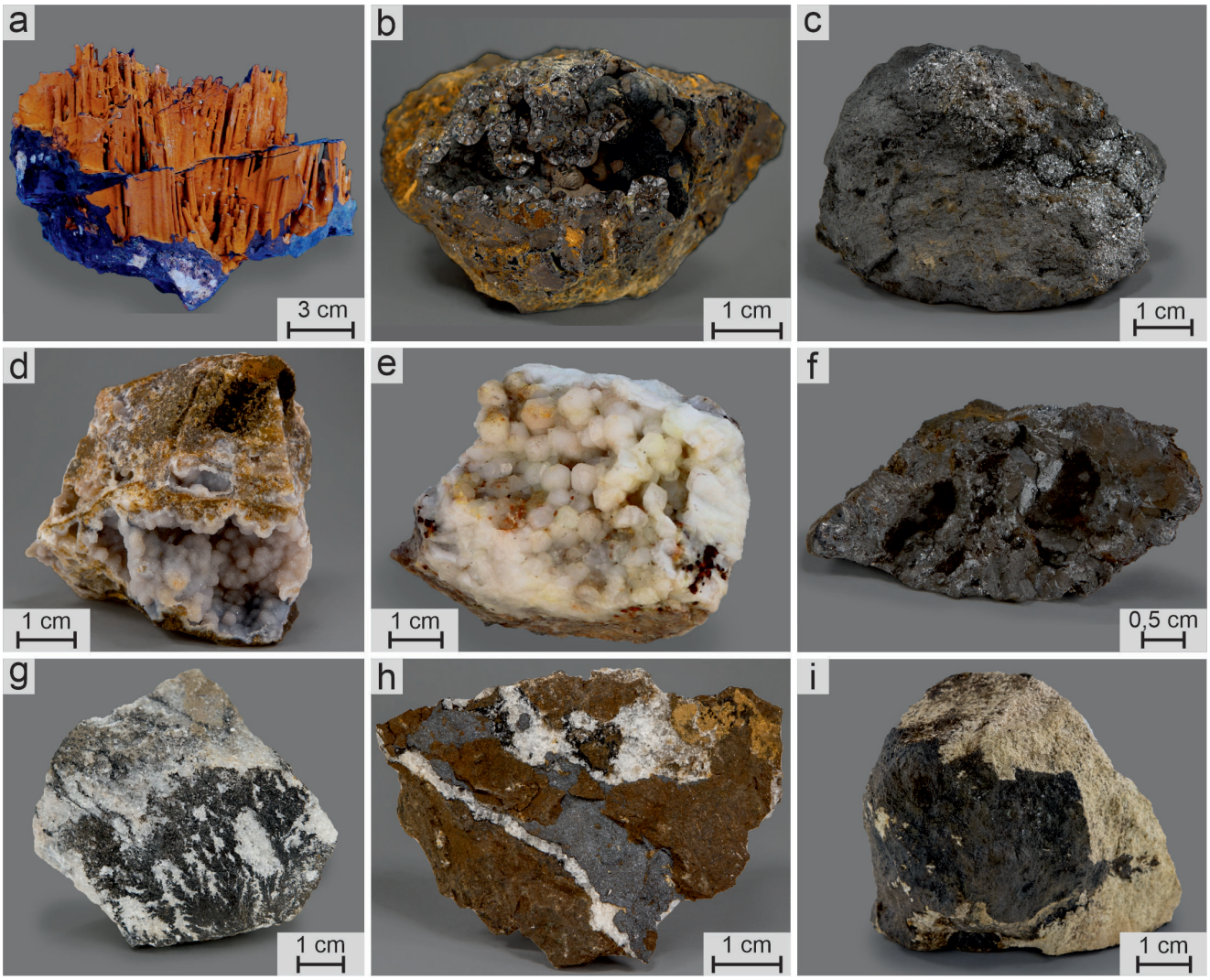

Fig. 32. Oxides and hydroxides of the Vorontsovskoe deposit, part II:

a – stalagmite-like goethite; b – dark brown to black botryoidal goethite on massive limonite; c – black sparkling pyrolusite crystals in dark gray massive pyrolusite aggregate; d – pale grayish violet bunch-shaped chalcedony crusts in of massive quartz; e – crust of quartz crystals; f – black shiny ramsdellite crystals on brown–black massive goethite crust; g – black todorokite dendrites on quartz–calcite aggregate; h – black romanèchite crust on brown calcite and romanèchite aggregates; i – dark brown to black powdery crust composed of vernadite, kaolinite, and halloysite-7Å on quartz–carbonate matrix.

Collections: Museum «Shtufnoi Kabinet», Severouralsk (a, e), A.V. Kasatkin (b–d, f–i). Photo: M.V. Tsyganko (a, e), A.D. Kasatkina (b–d, f–i).

Quartz SiO_2 is one of the major gangue minerals of the Vorontsovskoe deposit, however, its content varies. In metasomatites, milky white translucent quartz composes veins with poor sulfide (pyrite and chalcopyrite) mineralization. Quartz occurs as small anhedral grains up to hundredth part of a millimeter in assemblage with chlorites, micas, carbonates, albite, and K-feldspar. Quartz is one of the major minerals (up to 90 vol. %) of the weathering mantle (Sazonov et al., 1991a). In the oxidation zone, abundant fine-grained quartz forms aggregates up to 3–5 mm in size with a grain size of 0.01–0.05 mm. The quartz aggregates are enclosed in clay minerals and are often brown because of the presence of Fe oxides and hydroxides (Kabanov, 2001). Quartz metasomatites (jasperoids) occur in limestones and at the contacts of dikes with limestones. Quartz forms fine-grained and chalcedony-like aggregates and rice-like crystals with hexagonal sections. In some areas, the granoblastic quartz aggregates replace limestone breccias up to 80 vol. % and form veins up to 7.5 m thick along the dike contacts (Vikentyev et al., 2016). In our samples, abundant quartz

was found in assemblage nos. 2, 4, and, especially, nos. 1 and 6, where it is one of the breccia-forming minerals together with calcite and dolomite. Quartz is abundant in assemblage no. 9 of the oxidation zone. Striking samples of pale grayish violet bunchy chalcedony were collected from the dumps of the southern open pit (Fig. 32d), as well as large (up to 30 cm) geodes and druses of dull white quartz crystals up to 1.5 cm in size (Fig. 32e).

Ramsdellite MnO_2 was found in samples from the dumps of the southern open pit as black, highly lustrous lenticular crystals up to 0.5 mm in size, which are localized in areas up to 1 cm^2 on a brownish black radial fibrous goethite crust (Fig. 32f). The mineral contains only Mn and O in chemical composition. The parameters of its orthorhombic unit cell correspond to ramsdellite (Table 3). Our finding is most probably the first in the Russian Federation.

Ranciéite $(Ca,Mn^{2+})_{0.2}(Mn^{4+},Mn^{3+})O_2 \cdot 0.6H_2O$ intergrown with **todorokite** $(Na,Ca,K,Ba,Sr)_{1-x}(Mn,Mg,Al)_6O_{12} \cdot 3–4H_2O$ were identified in samples from the dumps of the southern open pit. Both minerals are present in subordinate amounts in a massive brown kaolinite–calcite aggregate. The minerals contain the dominant Mn, subordinate Ca, and minor Na. In the PXRD pattern of a mineral mixture, ranciéite is characterized by reflections at d = 7.51 (vs), 3.75 (s), 2.48, 2.07, and 1.42 Å and todorokite exhibits reflections at 9.55 (vs), 4.81 (m), 2.44 (s), 2.35 (s), and 1.90 Å. The calculated unit cell parameters of both oxides are given in Table 3. Samples with todorokite were also found at off-balance ore stockpile no. 2. The mineral composes black dendrites up to 3 cm long on quartz–calcite aggregates (Fig. 32g) and is associated with diopside, fluorapatite, pyrite, and talc. Its identification is based on a qualitative chemical analysis (strongly dominant Mn content with subordinate Ca, Mg, Na, and K contents) and a PXRD pattern (reflections at 9.66, 4.82, 3.06, 2.48, and 1.90 Å).

Romanèchite $(Ba,H_2O)_2(Mn^{4+},Mn^{3+})_5O_{10}$ was found in samples collected in the dumps of the southern open pit. It forms dark gray to black opaque fine-grained crusts up to 3 × 1 cm in size on calcite (Fig. 32h). The identification is supported by a qualitative chemical analysis (the presence of Ba, Mn, and O) and PXRD data (strong reflections at [d, Å (I)]: 9.66(30), 6.96(50), 5.58(40), 3.48(60), 3.29(60), 2.89(50), 2.40 (100), 2.18(80); the calculated parameters of the monoclinic unit cell are given in Table 3).

Rutile TiO_2 is rare and occurs in carbonate–talc matrix of breccias; it contains up to 0.75 wt. % WO_3 (Murzin, Varlamov, 2010). It is occasional among the gangue minerals of assemblages nos. 1, 4, and 6 and also occurs as microinclusions in manjiroite in assemblage no. 9. Rutile was identified by chemical composition (the presence of Ti and O) and reflections at 3.25, 2.49, and 1.69 Å in the PXRD patterns of mineral mixtures.

Vernadite $(Mn,Fe,Ca,Na)(O,OH)_2 \cdot nH_2O$ is an abundant accessory mineral of karst areas, where its content reaches several percents (Sazonov et al., 1991a). In samples from the dumps of the southern open pit, vernadite was found as monomineral dark brown crusts and in brown–black polymineral powdery aggregates, which are composed of clay minerals (kaolinite, dickite, halloysite), carbonates (calcite, rhodochrosite), fine-grained quartz and other supergene Mn oxides (birnessite, bixbyite, cryptomelane, todorokite) (Figs. 31d, 32i). Vernadite was identified by qualitative chemical composition (the presence of strongly dominant Mn and subordinate amounts of Fe, K, and Ca) and XRD data (characteristic broad reflections with d = 2.41 and 1.41 Å).

Carbonates

Azurite $Cu_3(CO_3)_2(OH)_2$ was found in several samples from the dumps of the southern open pit as dark blue grains up to 5 mm in size and thin coatings on oxidized quartz in assemblage with bayldonite, hemimorphite, malachite, galena, pyrite, sphalerite, and tennantite-(Zn) (Fig. 33i). Azurite was identified by qualitative chemical composition (the presence of Cu in cationic composition) and XRD data (Table 3).

Calcite $CaCO_3$ is a major gangue carbonate of the Vorontsovskoe deposit. It is ubiquitous in limestones, marbles, carbonate-bearing tuffites, eruptive breccias (limestone fragments, volcanic matrix) and occurs in post-ore assemblages of skarns. Similarly to dolomite, calcite is abundant in wollastonite skarns, beresites, listvenites, and jasperoids. Spectacular druses of the colorless scalenohedral calcite crystals up to 3 cm in size were collected from the dumps of the southern open pit (Fig. 33a). Calcite is described in details in many publications (Sazonov et al., 1991a; Murzin, Varlamov, 2010; Vikentyev et al., 2016; Stepanov et al., 2017; Soroka et al., 2017, 2018). Jasperoids contain Mg-, Mn- and Fe-bearing calcite (Sazonov et al., 1991a), whereas Mn-bearing calcite (up to 6.9 wt. % MnO) was reported from breccia matrix (Murzin, Varlamov, 2010). Mn-bearing calcite with up to 9.35 wt. % MnO was identified by us in assemblage no. 5.

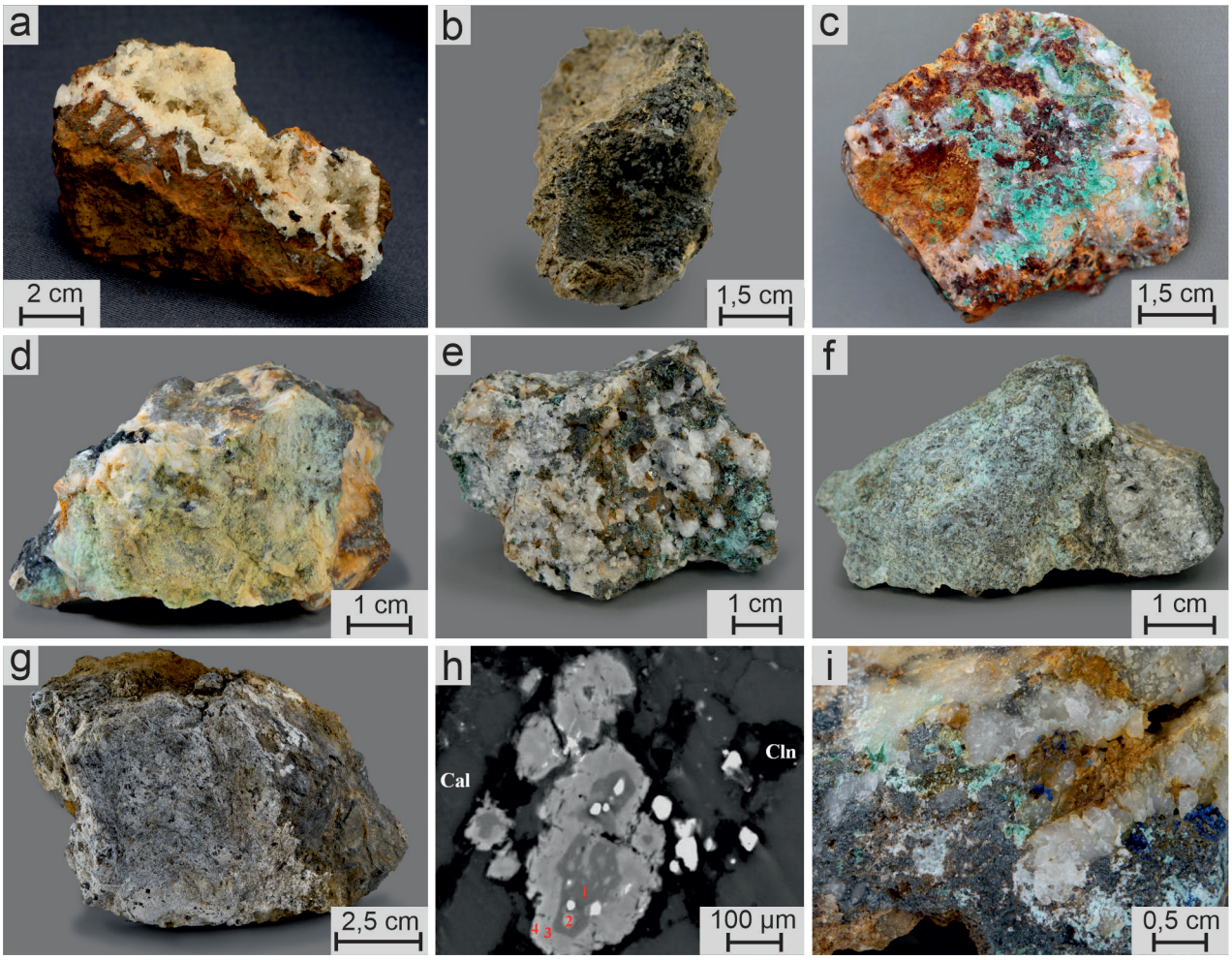

Fig. 33. Carbonates, sulfates, phosphates and arsenates of the Vorontsovskoe deposit:

a – crust of colorless calcite crystals; b – grayish black kutnohorite spherules with fine-grained manganite; c – green malachite crusts on oxidized quartz aggregate; d – yellow powdery beaverite-(Cu) on quartz with malachite; e – green fine-grained brochantite aggregates on quartz with calcite; f – pale blue thin chalcanthite crusts on quartz with calcite and oxidized sulfides; g – dirty white powdery crusts composed of pentahydrite, starkeyite, and gypsum; h – zoned grains composed of minerals of the apatite group in calcite and clinochlore with pyrite (white): 1 – fluorapatite; 2 – hydroxylapatite; 3 – chlorapatite; 4 – turneaurite (numbers correspond to the analyses in Table 9); i – green crusts of bayldonite on quartz in assemblage with pale blue and white hemimorphite and bright blue azurite.

Collections: Museum «Shtufnoi Kabinet», Severouralsk (a, c), A.V. Kasatkin (b, d–i). Photo: M.V. Tsyganko (a, c), A.D. Kasatkina (b, d–g, i), BSE image (h).

Cerussite $Pb(CO_3)$ was found in samples from the southern open pit dumps as colorless crusts with adamantine luster up to 1 × 0.5 mm in size, which replace galena in a quartz–sulfide aggregate from assemblage no. 9. Cerussite is associated with anglesite, pyrite, and sphalerite. The mineral was determined by EMPA, XRD data (Table 3) and Raman spectrum.

Dolomite $CaMg(CO_3)_2$ is one of the major gangue minerals of the Vorontsovskoe deposit. It is abundant in carbonate and carbonatized rocks, wollastonite skarns, beresites, listvenites, and jasperoids. The mineral is studied in details (Sazonov et al., 1991a; Vikentyev et al., 2016; Soroka et al., 2017, 2018). In our samples, dolomite is present in all mineral assemblages as a main gangue mineral of carbonate breccias. In jasperoids, Sazonov et al. (1991a) described a Fe- and Mn-rich dolomite coexisting with calcite. Assemblage no. 5 contains a Mn-rich dolomite with up to 11.1 wt. % MnO.

Kutnohorite $CaMn^{2+}(CO_3)_2$ was identified in one sample collected from the dumps of the southern open pit. It forms crusts and small spherulites of grayish white, locally dark gray color due to the presence of fine-grained manganite (Fig. 33b). The chemical com-

position of the mineral is as follows (wt. %, CO_2 is calculated by stoichiometry; average of three analyses): 24.24 CaO, 31.53 MnO, 3.29 FeO, 40.54 CO_2, total 99.60. The empirical formula based on six O atoms is $Ca_{0.94}Mn_{0.96}Fe_{0.10}(CO_3)_2$. The strongest reflections of the PXRD pattern [(*d*, Å (*I*)): 3.72(50), 2.90(100), 2.41(40), 2.20(30), 2.02(30), 1.85(10), 1.80(40), 1.47(10)] and the refined parameters of the hexagonal unit cell correspond to kutnohorite (Table 3).

Malachite $Cu_2(CO_3)(OH)_2$ is rare in the oxidation zone of the deposit. In samples collected at the dumps of the southern open pit, it forms green fibrous crystals and grains up to 0.5 cm in size, as well as thin films on quartz aggregates (Fig. 33c). It contains only Cu in cationic composition and the parameters of the monoclinic unit cell correspond to malachite (Table 3).

Rhodochrosite $Mn(CO_3)$ was identified in samples from the dumps of the southern open pit. It composes dark gray thin crusts together with kaolinite, cryptomelane, todorokite, and golden yellow pyrite crystals. The mineral contains only Mn in chemical composition; the parameters of the hexagonal unit cell are given in Table 3.

Siderite $Fe(CO_3)$ of supergene origin was found in a weathering mantle, where it occurs as small microglobular aggregates up to few tenths of a millimeter in size (Sazonov et al., 1991a). It contains numerous microinclusions of silicates and other minerals. In karst rocks, the fine-grained siderite is common and is associated with goethite, hematite, and, locally, vivianite. Siderite was identified by chemical composition and XRD data.

Sulfates

Anglesite $Pb(SO_4)$ intergrows with cerussite and forms colorless to pale green (due to the presence of Cu-bearing minerals) thin crusts on quartz with galena, pyrite, and sphalerite in samples with assemblage no. 9 from the dumps of the southern open pit. It contains only Pb and S with a ratio of ~1 : 1. The parameters of the orthorhombic unit cell are given in Table 3.

Baryte $Ba(SO_4)$ is one of the latest minerals of breccias (Vikentyev et al., 2016). Its interstitial aggregates 1–2 mm in size occur between all rock-forming minerals and pyrite. Baryte contains up to 1.5 wt. % SrO. Baryte was found in all mineral assemblages of the carbonate breccias and is one of major gangue minerals in assemblages nos. 1, 3 and 5. Baryte was also found as white radial aggregates up to 1 cm in size with a strong vitreous luster in fractures of volcanic rocks in samples of assemblage no. 9 from the southern open pit dumps and off-balance ore stockpile no. 2. Its chemical composition is close to ideal.

Beaverite-(Cu) $Pb(Fe^{3+}_2Cu)(SO_4)_2(OH)_6$ was found in the oxidation zone of the deposit. In samples with assemblage no. 9 from the dumps of the southern open pit, it forms yellow powdery crusts on oxidized quartz with covellite, djurleite, galena, and malachite (Fig. 33d). The mineral contains (wt. %, H_2O calculated by stoichiometry; average of four analyses) 1.41 K_2O, 13.18 CuO, 27.97 PbO, 23.93 Fe_2O_3, 3.06 As_2O_5, 22.45 SO_3, 8.18 H_2O, total 100.18. The empirical formula based on 14 O atoms is $(Pb_{0.83}K_{0.20})_{1.03}(Fe^{3+}_{1.98}Cu_{1.10})_{3.08}(S_{1.85}As_{0.18})_{2.03}O_8(OH)_6$. The strongest diffractions of the PXRD pattern and the parameters of the hexagonal unit cell correspond to the alunite structural type (Table 3).

Brochantite $Cu_4(SO_4)(OH)_6$ was found in samples with assemblage no. 9 from the dumps of the southern open pit as light green fine-grained aggregates up to 2 × 1 cm in size on quartz with bornite, calcite, chalcopyrite, galena, malachite, pyrite and tennantite-(Zn) (Fig. 33e). The mineral contains only Cu and S with a ratio of ~4 : 1. The strongest reflections of the PXRD pattern and the parameters of the monoclinic unit cell (Table 3) correspond to brochantite.

Chalcanthite $Cu(SO_4) \cdot 5H_2O$ is rare in samples with supergene assemblage no. 9 collected from the dumps of the southern open pit, where it forms thin pale blue crusts with a vitreous luster on an aggregate of quartz, calcite, and partly oxidized sulfides (pyrite, chalcopyrite, galena and sphalerite) (Fig. 33f). The mineral contains only Cu and S with a ratio of 1 : 1. The strongest diffractions of the PXRD pattern and the parameters of the triclinic unit cell (Table 3) correspond to the chalcanthite structural type.

Epsomite $Mg(SO_4) \cdot 7H_2O$, **gypsum** $Ca(SO_4) \cdot 2H_2O$, **pentahydrite** $Mg(SO_4) \cdot 5H_2O$ and **starkeyite** $Mg(SO_4) \cdot 4H_2O$ are typical products of post-mining mineral formation found in fragments of the supergene zone collected at the dumps of the southern open pit. Epsomite occurs as white monomineralic crusts on quartz–calcite aggregates. The aggregates of gypsum, pentahydrite, and starkeyite are found in dirty white crusts overgrowing aggregates of quartz, calcite, and fluorapatite with subordinate pyrite, sphalerite, galena, and tetrahedrite-(Zn) (Fig. 33g). Gypsum contains only Ca and S, whereas other sulfates exhibit only Mg and S in chemical composition with a metal/S close to 1 : 1. Strong reflections of the PXRD pattern of ep-

somite are [*d*, Å (*I*)]: 5.95(30), 5.32(40), 4.46(20), 4.19(100), 3.42(20), 2.97(20), 2.87(30), 2.65(50). The PXRD data of a gypsum, pentahydrite, and starkeyite mixture are given in Table 8. The unit cell parameters of all sulfates calculated from their PXRD patterns are shown in Table 3.

Wolframates

Scheelite $Ca(WO_4)$ is a subordinate mineral of assemblage no. 1. It forms dipyramidal crystals up to 30 × 10 μm in size in calcite and contains small realgar inclusions. Its chemical composition is characterized by significant As content (wt. %, average of two analyses): 73.62 WO_3, 20.52 CaO, 5.08 As_2O_5, total 99.22. The empirical formula based on four O atoms is $Ca_{1.02}(W_{0.89}As_{0.12})_{\Sigma 1.01}O_4$.

Phosphates, arsenates

Minerals of the apatite supergroup include chlorapatite, fluorapatite, hydroxylapatite, svabite, and turneaureite. Abundant **fluorapatite** $Ca_5(PO_4)_3F$ occurs as isometric grains 10–12 μm in size in Mn-bearing calcite of the breccias matrix and contains 6.3–7.2 wt. % As_2O_5* and 2.4–2.6 wt. % F (Murzin, Varlamov, 2010). Fluorapatite crystals up to 20 μm in size were found among the gangue minerals of metasomatites together with native arsenic and arsenopyrite (Murzin et al., 2011). Fluorapatite contains up to 0.7 wt. % SrO, 0.6 wt. % MnO, 0.2 wt. % As_2O_5, and 1.6 wt. % Cl. Some grains contain significant REE contents: up to 6.4 wt. % Ce_2O_3, 3.2 wt. % La_2O_3, and 2.0 wt. % Nd_2O_3.

In our samples, fluorapatite was found in all mineral assemblages except for assemblages no. 2 and 8. In assemblages nos. 1, 4 and 5, it is rare in contrast to other ones. The most interesting zoned fluorapatite from assemblage no. 7 exhibits a broad P–As and F–Cl–OH isomorphic substitutions up to the zones corresponding to **hydroxylapatite** $Ca_5(PO_4)_3OH$, **chlorapatite** $Ca_5(PO_4)_3Cl$, and **turneaureite** $Ca_5(AsO_4)_3Cl$ in composition. These members of the apatite group occur in zoned oval grains up to 40 μm in size, which are enclosed in calcite and clinochlore and contain pyrite microinclusions (Fig. 33h). The Cl and As content increases from the center of the grain to the edges, thus the central part always corresponds to fluorapatite and most edges locally match the composition of turneaureite. Assemblage no. 1 hosts **svabite** $Ca_5(AsO_4)_3F$ as inclusions up to 30 μm in size in baryte with calcite. It contains low amounts of Si and S. The chemical composition of minerals of the apatite supergroup is given in Table 9.

Bayldonite $Cu_3PbO(AsO_3OH)_2(OH)_2$ is a rare supergene mineral found in samples with assemblage no. 9 from the dumps of the southern open pit. It forms minute green crusts on quartz with azurite, hemimorphite, and tennantite-(Zn) relics (Fig. 33i). The mineral contains (wt. %, H_2O calculated by stoichiometry; average of three analyses): 30.82 CuO, 2.09 ZnO, 31.63 PbO, 30.58 As_2O_5, 0.37 SO_3, 4.94 H_2O, total 100.43. The empirical formula based on eleven O atoms is $Pb_{1.03}(Cu_{2.83}Zn_{0.19})_{3.02}(As_{1.94}S_{0.03})_{1.97}O_7(OH)_4$. The strongest reflections of the PXRD pattern [(*d*, Å (*I*)): 4.90(40), 4.52(40), 3.18(100), 2.93(50), 2.68(50), 2.50(40), 2.27(30)] and the calculated parameters of the monoclinic unit cell correspond to bayldonite (Table 3).

Chernovite-(Y) $Y(AsO_4)$ was found in one sample from assemblage no. 5 as rare dipyramidal crystals up to 30 μm in size in Mn-bearing dolomite. The mineral contains a significant xenotime (0.30 apfu) and low wakefieldite (0.04 apfu) components. Its chemical composition is (wt. %, average of three analyses): 1.23 CaO, 41.06 Y_2O_3, 0.44 La_2O_3, 0.74 Ce_2O_3, 2.25 Nd_2O_3, 1.01 Sm_2O_3, 2.36 Gd_2O_3, 4.09 Dy_2O_3, 2.09 Er_2O_3, 1.93 Yb_2O_3, 9.36 P_2O_5, 1.45 V_2O_5, 32.72 As_2O_5, total 100.73. The empirical formula based on four O atoms is $(Y_{0.82}Dy_{0.05}Nd_{0.03}Gd_{0.03}Er_{0.02}Yb_{0.02}La_{0.01}Ce_{0.01}Sm_{0.01}Ca_{0.05})_{1.05}(As_{0.64}P_{0.30}V_{0.04})_{0.98}O_4$.

Gasparite-(La) $La(AsO_4)$ was determined as a single grain 20 × 10 μm in size in assemblage no. 7 at the contact with alabandite in calcite–dolomite rock. It is associated with tsygankoite and arsenopyrite. Gasparite-(La) contains (wt. %, average of three analyses): 2.23 CaO, 36.73 La_2O_3, 14.70 Ce_2O_3, 1.37 Pr_2O_3, 2.39 Nd_2O_3, 41.98 As_2O_5, total 99.40. Its empirical formula based on four O atoms is $(La_{0.62}Ce_{0.25}Nd_{0.04}Pr_{0.02}Ca_{0.11})_{1.04}As_{1.00}O_4$.

Tilasite $CaMg(AsO_4)F$ was found in assemblage no. 7, where it forms anhedral grains up to 0.2 mm in size intergrown with duranusite, tsygankoite, orpiment, and realgar in dolomite and calcite (Figs. 8d, 26g). The mineral contains (wt. %, average of five analyses) 50.85 As_2O_5, 24.97 CaO,18.02 MgO, 9.21 F, –3.88 O = F, total 99.17. Its empirical formula based on O + F = 5 anions is $Ca_{0.99}Mg_{1.00}(As_{0.99}O_{3.92})_{4.91}F_{1.08}$. The strongest reflections of the PXRD pattern and the

* The original values in As_2O_3 given by authors (Murzin and Varlamov, 2010; Murzin et al., 2011) were recalculated by us to As_2O_5

Table 8

Powder XRD data of sample 1091P with pentahydrite, starkeyite and gypsum

***d*, Å (*I*, %) sample 1091P**	Pentahydrite [JCPDS-ICDD, 25-0532]	Starkeyite [JCPDS-ICDD, 24-0720]	Gypsum [JCPDS-ICDD, 33-0311]
10.358(5)	10.31(5)		
7.682(10)			7.63(100)
6.896(25)		6.83(45)	
5.853(15)	5.84(20)		
5.648(10)	5.62(10)		
5.470(60)		5.43(75)	
5.160(15)	5.15(30)	5.15(8)	
4.966(30)	4.93(100)		
4.828(5)	4.83(5)		
4.735(30)		4.70(35)	
4.491(100)		4.46(100)	
4.351(10)	4.34(5)		
4.283(5)			4.283(100)
3.974(60)		3.951(65)	
3.817(10)		3.794(8)	3.799(17)
3.667(20)	3.65(30)		
3.616(10)		3.598(12)	
3.475(10)	3.46(15)		
3.415(50)		3.398(45)	
3.272(15)	3.26(40)	3.263(6)	
3.231(40)		3.216(40)	
3.165(5)	3.15(10)		
3.078(5)			3.065(75)
3.043(15)	3.03(20)		
3.019(5)	3.00(20)		
3.007(5)			
2.989(20)	2.99(5)	2.978(20)	
2.958(70)	2.95(30)	2.946(55)	
2.907(5)	2.90(5)	2.892(8)	2.873(45)
2.800(10)	2.79(25)		
2.779(25)		2.769(25)	2.789(10)
2.765(20)		2.755(14)	
2.707(10)	2.69(15)	2.702(6)	
2.685(20)	2.68(25)		2.685(35)
2.564(25)		2.555(20)	
2.546(10)	2.537(20)		
2.485(10)	2.489(5)	2.478(8)	2.495(11)
2.465(20)	2.466(5)	2.458(14)	
2.430(25)		2.422(20)	
2.406(5)	2.407(15)		
2.361(15)	2.360(5)	2.351(14)	
2.285(15)	2.280(5)	2.279(10)	
2.273(20)		2.266(25)	
2.228(5)			2.219(15)
2.186(5)	2.182(5)		
1.998(5)	1.995(35)	1.965(8)	
1.882(10)	1.880(5)	1.877(8)	
1.799(10)		1.795(10)	
1.721(5)	1.729(10)	1.718(6)	

Note. Only reflections with $I_{rel.} \geq 5\%$ are included.

Table 9

Chemical composition (wt. %) of minerals of the apatite group

An. no.	As. no.	Mineral	CaO	P_2O_5	As_2O_5	F	Cl	H_2O	–O = F,Cl	Total	Formula
1	7	Fluorapatite	54.75	41.35	0.67	2.62	0.52	0.41	–1.22	99.1	$Ca_{4.98}(P_{2.97}As_{0.03})_{3.00}O_{12}[F_{0.70}(OH)_{0.23}Cl_{0.07}]_{1.00}$
2		Hydroxylapatite	50.91	27.21	19.31	0.56	1.45	1.03	–0.56	99.91	$Ca_{4.96}(P_{2.10}As_{0.92})_{3.02}O_{12}[(OH)_{0.62}Cl_{0.22}F_{0.16}]_{1.00}$
3		Chlorapatite	50.72	27.66	17.56	1.29	3.03	0.25	–1.23	99.28	$Ca_{5.00}(P_{2.15}As_{0.84})_{2.99}O_{12}[Cl_{0.47}F_{0.38}(OH)_{0.15}]_{1.00}$
4		Turneaureite	47.3	17.33	30.54	0.75	2.93	0.43	–0.98	98.3	$Ca_{4.98}(As_{1.57}P_{1.44})_{3.01}O_{12}[Cl_{0.49}(OH)_{0.28}F_{0.23}]_{1.00}$
5	1	Svabite	44.18	–	50.9	1.6	1.98	0.14	–1.12	99.54	$Ca_{5.02}(As_{2.82}Si_{0.11}S_{0.07})_{3.00}O_{12}[F_{0.54}Cl_{0.36}(OH)_{0.10}]_{1.00}$

Note. The H_2O content is calculated by stoichiometry. Analysis no. 5 contains 1.02 wt. % SiO_2 and 0.84 wt. % SO_3. Samples: Vor-10bis-3c – an. 1–4; Vor-01/19-1tf – an. 5.

parameters of the monoclinic unit cell correspond to tilasite (Table 3).

Vivianite $Fe^{2+}_3(PO_4)_2 \times 8H_2O$ was found in Fe-rich ocher montmorillonite areas of karst rocks (Sazonov et al., 1991a). It forms gray blue to indigo blue fractured lenses up to 3 mm long and up to 1 mm thick. The identification of vivianite is supported by chemical composition and PXRD data.

Silicates

Amphiboles were found in propylitized rocks of the deposit (Sazonov et al., 1991a). They include hornblende and an amphibole of the actinolite–tremolite series. According to the current nomenclature, the composition of this «hornblende» (Sazonov et al., 1991a) corresponds to **magnesio-ferri-hornblende** $\square Ca_2(Mg_4Fe^{3+})(AlSi_7O_{22})(OH)_2$. Colorless acicular **tremolite** crystals $\square Ca_2(Mg_{5.0\text{-}4.5}Fe^{2+}_{0.0\text{-}0.5})Si_8O_{22}(OH)_2$ were found in skarns and wollastonite skarns. The mineral was determined by optical properties. Tremolite was also described as a rare mineral in the matrix of the carbonate breccias (Murzin, Varlamov, 2010).

In our samples, tremolite occurs as creamy white radial aggregates of fine-fibrous crystals up to 0.5 cm long in assemblage with brownish massive talc enclosed in white marble (Fig. 34a). The chemical composition of the mineral is given in Table 10. The calculated parameters of the monoclinic unit cell are given in Table 3.

Pargasite $NaCa_2(Mg_4Al)(Si_6Al_2)O_{22}(OH)_2$ was found in samples from the dumps of the northern open pit. The mineral forms black prismatic crystals with a vitreous luster up to 1 × 0.5 cm in size in lamprophyre (Fig. 34b). Its chemical composition and calculated parameters of the monoclinic unit cell are given in Tables 10 and 3, respectively.

Armenite $BaCa_2(Al_6Si_9)O_{30} \cdot 2H_2O$ was identified in samples with assemblage no. 1 from the main ore stockpile specimens (Kasatkin, 2019). It forms white aggregates up to 1 mm in size with a vitreous luster and intergrows with calcite, clinochlore, dolomite, muscovite, and pyrite in metasomatite (Fig. 34c). Other associated ore minerals include boscardinite, chabournéite, christite, cinnabar, coloradoite, dalnegroite, native gold, metacinnabar, parapierrotite, and routhierite. The reflectance values of armenite are much higher than of the associated gangue minerals. In reflected light, it looks light gray at the contact with dark gray clinochlore, muscovite, and calcite. In immersion, the reflectance values of armenite strongly decrease: it looks dark gray in comparison with almost black associated

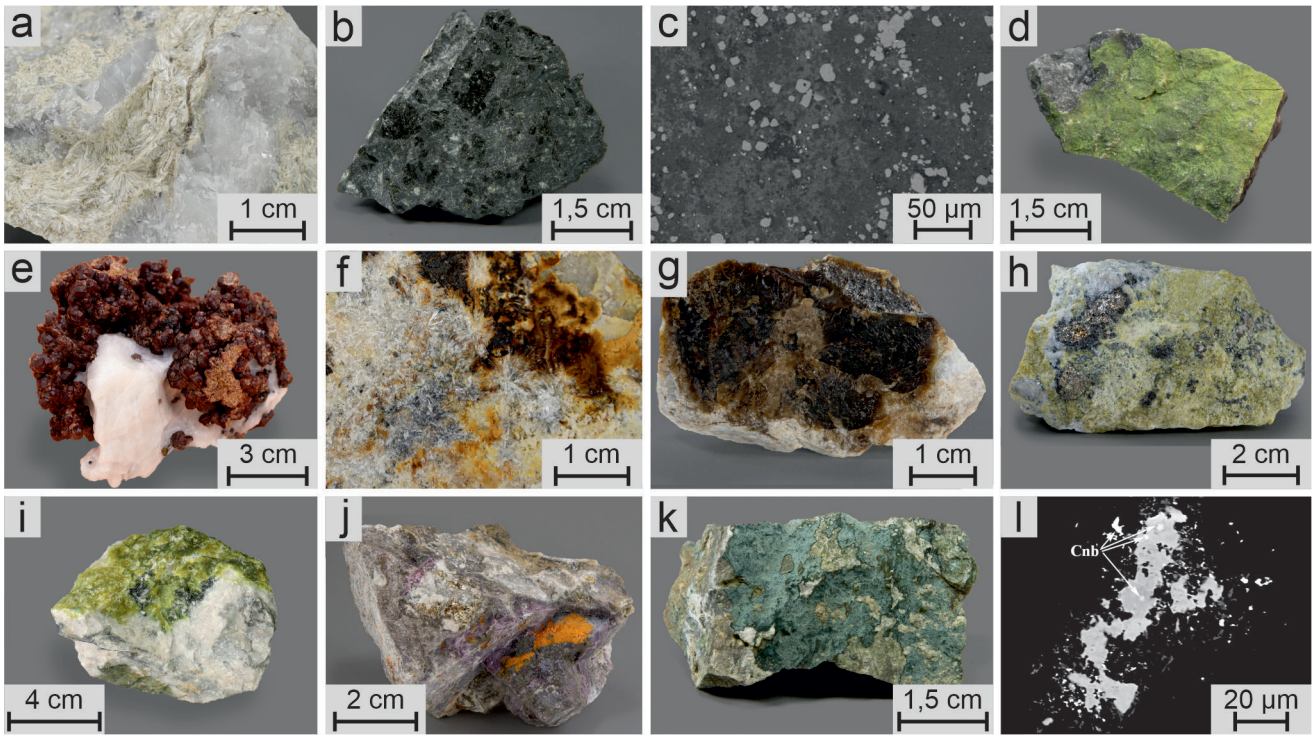

Fig. 34. Silicates of the Vorontsovskoe deposit:

a – veinlet of creamy white radial aggregates of fibrous tremolite in white marble; b – black prismatic pargasite crystals in lamprophyre; c – abundant aggregates of armenite (moderate gray) intergrown with muscovite and clinochlore (dark gray zones) and pyrite (numerous light gray rounded grains); d – greenish yellow powdery aggregates of chapmanite on calcite with quartz and stibnite; e – crust of andradite crystals on calcite; f – radial aggregates of colorless prismatic hemimorphite crystals on quartz in assemblage with dark brown earthy crusts of cesàrolite; g – dark brown massive chrysotile-2Or_{c1} on calcite; h – yellow aggregates of chrysotile-2Or_{c1} on dolomite with pyrite and magnetite; i – light green massive pigeonite intergrown with chrysotile-2O_{rc1} in dark matrix; j – violet aggregates of Ba,Mg,Mn-bearing muscovite in dolomite–calcite marble with pyrite and orange realgar; k – greenish blue crust of celadonite–ferroceladonite on carbonate matrix; l – thorite aggregate with cinnabar inclusions in microcline.

Collections: A.V. Kasatkin (a–c, f–h, j–l), Museum «Shtufnoi Kabinet», Severouralsk (d, e, i). Photo: A.D. Kasatkina (a, b, f–h, j, k), M.V. Tsyganko (d, e, i); BSE images (c, l).

gangue minerals. Bireflectance and anisotropy are distinct in gray tones and are much more intense in immersion. The chemical composition of armenite and the parameters of its orthorhombic unit cell are given in Tables 10 and 3, respectively. This is the first finding of the mineral in the Russian Federation.

Chapmanite $Fe^{3+}{}_2Sb^{3+}(SiO_4)_2(OH)$ was established in samples from the main ore stockpile of the deposit (Kasatkin, 2019). The mineral forms thin greenish yellow crusts and powdery coatings on brecciated rock, which is composed of calcite, quartz, and stibnite (Fig. 34d). Chapmanite contains (wt. %, H_2O calculated by stoichiometry; average of five analyses): 32.90 Fe_2O_3; 35.06 Sb_2O_3; 27.45 SiO_2, 2.04 Al_2O_3; 2.06 H_2O, total 99.51. Its empirical formula based on nine O atoms is $(Fe^{3+}{}_{1.79}Al_{0.17})_{1.96}Sb^{3+}{}_{1.05}Si_{1.99}O_8(OH)$. The strongest reflections of the PXRD pattern are [*d*, Å (*I*)]: 7.614(100), 4.168(20), 3.874(40), 3.573(60), 3.182(40), 2.908(20), 2.587(30). The calculated parameters of the monoclinic unit cell are consistent with those of chapmanite (Table 3). This is the first finding of this mineral in the Russian Federation.

Chlorites are the most abundant minerals in altered rocks of the deposit. They are widely distributed in skarns, propylites, beresites, and listvenites. Chlorites include a common **clinochlore** $Mg_5Al(AlSi_3O_{10})(OH)_8$ and a rarer **chamosite** $(Fe^{2+},Mg,Al,Fe^{3+})_6(Si,Al)_4O_{10}(OH,O)_8$. They compose colorless (in limestones) to grayish green and green (in metasomatites) flakes few tens of micrometers and smaller. Chlorites were determined by chemical composition, PXRD patterns and optical parameters (Sazonov et al., 1991a). The rock-forming clinochlore was found in assemblages nos. 1, 2 and 7. The colorless clinochlore from assemblage no.

Table 10

Chemical composition (wt. %) of silicates

An. no.	Mineral	Na_2O	K_2O	CaO	BaO	MgO	MnO	FeO	Al_2O_3	Fe_2O_3	TiO_2	SiO_2	H_2O*	Total	Formula
1	Andradite	–	–	35.2	–	–	–	–	8.11	18.94	1.49	37.94		101.68	$Ca_{2.99}Fe^{3+}_{1.13}Al_{0.76}Ti_{0.09}Si_{3.00}O_{12}$
2	Armenite	–	–	9.85	13.09	–	–	–	26.72	–	–	47.08	3.14	99.88	$Ba_{0.98}Ca_{2.02}Al_{6.01}Si_{8.99}O_{30} \cdot 2H_2O$
3	Augite	–	–	15.14	–	19.41	1.80	0.96	7.67	–	–	55.07		100.05	$(Mg_{1.01}Ca_{0.57}Al_{0.32}Mn_{0.05}Fe^{2+}_{0.03})_{1.98}Si_{1.93}O_6$
4	Celadonite	–	11.01	–	–	5.34	–	8.12	4.98	10.78	–	56.79	4.26	101.28	$K_{0.99}Mg_{0.56}Fe^{2+}_{0.48}Fe^{3+}_{0.57}Al_{0.41}Si_{4.00}O_{10}(OH)_2$
5	Chabazite-Ca	–	1.75	7.56	2.57	–	–	–	18.56	–	–	47.16	22.32	99.92	$(Ca_{1.42}K_{0.39}Ba_{0.18})_{1.99}Al_{3.82}Si_{8.24}O_{24} \cdot 13H_2O$
6	Chamosite	–	–	–	–	9.14	–	34.43	16.16	–	–	27.86	10.86	98.45	$Fe^{2+}_{3.18}Mg_{1.51}Al_{2.10}Si_{3.08}O_{10}(OH)_8$
7	Chrysotile-2Or_{c1}	–	–	–	–	40.65	–	3.81	–	–	–	43.24	12.88	100.58	$(Mg_{2.82}Fe^{2+}_{0.15})_{2.97}Si_{4.01}O_5(OH)_4$
8	Clinochlore	–	–	–	–	39.15	–	–	13.47	–	–	33.86	12.84	99.32	$Mg_{5.45}Al_{1.48}Si_{3.16}O_{10}(OH)_8$
9	Diopside	–	–	25.99	–	17.19	–	1.64	–	–	–	54.44		99.22	$Ca_{1.02}Mg_{0.94}Fe^{2+}_{0.05}Si_{2.00}O_6$
10	Ferroceladonite	–	10.45	–	–	4.08	–	9.46	5.16	11.17	–	56.69	4.24	101.25	$K_{0.94}Fe^{2+}_{0.56}Mg_{0.43}Fe^{3+}_{0.59}Al_{0.43}Si_{4.00}O_{10}(OH)_2$
11	Grossular	–	–	36.56	–	–	–	–	14.40	11.17	0.83	39.45		102.41	$Ca_{2.99}Al_{1.29}Fe^{3+}_{0.64}Ti_{0.05}Si_{3.01}O_{12}$
12	Harmotome	–	1.28	0.36	21.82	–	–	–	15.62	–	–	45.68	14.48	99.24	$(Ba_{2.13}K_{0.41}Ca_{0.10})_{2.64}(Al_{4.58}Si_{11.36})O_{32} \cdot 12H_2O$
13	Johannsenite	–	–	23.38	–	1.79	25.25	0.88	0.55	–	–	47.58		99.43	$Ca_{1.03}Mn_{0.88}Mg_{0.11}Fe^{2+}_{0.03}Al_{0.03}Si_{1.96}O_6$
14	Laumontite	–	0.87	11.78	–	–	–	–	22.02	–	–	51.44	15.50	101.61	$(Ca_{0.98}K_{0.09})_{1.07}Al_{2.01}Si_{3.98}O_{12} \cdot 4H_2O$
15	Muscovite-2M_1	–	9.39	1.74	0.95	5.99	0.92	–	28.96	–	1.79	45.73	4.45	99.92	$(K_{0.81}Ca_{0.13}Ba_{0.03})_{0.97}(Al_{2.30}Mg_{0.60}Ti_{0.09}Mn_{0.05})_{3.04}Si_{3.08}O_{10}(OH)_2$
16	Pargasite	2.43	0.90	12.71	–	14.20	–	8.32	15.64	–	0.66	42.55	2.07	99.48	$(Na_{0.66}K_{0.17})(Na_{0.02}Ca_{1.98})_{2.00}(Mg_{3.07}Fe^{2+}_{1.01}Al_{0.86}Ti_{0.07})_{5.01}(Si_{6.18}Al_{1.82}O_{22})(OH)_2$
17	Pigeonite	–	–	5.50	–	34.08	–	1.71	3.15	–	–	55.17		99.61	$(Mg_{1.75}Ca_{0.20}Fe^{2+}_{0.05})_{2.00}(Si_{1.90}Al_{0.13})_{2.03}O_6$
18	Prehnite	–	–	27.02	–	–	–	–	24.17	–	–	44.55	4.38	100.12	$Ca_{1.98}Al_{1.95}Si_{3.05}O_{10}(OH)_2$
19	Pumpellyite-Mg	–	–	23.49	–	4.47	0.38	0.08	23.70	–	–	37.81	6.81	100.00	$Ca_{2.00}(Al_{2.22}Mg_{0.53}V^{3+}_{0.21}Mn_{0.02}Fe^{2+}_{0.01})_{2.99}Si_{3.00}O_{11.40}(OH)_{1.60} \cdot H_2O$
20	Talc	–	–	–	–	28.02	1.10	4.21	–	–	–	62.23	4.65	100.21	$(Mg_{2.69}Mn_{0.23}Fe_{0.06})_{2.98}Si_{4.01}O_{10}(OH)_2$
21	Tremolite	0.16	0.25	13.23	–	21.69	0.27	3.35	1.29	–	–	57.10	2.17	99.51	$K_{0.04}(Na_{0.04}Ca_{1.96})_{2.00}(Mg_{4.47}Fe^{2+}_{0.39}Al_{0.11}Mn_{0.03})_{5.00}(Si_{7.90}Al_{0.10}O_{22})(OH)_2$
22	Vesuvianite	–	–	36.37	–	0.25	3.04	1.51	19.76	–	–	36.52	2.55	100.00	$Ca_{19}(Al_{11.36}Mn_{1.26}Fe_{0.62}Mg_{0.18})_{13.42}Si_{69.56}O_{74}(OH)_{8.29}$

Note. The H_2O content is calculated by stoichiometry in all analyses except analyses nos. 19 and 22, where it is calculated by total deficiency. The Fe^{2+}/Fe^{3+} ratio in analyses nos. 4 and 10 is calculated from the charge balance. The analysis no. 19 contains 3.26 wt. % V_2O_3.

Samples: 1044A – an. 1; 928A – an. 2; Vor-8bis-1 – an. 3; 1002C – an. 4, 10; 312Sh – an. 5; Vor-08/18-15 – an. 6; 547Ch – an. 7; Vor-10/2017-1 – an. 8; Vor-CC-1b – an. 9; Vor-05/18-9 – an. 11; Vor-2013new–1 – an. 12; Vor-08/20-9 – an. 13; 535L – an. 14; 1374M – an. 15; 920P – an. 16; 1073P – an. 17; Vor-01/19-22 – an. 18; Vor-2013-8-1 – an. 19; 661T – an. 20; 795T – an. 21; Vor-08/18-13 – an. 14.

The mineral formulas are recalculated to four Si and 12 O atoms (celadonite, ferroceladonite), six (augite, diopside, johannsenite, pigeonite), nine (chrysotile-2Or_{c1}), 12 (andradite, grossular, muscovite-2M_1, prehnite, talc), 18 (chamosite, clinochlore) and 24 (pargasite, tremolite), 12 O atoms and 4 H_2O molecules (laumontite), 13 O and one H_2O molecule (pumpellyite-Mg), 24 O atoms and 13 H_2O molecules (chabazite-Ca), 30 O atoms and 2 H_2O molecules (armenite), 32 O atoms and 12 H_2O molecules (harmotome) and 19 Ca atoms (vesuvianite).

4 contains no Fe in its composition (Table 10). Chamosite was identified only in sample Vor-08/18-15 (Table 10). The parameters of the triclinic unit cells of chlorites calculated from their PXRD patterns are given in Table 3.

Epidote $Ca_2(Al_2Fe^{3+})[Si_2O_7][SiO_4]O(OH)$ is abundant in various metasomatites of the deposit. Sazonov et al. (1991a) describe three morphological varieties of the mineral: isometric grains up to 2 mm thick, veinlets up to 3 mm thick, and powder aggregates. The mineral was identified by its chemical composition. In calcite–garnet–epidote skarns with late magnetite–sulfide mineralization (the dumps of the southern open pit), epidote was found in assemblage no. 8 with rare Bi and Te minerals.

Feldspars include albite, microcline, and orthoclase. **Albite** $Na(AlSi_3O_8)$ (including oligoclase) is rare in metasomatites and forms aggregates of μm-sized grains with microinclusions of other minerals. **Microcline** $K(AlSi_3O_8)$ occurs in zones of K-feldspar alteration of rocks of the intrusive diorite–granodiorite complex and associated andesites. **Orthoclase** $K(AlSi_3O_8)$ was found in metasomatites with gold mineralization in form of fine (few tens of micrometers) grains with microinclusions of chlorites and other minerals. All feldspars were identified by chemical composition and PXRD patterns (Sazonov et al., 1991a). Kabanov (2001) mentioned feldspars in the oxidation zone. Later, microcline and orthoclase from igneous rocks of diorite–granodiorite composition and volcanosedimentary rocks (tuffites, tuffaceous siltstones and tuffaceous sandstones) were studied by XRD and thermal analyses (Rovnushkin et al., 2010). Feldspars are extremely rare in carbonate breccias. Only rare grains of albite and Ba-bearing orthoclase (hyalophane, up to 9.6 wt. % BaO) were found in gangue minerals of breccias (assemblage no. 1).

Garnets of the Vorontsovskoe deposit include andradite and grossular. **Andradite** $Ca_3Fe^{3+}{}_2(SiO_4)_3$ was found in samples from the dumps of the southern open pit. It is present in calcite–garnet–epidote skarns with late magnetite–sulfide mineralization. Striking druses of dark red opaque andradite tetragontrioctahedra up to 1 cm in size were etched from calcite (Fig. 34e). The associated minerals include chalcopyrite, epidote, magnetite, pyrite, and sphalerite. Andradite contains a significant grossular component in chemical composition (Table 10). **Grossular** $Ca_3Al_2(SiO_4)_3$ was described in fine-grained mica–calcite–chlorite and medium-grained pyrite–calcite–grossular metasomatites (Sazonov et al., 1991a). It occurs as finest dissemination and, less often, veinlets up to several millimeters thick. The color of grossular is light yellow, locally, white, olive–green or green. It was determined by chemical composition and PXRD data. In calcite–garnet–epidote skarns with andradite, grossular forms significantly rare smaller (<0.5 mm) transparent greenish yellow crystals. The chemical composition is given in Table 10.

Hemimorphite $Zn_4(Si_2O_7)(OH)_2 \cdot H_2O$ is a rare mineral of the oxidation zone identified in samples from the dumps of the southern open pit. It forms radial aggregates of the colorless prismatic crystals up to 0.7 cm long on quartz in assemblage with cesàrolite, galena, chalcopyrite, and malachite (Figs. 31e, 34f). Hemimorphite also occurs as small white and pale blue (probably, due to a low Cu content) spherules on quartz with bayldonite, malachite, pyrite, and tennantite-(Zn) (Fig. 33i). The mineral contains only Zn and Si at a 2:1 ratio. The parameters of the orthorhombic unit cell are given in Table 3.

Hingganite-(Y) $Y_2\square Be_2Si_2O_8(OH)_2$ and **hingganite-(Nd)** $Nd_2\square Be_2Si_2O_8(OH)_2$ were identified in a sample collected from the main ore stockpile of the deposit. Both minerals compose the grains up to 10 μm in size in dolomite–calcite rock and are associated with baryte, fergusonite-(Y), Cr-bearing magnetite, pyrite, realgar, routhierite, and wakabayashilite. These grains are chemically heterogeneous with areas dominated by Y or Nd among REEs. Hingganite-(Y)/hingganite-(Nd) contain (wt.%, BeO and H_2O calculated by stoichiometry): 10.10/10.43 BeO, 1.21/1.78 CaO, 4.19/2.60 FeO, 12.71/11.03 Y_2O_3, 1.05/0.99 La_2O_3, 8.45/7.36 Ce_2O_3, 2.34/2.15 Pr_2O_3, 14.17/17.89 Nd_2O_3, 5.84/5.86 Sm_2O_3, 1.05/1.14 Eu_2O_3, 5.92/6.12 Gd_2O_3, 0.52/0.48 Tb_2O_3, 2.98/2.87 Dy_2O_3, 0.44/0.34 Ho_2O_3, 1.19/1.09 Er_2O_3, 0.75/0.88 Tm_2O_3, 0.58/0.52 Yb_2O_3, 24.46/24.66 SiO_2, 3.24/3.25 H_2O, total 101.19/101.44. The empirical formulas on the basis of two Si atoms and O + OH = 10 apfu are: $(Y_{0.55}Nd_{0.41}Ce_{0.25}Sm_{0.16}Gd_{0.16}Dy_{0.08}Pr_{0.07}La_{0.03}Eu_{0.03}Er_{0.03}Tm_{0.02}Tb_{0.01}Ho_{0.01}Yb_{0.01}Ca_{0.11})_{1.93}(\square_{0.71}Fe^{2+}_{0.29})_{1.00}Be_{2.00}Si_{2.00}O_{8.24}(OH)_{1.76}$ and $(Nd_{0.52}Y_{0.48}Ce_{0.22}Sm_{0.16}Gd_{0.16}Dy_{0.08}Pr_{0.06}La_{0.03}Eu_{0.03}Er_{0.03}Tm_{0.02}Tb_{0.01}Ho_{0.01}Yb_{0.01}Ca_{0.15})_{1.97}(\square_{0.82}Fe^{2+}_{0.18})_{1.00}Be_{2.00}Si_{2.00}O_{8.24}(OH)_{1.76}$, respectively. In spite of the absence of XRD data because of the small grain size of minerals, the above compositions, in our opinion, belong to the minerals of the hingganite series. The deficit in totals is correlated with the calculated BeO and H_2O contents. The Fe content of both minerals is typical of hingganite; other silicates with an atomic REE/Si ratio close to 1 : 1 contain no Fe. Similar chemical zonation with

dominant Y or Nd in various zones was described in hingganite-(Nd) from its type locality, Mt. Zagi in Pakistan (Kasatkin et al., 2020d). The finding of hingganite-(Nd) is the first in the Russian Federation.

The **kaolinite–serpentine** group at the deposit includes four minerals.Three polymorphs of the kaolinite subgroup (dickite, halloysite, kaolinite $Al_2(Si_2O_5)(OH)_4$) and a member of the serpentine subgroup (chrysotile-2Or_{c1}) were identified in samples with assemblage no. 9 collected at the dumps of the southern open pit.

Dickite is a subordinate mineral in yellow–white powdery aggregates with major kaolinite. It was determined by chemical composition (Al/Si ratio of ~1 : 1) and IR spectrum (the main bands at 430, 470, 537, 695, 797, 912, 1007, 1031, 1625, 3650 cm^{-1}). Dickite differs from kaolinite by a characteristic band at 3650 cm^{-1} in a region of O–H stretching vibrations.

Halloysite was mentioned in the oxidation zone of the deposit (Kabanov, 2001). In our samples, this mineral was found in brown and black powdery polymineral crust with kaolinite, calcite, quartz, and rhodochrosite (Fig. 32i). The mineral was identified by qualitative chemical composition (Al/Si ratio of ~1 : 1), PXRD pattern (the strongest reflections at [*d*, Å (*I*)]: 7.27(100), 4.44(80), 3.65(50), 2.57(20), 1.70(10), 1.48(10)), and IR spectrum. The parameters of the monoclinic unit cell correspond to halloysite-7Å (Table 3).

Kaolinite is abundant in the deposit and is a subordinate mineral in the supergene zone. It was determined by XRD in polymineral samples of various rocks of the deposit (Sazonov et al., 1991a). In our samples from the oxidation zone from dumps of the southern open pit, kaolinite is one of the major rock-forming minerals. In some samples, it composes up to 80 vol. % hosting the fine-grained quartz. Due to the presence of Fe and Mn oxides, kaolinite is often characterized by a brown color (Figs. 31d, 32i). It contains only Al and Si at an approximate ratio of 1 : 1. The strong reflections of the PXRD pattern [(*d*, Å (*I*)): 7.12(100), 4.39(40), 4.17(30), 3.54(50), 2.55(30), 1.97(10), 1.66(10), 1.49(20)], the parameters of the triclinic unit cell (Table 3), and the main bands in IR spectrum (at 432, 469, 536, 691, 796, 912, 1008, 1031, 1627, 3620, 3697 cm^{-1}) correspond to kaolinite. A characteristic feature of the mineral is a doublet in the IR spectrum in a region of OH-groups that consists of two narrow bands at 3620 and 3697 cm^{-1}, which is absent in the IR spectrum of dickite and halloysite.

Chrysotile-2Or_{c1} $Mg_3Si_2O_5(OH)_4$ forms dark brown and yellow aggregates on calcite and dolomite with pyrite and magnetite (Figs. 34g, 34h) and light green massive aggregates with pigeonite in a dark gray rock mainly consisting of clinochlore, Fe-bearing grossular, fluorapatite, titanite, baryte, pyrite, and chalcopyrite (Fig. 34i). Chrysotile contains a low Fe content (Table 10). The parameters of the orthorhombic unit cell correspond to the 2Or_{c1} polytype (Table 3). The characteristic bands in the IR spectrum are at 384, 404, 438, 564, 613, 960, 1025, 1074, 3687 cm^{-1}.

The minerals of the **mica group** at the deposit, first of all, include **muscovite** $KAl_2(Si_3Al)O_{10}(OH)_2$, which is abundant in quartz–sericite metasomatites and, to a lesser extent, in beresites and listvenites. In addition, muscovite occurs in propylites after intermediate–mafic volcanic rocks and rocks of the intrusive diorite–granodiorite complex. Muscovite composes flakes up to 1 mm in size that are dispersed among the grains of other minerals. It is identified by chemical composition and PXRD pattern (Sazonov et al., 1991a).

In our samples, muscovite was found in four mineral assemblages. In assemblage no. 1, it is a rock-forming mineral, which is associated with clinochlore and armenite. An atypical purple aggregates of Ba,Ca,Mg,Mn,Ti-bearing muscovite were found in a dolomite–calcite marble with pyrite and realgar (Fig. 34j; Table 10). The parameters of its monoclinic unit cell correspond to the $2M_1$ polytype (Table 3).

Celadonite $KMgFe^{3+}Si_4O_{10}(OH)_2$ and **ferroceladonite** $KFe^{2+}Fe^{3+}Si_4O_{10}(OH)_2$ were found in samples collected at the dumps of the northern open pit. Together with calcite, the micas form pale greenish blue crusts that are overgrown by late colorless calcite crystals (Fig. 34k). Celadonite and ferroceladonite are macroscopically indistinguishable and even grains of few tens of micrometer in size could be composed of both minerals. The chemical compositions of the minerals are given in Table 10. The parameters of the monoclinic unit cell correspond to a Si-rich dioctahedral mica (Table 3).

Prehnite $Ca_2Al(Si_3Al)O_{10}(OH)_2$ occurs in propylitizes rocks (Sazonov et al., 1991a). In assemblage no. 1, prehnite is a rock-forming mineral of propylites superimposed on carbonate breccias. It was also found in gangue minerals of breccias in assemblages nos. 4 and 5. Its chemical composition is close to ideal (Table 10).

Pumpellyite was described in propylites (Sazonov et al., 1991a; Vikentyev et al., 2016). We identified **pumpellyite-(Mg)** $Ca_2MgAl_2(Si_2O_7)(SiO_4)(OH)_2 \cdot H_2O$ that forms 50–70 μm aggregates in assemblage

no. 1 of metasomatic rocks superimposed on carbonate breccias. The mineral is associated with armenite, baryte, calcite, fluorapatite, muscovite, chabournéite, christite, cinnabar, native gold, pyrite, routhierite, and sphalerite. Pumpellyite-(Mg) contains small amount of V, which is an atypical chemical element for the Vorontsovskoe deposit (Table 10).

Pyroxenes are the subordinate to rare minerals of the deposit. **Augite** $(Ca,Mg,Fe)_2Si_2O_6$ rarely occurs in metasomatites, which are superimposed on carbonate breccias with minerals of assemblage no. 1. **Diopside** $CaMgSi_2O_6$ is abundant amid gangue minerals of assemblage no. 5 and is rarer in assemblages nos. 1, 4 and 6. In a sample from off-balance ore stockpile no. 2, we detected a diopside rich in Mn up to the compositions corresponding to **johannsenite** $CaMnSi_2O_6$. **Pigeonite** $(Mg,Fe,Ca)_2Si_2O_6$ was found in samples from the dumps of the southern open pit, where it intergrows with chrysotile-2*Or*$_{c1}$ in large (up to 5 × 3 cm) massive yellow–green grains in light calcite–dolomite marble (Fig. 34i). The chemical composition and the parameters of the monoclinic unit cell of pigeonite are given in Tables 10 and 3, respectively. The chemical composition of other pyroxenes is also shown in Table 10.

Subordinate **smectites** are typical of the oxidation zone of the deposit. **Beidellite** $(Na,Ca)_{0.3}Al_2(Si,Al)_4O_{10}(OH)_2 \cdot nH_2O$, **montmorillonite** $(Na,Ca)_{0.3}(Al,Mg)_2Si_4O_{10}(OH)_2 \cdot nH_2O$, and **nontronite** $Na_{0.3}Fe^{3+}{}_2(Si,Al)_4O_{10}(OH)_2 \cdot nH_2O$ were identified by chemical composition and PXRD patterns in several samples (Sazonov et al., 1991a). **Nontronite-15Å** was identified in a sample from the dumps of the northern open pit as a yellow powdery films on fine-grained calcite. Its identification is confirmed by qualitative chemical analysis (major Fe, Si and O and minor Na and Ca) and PXRD pattern (strong reflections at [*d*, Å (*I*)]: 15.20(100), 4.50(20), 3.04(50), 2.58(10), 2.28(20), 1.71(5), 1.52(20) и 1.34(5) Å)) and IR spectrum (main bands at 428, 490, 682, 818, 1017, 1100 (a shoulder), 1636, 3419, 3560 cm^{-1}).

Talc $Mg_3Si_4O_{10}(OH)_2$ composes leaf aggregates in carbonates of the breccia matrix (Murzin, Varlamov, 2010). Talc in samples from the main ore stockpile forms bluish green massive aggregates in dolomite in assemblage with arsenopyrite crystals. In some samples, talc forms white and brownish films on calcite and intergrows with clinochlore and muscovite. Talc is identified as a rare mineral of metasomatites in assemblage no. 3. The mineral contains up to 1.1 wt. % MnO (Table 10). The parameters of the triclinic unit cell correspond to talc (Table 3).

Thorite $Th(SiO_4)$ (or, possibly, its dimorph huttonite) was found in assemblage no. 1 as a grain 0.1 × 0.03 mm in size in Ba-containing orthoclase with diopside. Thorite hosts a small cinnabar inclusions (Fig. 34l). It contains only Th and Si at a ratio close to 1 : 1. The mineral is X-ray amorphous as a result of metamictic decay.

Titanite $CaTi(SiO_4)O$ forms rare crystals up to 20 μm in size in siliceous breccia fragments. It contains up to 1.3 wt. % Al_2O_3 and 0.9 wt. % V_2O_5 (Murzin, Varlamov, 2010). Titanite was also found as a rare accessory of assemblages nos. 1 and 6. It is more common for the gangue minerals of breccias (assemblage no. 7).

Vesuvianite $(Ca,Na)_{19}(Al,Mg,Fe)_{13}(SiO_4)_{10}(Si_2O_7)_4(OH,F,O)_{10}$ is a rare mineral of metasomatites and was found in assemblage no. 6 in aggregates with diopside and fluorapatite. It contains numerous inclusions of arsenopyrite, benavidesite, galena, native arsenic, orpiment, pyrite, ramdohrite, realgar, tetrahedrite-(Fe), and tetrahedrite-(Zn). The chemical composition of vesuvianite is given in Table 10.

Wollastonite $CaSiO_3$ occurs in skarns and wollastonite skarns confined to faults (Sazonov et al., 1991a). In skarns, it composes almost monomineralic rims between the zones of garnet skarns and marblized limestones. The wollastonite crystals form colorless sheaf-like aggregates. The mineral was identified by its chemical composition, XRD, and optical data.

The minerals of the **zeolite group** include chabazite-Ca, harmotome, and laumontite. **Chabazite** was described as an abundant mineral that forms veins in propylitized andesites, basaltic andesites, mafic dikes, rocks of the intrusive diorite–granodiorite complex, skarns, and epidosites (Sazonov et al., 1991a). **Chabazite-Ca** $Ca_2[Al_4Si_8O_{24}] \cdot 13H_2O$ was found in a sample from the dumps of the southern open pit (Table 10). It forms pinkish fine-grained crusts on marblized limestone and is associated with small (up to 0.3 mm) pyrite crystals. The parameters of the triclinic unit cell correspond to the mineral of the chabazite series (Table 3).

Harmotome $Ba_2(Si_{12}Al_4)O_{32} \cdot 12H_2O$ was identified in assemblage no. 1 as anhedral grains up to 0.2 × 0.1 mm in size in calcite with pyrite, realgar, orpiment, Ag-bearing native gold, chabournéite, parapierrotite, routhierite, and weissbergite. The identification of the mineral was confirmed by EMPA (Table 10).

Laumontite $CaAl_2Si_4O_{12} \cdot 4H_2O$ was first found in a stringer-disseminated zone with gold mineralization in assemblage with grossular, K-feldspar, and quartz (Sazonov et al., 1991a). In samples from the dumps

of the northern open pit, laumontite forms creamy pockets up to 5 × 5 mm in size in white calcite with pyrite crystals. In contrast to laumontite described by (Sazonov et al., 1991a), the mineral from the northern open pit contains only low amount of K (Table 10). The parameters of the monoclinic unit cell correspond to laumontite (Table 3).

Zircon $Zr(SiO_4)$ is a rare accessory mineral of assemblage no. 1 from metasomatites superimposed on carbonate breccias. Its chemical composition is close to ideal.

Specific features of mineralogy of the Vorontsovskoe gold deposit

Most researchers agree that the Vorontsovskoe deposit has several stages of mineral formation. The early ore types (skarns and disseminated ores) of the deposit are hosts to the arsenopyrite–pyrite–chalcopyrite–sphalerite–galena assemblage and the tuffaceous rocks are characterized by pyrite–arsenopyrite–fahlore assemblage with native arsenic and realgar, the presence of which indicates an increasing S fugacity (Sazonov et al., 1991a, Stepanov et al., 2017, 2021; Murzin et al., 2017, Vikentyev et al., 2019). The carbonate breccias with carbonate-tuffaceous matrix contain gold–pyrite–realgar ores with remarkably diverse sulfosalts. Evaluation of the formation conditions of the sulfosalt assemblages is complicated by fine grain size of ore minerals and their close assemblage with other minerals formed at different hydrothermal stages.

On the one hand, a number of sulfosalts including new minerals are characterized by unique chemical composition and structure. On the other hand, many of them belong to an homologous series that are typical of geochemical conditions similar to that observed at the Vorontsovskoe deposit. Eleven Pb–Tl–Sb–As sulfosalts (boscardinite, chabournéite, dufrénoysite, écrinsite, enneasartorite, guettardite, heptasartorite, parapierrotite, philrothite, twinnite, veenite) belong to the sartorite homologous series. Minerals of this series consist in principle of diagonal slabs formed by As(Sb)-S double-ribbons, which are separated by zigzag walls of large coordination polyhedra of Pb and Tl, and joined into a herringbone-like structure (Berlepsch et al., 2001; Makovicky, Topa, 2015).

Five Pb–Tl–Sb–As sulfosalts (lillianite, andorite-VI, ramdohrite, roshchinite, vikingite) are the members of the lillianite homologous series. Lillianite occurs in magnetite–garnet–epidote skarns, whereas other members of its group are hosted in carbonate breccias. Most of them are combinations of Pb–Ag–Sb(As)–S in the andorite subseries, whereas the members of the Pb–Ag–Bi–S, lillianite–gustavite subseries are rare at the Vorontsovskoe deposit. In this series, the diagonal slabs with galena-like arrangement are mirror-twinned to form the structure, which, thanks to its properties, shows preference for Sb and/or Bi over As (Makovicky, Topa, 2014).

The pavonite homologous series includes rare pavonite and luboržákite, a new Bi-free As–Sb–Mn mineral. These two minerals are also observed in different assemblages: pavonite (as well as the most Bi minerals of the deposit) occurs in magnetite–garnet–epidote skarns, whereas luboržákite is confined to carbonate breccias. In the luboržákite structure, the right mixture of lone-electron pair active and inactive elements allows the pavonite-like motif to form (Kasatkin et al., 2020a).

The plagionite homologous series includes three Pb–Sb members: heteromorphite, plagionite, and semseyite. The jordanite homologous series is characterized by the presence of jordanite and geocronite, another important Pb–Sb structure present is meneghinite, and the Tl–As homologous pair bernardite–hutchinsonite. To the latter, we can add the modified quasimember, imhofite, too. The polybasite series consists of polybasite, cupropolybasite, and benleonardite. The tetrahedrite–vorontsovite «over-group», which combines minerals with perfect-to-defect tetrahedrite-like structures, includes, on the one hand, argentotetrahedrite-(Fe), argentotetrahedrite-(Zn), tennantite-(Fe), tennantite-(Zn), tetrahedrite-(Fe), and tetrahedrite-(Zn), and, on the other hand, minerals with Tl in the structure cages (galkhaite, vorontsovite, ferrovorontsovite, routhierite, arsiccioite, stalderite). Aktashite, nowackiite, sinnerite, and laffittite are related to these minerals in chemical composition and structures.

The presence of sulfosalts of various homologous series and structural types means that these minerals are successfully adjusted to the variable chemical and physical conditions of mineral formation via, e.g., cation substitution (Sb,Bi) + Ag ↔ 2 Pb and/or As(Sb)+Tl ↔ 2 Pb with preservation of their structure schemes (Moëlo et al., 2008). The examples of broad cation substitution include andorite, philrothite, écrinsite, boscardinite, ramdohrite, etc.

The Vorontsovskoe deposit is As-rich, whereas the high Sb contents are locally detected and Bi contents are low. The deposit is also Mn-rich in contrast to similar Lengenbach (Switzerland) and Allchar (North Macedonia) deposits. Rock-forming Mn-bearing dolomite and calcite are most likely the source of Mn for

numerous ore minerals: sulfides (alabandite) and sulfosalts (auerbakhite, benavidesite, clerite, luboržákite, tsygankoite, etc.). Manganese is also present as a species-defining element in oxides, hydroxides, carbonates and silicates.

Twenty three Ag minerals have been identified at the Vorontsovskoe deposit, but most Ag minerals occur as single grains, e.g., acanthite, arsiccioite, jalpaite, laffittite, manganoquadratite, oyonite, pavonite, ramdohrite, sicherite, and tsnigriite. Only two sulfosalts (boscardinite, écrinsite) are relatively abundant, however, they contain minor Ag amount. Bismuth is mainly present in assemblage no. 8, which is confined to skarns. Eight Bi minerals are identified at the deposit and only vikingite and bismoclite were found in breccias. Tellurium is a trace element of the deposit, which is hosted in five minerals. Coloradoite is relatively common in comparison with other Te minerals that are confined only to skarns. No Se minerals have been found at the deposit. Selenium is detected in a minor amounts only in cinnabar.

Telescoping of various geological processes and the formation of metasomatites after various rocks were responsible for the crystallization of specific ore and gangue minerals in ores of the Vorontsovskoe deposit. The formation of various assemblages of oxygen-bearing minerals is a result of a successive evolution of the ore-forming system from the high-temperature skarns to low-temperature argillisites. Skarns are the earliest metasomatic rocks. Their major rock-forming minerals are garnets of the grossular–andradite series, diopside, clinochlore, vesuvianite, and wollastonite. A decrease in temperature resulted in the replacement of skarns by medium-temperature quartz–sericite metasomatites and then low-temperature argillisites. Their major rock-forming minerals are quartz and muscovite. The quartz–sericite metasomatites also contain subordinate carbonates with dominant Fe-bearing dolomite and accessory scheelite. Argillisites contain Ba-bearing orthoclase and baryte. The low-temperature ores host accessory prehnite, pumpellyite-(Mg), and talc. A diversity of gangue minerals in breccias is caused by both telescoping of ore-forming processes and mechanical contamination of breccias by rock-forming minerals of host rocks. It was found that some varieties of these rocks exhibit two or, less often, three successive assemblages of metasomatic minerals (Stepanov et al., 2017). Some minerals, such as Cr-spinels, geikielite, pyrophanite, augite, monoclinic amphiboles, albite, orthoclase, etc. were mechanically emplaced into the breccia matrix during hydrothermal-explosive processes.

Conclusions

Although the open pit mining at the Vorontsovskoe deposit has been finished, the mineralogical potential of the deposit is far from being exhausted. Exploration drilling in 2017–2019 revealed a significant gold mineralization under the northern open pit. In 2020, the Polymetal Company conducted technical studies in order to determine the feasibility of the underground mining, as well as the open pit mining of oxidized ores in the western flank of the open pit. In 2022, the company planned to continue the geological exploration of neighboring promising areas. All this gives hope for the appearance of new mineralogical material, the study of which can yield interesting mineralogical findings at the deposit.

Acknowledgments

We are sincerely grateful to Igor Pekov, Vlad Gurzhiy, Elena Belogub, and Irina Melekestseva for valuable comments and editing that substantially improved the manuscript. We also acknowledge Nikita Chukanov for the IR spectroscopic study and assistance in the interpretation of Raman spectra of sulfosalts, Leonid Pautov for the help in optical studies and measurement of reflectance spectra of vorontsovite and ferrovorontsovite, and Anastasia Kasatkina, Victor Levitskiy, Maria Milshina, and Tim Pashko for the photographing of minerals. We appreciate the help of the management of the Uralian Branch of the Polymetal Company: Director Andrey Novikov in assistance of field works and Chief geologist Andrey Gottman for providing samples with native arsenic.

The field works were partly supported by state contracts of the IGG UB RAS no. AAAA-A18-118052590032-6 and SU FRC MG UB RAS no. 075-00880-22 ПР.

References

Anastassakis E., Perry C.H. (1976) Light scattering and IR measurements in XS_2 pyrite–type compounds. *The Journal of Chemical Physics*, **64**, 3604–3609.

Balić-Žunić T., Šćavnićar S., Engel P. (1982) The crystal structure of rebulite, $Tl_5As_8Sb_5S_{22}$. *Zeitschrift für Kristallographie*, **160**, 109–125.

Baryshev A.N., Zlotnik-Khotkevich A.G., Cheremisin A.A. (1993) [Vorontsovskoe gold deposit in the Northern Urals, structure and forecast-prospecting criteria]. Materiali nauchno-tekhnicheskoy konferencii NTD-92-TSNIGRI.

[*Proceedings of the scientific and technical conference 12–24 March 1993]*. Moscow, TsNIGRI, 31–32. (in Russian)

Begetnev S.V. (1998) [Morphology of «rice-like» jasperoid quartz of the Vorontsovskoe gold deposit (Northern Urals)]. *Ural'skaya letnyaya mineralogicheskaya shkola–98 [Urals Summer Mineralogical School-98]*. Yekaterinburg, UGGU, 67–68. (in Russian)

Berlepsch P., Makovicky E., Balić-Žunić T. (2001) Crystal chemistry of sartorite homologues and related sulfosalts. *Neues Jahrbuch für Mineralogie-Abhandlungen*, **176**, 45–66.

Bezsmertnaya M.S., Kozerenko S.V., Kolpakova N.N. (1973) [Seligmannite and sinnerite from Elbrus polymetallic deposit]. In.: *Issledovania v oblasti rudnoy mineralogii [Researches in Area of Ore Mineralogy]*. Moscow, Nauka, 5–14. (in Russian)

Biagioni C., Bonaccorsi E., Moëlo Y., Orlandi P., Bindi L., D'Orazio M., Vezzoni S. (2014) Mercury–arsenic sulfosalts from Apuan Alps (Tuscany, Italy). III. Arsiccioite, $AgHg_2TlAs_2S_6$, a new mineral from the Monte Arsiccio mine: occurrence, crystal structure, and crystal chemistry of the routhierite isotypic series. *Mineralogical Magazine*, **78**, 101–117.

Biagioni C., George L.L., Cook N.J., Makovicky E., Moëlo Y., Pasero M., Sejkora J., Stanley C.J., Welch M.D., Bosi F. (2020) The tetrahedrite group: nomenclature and classification. *American Mineralogist*, **105**, 109–122.

Biagioni C., Moëlo Y. (2017) Lead–antimony sulfosalts from Tuscany (Italy). XVIII. New data on the crystal–chemistry of boscardinite. *Mineralogical Magazine*, **81**, 47–60.

Biagioni C., Moëlo Y., Favreau G., Bourgoin V., Boulliard J.-C. (2015) Crystal structure of Pb-rich chabournéite from Jas Roux, France. *Acta Crystallographica*, **71**, 81–88.

Bindi L. Biagioni C., Keutsch F.N. (2018) Oyonite, $Ag_3Mn_2Pb_4Sb_7As_4S_{24}$, a new member of the lillianite homologous series from the Uchucchacua base-metal deposit, Oyon district, Peru. *Minerals*, **8**, 192.

Bindi L., Nestola F., Guastoni A., Secco L. (2010) The crystal structure of dalnegroite, $Tl_{5-x}Pb_{2x}(As,Sb)_{21-x}S_{34}$: a masterpiece of structural complexity. *Mineralogical Magazine*, **74**, 999–1012.

Bindi L., Nestola F., Makovicky E., Guastoni A., de Battisti L. (2014) Tl-bearing sulfosalt from the Lengenbach quarry, Binn valley, Switzerland: Philrothite, $TlAs_3S_5$. *Mineralogical Magazine*, **78**, 1–9.

Bindi L., Popova V., Bonazzi P. (2003) Uzonite, As_4S_5, from the type locality: single-crystal X-ray study and effects of exposure to light. *The Canadian Mineralogist*, **41**, 1463–1468.

Bindi L., Stanley C.J., Spry P.G. (2015) New structural data reveal benleonardite to be a member of the pearceite–polybasite group. *Mineralogical Magazine*, **79**, 1213–1221.

Bobrov V.N. (2013) [Vorontsov's treasure. Prospecting and discoveries]. Karpinsk, Perspektiva, 32 p. (in Russian)

Boev B., Jovanovski G., Makreski P. (2012) Geology and mineralogy of Allchar Sb–As–Tl–Au deposit. *Geologica Macedonica*, **3**, 215–233.

Bonazzi P., Bindi L., Keutsch F.N. (2012) Manganoquadratite, $AgMnAsS_3$, a new manganese-bearing sulfosalt from the Uchucchacua polymetallic deposit, Lima department, Peru: description and crystal structure. *American Mineralogist*, **97**, 1199–1205.

Bonazzi P., Menchetti S., Pratesi G. (1995) The crystal structure of pararealgar, As_4S_4. *American Mineralogist*, **80**, 400–403.

Bryzgalov I.A., Krivitskaya N.N., Spiridonov E.M. (2011) [First find of minerals of jordanite-geocronite-schulzite series at one deposit (Darasun, Eastern Transbaikalia)]. *Doklady RAN [Doklady Russian Academy of Sciences]*, **438**(5), 635–638. (in Russian).

Burri G., Graeser S., Marumo F., Nowacki W. (1965) Imhofit, ein neues Thallium–arsensulfosalz aus dem Lengenbach (Binnatal, Kanton Wallis). *Chimia*, **19**, 499–500. (in German)

Cheremisin A.A., Zlotnik-Khotkevich A.G. (1997) [The Vorontsovskoe gold deposit]. *Rudy i metally [Ores and Metals]*, (1), 59–70. (in Russian)

Chvileva T.N., Bezsmertnaya M.S., Spiridonov E.M., Agroskin A.S., Papayan G.V., Vinogradova R.A., Lebedeva S.I., Zavyalov E.N., Filimonova A.A., Petrov V.K., Rautian L.P., Sveschnikova O.L. (1988) [Handbook of ore minerals in reflected light]. Moscow, Nedra, 504 p. (in Russian).

Dickson F.W., Radtke A.S., Peterson J.A. (1979) Ellisite, Tl_3AsS_3 a new mineral from the Carlin gold deposit, Nevada, and associated sulfide and sulfosalt minerals. *American Mineralogist*, **64**, 701–707.

Dincă G., Popescu G.C. (2019) Manganoquadratite and Cd-manganoquadratite from Săcărâmb Au–Ag–Te ore deposit, Metaliferi Mountains, Romania. *Carpathian Journal of Earth and Environmental Sciences*, **14**(1), 131–136.

Engel P. (1980) Die Kristallstruktur von synthetischem Parapierrotit, $TlSb_5S_8$. *Zeitschrift für Kristallographie,* **151**, 203–216. (in German)

Fleet M.E. (1973) The crystal structure and bonding of lorandite, $Tl_2As_2S_4$. *Zeitschrift für Kristallographie,* **138**, 147–160.

Forneris R. (1969) Infrared and Raman spectra of realgar and orpiment. *American Mineralogist*, **54**(7–8), 1062–1074.

Frost R.L., Bahfenne S., Keeffe E.C. (2010) Raman spectroscopic study of the mineral gerstleyite $Na_2(Sb,As)_8S_{13} \cdot 2H_2O$ and comparison with some heavy-metal sulfides. *Journal of Raman Spectroscopy*, **41**(12), 1779–1783.

Gladkovsky B.A. (2002) [The history of discovery of the Vorontsovskoe gold deposit]. *Ural'skiy geologicheskiy zurnal [Urals Geological Journal]*, (5), 165–170. (in Russian)

Gostojić M., Edenharter A., Nowacki W., Engel P. (1982) The crystal structure of synthetic $Tl_2MnAs_2S_5$. *Zeitschrift fur Kristallographie*, **158**, 43–51.

Graeser S., Berlepsch P., Makovicky E., Balić-Zunić T. (2001) Sicherite, $TlAg_2(As,Sb)_3S_6$, a new sulfosalt

mineral from Lengenbach (Binntal, Switzerland): description and structure determination. *American Mineralogist*, **86**, 1087–1093.

Graeser S., Schwander H., Wulf R. (1995) Stalderite $TlCu(Zn,Fe,Hg)_2As_2S_6$ – a new mineral related to routhierite: description and crystal structure determination. *Schweizerische mineralogische und petrographische Mitteilungen*, **75**, 337–345.

Grigoriev N.A., Sazonov V.N., Murzin V.V. (1991) [Mineral balance of gold in Carlin type rocks]. *Mineral'niy balans khimicheskikh elementov v gornykh porodakh i rudakh Urala* [Mineral balance of chemical elements in rocks and ores of the Urals], **2**, 14–19. (in Russian)

Gruzdev V.S., Stepanov V.I., Shumkova N.G., Chernitsova M.M., Yudin R.N., Bryzgalov I.A. (1972) [Galkhaite, $HgAsS_2$, a new mineral from arsenic–antimony–mercury deposits of the USSR]. *Doklady AN SSSR [Doklady Academy of Sciences USSR]*, **205**(5), 1194–1197. (in Russian)

Gvozdev V.I., Grebennikova A.A., Vakh A.S., Goryachev N.A., Fedoseev, D.G. (2020) [Mineral evolution of during formation of gold–rare–metals ores of Sredne-Golgotai deposit (Eastern Transbaikalia)]. *Russian Journal of Pacific Geology*, **14**, 66–86.

Isakovich I.Z. (1996) [Mineralogical aureoles of the Vorontsovskoe gold deposit]. *Otechestvennaja geologiya [Native Geology]*, **8**, 26–30. (in Russian)

Ivashchenko V.I., Valkama M., Sundblad K., Golubev A.I., Alekseev V.Y. (2011) [New data on mineralogy and metallogeny of scarns of Pitkyaranta ore region]. *Doklady Akademii nauk [Doklady Earth Sciences],* **440**(1), 1307–1311.

Johan Z., Mantienne J., Picot P. (1981) La chabournéite, un nouveau minéral thallifère. *Bulletin de Minéralogie*, **104**, 10–15 (in French).

Kabanov A.A. (2001) [Oxidized ores as a new geological and economic type of supergene gold deposits: example of the Vorontsovskoe deposit in the Urals]. *[Dissertation of Candidate of Geological-Mineralogical Sciences]*. St. Petersburg, 142 p. (in Russian)

Kasatkin A.V. (2019) New findings of rare minerals from former Soviet Union countries. *Mineralogical Almanac*, **24**(2), 4–47.

Kasatkin A.V., Nestola F., Agakhanov A.A., Škoda R., Karpenko V.Y., Tsyganko M.V., Plášil J. (2018a) Vorontsovite, $(Hg_5Cu)_{\Sigma6}TlAs_4S_{12}$, and ferrovorontsovite, $(Fe_5Cu)_{\Sigma6}TlAs_4S_{12}$: The Tl- and Tl–Fe-analogues of galkhaite from the Vorontsovskoe gold deposit, Northern Urals, Russia. *Minerals*, **8**, 185.

Kasatkin A.V., Makovicky E., Plášil J., Škoda R., Agakhanov A.A., Karpenko V.Y., Nestola F. (2018b) Tsygankoite, $Mn_8Tl_8Hg_2(Sb_{21}Pb_2Tl)_{\Sigma24}S_{48}$, a new sulfosalt from the Vorontsovskoe gold deposit, Northern Urals, Russia. *Minerals*, **8**, 218.

Kasatkin A.V., Makovicky E., Plášil J., Škoda R., Chukanov N.V., Stepanov S.Y, Agakhanov A.A., Nestola F. (2019) Gladkovskyite, $MnTlAs_3S_6$, a new thallium sulfosalt from the Vorontsovskoe gold deposit, Northern Urals, Russia. *Journal of Geosciences*, **64**(3), 207–218.

Kasatkin A.V., Makovicky E., Plášil J., Škoda R., Agakhanov A.A., Stepanov S.Y., Palamarchuk R.S. (2020a) Luboržákite, Mn_2AsSbS_5, a new member of pavonite homologous series from Vorontsovskoe gold deposit, Northern Urals, Russia. *Mineralogical Magazine*, **84**, 738–745.

Kasatkin A.V., Pautov L.A. (2020) [Optical properties of vorontsovite and ferrovorontsovite: new data]. *Novye dannye o mineralakh [New Data on Minerals]*, **54**(2), 69–72. (in Russian)

Kasatkin A.V., Plášil J., Makovicky E., Chukanov N.V., Škoda R., Agakhanov A.A., Tsyganko M.V. (2020c) Gungerite, IMA 2020-009. CNMNC Newsletter No. 56. *Mineralogical Magazine*, **84**, 485–488.

Kasatkin A.V., Nestola F., Škoda R., Chukanov N.V., Agakhanov A.A., Belakovskiy D.I. (2020d) Hingganite-(Nd), $Nd_2\square Be_2Si_2O_8(OH)_2$, a new gadolinite-supergroup mineral from Zagi Mountain, Pakistan. *The Canadian Mineralogist*, **58**, 549–562.

Kasatkin A.V., Plášil J., Makovicky E., Chukanov N.V., Škoda R., Agakhanov A.A., Stepanov S.Y., Palamarchuk R.S. (2021) Auerbakhite, $MnTl_2As_2S_5$, a new thallium sulfosalt from the Vorontsovskoe gold deposit, Northern Urals, Russia. *Journal of Geosciences*, **66**(2), 89–96.

Kasatkin A.V., Plášil J., Makovicky E., Hornfeck W., Chukanov N.V., Škoda R., Agakhanov A.A., Tsyganko M.V. (2022a) Gungerite, $TlAs_5Sb_4S_{13}$, a new thallium sulfosalt with a giant structure containing covalent As–As bonds. *American Mineralogist*, in press, DOI: doi.org/10.2138/am-2022-8003.

Kasatkin A.V., Plášil J., Makovicky E., Škoda R., Agakhanov A.A., Tsyganko M.V. (2022b) Pokhodyashinite, $CuTlSb_2(Sb_{1-x}Tl_x)AsS_{7-x}$, a new thallium sulfosalt from the Vorontsovskoe gold deposit, Northern Urals, Russia. *Journal of Geosciences*, **67**(1), in press, DOI: 10.3190/jgeosci.342.

Kemkina R.A., Kemkin I.V., Khanchuk A.I., Ivanov V.V. (2018) [First find of trace metal minerals at the Albaza gold deposit]. *Doklady Akamenii nauk [Doklady Earth Sciences], 481, 943–947.*

Kharbish S. (2011) Raman spectroscopic investigations of some Tl-sulfosalt minerals containing pyramidal $(As,Sb)S_3$ groups. *American Mineralogist*, **96**(4), 609–616.

Kharbish S., Libowitzky E., Beran A. (2009) Raman spectra of isolated and interconnected pyramidal XS_3 groups (X = Sb, Bi) in stibnite, bismuthinite, kermesite, stephanite and bournonite. *European Journal of Mineralogy*, **21**(2), 325–333.

Korzhinsky D.S. (1948) [Petrology of the Turinsky skarn copper deposits]. Moscow, AN SSSR, 148 p. (in Russian)

Krasnobaev A.A., Fershtater G.B., Bogomolov E.S., Larionov A.N., Berezhnaya N.G. (2007) [Auerbakh pluton: zircons, age, polychronism]. *Ezhegodnik-2006 IGiG UrO RAN [Yearbook-2006 of the Institute of Geology and Geochemistry UB RAS]. Yekaterinburg, IGG UrO RAN,* 191–196. (in Russian)

Makovicky E. (2019) Algorithms for calculations of homologue order *N* in the homologous series of sulfosalts. *European Journal of Mineralogy*, **31**, 83–97.

Makovicky E., Plášil J., Kasatkin A.V., Škoda R. (2021) The crystal structure of $Tl_{2.355}Sb_{5.984}As_{4.591}S_{17}$, the lead-free end-member of the chabournéite homeotypic family. *The Canadian Mineralogist*, **59**, 533–549.

Makovicky E., Topa D. (2014) Lillianites and andorites: new life for the oldest homologous series of sulfosalts. *Mineralogical Magazine*, **78**, 387–414.

Makovicky E., Topa D. (2015) Crystal chemical formula for sartorite homologues. *Mineralogical Magazine*, **79**, 25–31.

Makreski P., Jovanovski G., Boev B. (2014) Micro-Raman spectra of extremely rare and endemic Tl-sulfosalts from Allchar deposit. *Journal of Raman Spectroscopy*, **45**(7), 610–617.

Melkov V. G., Belova L. N., Gorshkov A. I., Ivanova O. A., Sivtsov A.V., Boronikhin V. A. (1983) [New data on lermontovite]. *Mineralogicheskiy zhurnal [Mineralogical Journal]*, **55**(1), 82–87. (in Russian)

Merlet C. (1994) An accurate computer correction program for quantitative electron probe microanalysis. *Microchimica Acta*, **114/115**, 363–376.

Minceva-Sukarova B., Jovanovski G., Makreski P., Soptrajanov B., Griffith W., Willis R., Grzetic I. (2003) Vibrational spectra of $M^{I}M^{III}S_2$ type synthetic minerals (M^{I} = Tl or Ag and M^{III} = As or Sb). *Journal of Molecular Structure*, **651–653**, 181–189.

[Mineralogy of the Urals: arsenides and stibnides. Tellurides. Selenides. Fluorides. Chlorides and bromides]. (1991) Sverdlovsk, UO AN SSSR, 215 p. (in Russian)

Minina O.V. (1994) [Auerbakh complex ore-magmatic system in the Central Urals]. *Otechestvennaya geologiya [Native Geology]*, (7), 17–23. (in Russian)

Miyawaki R., Hatert F., Pasero M., Mills S. J. (2021) IMA Commission on New Minerals, Nomenclature and Classification (CNMNC) – Newsletter 63. *European Journal of Mineralogy*, **33**, 639–646.

Moëlo Y., Makovicky E., Mozgova N.N., Jambor J.L., Cook N., Pring A., Paar W., Nickel E.H., Graeser S., Karup–Möller S., Balic-Žunic T., Mumme W.G., Vurro F., Topa D., Bindi L., Bente K., Shimizu M. (2008) Sulfosalt systematics: a review. Report of the sulfosalt subcommittee of the IMA Commission on Ore Mineralogy. *European Journal of Mineralogy,* **20***,* 7–46.

Moëlo Y., Marcoux E., Makovicky E., Karup-Möller S., Legendre O. (1987) Homologues de la lillianite (gustavite, vikingite, heyrovskyite riche en Ag et Bi...) de l'indice à W-As-(Pb,Bi,Ag) de La Roche-Balue (Loire Atlantique, France). *Bulletin de Minéralogie*, **110**, 43–64. (in French)

Mozgova N.N., Borodaev Yu.S., Senderova V.M., Ronami G.N., Yakovlevskaya T.A. (1971) [The find of heteromorphite in a collection of the Mineralogical Museum of Academy of Sciences of the USSR]. *Trudy mineralogicheskogo muzeia im. Fersmana [Proceedings of the Fersman Mineralogical Museum]*, **20**, 114–119. (in Russian)

Murzin V.V., Bushmakin A.F., Sustavov S.G., Shcherbachov D.K. (1996) [Clerite $MnSb_2S_4$ – a new mineral from Vorontsovskoe gold deposit in the Urals]. *Zapiski VMO [Proceedings of the Russian Mineralogical Society]*, **125**(3), 95–101. (in Russian)

Murzin V.V., Naumov E.A., Azovskova O.B., Varlamov D.A., Rovnushkin M.Yu., Pirajno F. (2017) The Vorontsovskoe Au–Hg–As ore deposit (Northern Urals, Russia): geological setting, ore mineralogy, geochemistry, geochronology and genetic model. *Ore Geology Reviews*, **85**, 271–298.

Murzin V.V., Sazonov V.N. (1990) [Mineralogical features of Carlin type gold mineralization in an andesite volcano-plutonic belt (Urals)]. *Mineralogiya mestorozhdeniy Urala: tezisy dokladov II regionalnogo soveshchaniya «Mineralogiya Urala» [Mineralogy of the Urals Deposits: Abstracts of the II Regional Meeting «Mineralogy of the Urals»]*. Sverdlovsk, UrO AN SSSR, 95–98. (in Russian)

Murzin V.V., Sazonov V.N., Grigoriev N.A., Ryabinin V.F. (1990) A genetic model for Carlin-type gold ores in the Urals. *Proceedings of Eighth Quaddrennial IAGOD Symposium*, Schweizerbart'sche Verlagsbuchhandlung, Stuttgart, 647–652.

Murzin V.V., Sazonov V.N., Ronkin Yu.L. (2010) [Model of formation of the Carlin type Vorontsovskoe gold deposit in the Urals: new data and problems]. *Litosfera [Lithosphere]*, **6**, 66–73. (in Russian).

Murzin V.V., Sustavov S.G. (1997) [Prospects of discovery of new ore minerals in the Urals]. *Struktura i evolutsiya mineral'nogo mira. Materiali k mezhdunarodnomu mineralogicheskomu seminaru [Structure and Evolution of the Mineral World. Materials of the International Mineralogical Seminar]*. Syktyvkar, 105–106. (in Russian)

Murzin V.V., Varlamov D.A. (2010) [Gold–sulfide–sulfosalt mineral assemblage in breccias with siliceous fragments from the Vorontsovskoe deposit (Central Urals)]. *Vestnik Uralskogo otdeleniya RMO [Bulletin of the Urals Branch of the Russian Mineralogical Society]*, **7**, 92–100 (in Russian).

Murzin V.V., Varlamov D.A., Rovnushkin M.Yu. (2011) [Assemblage of native arsenic and arsenopyrite at the Vorontsovskoe gold deposit (Northern Urals)]. *Vestnik Uralskogo otdeleniya RMO [Bulletin of the Urals Branch of the Russian Mineralogical Society]*, **8**, 80–87. (in Russian)

Nestola F., Guastoni A., Bindi L., Secco L. (2009) Dalnegroite,$Tl_{5-x}Pb_{2x}(As,Sb)_{21-x}S_{34}$, a new thallium sulphosalt from Lengenbach quarry, Binntal, Switzerland. *Mineralogical Magazine*, **73**(6), 1027–1032.

Orlandi P., Biagioni C., Bonaccorsi E., Moëlo Y., Paar W.H. (2012) Lead antimony sulfosalts from Tuscany (Italy). XII. Boscardinite, $TlPb_4(Sb_7As_2)_{\Sigma 9}S_{18}$, a new species from Monte Arsiccio mine: occurrence and crystal structure. *The Canadian Mineralogist*, **50**, 235–251.

Orlandi P., Biagioni C., Moëlo Y., Bonaccorsi E., Paar W.H. (2013) Lead antimony sulfosalts from Tuscany (Italy). XIII. Protochabournéite, ~ $Tl_2Pb(Sb_{9-8}As_{1-2})_{\Sigma 10}S_{17}$, from the Monte Arsiccio mine: occurrence, crystal structure and relationship with chabournéite. *The Canadian Mineralogist*, **51**, 475–494.

Plášil J., Kasatkin A.V., Škoda R., Stepanov S.Yu. (2018) [Parapierrotite from the Vorontsovskoe gold deposit, Northern Urals, Russia: crystal structure and chemical composition]. *Zapiski RMO [Proceedings of the Russian Mineralogical Society]*, **147**(1), 68–78.

Popov V.A., Kolisnichenko S.V. (2008) [On the mineralogy of carbonatites of Russian Brazil in the Southern Urals]. *Ural'skij mineralogicheskij sbornik [Ural mineralogical digest]*, **15**, 75–84. (in Russian)

Raber T., Roth P. (2018) The Lengenbach quarry in Switzerland: Classic locality for rare thallium sulfosalts. *Minerals*, **8**, 409.

Radtke A. (1985) Geology of the Carlin gold deposit, Nevada. *USGS Professional Paper* 1267, 124 p.

Rakhov E.V. [The ore-bearing breccias of the Vorontsovskoe deposit: composition, genesis and role in formation of gold mineralization]. *Abstract of Dissertation of Candidate of Geological-Mineralogical Sciences*. Yekaterinburg, 1999, 17 p. (in Russian)

Rindzunskaya N.M., Berzon R.O., Polyakova T.P. (1995a) [Geological and genetic bases of forecast and prospect of gold deposits in weathering mantle]. Moscow, TsNIGRI, 300 p. (in Russian)

Rindzunskaya N.M., Polyakova T.P., Bobrov V.N. (1995b) [Geological and mineralogical characteristics of a supergene zone of the Vorontsovskoe gold deposit]. *Rudy i metally [Ores and Metals]*, **4**, 42–52. (in Russian)

Roth P., Raber T., Favreau G. and Meisser N. (2017) Thallium sulfosalts from the Shimen As deposit, Hunan, China. *Mineral Up,* **4**(6), 8–22.

Rovnushkin M.Yu., Gulyaeva T.Ya., Galakhova O.L. (2010) [Occurrence of K-feldspar metasomatosis within the Vorontsovskoe gold deposit (Northern Urals)]. *Ezhegodnik-2009 IGG UrO RAN [Yearbook-2009 of the Institute of Geology and Geochemistry UB RAS]*. Yekaterinburg, IGG UrO RAN, 241–244. (in Russian)

Ryabinin V.F., Murzin V.V., Surganov A.V. (1992) [Features of gold and silver distribution in sulfidized skarns of the Vorontsovskoe gold deposit]. *Ezhegodnik-1991 IGG UrO AN SSSR [Yearbook-1991 of the Institute of Geology and Geochemistry UB AS USSR]*. Yekaterinburg, IGG UrO RAN, 65–66. (in Russian)

Savel'eva K.P., Kostromin D.A. (1991) [Polygenic and polychronous metasomatosis of one of the Ural gold deposits]. *Rudonosnye metasomaticheskie formatsii Urala [Ore-Bearing Metasomatic Complexes of the Urals]*, Sverdlovsk, UrO AN SSSR, 77–78. (in Russian)

Savel'eva K.P., Kostromin D.A. Melnichuk G.D. (1991) [Features of formation of gold deposits of the Northern Urals]. *Materialy po geologii i metallogenii Urala [Materials on Geology and Metallogeny of the Urals*. Sverdlovsk, UrO AN SSSR, 60–64. (in Russian)

Sazonov V.N., Artemenko N.A., Voronina L.K. (1995) [Light micas of the Vorontsovskoe gold deposit (Northern Urals)]. *Ezhegodnik-1994 IGG UrO RAN [Yearbook-1994 of the Institute of Geology and Geochemistry UB RAS]*, Yekaterinburg, IGG UrO RAN, 93–94. (in Russian)

Sazonov V.N., Murzin V.V., Grigor'ev, N.A. (1998) [Vorontsovskoe gold deposit: an example of Carlin-type mineralization in the Urals, Russia]. *Geologiya rudnykh mestorozhdenii [Geology of Ore Deposits]*, **40**(2), 139–151.

Sazonov V.N., Murzin V.V., Grigoriev N.A. (1990a) [Gold content of ore in area of andesite marginal belts: example of the Urals]. *Doklady AN SSSR* [*Doklady Academy of Sciences USSR*], **314**(3), 677–681. (in Russian)

Sazonov V.N., Murzin V.V., Grigoriev N.A., Gladkovsky B.A. (1990b) [The Carlin-type gold mineralization in the Urals]. *Novye dannye po zolotorudnym mestorozhdeniyam Urala [New Data on the Urals Gold Deposits]*. Sverdlovsk, UrO AN SSSR, 26–49 (in Russian).

Sazonov V.N., Murzin V.V., Grigoriev N.A., Gladkovsky B.A. (1991a) [Endogenic mineralization of the Devonian andesite volcano-plutonic complex (Urals)]. Sverdlovsk, UrO AN SSSR, 184 p. (in Russian)

Sazonov V.N., Murzin V.V., Grigoriev N.A., Ogorodnikov V.N., Ryabinin V.F. (1991b) [Unconventional gold mining in the Urals]. *Materialy po geologii i metallogenii zolota Urala [Materials on Geology and Metallogeny of the Urals Gold]*. Sverdlovsk, UrO AN SSSR, 3–36. (in Russian)

Sazonov V.N., Murzin V.V., Shumilov I.A. (1993) [Isotopic-geochemical model of the Auerbakh ore field (Northern Urals)]. *Doklady Akademii nauk [Doklady of Academy of Sciences*], **331**(4), 456–458. (in Russian)

Soroka E.I., Pritchin M.E., Azovskova O.B., Rovnushkin M.Yu., Lyutoev V.P., Smoleva I.V. (2018) [Physical and chemical studies of vein carbonates of the Vorontsovskoe gold deposit]. *Vestnik Permskogo universiteta [Bulletin of the Perm University]*, **17**(1), 41–51. (in Russian)

Soroka E.I., Pritchin M.E., Azovskova O.B., Rovnushkin M.Yu., Smoleva I.V., Galakhova O.L. (2017) [Vein carbonates of ore-bearing rocks of the Vorontsovskoe gold deposit]. *Problemy mineralogii, petrografii i metallogenii. Nauchnye chteniya pamyati P.N. Chirvinskogo [Problems of Mineralogy, Petrography and Metallogeny. Scien-*

tific Readings in Memory of P.N. Chirvinsky], **20**, 242–248. (in Russian)

Spiridonov E.M., Petrova I.V., Dashevskaya D.M., Balashov E.P., Klimova L.M. (1990) [Roshchinite $Ag_{19}Pb_{10}Sb_{51}S_{96}$ – new mineral of the andorite group]. *Zapiski VMO [Proceedings of the Russian Mineralogical Society]*, **119**(5), 32–43. (in Russian)

Stanley C.J., Criddle A.J., Chisholm J.E. (1986) Benleonardite, a new mineral from the Bambolla mine, Moctezuma, Sonora, Mexico. *Mineralogical Magazine*, **50**, 681–686.

Stepanov S.Yu., Palamarchuk R.S., Cherepanov A.V., Proskurnin V.F. (2019) [Geological and genetic type of the Vorontsovskoe gold deposit (Northern Urals)]. *Ural'skaya mineralogicheskaya shkola-2019 [Urals Mineralogical School-2019].* Yekaterinburg, IGG UrO RAN, 163–168. (in Russian)

Stepanov S.Yu, Sharpenok L.N., Antonov A.V. (2017) [Fluid-explosive breccias of the Vorontsovskoe gold deposit (The North Urals)]. *Zapiski RMO [Proceedings of the Russian Mineralogical Society]*, **146**(1), 29–43. (in Russian)

Stepanov S.Yu., Palamarchuk R.S., Varlamov D.A., Kiseleva D.V., Sharpyonok L.N., Škoda R., Kasatkin A.V. (2021) The Features of Native Gold in Ore-bearing Breccias with Realgar-orpiment Cement of the Vorontsovskoe Deposit (Northern Urals, Russia). *Minerals*, **11**, 541.

Thomas R., Davidson P. (2010) Hambergite-rich melt inclusions in morganite crystals from the Muiane pegmatite, Mozambique and some remarks on the paragenesis of hambergite. *Mineralogy and Petrology*, **100**(3–4), 227–239.

Tomkins A.G., Frost B.R., Pattison D.R.M. (2006) Arsenopyrite melting during metamorphism of sulfide ore deposits. *The Canadian Mineralogist*, **44**, 1045–1062.

Topa D., Graeser S., Stoeger B., Raber T., Stanley C. (2019) Drechslerite, IMA 2019-061. CNMNC Newsletter No. 52. *Mineralogical Magazine*, **83**, https://doi.org/10.1180/mgm.2019.73

Topa D., Kolitsch U. (2018) The crystal chemistry of rathite based on new electron-microprobe data and single-crystal structure refinements: the role of thallium. *Minerals,* **8**, 466.

Topa D., Kolitsch U., Makovicky E., Stanley C. (2017a) Écrinsite, $AgTl_3Pb_4As_{11}Sb_9S_{36}$, a new thallium-rich homeotype of baumhauerite from the Jas Roux sulphosalt deposit, Parc national des Écrins, Hautes-Alpes, France. *European Journal of Mineralogy*, **29**, 689–700.

Topa D., Makovicky E. (2017) The crystal structure of veenite. *Mineralogical Magazine*, **81**, 355–368.

Topa D., Makovicky E., Putz H., Zagler G. (2013) Lopatkaite, IMA 2012–083. CNMNC Newsletter No. 15, February 2013, page 11. *Mineralogical Magazine*, **77**, 1–12.

Topa D., Makovicky E., Stöger B., Stanley C. (2017b) Heptasartorite, $Tl_7Pb_{22}As_{55}S_{108}$, enneasartorite, $Tl_6Pb_{32}As_{70}S_{140}$ and hendekasartorite, $Tl_2Pb_{48}As_{82}S_{172}$, three members of the anion-omission series of 'sartorites' from the Lengenbach quarry at Binntal, Wallis, Switzerland. *European Journal of Mineralogy*, **29**, 701–712.

Topa D., Keutsch F.N., Kolitsch U., Lengauer C., Giester G., Stanley C. (2021a) Shimenite, IMA 2019-069, in: CNMNC Newsletter 63. *European Journal of Mineralogy*, **33**, 639–646.

Topa D., Kolitsch U., Stoeger B., Keutsch F., Stanley C. (2021b) Dewitite, IMA 2019-098, in: CNMNC Newsletter 63. *European Journal of Mineralogy*, **33**, 639–646.

Vakh A. S., Avchenko O. V., Gvozdev V. I., Goryachev N. A., Karabtsov A. A., Vakh *E. A. (*2019*)* Minerals of the Pb–As–Sb–S and Cu–Pb–As–Sb–S systems in ores of the Berezitovoe gold-polymetallic deposit, Upper Amur region, Russia. *Geology of Ore Deposits*, **61**, 256–273.

Vakh A.S., Khomich V.G., Boriskina N.G., Santosh M. (2016) The Berezitovoe gold-polymetallic deposit (Upper Amur region, Russia): structure, mineralogy and genetic aspects. *Geoscience Frontiers*, **7**(3), 483–494.

Vasiliev V.I. (2011) New data on the composition of metacinnabar and Hg-sphalerite with an isomorphous Cd admixture. *Russian Geology and Geophysics*, **52**(7), 701–708.

Vikent'eva O., Vikentev I. (2016) Occurrence modes of As, Sb, Te, Bi, Ag in sulfide assemblages of gold deposits of the Urals. *3rd International Conference on Competitive Materials and Technology Processes (IC–CMTP3). IOP Conference Series: Materials Science and Engineering*, **123,** 012028.

Vikentyev I.V., Tyukova E.E., Murzin V.V., Vikentyeva O.V., Pavlov L.G. (2016) [Vorontsovskoe gold deposit. Geology, gold modes, genesis]. Yekaterinburg, Fort Dialog-Iset, 204 p. (in Russian)

Vikentyev I.V., Tyukova E.E., Vikentyeva O.V., Chugaeva A.V., Dubinina E.O., Prokofiev V.Yu., Murzin V.V. (2019) Vorontsovka Carlin-style gold deposit in the North Urals: Mineralogy, fluid inclusion and isotope data for genetic model. *Chemical Geology*, **508**, 144–166.

Volkov A.V., Sidorov A.V. (2016) [Geological-genetic model of Carlin type gold deposits]. *Litosfera [Lithosphere]*, (6), 145–165. (in Russian)

White N.C., Hedenquist J.W. (1995) Epithermal gold deposits: styles, characteristics and exploration. *SEG Newsletter*, (23), 9–13.

Wilson J.R., Robinson P.D., Wilson P.N., Stanger L.W., Salmon G.L. (1991) Gillulyite, $Tl_2(As,Sb)_8S_{13}$, a new thallium arsenic sulfosalt from the Mercur gold deposit, Utah. *American Mineralogist*, **76**, 653–656.

Yazeva R.G., Puchkov V.N., Bochkarev V.V. (1991) [Geodynamics and metallogeny of the eastern paleocontinental margin and marginal volcanic-plutonic belts of the Urals]. *Geodinamika i metallogeniya Urala [Geodynamics and Metallogeny of the Urals]*. Yekaterinburg, IGG UrO RAS, 43–45. (in Russian)